Dissertation zur Erlangung des Doktorgrades
der Fakultät für Chemie und Pharmazie
der Ludwig-Maximilians-Universität München

Role of the ubiquitin-editing enzyme A20 in B cell function and disease

Yuanyuan Chu

aus

Xian, China

2012

Erklärung

Diese Dissertation wurde im Sinne von § 7 der Promotionsordnung vom 28. November 2011 von Herrn Prof. Dr. Reinhard Fässler betreut.

Eidesstattliche Versicherung

Diese Dissertation wurde eigenständig und ohne unerlaubte Hilfe erarbeitet.

München, am 29.10.2012

_____

Yuanyuan Chu

Dissertation eingereicht am 29.10.2012

1. Gutachter: Prof. Dr. Reinhard Fässler

2. Gutachterin: PD Dr. Ursula Zimber-Strobl

Mündliche Prüfung am 30.11.2012

Table of contents

Table of contents ..... **I**

List of publications ..... **II**

Abbreviations ..... **III**

Summary ..... **V**

Acknowledgements ..... **VII**

Introduction **1**

1 B cell biology and B cell-mediated diseases **1**
1.1 Overview of immune cells 1
1.2 B cell development 2
1.2.1 Early B cell development in the bone marrow 2
1.2.2 Peripheral B cell maturation 3
1.2.3 Germinal center reaction 4
1.3 The role of B cells in autoimmunity 6

2 NF-κB coordinates immune cell function and inflammation **9**
2.1 The family of NF-κB transcription factors 9
2.2 Canonical and non-canonical NF-κB signaling 11
2.3 The role of NF-κB in B cell differentiation and function 13
2.4 The role of NF-κB in inflammatory responses 15

3 Regulation of NF-κB signaling by ubiquitination **17**
3.1 The ubiquitin system 17
3.2 The role of ubiquitination in NF-κB signal transduction pathways 20

4 A20, a central negative regulator of NF-κB activation **24**
4.1 Cellular functions of the ubiquitin-editing enzyme A20 24
4.2 Mechanisms of NF-κB inhibition by A20 26
4.3 CYLD: tumor suppressor and negative regulator of NF-κB signaling 28
4.4 Physiological functions of A20 29
4.5 Association of A20 with human diseases 30
4.5.1 Association of A20 polymorphisms with human autoimmune diseases 30
4.5.2 Loss of A20 function in human lymphomas 31

Aim of the thesis **33**

Brief summaries of the publications **34**

Curriculum Vitae **38**

References **39**

Supplements **52**

List of publications

The thesis is based on the following publications which are referred to in the text by their Roman numerals (I–IV):

I. Vereecke, L., Sze, M., Mc Guire, C., Rogiers, B., **Chu, Y.,** Schmidt-Supprian, M., Pasparakis, M., Beyaert, R., and van Loo, G., 2010.
Enterocyte-specific A20 deficiency sensitizes to tumor necrosis factor-induced toxicity and experimental colitis.
Journal of Experimental Medicine 207: 1513–1523.

II. **Chu, Y.**, Vahl, C.J., Kumar, D., Heger, K., Bertossi, A., Wójtowicz, E., Soberon, V., Schenten, D., Mack, B., Reutelshöfer, M., Beyaert, R., Amann, K., van Loo, G. and Schmidt-Supprian, M., 2011.
B cells lacking the tumor suppressor TNFAIP3/A20 display impaired differentiation and hyperactivation and cause inflammation and autoimmunity in aged mice.
Blood 117: 2227–2236. Epub 2010 Nov 18.

III. Matmati, M., Jacques, P., Maelfait, J., Verheugen, E., Kool, M., Sze, M., Geboes, L., Louagie, E., Mc Guire, C., Vereecke, L., **Chu, Y.,** Boon, L., Staelens, S., Matthys, P., Lambrecht, B.N., Schmidt-Supprian, M., Pasparakis, M., Elewaut, D., Beyaert, R., and van Loo, G., 2011.
A20 (TNFAIP3) deficiency in myeloid cells triggers erosive polyarthritis resembling rheumatoid arthritis.
Nature Genetics 43: 908–912.

IV. **Chu, Y.,** Soberon, V., Glockner, L., Beyaert, R., Massoumi, R., van Loo, G., Krappmann, D., and Schmidt-Supprian, M., 2012.
A20 and CYLD do not share significant overlapping functions during B cell development and activation.
Journal of Immunology. Epub 2012 Sep 21.

Abbreviations

AID	Activation-induced cytidine deaminase
APC	Antigen-presenting cell
BAFF	B cell-activating factor belonging to TNF family
Bcl-10	B cell lymphoma 10
BCL-3	B cell lymphoma 3
BCR	B cell receptor
CARMA1	Caspase recruitment domain, CARD, membrane-associated guanylate kinase, MAGUK, protein 1
cIAP	Cellular inhibitor of apoptosis
CLP	Common lymphoid progenitor
CMP	Common myeloid progenitor
CXCR	CXC-chemokine receptor
CYLD	Cylindromatosis
DC	Dendritic cells
DLBCL	Diffuse large B cell lymphoma
DNA	Deoxyribonucleic acid
DUB	Deubiquitinase
EBV	Epstein Barr Virus
EDA-ID	Anhidrotic ectodermal dysplasia with immunodeficiency
FDC	Follicular dendritic cell
FL	Follicular lymphoma
GC	Germinal center
GWAS	Genome-wide association study
HL	Hodgkin lymphoma
HSC	Hematopoetic stem cell
HTLV	Human T lymphotropic virus
ICAM	Intracellular adhesion molecule
IEC	Intestinal epithelial cell
IFN	Interferon
Ig	Immunoglobulin
IgH	Immunoglobulin heavy chain
IgL	Immunoglobulin light chain
IKK	IκB kinase
IL	Interleukin
IRF	Interferon regulatory factor
IκB	Inhibitor of nuclear factor-κB
JAMM	JAB1/MPN/MOV34 metalloenzyme
LMP1	Latent membrane protein
LPS	Lipopolysaccharide
LT	Lymphotoxin
LUBAC	Linear ubiquitin chain assembly complex
LUBIC	Linear ubiquitin binding domain
MALT1	Mucosa-associated lymphoid tissue lymphoma translocation protein1
MCL	Mantle cell lymphoma
MCPIP	Monocyte chemotactic protein-induced protein
MZ	Marginal zone

NEMO	NF-κB essential modulator
NF-κB	Nuclear factor-κB
NIK	NF-κB inducing kinase
NK	Natural killer cell
NLR	Nucleotide-binding oligomerization domain-like receptor
NLS	Nuclear localization signal
OTU	Ovarian tumor
PAMP	Pathogen-associated molecular pattern
PKC	Protein kinase C
PMBL	Primary mediastinal lymphoma
PRR	Pattern recognition receptor
RA	Rheumatoid arthritis
RANK	Receptor activator for NF-κB
RHD	Rel homology domain
RIG	Retinoic acid inducible gene
RIP	Receptor-interacting protein
SHM	Somatic hypermutation
SLE	Systemic lupus erythematosus
SNP	Single nucleotide polymorphism
SS	Sjögren's syndrome
TAB	TAK1 associated binding protein 2
TAD	Transcription activation domain
TAK	TGFβ activated kinase
Tax1bp1	Tax1-binding protein 1
TBK	TANK-binding kinase
TCR	T cell receptor
TD	T cell dependent
T_{FH}	T follicular helper
TGF	Transforming growth factor
TLR	Toll-like receptor
TNF	Tumor necrosis factor
TNFAIP3	TNFα-induced protein 3
TNFR	Tumor necrosis factor family
TRADD	Tumor necrosis factor receptor type 1-associated DEATH domain
TRAF	Tumor necrosis factor receptor associated factor
TSH	Thyroid stimulating hormone
Ub	Ubiquitin
UBAN	Ubiquitin binding in ABIN and NEMO domain
USH	Ubiquitin C-terminal hydrolase
USP	Ubiquitin-specific protease
VCAM	Vascular cell adhesion molecule
WM	Waldenström Macroglobulinemia

Summary

Multicellular organisms protect themselves against invading pathogens via sophisticated effector mechanisms of their immune system. In particular, B and T lymphocytes of the adaptive branch of immunity, generate a huge repertoire of receptor specificities against foreign antigens through random recombination of antigen receptor encoding gene segments. A key function of adaptive immunity is attributed to B cells, which provide high-affinity antibodies and long-term memory. However, the large pool of B cells harboring diverse antigen specificities also bears autoreactive B cells recognizing self-antigens. Recognition of self, also termed autoimmunity, can be of deleterious outcome for its host. Over the last decade, genome-wide association studies contributed significantly to the identification of a growing number of genetic risk variants associated with an increased susceptibility to human autoimmune diseases.

Recently, polymorphisms in the *A20* (*TNFAIP3*) gene were linked with several human autoimmune diseases such as systemic lupus erythematosus, rheumatoid arthritis, Crohn's disease, coeliac disease and psoriasis. Moreover, A20 is frequently inactivated in multiple human B cell lymphomas. A20 is an ubiquitin-editing enzyme that functions as a central negative regulator of signaling pathways leading to the activation of NF-κB transcription factors. The family of NF-κB transcription factors drives the expression of genes that are involved in a wide variety of physiological functions and inflammatory responses. In particular, NF-κB plays an important and evolutionarily conserved role in the immune system. NF-κB activation is critically regulated through ubiquitination of key signaling molecules. Failure to control these posttranslational events by negative regulators such as A20 contributes significantly to chronic inflammation, autoimmunity and cancer.

Therefore, to uncover the role of A20 during immune responses and its contribution to prevent autoimmunity *in vivo*, we studied effects of cell-type specific ablation of A20 in mice. Given the critical role of B cells in autoimmune pathology and the strong implication of A20 in human B cell lymphomas, we focused on studying the role of A20 in B cell development, function and autoimmunity (Paper II). A20 deficiency in B cells impairs the development, function and possibly localization of several mature B cell subsets. Importantly, loss of A20 in B cells lowers their activation threshold in a gene-dose-dependent manner, resulting in the spontaneous

secretion of pro-inflammatory cytokines, most notably IL-6. Through their spontaneous activation, A20-deficient B cells initiate expansion of myeloid and T cells in naïve mice, which progresses to chronic inflammation and autoimmune manifestations in old age.

In addition to A20, NF-κB activation is also controlled by other deubiquitinases such as CYLD. It is remarkable that A20 and CYLD share similar mechanisms and molecular targets in the negative regulation of NF-κB signaling, suggesting potential overlapping functions. Therefore, we generated and characterized a mouse model for A20/CYLD double-deficiency in B cells (Paper IV). Interestingly, the combined loss of A20 and CYLD did not exacerbate the developmental defects and hyperresponsive activity of A20-deficient B cells.

Finally, in the context of Crohn's disease and rheumatoid arthritis, we also contributed to studies on the cell-type-specific function of A20 in intestinal epithelial (Paper I) and myeloid cells (Paper III) to contain inflammation and autoimmunity. A20 deficiency in intestinal epithelial cells sensitized mice to experimental colitis and TNF-induced lethality (Paper I). TNF induces apoptosis in A20-deficient intestinal epithelial cells, resulting in disruption of the intestinal epithelial barrier and infiltration of commensal bacteria that trigger a systemic inflammatory response.

Mice lacking A20 specifically in myeloid cells develop spontaneous severe destructive polyarthritis, which is similar to human rheumatoid arthritis (Paper III). Moreover, myeloid-specific A20-deficient mice have high levels of pro-inflammatory cytokines including TNF, IL-1β and IL-6 systemically and in local joint tissue. Given the strong association of TNF with the pathogenesis of rheumatoid arthritis, it is of clinical interest that the polyarthritis in myeloid-specific A20-deficient mice does not depend on TNF, but is mediated by the TLR4/MyD88 signalling axis and IL-6.

Taken together, we defined the important role of A20 in maintaining B cell homeostasis and in preventing B cell-mediated chronic inflammation and autoimmunity. Interestingly, A20 does not have overlapping functions with the deubiquitinase CYLD in B cells. In the intestinal epithelium, A20 acts as a critical anti-apoptotic protein to maintain the epithelial barrier function. In addition, A20 also plays a crucial role in myeloid cells to prevent autoimmune diseases such as rheumatoid arthritis.

Acknowledgements

During the four and a half years of my PhD studies, I have benefited from the knowledge, support, help and advices of many great people.

In particular, I want to express my deep gratitude to two persons: my thesis advisor Dr. Marc Schmidt-Supprian and my doctor father Prof. Dr. Reinhard Fässler.
It was my great fortune to have the privilege of joining Dr. Marc Schmidt-Supprian's research group as one of his first PhD students. Throughout the years, he has always been supportive and encouraging both in research and in life. I am deeply grateful to him for the exciting projects, excellent supervision and his brilliant ideas.
It was also my great fortune to have Prof. Dr. Reinhard Fässler as my doctor father. His broad knowledge and sharp insight on various topics have always been inspiring to me. I am deeply grateful to him for his constant interest in my projects, his invaluable advices, his support and the excellent working conditions that he provided for the Schmidt-Supprian lab.

I greatly appreciate the members of the thesis committee for their time and dedication to review my thesis: Prof. Dr. Reinhard Fässler as first referee, Dr. Ursula Zimber-Strobl as second referee, Prof. Dr. Martin Biel, Prof. Dr. Klaus Förstemann, Prof. Dr. Christian Wahl-Schott and Prof. Dr. Karl-Peter Hopfner.

Special thanks go to our collaboration partners: Dr. Geert van Loo for sharing the conditional A20 allele and the fruitful collaboration projects, Dr. Daniel Krappmann for his deep expertise in NF-κB signaling and the great help he always offered, Laura Glockner for tremendous help with EMSA, Dr. Ursula Zimber-Strobl for sharing reagents and numerous discussions on my projects, Prof. Dr. Ludger Klein for tissues of $RAG2^{-/-}$ mice, Dr. Guru Krishnamoorthy for help with thymidine incorporation assays, Dr. Dominik Schenten for sharing the conditional MyD88 allele and his expertise on somatic hypermutation analysis, Miriam Reutelshöfer and Prof. Dr. Kerstin Amann for their expertise on organ pathology and tremendous help with IHC, Brigitte Mack for help with IHC staining of marginal zone B cells, Dr. David Komander for providing purified A20 OTU protein, Prof. Dr. Rudi Beyaert and Dr. Ramin Massoumi for helpful discussions.

I am very thankful to the present and former members of the Schmidt-Supprian lab for their help, scientific expertise, input, companionship and the fun we had along the road: Julia Knogler and Barbara Habermehl for tremendous help in the lab and Julia for her delicious cakes, Christoph Vahl for always being a helpful friend, Arianna Bertossi for all the pleasant trips we spent together, Klaus Heger for his deep understanding of immunology and stimulating discussions, Dilip Kumar for numerous conversations about science and life, Valeria Soberon for precious help with the A20/CYLD project and nice chats, Maike Kober for the good mood she spreads in the lab, my bench neighbour David Riess for friendship and discussions about anything in science and life, and also the students Edyta Wójtowicz, Sarah Schmalbrock and Basma Abdel-Motaal for help with experiments during their visit.

Many thanks are due to all present and former members of the department, in particular: Tim Lämmermann who introduced me into the fascinating world of immunofluorescence on lymphoid tissues, Michael Sixt for numerous advices, Karin Hirsch and Kathrin Schumann for help with migration assays, Raphael Ruppert for help with i.v. injections, pouch bleeding and his expertise on BM chimeras, Markus Moser for help with irradiation, Daniel Moik for help with rabbit immunization, and Aurelia Raducanu who offered her help whenever it was needed.
Moreover, I want to thank Dr. Walter Göhring, Dr. Armin Lambacher, Ines Lach-Kusevic, Klaus Weber and Carmen Schmitz for technical and administrative support and all animal caretakers, in particular Jens Pässler.

I also want to thank my friends and science fellows Franziska Jadghuber, Caroline Hojer and Nathalie Knies for their help, scientific expertise and support.

I am forever indebted to my parents and Andreas. Their love, support and encouragement have been the driving force for my scientific journey.
To them, I dedicate this thesis.

Introduction

1 B cell biology and B cell-mediated diseases

1.1 Overview of immune cells

The immune system protects us against the constant threat of hostile invasion by foreign pathogens, such as bacteria, viruses or parasites. This system consists of many different cell types, which can roughly be subdivided into the innate or inborn and adaptive or acquired branch of immunity. B lymphocytes, which can differentiate into antibody producing plasma cells, belong to the adaptive immune system.

In mammals, all immune cells including B cells are derived from pluripotent hematopoietic stem cells (HSCs) in the fetal liver before birth and in the bone marrow after birth[1]. In sequential steps, these HSCs differentiate through multipotent progenitors into more committed common myeloid progenitor (CMP) cells or common lymphoid progenitor (CLP) cells. CMPs give rise to the myeloid lineage, consisting of granulocytes (neutrophils, eosinophils and basophils), mast cells and macrophages[2,3]. Myeloid cells represent cellular components of the innate immunity and have phagocytic properties in common[4]. However, myeloid cells not only contribute to the clearance of pathogens, dead cells and cell debris but are also critical sentinel cells to induce inflammation by secreting cytokines and chemokines to activate and recruit additional immune cells[4].

CLPs are the precursors of B and T lymphocytes, natural killer (NK) cells and dendritic cells (DC)[2,3]. In particular, B and T cells are the key players of the adaptive immune response. Both types of lymphocyte have the high variability of their antigen receptors in common: the B cell receptor (BCR) and the T cell receptor (TCR). Through recombination of a large pool of different gene segments encoding the antigen receptors, each lymphocyte expresses a unique variant of the antigen receptor, which is specific for a certain antigen. A special immune function is also attributed to dendritic cells, which do not solely act as phagocytic cells but are essential to initiate the adaptive immune response by functioning as antigen-presenting cells (APCs) for B and T cells[5].

1.2 B cell development

1.2.1 Early B cell development in the bone marrow

During their development, B cells randomly assemble a functional B cell receptor (BCR) from different gene segment families. Therefore, each B cell carries a unique BCR, which endows them with specificity for a unique antigen. Adult B cell development in the bone marrow occurs in several steps to generate immature B cells harboring a productive BCR. These early developmental stages also encompass essential processes to eliminate B cells expressing self-reactive BCR. The BCR consists of pairs of immunoglobulin heavy (IgH) and light (IgL) chains[6]. The IgH chain is encoded by one locus, whereas the IgL chain is encoded by two loci: λ and κ[6]. The antigen specificity of an immunoglobulin is determined by the variable (V) region of Ig heavy and light chain[6]. Through a process, termed V(D)J recombination, which is initiated by the lymphoid-specific enzymes recombination-activating genes 1 and 2 (RAG1 and RAG2), gene segments encoding the variable region are rearranged[7]. The V region of the IgH chain is assembled by joining a variable (V_H), diversity (D_H) and joining (J_H) gene segment[6]. In contrast, the V region of the IgL chain does not contain D segments, but only rearranged V_L and J_L gene segments[6].
During early B cell development, the rearrangement of the IgH chain occurs in pro B cells (Fig. 1). Pro B cells harboring a productive IgH rearrangement further proceed to the pre B cell stage. In pre B cells, the IgH chain is associated with a surrogate light chain, consisting of the λ5 and VpreB molecules, to form the pre-BCR[8]. During this developmental stage, pre B cells rearrange their IgL chain on the κ locus first, followed by Igλ rearrangement in case the Igκ rearrangement does not result in a productive IgL chain[9]. Immature B cells with successfully rearranged IgH and IgL chain further undergo negative selection for the recognition of self-antigens[9]. Autoreactive immature B cells either rearrange the V region of their IgL chain, a process termed receptor editing, or are eliminated by apoptosis[9]. Non-autoreactive immature B cells exit the bone marrow as transitional B cells[10]. The transitional stage consists of three developmental phases: T1, T2 and T3. Transitional type 1 (T1) B cells migrate from the bone marrow to the splenic B cell follicles where they differentiate into non-circulatory T2 B cells[10]. T3 B cells, originally proposed as late transitional B cells, have been identified as anergic B cells[11]. Anergic B cells are

autoreactive, but persist in an antigen-unresponsive state in the periphery[12]. Thus, besides clonal deletion and receptor editing in the bone marrow, anergy represents a third mechanism by which autoreactive B cells are tolerized[12].

1.2.2 Peripheral B cell maturation

B cells can mature into several subtypes, which are characterized by different effector functions and distinct localization in the organism.

Mature B cells are generated both in the bone marrow and secondary lymphoid organs with the majority of B cells mature in the periphery[13]. Mature B cells in the periphery can be divided into three subsets: follicular (FO) B cells, marginal zone (MZ) B cells and B1 cells. During transition from immature to mature B cells, the response to BCR crosslinking changes from an apoptotic to a proliferative signal[14]. In addition, BCR-mediated signal strength critically determines lineage commitment in peripheral B cells[14].

T2 B cells either differentiate into FO B cells or via MZ precursors into MZ B cells (Fig. 1). FO B cells represent the major subset of mature B cells[14]. In addition, they are recirculating and the major source of T cell-dependent (TD) immune response (in detail under 1.2.3) and B cell memory[14].

In contrast, in the mouse, MZ B cells are non-recirculating and localized at the border of the splenic marginal sinus where they can rapidly respond to blood-borne pathogens in a T cell-independent manner[14,15]. This response does not involve germinal center formation (in detail under 1.2.3), but is still accompanied by somatic hypermutation and Ig class switching[14,15]. In addition, MZ B cells also contribute to T cell-dependent (TD) immunity by shuttling antigens in immune complexes into splenic follicles[16].

B1 cells represent the third mature B cell subset in the periphery. They populate the peritoneal and pleural cavities and represent the main source of natural IgM antibodies, thereby contributing to innate immunity[17]. B1 cells are mainly derived from fetal precursors and maintained by self-renewal throughout life[17]. However, they can also be generated from less abundant precursors in adult bone marrow[18].

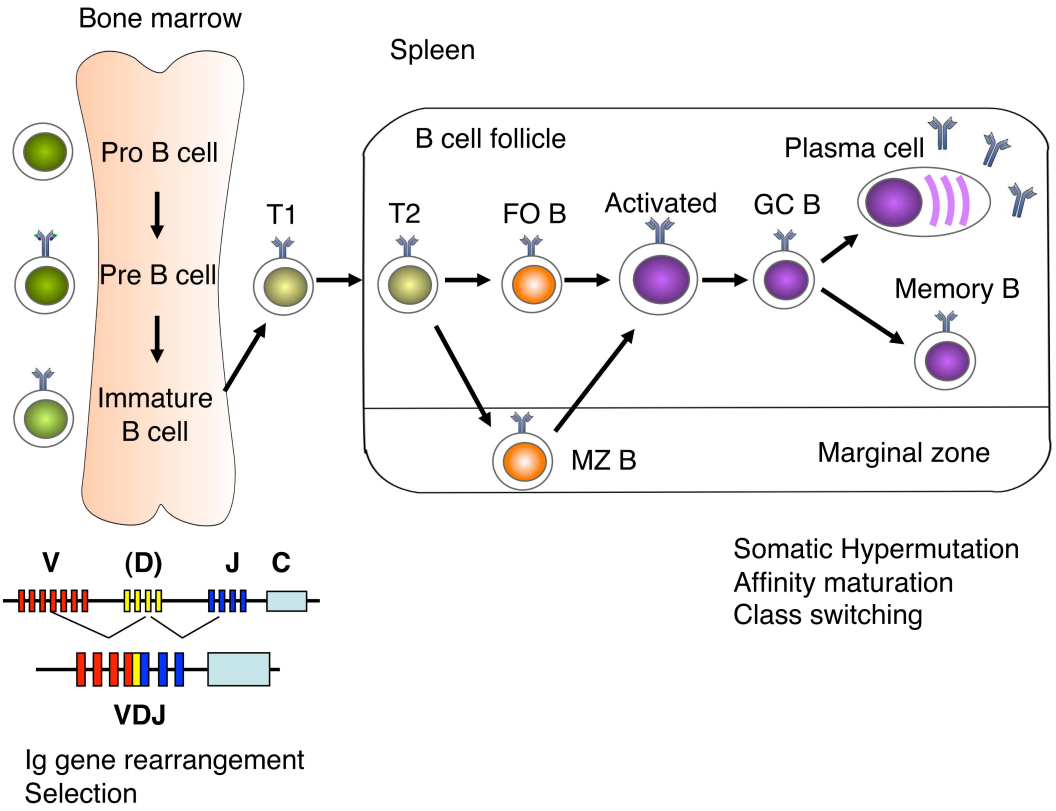

Figure 1: **Simplified scheme of B cell differentiation in bone marrow and periphery.**
Postnatally, early B cell differentiation takes place in the bone marrow. This phase is characterized by the generation of functional B cell receptors through V(D)J recombination and the negative selection of autoreactive B cells. Successfully selected B cells mature to follicular or marginal zone B cells in the spleen. Upon antigen encounter, activated B cells can undergo the germinal center reaction where somatic hypermutation and class switch recombination of the BCR occur. Finally, germinal center B cells differentiate either into antibody-secreting plasma cells or long-lived memory B cells. Abbreviations: FO B = Follicular B cell; MZ B = Marginal zone B cell; GC B = Germinal center B cell.

1.2.3 Germinal center reaction

The huge repertoire of B cells recognizing a specific antigen is generated by V(D)J recombination in the bone marrow. However, additional somatic mutations in the variable region of the B cell receptor, determining antigen recognition, contribute significantly to increased antigen affinity of the generated antibodies. This process occurs in a lymphoid structure termed germinal center and requires help from specialized immune cells, in particular T cells.

The germinal center (GC) reaction is the basis of T cell-dependent (TD) immune response (Fig. 1)[19]. It provides a cellular environment for the affinity maturation of

antibody responses and generates long-term B cell memory[19]. Recirculating follicular B cells encountering an antigen through their BCR in secondary lymphoid organs such as lymph node and spleen can undergo two routes of TD-B cell activation: extrafollicular response or follicular germinal center reaction[20,21]. First, upon activation, most B cells differentiate into short-lived plasma cells at the outer T cell zone, where they secrete low-affinity antibodies[20,22,23]. Second, only B cells presenting high-affinity peptide-MHCII molecules (pMHCII) to a limited number of antigen-primed T cells at the T:B cell border can compete to seed the follicles and give rise to germinal centers[22,23]. With ongoing immune reaction, the germinal center acquires a polarized structure, which is divided into the dark and light zone[24]. In the dark zone, adjacent to the T cell zone, B cells – at this stage, they are termed centroblasts - undergo extensive proliferation and somatic hypermutation (SHM)[22-24]. The last process requires the enzymes Activation-induced cytidine deaminase (AID)[25] and Polymerase η[26,27], which introduce mutations into the variable region of the rearranged immunoglobulin to generate antibodies of higher affinities. Centroblasts further migrate to the light zone where they turn into non-proliferating centrocytes to undergo affinity selection and Ig class switching[22-24].

Selection and class switching of GC B cells require the presence of two additional cell types in the light zone: follicular dendritic cells (FDC) and T follicular helper (T_{FH}) cells[28]. First, only GC B cells expressing high-affinity BCR are positively selected by FDCs, which present unprocessed antigen deposited as immune complexes on Fc receptors[28]. GC B cells with no or low antigen affinity will die due to lack of BCR signals[28]. Second, GC B cells are further selected by T_{FH} cells. The BCR affinity defines the level of pMHCII molecules on the B cell surface. In a competitive manner, centrocytes expressing high level of pMHCII molecules preferentially interact with a limited number of T_{FH} cells[29]. Importantly, T cell help initiates through CD40L and cytokines class switch recombination, the modification of IgM to other Ig isotypes, and terminal differentiation to plasma cells[28]. Positively selected GC B cells can either reenter the dark zone and undergo additional rounds of proliferation, hypermutation and selection (“cyclic re-entry” model)[30] or exit the germinal center as long-lived plasma cells[31] or memory B cells[32]. The correct positioning of B cells during the two routes of extrafollicular and follicular GC reaction is guided by chemokine gradients and the regulated expression of chemokine receptors including

EBI2[33,34], $S1P_2$[35], CXCR4 and CXCR5[36]. Chemokines also guide long-lived plasma cells to the bone marrow[37], whereas memory B cells are retained in secondary lymphoid organs where they can be rapidly recruited into a secondary immune response[38].

1.3 The role of B cells in autoimmunity

Autoimmunity is the aberrant immune response directed against self-antigens and can result in a pathological condition of tissue destruction termed autoimmune disease. Autoimmune diseases can manifest either in a systemic or organ-specific manner. Examples of systemic autoimmune diseases are systemic lupus erythematosus (SLE), rheumatoid arthritis (RA) and Sjögren's syndrome (SS). SLE and RA are characterized by the production of several auto-antibodies targeting widely distributed auto-antigens in multiple organs such as skin, joints, kidney, brain, blood vessels, lung and heart. In SS, exocrine glands are attacked and destroyed by the autoimmune reaction. In contrast, in organ-specific autoimmune diseases such as type 1 diabetes, psoriasis, multiple sclerosis and inflammatory bowel disease (including Crohn's disease and coelic disease), the autoimmune response is directed against tissue-specific auto-antigens.

The etiology of autoimmune diseases is highly complex and involves both environmental and genetic components[39]. Environmental factors such as diet and infections can trigger autoimmunity in genetically susceptible patients. Since the last decade, genome-wide association studies (GWAS) have identified a growing number of genetic variants such as single nucleotide polymorphisms (SNPs), which are associated with an increased risk to develop autoimmune diseases[39,40].

Immune factors contributing to autoimmunity include both humoral and cellular components, in particular B and T cells, macrophages and dendritic cells. In fact, auto-antibodies produced by autoreactive B cells directly mediate some of the tissue pathology observed in autoimmune diseases such as SLE[41]. Moreover, the therapeutic benefit of B cell depletions with monoclonal antibodies directed against the B cell specific surface antigen CD20 in human trials implies that B cells play an integral role in autoimmune diseases[42].

The huge repertoire of B cell specificities against foreign antigens is shaped by V(D)J recombination in the bone marrow and somatic hypermutation in the germinal center. However, these mechanisms to increase BCR diversity and affinity simultaneously also lead to the generation of self-reactive B cells. Despite different mechanisms of tolerance at several checkpoints during B cell development including clonal deletion, receptor editing and anergy, autoreactive B cells can escape tolerance and contribute to autoimmunity[12].

B cells contribute to autoimmunity through five major mechanisms (Fig. 2)[43,44]: (1) generation of auto-antibodies; (2) antigen-presentation; (3) co-stimulation of T cells; (4) production of pro-inflammatory cytokines; (5) formation of ectopic lymphoid structures.

(1) Auto-antibodies, which can also be found in healthy individuals, are not necessarily pathogenic. In particular, low-affinity IgM auto-antibodies, constituting the majority of natural auto-antibodies, are crossreactive and serve a protective role in autoimmunity by neutralizing auto-antigens[45]. In contrast, pathological functions are mediated by high-affinity and class-switched auto-antibodies of the IgG isotype. They are generated from GC-derived plasma cells, which underwent somatic hypermutation and class switch recombination. High-affinity IgG auto-antibodies cause disease pathology through three major effects (Fig. 2)[43,44]. First, they can mediate direct cytopathic effects in autoimmune diseases such as myasthenia gravis and Graves disease[43,44]. In myasthenia gravis, the acetylcholine receptors are targeted by auto-antibodies, resulting in receptor endocytosis and neuromuscular dysfunction[43,44]. Auto-antibodies against thyroid stimulating hormone (TSH) receptor in Graves disease constantly activate the TSH-receptor, thereby causing hyperthyroidism[43,44]. Second, auto-antibodies can cause cytotoxicity through complement activation. In hemolytic anemia, erythrocytes are lysed in a complement-dependent manner by auto-antibodies recognizing erythrocyte-specific antigens[43,44]. Third, auto-antibodies can form immune complexes with soluble antigens and deposition of immune complexes in organs is a common feature of several autoimmune diseases including SLE[43,44]. Immune complexes deposited in renal glomeruli can cause complement-induced inflammation, resulting in glomerulonephritis[43,44].

(2) Besides the production of pathogenic auto-antibodies, autoreactive B cells can activate $CD4^+$ T cells by functioning as antigen-presenting cells (Fig. 2)[43,44].

(3) Simultaneously, through the expression of co-stimulatory molecules including B7, CD40 and OX40L, B cells can enhance T cell priming (Fig. 2)[43,44].

(4) Less studied is the contribution of B cells to autoimmunity as cytokine producing cells (Fig. 2). In fact, B cells can modulate immune homeostasis through the secretion of pro-inflammatory cytokines such as IL-6, IFNγ and LTα[43,44]. In particular, IL-6 production by B cells was recently proposed as the key mechanism of autoimmune pathogenesis in a murine EAE-model for human multiple sclerosis[46].

(5) Uniquely, B cells can initiate the formation of lymphoid follicles in non-lymphoid organs (Fig. 2). Ectopic lymphoid structures or germinal centers have been found in the synovium of RA patients, in the salivary glands of SS patients and in the kidney of SLE patients[43,44]. Local initiation of the immune response in the diseased organ significantly amplifies the inflammatory response and disease pathology[43,44].

The molecular mechanisms underlying aberrant B cell function in autoimmunity is complex. However, studies using mouse models for autoimmune diseases revealed two major molecular factors driving altered B cell function: increased B cell survival and altered B cell activation.

First, intrinsic survival signals generated e.g. by overexpression of Bcl-2[47] or deletion of Fas[48] help autoreactive B cells to overcome apoptosis during negative selection. In addition, extrinsic survival signals are provided by the cytokine BAFF, which is also essential for normal B cell maturation[49,50]. BAFF protects autoreactive B cells from negative selection by upregulating Bcl-2 through alternative NF-κB signaling[49,50].

Second, the generation and maintenance of autoreactive B cells depend on signaling through the BCR[51]. Altered intrinsic signal tranduction can decrease the threshold of signal strength for cellular activation, resulting in hyperactivity and spontaneous production of pro-inflammatory cytokines[51].

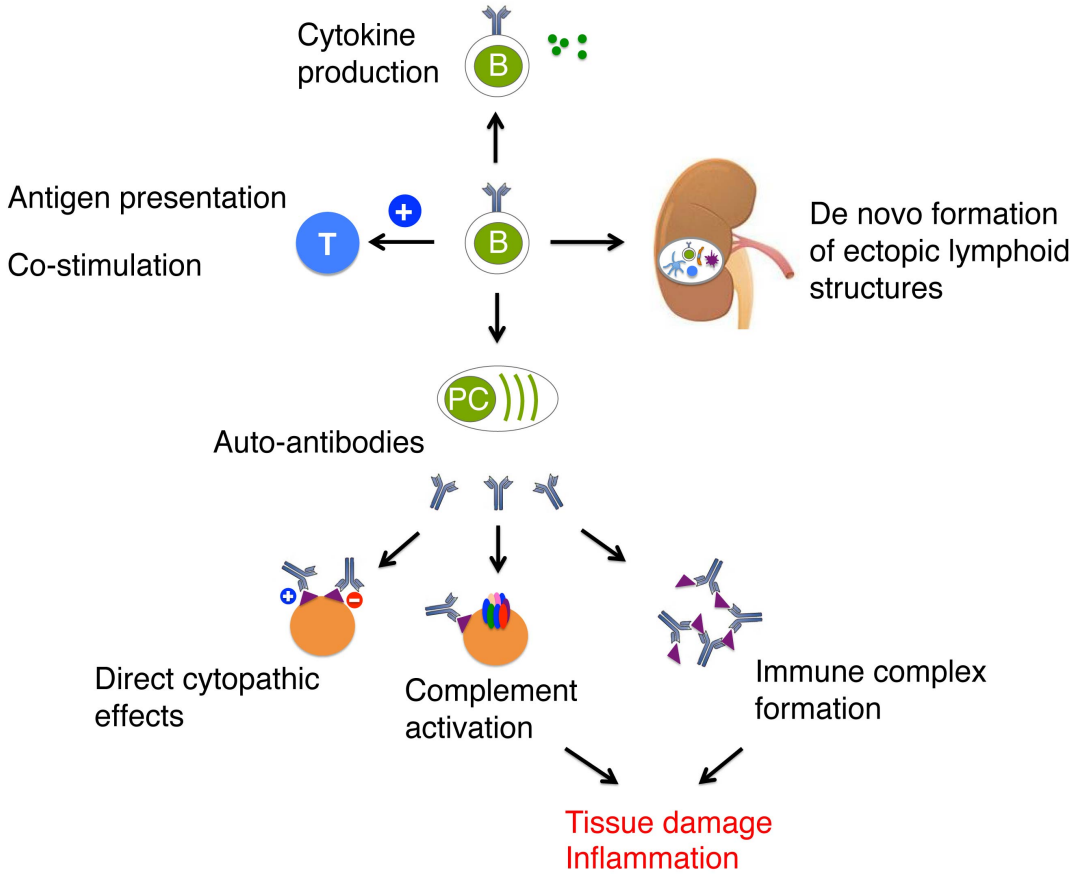

Figure 2: **B cells are the central players in autoimmune diseases.**
B cells contribute to autoimmunity through the production of auto-antibodies, by antigen presentation and co-stimulation of T cells, through the secretion of pro-inflammatory cytokines and the formation of ectopic lymphoid structures. Abbreviations: B = B cells; PC = Plasma cell; T = T cells.

2 NF-κB coordinates immune cell function and inflammation

2.1 The family of NF-κB transcription factors

The family of nuclear factor-κB (NF-κB) transcription factors controls the expression of genes that are involved in various physiological contexts such as cell survival and proliferation, immune and inflammatory responses[52-54]. In mammals, the NF-κB family consists of five related transcription factors: NF-κB1 (p105/p50), NF-κB2 (p100/p52), RelA (p65), RelB and c-Rel (Fig. 3)[54]. All are characterized by the presence of a N-terminal Rel homology domain (RHD) responsible for both homo- and heterodimerization and sequence-specific DNA binding[54]. Dimers of NF-κB bind

to κB sites in promoters and enhancers of target genes and regulate transcription through the recruitment of co-activators and co-repressors[52]. Positive gene regulation requires the transcription activation domain (TAD) that is only present in RelA, RelB and c-Rel[52]. Since the p50 and p52 subunits lack the TAD, they may repress transcription as homodimers or activate transcription when associated with a TAD-containing NF-κB member or other proteins capable of co-activator recruitment[52]. RelA and c-Rel heterodimerize in particular with p50, whereas RelB preferentially heterodimerizes with p100 or its processed form p52[52-54].

In unstimulated cells, NF-κB is sequestered in the cytoplasm as inactive precursors, p100 and p105 or by association with one of three typical inhibitors of NF-κB (IκB) proteins, IκBα, IκBβ and IκBε (Fig. 3)[53,55]. The NF-κB inhibiting function of these proteins is mediated by the presence of multiple ankyrin repeats that interfere with the nuclear localization signals (NLS) of NF-κB to retain it in the cytoplasm[53]. Upon stimulation, the three major IκBs undergo signal-induced proteosomal degradation and NF-κB-dependant resynthesis with distinct kinetics[53]. The prototypical and most studied member of IκBs, IκBα, is rapidly degraded in response to NF-κB activating stimuli leading to the release of NF-κB dimers into the nucleus[53]. The current model suggests that IκBα and its preferred target, RelA:p50, constantly shuttle between the cytoplasm and the nucleus[56]. Signal-induced degradation of IκBα alters the dynamic balance between cytosolic and nuclear localization, thereby favoring nuclear localization of NF-κB[56]. Finally, NF-κB-induced resynthesis of IκBα constitutes a negative feedback mechanism to terminate NF-κB activation.

Since p105 and p100 contain ankyrin repeats in their C-terminus, they can function as IκB-like proteins[52]. In unstimulated cells, p105 is constitutively processed to p50 and the interaction of p105 with p50, RelA or c-Rel sequester the NF-κB dimers in the cytoplasm[52]. In contrast, p100 preferentially forms a complex with RelB to retain it in the cytosol and is only processed to p52 upon stimulation[52].

In addition, a novel family of inducibly expressed IκBs, also termed atypical IκB proteins, including BCL-3 (B cell CLL/ lymphoma 3)[57] and IκBζ[58], may function both as transcriptional co-activators and inhibitors of NF-κB in a context-specific manner (Fig. 3). BCL-3, which contain a TAD, can form transcriptionally active complexes with p50 or p52 homodimers[59,60] and thereby transactivate Cyclin D1 expression[61]. Cyclin D1 as a BCL-3 target gene is of particular interest due to its association with cell proliferation and tumorigenesis[62]. Similar to BCL-3, IκBζ can act as a

transcriptional co-activator for p50 dimers in an IL-1 or LPS-dependant manner[63]. However, its transactivation ability is blocked when associated with RelA-containing NF-κB dimers[64].

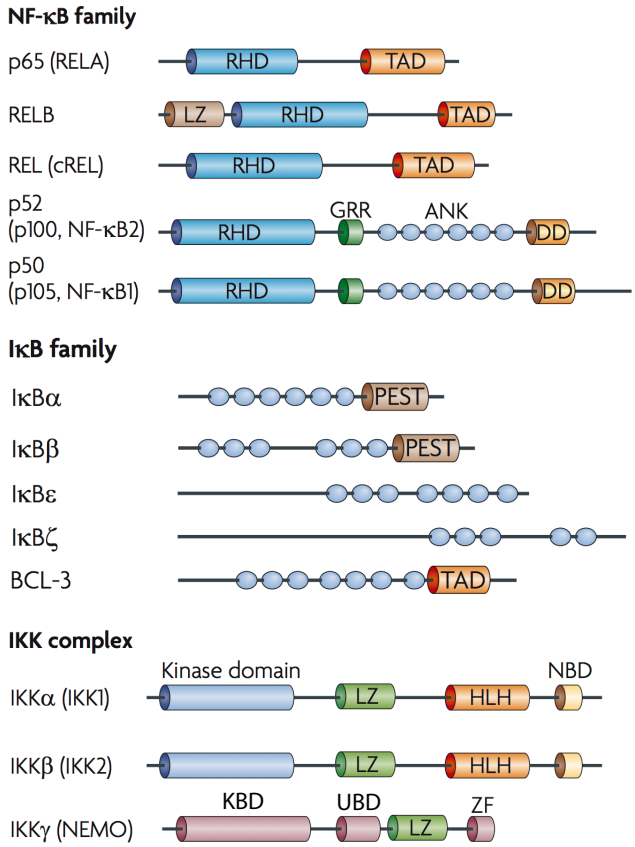

Figure 3: **Members of the NF-κB, IκB and IKK protein family.**
ANK, ankyrin repeat; BCL-3, B cell lymphoma 3; DD, death domain; GRR, glycine-rich region; HLH, helix–loop–helix; IKK, IκB kinase; KBD, Kinase- binding domain; LZ, leucine zipper; NBD, NEMO- binding domain; PEST, proline-, glutamic acid-, serine- and threonine-rich; RHD, REL homology domain; TAD, transactivation domain; UBD, ubiquitin-binding domain; ZF, zinc-finger (scheme modified from[53]).

2.2 Canonical and non-canonical NF-κB signaling

Activation of NF-κB occurs through two distinct mechanisms. Canonical NF-κB activation depends on the phosphorylation and subsequent proteosomal degradation of IκB proteins[53,54]. The phosphorylation is catalyzed by the IκB kinase (IKK) complex consisting of three main subunits: IKK1 (IKKα), IKK2 (IKKβ), and NEMO (NF-κB essential modulator) (IKKγ)[65,66]. IKK1 and IKK2 are highly similar in structure and contain a N-terminal kinase domain mediating their catalytic function[53,54]. Both

kinases interact with NEMO through their C-terminal NEMO-binding domain[66]. NEMO represents the regulatory core of the IKK complex and consists of a kinase-binding domain and an ubiquitin-binding domain[53,54]. The three components form a hexameric complex consisting of four catalytic subunits and two NEMO molecules[52]. NEMO is essential for canonical NF-κB signaling since it recruits through ubiquitin-binding upstream regulators that are required for IKK activation[67]. Canonical NF-κB signaling mediates diverse biological functions and can be activated by engagement of TNFR1, antigen receptors such as B cell receptor (BCR) and T cell receptor (TCR), Toll-like receptors (TLR) and other pattern recognition receptors (PRR) (Fig. 4)[52].

In addition, an alternative pathway of NF-κB activation exists to mediate more specific functions including lymphoid organogenesis, bone metabolism, B cell survival and maturation[68-70]. These specific biological functions of alternative NF-κB signaling are mediated through few members of the TNFR superfamily such as CD40, B cell-activating factor belonging to TNF family receptor (BAFFR), lymphotoxin β-receptor (LTβR) and receptor activator for NF-κB (RANK) (Fig. 4)[69,70]. Engagement of these receptors results in the stabilization of the NF-κB inducing kinase (NIK), which activates IKK1 by phosphorylation[71,72]. Active IKK1 triggers phosphorylation-induced processing of p100 to p52[72] that results in the nuclear translocation of transcriptionally active p52/RelB complexes. In contrast to the canonical pathway, alternative NF-κB activation is independant of the trimeric IKK complex but relies on NIK and IKK1[73]. However, both mechanisms do not exist in isolation, but activated p65 induces p100 production and thereby feeds the alternative NF-κB pathway[74].

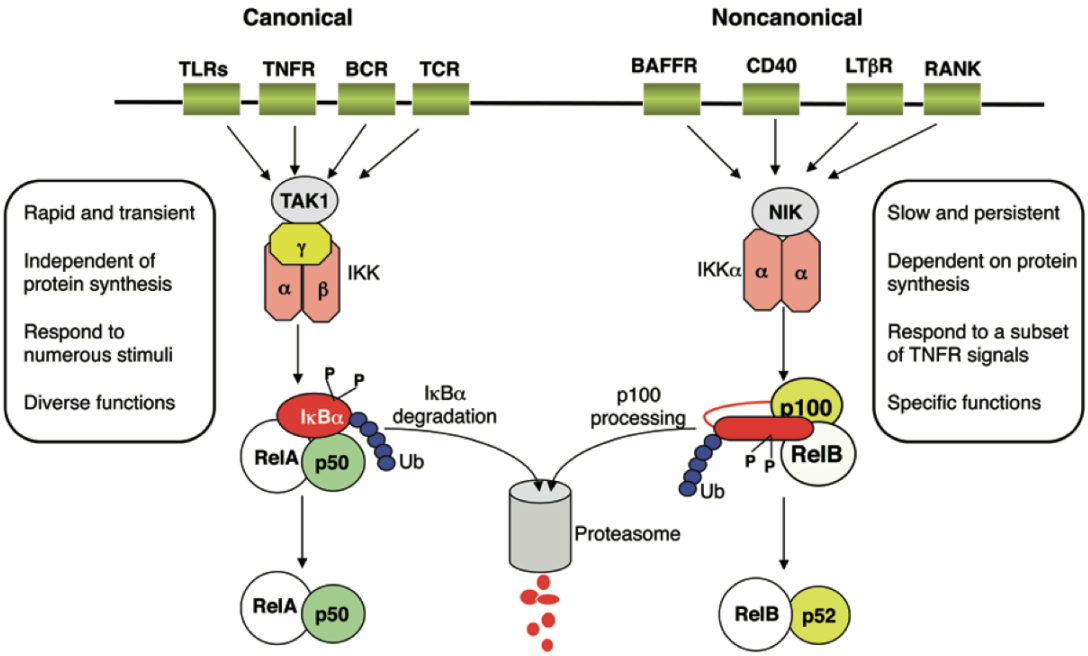

Figure 4: **Canonical and non-canonical NF-κB signaling pathways.**
Canonical NF-κB signaling is triggered by diverse signals such as TLR ligands, TNF and antigens. It depends on IKK-mediated IκBα phosphorylation and subsequent proteosomal degradation, resulting in the release and nuclear translocation of NF-κB dimers such as RelA/p50. Non-canonical NF-κB signaling is activated by cell type-specific signals such as BAFF, Lymphotoxin and RANK ligand. This alternative pathway requires NIK and IKK1 for p100 phosphorylation and processing to p52. p52 preferentially forms a complex with RelB (scheme from[70]).

2.3 The role of NF-κB in B cell differentiation and function

NF-κB plays a pivotal role in the development and function of immune cells since most of the receptors that either activate the canonical or the alternative pathway are expressed on hematopoietic cells[52]. Many of the insights about the role of NF-κB in physiology arise from studies where NF-κB family members, IKK members, IκBs or signal intermediates are lacking or overexpressed. Deletion of different NF-κB family members results in severe defects of immune cells, ranging from impaired myelopoiesis and erythrocyte differentiation to blockage of B and T cells at different developmental stages[75]. Deficiency of IKK members does not have a direct effect on myeloid cells but strongly affects B and T cell survival resulting in partial till complete absence of mature B and T cell subtypes[76,77]. The primary role of NF-κB signaling in lymphocytes, in particular B cells is to transmit survival signals.

Canonical NF-κB signaling through the pre-BCR contributes to the survival of early B cell progenitors in the bone marrow[78]. NF-κB was originally identified as a

regulator of κ immunoglobulin light chain (IgL) expression in B cells[79]. Interestingly, IKK-mediated activation of NF-κB is dispensable for the generation of immature B cells that express the κ Ig light chain but is required for the survival of λ IgL expressing immature B cells[80]. In accordance, the anti-apoptotic protein Pim2 is downregulated in NF-κB-deficient small pre B cells but the missing NF-κB signals can be replaced by the transgenic expression of the pro-survival protein Bcl-2[80]. However, the receptor that mediates NF-κB survival signals in λ positive immature B cells is not elucidated yet. Immature B cells that receive strong autoreactive signals through the BCR are subject to negative selection in the bone marrow[9]. To impede immediate apoptosis, autoreactive B cells can undergo receptor editing, a tolerance mechanism through which they rearrange their immunoglobulin light chain to generate a non-autoreactive BCR[9]. NF-κB was suggested to play a role during this process of negative selection by regulating the reactivation of RAG recombinase that is involved in the rearrangement of the Ig light chain[81]. In contrast, Derudder et *al.* did not find evidence for a role of IKK-mediated NF-κB activation during receptor editing, whereas another group[82] reported a correlation between elevated autoreactive BCR-induced NF-κB activation and receptor editing. However, several studies point to a possible contribution of NF-κB to the survival of immature B cells during negative selection in the bone marrow[83].

Immature B cells leaving the bone marrow become transitional B cells in the spleen before they progress further to mature follicular or marginal zone B cells. The transitional phase consists of at least two stages, T1 and T2. With ongoing maturation, NF-κB becomes absolutely essential for the long-term survival of B cells[78,83]. Compound loss of p105 and p100 or cRel and RelA result in the developmental blockage at the T1 to T2 transitional stage and the absence of mature B cells[78,83]. Canonical NF-κB signaling is absolutely required during all stages of B cell maturation, whereas BAFFR-mediated alternative NF-κB signaling strongly contributes to the survival of T2 and mature B cells[78,83]. In accordance, loss of the canonical pathway through deficiency of NEMO in B cells strongly reduces the number of T2 and mature B cells[80]. Ablation of the canonical and alternative pathway in mice with IKK1/IKK2-double deficient B lineage completely blocks B cell development at the T1 stage[80]. The absence of BAFFR-mediated alternative signaling can be compensated by the presence of a constitutive active form of IKK2 (IKK2ca), suggesting that canonical NF-κB signaling is sufficient to promote the maturation of

B cells in the absence of alternative signals[84].

Besides providing survival, canonical NF-κB signaling also contributes to mitogen-induced B cell proliferation by regulating the expression of Cyclin D1[85]. Resting B cells enter the G1 phase following stimulation through BCR, TLR4/9 or[52,83]. However, NF-κB is only required for entry into the S phase. The transition to the G2/S phase occurs in a NF-κB-independent manner[83]. *In vivo*, antigen activated B cells undergo extensive proliferation in the germinal center (GC) that is characterized by clonal expansion and BCR affinity maturation[86]. Remarkably, the gene expression profile of GC B cells lacks NF-κB signature genes but is dominated by G2/M phase regulators, indicating that NF-κB signaling is dispensable in GC B cells[87]. These findings are consistent with the shortened G1 phase of rapidly dividing GC B cells[86]. NF-κB is therefore important to initiate the proliferation of resting B cells by controlling the G0/G1 phase of the cell cycle but is potentially not involved in the division of GC B cells.

2.4 The role of NF-κB in inflammatory responses

NF-κB is not only essential for immune cell survival and function, but is clearly also the key regulator of inflammatory responses. Inflammation is defined as the manifestation of innate immunity to microbial infection or local injury in vascularized tissues[88]. Inflammation can be triggered by invading pathogens, which are sensed by innate immune receptors such as Toll-like receptors (TLRs) on tissue-resident dendritic cells, macrophages or mast cells[88,89]. These activated innate immune cells induce the production of pro-inflammatory cytokines (e.g., TNFα, IL-1β, IL-6), chemokines (e.g., CCL2 and CXCL8), prostaglandins and the upregulation of cell adhesion molecules (E-Selectin, VCAM-1, ICAM-1), thereby promoting infiltration of neutrophils and other leucocytes, vasodilatation of blood vessels and leakage of plasma into the tissue[88,89]. In addition, the pro-inflammatory cytokines TNFα, IL-1β and IL-6, if present in high amounts, also induce systemic effects, i.e. the hepatic acute phase response such as fever[89].

Inflammation can also be initiated by sterile tissue injury in the absence of infectious agents, thereby promoting tissue repair[89]. At the molecular level, factors triggering sterile inflammation include products from dying cells and breakdown components of

the extracellular matrix[89]. These triggering factors are sensed by tissue-resident macrophages, which induce inflammatory and reparative responses, and nociceptors mediating pain sensation[89].

Acute inflammation is resolved once the triggering stimulus has been removed[90,91]. The termination process is initiated through the switch from pro-inflammatory prostaglandins to anti-inflammatory lipoxins[90,91]. Lipoxins impede neutrophil infiltration and stimulate the clearance of apoptotic cells by macrophages[90,91]. In addition, stimulated macrophages secrete the anti-inflammatory cytokine transforming growth factor-β1 (TGF-β1), which counteracts pro-inflammatory TLR-signaling[90-92].

However, failure to terminate an acute inflammation can establish a chronic inflammatory state[89,92]. Chronic inflammation is classically caused by persistent infections, but also include conditions where neither infections nor tissue damage are involved[89,92]. An increasing number of human chronic inflammatory diseases have the loss of cellular homeostasis in common[89,92]. Chronic inflammation is not necessary the primary cause but contributes significantly to the pathogenesis of these diseases including atherosclerosis, obesity, cancer, neurodegenerative diseases, allergy and autoimmune diseases such as multiple sclerosis and rheumatoid arthritis[89,92].

NF-κB is critically involved both in the onset and resolution of acute inflammation. Tissue-resident sentinel cells such as macrophages are activated by pathogen-associated molecular patterns (PAMPs) through TLRs to trigger a signal cascade resulting in canonical NF-κB activation[93,94]. NF-κB regulates the expression of all key factors orchestrating inflammation including cytokines (e.g. TNFα, IL-1β, IL-6), chemokines (e.g. CCL2 and CXCL8), cell adhesion molecules (E-Selectin, VCAM-1, ICAM-1) and inflammatory enzymes (e.g. COX-2)[93,94].

NF-κB contributes also to the termination of inflammatory responses through several mechanisms. Infiltrating neutrophils are cleared from the inflamed tissue by NF-κB-mediated apoptosis[95]. In addition, NF-κB favors the differentiation of M2 macrophages secreting anti-inflammatory IL-10[95,96]. Finally, NF-κB attenuates the inflammatory gene expression by inducing the expression of several negative regulators such as IκBα and the deubiquitinase A20[96].

Increased NF-κB activation has been found in many chronic inflammatory diseases including inflammatory bowel disease[97], rheumatoid arthritis[94] and psoriasis[98].

However, besides its pro-inflammatory role, NF-κB also exerts anti-inflammatory

functions in non-immune cells to maintain tissue homeostasis. Loss of NF-κB activity in epithelial cells causes the development of severe chronic inflammation. In intestinal epithelial cells (IECs), deletion of IKK2[99] or NEMO[100] in the mouse results in higher susceptibility to chemical-induced colitis and spontaneous intestinal inflammation. Similarly, inhibition of NF-κB in mouse keratinocytes disturbs skin homeostasis and induces TNF-dependent inflammation and epidermal hyperplasia, which are reminiscent of a psoriasis-like disease[101,102].

3 Regulation of NF-κB signaling by ubiquitination

3.1 The ubiquitin system

The posttranslational modification of signaling molecules with polyubiquitin chains plays a pivotal role in signal transduction pathways such as NF-κB signaling. Ubiquitin (Ub) is a highly conserved eukaryotic protein, consisting of 76 amino acids[103]. In addition to its role in signal transduction, conjugation of ubiquitin to target proteins controls diverse cellular processes, ranging from protein degradation, cell cycle control, DNA repair, immune response, transcriptional regulation to endocytosis and vesicle trafficking[103,104].

Ubiquitin is covalently conjugated to target proteins through an isopeptide bond between its C-terminal glycine and the ε-amino group of lysine of the target protein[103,104]. Ubiquitination of target proteins is orchestrated by three classes of enzymes: Ub-activating enzyme E1, Ub-conjugating enzyme E2 and Ub ligase E3 (Fig. 5)[103,104]. First, E1 activates ubiquitin in an ATP-dependent manner by forming a thioester linkage between the catalytic cysteine of E1 and the C-terminal glycine of ubiquitin[103,104]. Second, activated ubiquitin is transferred and linked to E2 through a thioester bond (Fig. 5)[103,104]. In the final step, E3 conjugates ubiquitin to a lysine residue of the target protein (Fig. 5)[103,104]. In humans, two E1s, around 50 E2s and more than 700 E3s exist[105]. The high number of E3s is required for the temporal and spatial regulation of ubiquitination of a plethora of different substrates. There are two main groups of E3 Ub ligases: E3 ligases containing the really interesting new gene (RING) and the homologous to E6-associated protein C-terminus (HECT) domains, respectively[106]. The RING family of E3 ligases function as adapters and bind

simultaneously to the substrate and E2[106]. In addition, E3 binding induces conformational changes in E2, thereby stimulating ubiquitin transfer to the target protein[107]. In contrast, HECT E3 ligases directly catalyze substrate conjugation in two steps. First, ubiquitin is transferred from E2 to HECT E3. In a second step, the E3-Ub thioester complex conjugates Ub to the target protein[106].

The biological function of mono- or polyubiquitination of substrates depends on the type of linkage between ubiquitin proteins within an ubiquitin chain and its length. Proteins can be conjugated with a single ubiquitin on one (monoubiquitin) or several lysine residues (multi-monoubiquitin) or with a polymeric chain of ubiquitin (polyubiquitin)[108]. Monoubiquitin plays a role in endocytosis of plasma membrane proteins, in protein sorting and subnuclear trafficking[109]. In contrast, significant complexity adds up in the case of polyubiquitin chains. Ubiquitin contains seven internal lysine residues (K6, K11, K27, K29, K33, K48 and K63) and a N-terminal methionine residue[108]. Each of these residues can contribute to linkage formation with the C-terminal glycine of another ubiquitin molecule[108]. Linkage assembly involving the N-terminal methionine and the C-terminal glycine results in linear polyubiquitin chains (Fig. 5)[110].

Whereas substrate specificity is mediated by E3 ligases, both E2 and E3 determine ubiquitin chain assembly linked through a specific lysine residue of ubiquitin. Although most E2s such as UbcH5 do not show preference for a specific lysine residue in ubiquitin chain assembly, some E2s control chain formation linked through a specific lysine[108,111,112]. For example, the E2s Ubc13 and Uev1a specifically synthesize K63-linked polyubiquitin chains[113].

Among the different linkage options, K63-linked and K48-linked polyubiquitin chains have been most extensively studied and both chain types are critically involved in NF-κB signaling. Proteins conjugated with K48-linked polyubiquitin chains are targeted for 26S proteosomal degradation (Fig.5)[103]. In contrast, K63-linked polyubiquitin chains participate in non-proteolytic functions including signal transduction, kinase activation, receptor endocytosis and DNA repair (Fig. 5)[114]. Additional chain types such as K11, K27 and K29-linked polyubiquitin chains may serve as degradation signals (Fig. 5)[115-119]. However, K11-linked polyubiquitin chains are also suggested to exert non-degradative functions during NF-κB activation (Fig. 5)[120]. Recently, linear polyubiquitination of signaling molecules has emerged as critical regulator of NF-κB signaling in inflammatory pathways[110,121]. Linear polyubiquitin chains are assembled

by an E3 ligase complex termed LUBAC (linear ubiquitin chain assembly complex), which consists of three components, HOIL-1L, HOIP and SHARPIN[110,121]. K63-linked and linear polyubiquitin chains are thought to influence signal transduction events by providing assembly platforms for protein complexes. These chains attached to proteins serve as docking anchors to which other proteins can bind via their ubiquitin-binding motifs.

Ubiquitination is a reversible process and is counterregulated by deubiquitinating enzymes (DUBs). The human genome encodes nearly 100 DUBs, which are subdivided into six families: ubiquitin-specific proteases (USPs), ubiquitin C-terminal hydrolases (USHs), ovarian tumor proteases (OTUs), Machado–Joseph disease protein domain proteases, JAB1/MPN/MOV34 metalloenzymes (JAMMs) and the recently discovered monocyte chemotactic protein-induced protein (MCPIP) family[122,123]. DUBs contribute to the regulation of ubiquitination by exerting three major functions: ubiquitin precursor processing, ubiquitin editing and ubiquitin deconjugation[122,123]. First, ubiquitin proteins are encoded in the genome at four loci. Two of them code for polyubiquitin precursors containing several Ubs in an exact head to tail array. These Ub precursors are processed by DUBs to generate free ubiquitin monomers. Second, some DUBs are involved in editing of polyubiquitin chains and thereby change the type of ubiquitin chain attached to a particular substrate. Third, DUBs deconjugate polyubiquitin chains from modified proteins, thereby blocking signal transduction or preventing proteosomal degradation. In parallel, DUBs rescue the removed ubiquitin from 26S proteosomal degradation and recycle it to the free ubiquitin pool. Thus, DUBs also play an important role in the maintenance of ubiquitin homeostasis[122,123].

Deubiquitination can occur in a linkage- or substrate-specific manner, coordinated by distinct ubiquitin-binding motifs. Ub chain type-specific DUBs hydrolyse polyubiquitin chains either from the ends (exo) or within a chain (endo)[122]. In contrast, substrate-specific DUBs cleave the entire polyubiquitin chain in a single step from its target protein[122].

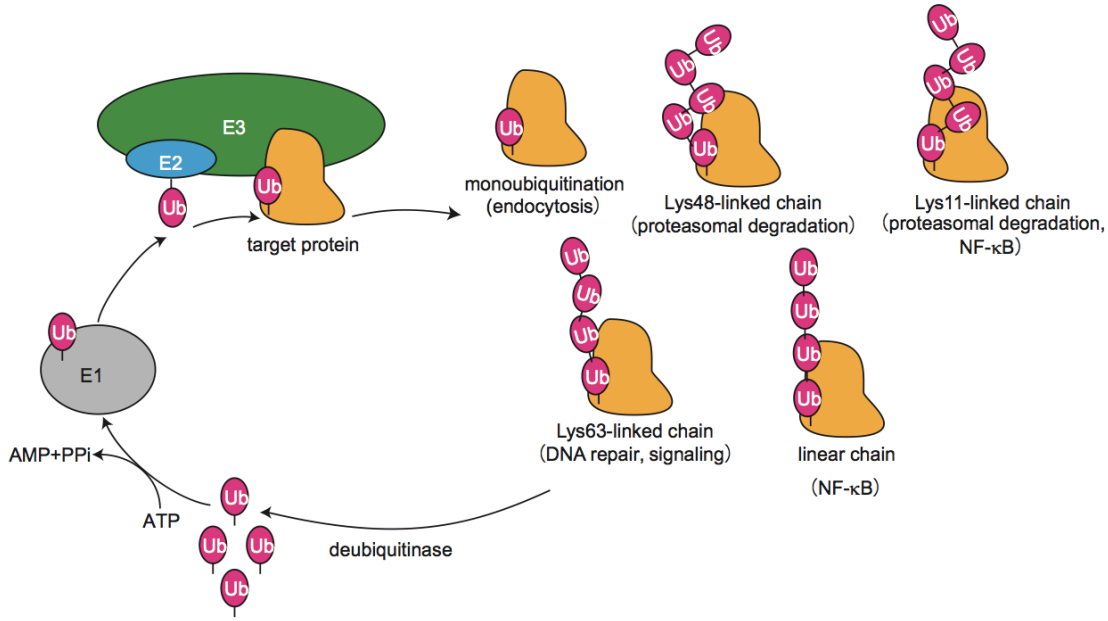

Figure 5: **The ubiquitin system and the cellular functions of diverse ubiquitin chain linkages.**
Ubiquitin conjugation of target proteins is orchestrated by E1 (ubiquitin-activating enzyme), E2 (ubiquitin-conjugating enzyme) and E3 (ubiquitin ligase). Depending on the linkage type and the number of conjugated ubiquitins, ubiquitination exerts different cellular functions (scheme from[124]).

3.2 The role of ubiquitination in NF-κB signal transduction pathways

NF-κB signal transduction pathways are highly regulated through ubiquitination of signaling molecules. In TNFR-mediated NF-κB signaling, TNF binding to its receptor initiates trimerization of the TNF receptor and recruitment of several signaling molecules including the adapter protein TRADD, the protein kinase RIP1 and the E3 ligases TRAF2 and cIAP1/2[67,125]. TRAF2 and cIAP1/2 catalyze K63-linked polyubiquitination of RIP1, which serves as a scaffold molecule to bring TAK1 via TAB2 and the IKK complex via NEMO into close proximity[67,125]. Ubiquitin-binding of TAB2 and NEMO allows proximity-mediated phosphorylation of IKK2 by TAK1[67,125]. Finally, the activated IKK complex phosphorylates IκBα, which induces its K48-linked polyubiquitination, resulting in proteosomal degradation of IκBα and release of NF-κB into the nucleus (Fig. 6)[67,125].

In a similar manner, K63-linked polyubiquitin chains play also a central role in IL-1 receptor/TLR-mediated NF-κB signaling. Upon TLR engagement, the adaptor molecule MyD88 is recruited to the receptor and further recruits the kinases IRAK1 and IRAK4[67,125]. IRAK1 induces TRAF6 K63-linked autoubiquitination involving the

E2 complex Ubc13/Uev1A[67,125]. Recently, it was suggested that TRAF6 and Ubc13/Uev1A also catalyze the formation of unanchored K63-linked polyubiquitin chains[126]. Both K63-polyubiquitin chains on TRAF6 as well as free K63-linked polyubiquitin chains can serve as a scaffold to recruit TAK1 via TAB2 and IKK via NEMO, thereby facilitating IKK2 phosphorylation by TAK1 (Fig. 6)[67,125].

Antigen receptor-mediated NF-κB signaling such as signaling through the B cell receptor is initiated through recruitment and activation of proximal tyrosine kinases such as Syk[127]. Following several cascade steps, the phospholipase PLCγ2 activates the protein kinase PKCβ, which phosphorylates the scaffold protein CARMA1 (CARD11)[127,128]. CARMA1 phosphorylation facilitates its association with Bcl-10 and the paracaspase MALT1 to form the CBM complex, which plays a critical role in IKK complex activation during both BCR and TCR-induced NF-κB signaling[67,127,128]. In T cells, the CBM complex activates IKK by recruiting TRAF6 and Ubc13/Uev1A[67]. TRAF6 K63-linked autoubiquitination further recruits TAK1 and IKK[67]. In contrast, it is not clear whether TRAF6 is also involved in IKK activation in B cells. However, it has been suggested that both TAK1 and IKK are recruited to CARMA1 through Bcl-10 and MALT1, thereby enabling IKK activation by TAK1 (Fig. 6)[127,128].

Ubiquitination events also control the activation of the alternative NF-κB signaling pathway downstream of BAFFR- or CD40-mediated signaling[125,129]. Under resting conditions, NIK is bound to TRAF3, which exist in a dimeric complex with TRAF2[129]. cIAP1 and cIAP2 are recruited to TRAF2 and constantly ubiquitinate NIK with K48-linked polyubiquitin chains to induce its proteosomal degradation[129]. Upon ligation by BAFF or CD40 ligand (CD40L), the complex consisting of TRAF2, TRAF3 and cIAP1/2 is recruited to the receptor[129]. Binding of the complex to BAFFR or CD40 stimulate the E3 ligase activity of TRAF2 and TRAF3, which add K63-linked polyubiquitin chains to cIAP1/2[129]. The addition of these chains alters the substrate specificity of cIAP1/2, and they now target TRAF3 and, to a lesser extent, TRAF2, for degradation via K48-linked polyubiquitination[130]. Proteosomal degradation of TRAF2 and TRAF3 finally allows NIK release, stabilization and autophosphorylation. Activated NIK phosphorylates IKK1, thereby enabling p100 processing to p52 and release of p52/RelB into the nucleus (Fig. 6)[125,129].

The role of additional polyubiquitin linkage types in the regulation of NF-κB signaling has been elucidated recently, adding further complexity to this process. In

particular, linear polyubiquitin chains emerged as critical regulator of canonical NF-κB signaling via the linear polyubiquitination of RIP1 and NEMO by the LUBAC complex (Fig. 6)[131,132]. Interestingly, NEMO recognizes ubiquitin through its ubiquitin-binding domain, termed UBAN domain and the binding affinity of this domain is 100-fold higher for linear than for K63-linked diubiquitin[133]. Therefore, it is hypothesized that both IKK complex binding via NEMO to linear ubiquitin chains on RIP1 as well as linear ubiquination of NEMO induce trans-autophosphorylation of IKK2[131,132]. The significance of linear ubiquitin chains in canonical NF-κB signaling manifests both in human genetics and mouse studies. Human mutations in the UBAN domain of NEMO are the cause for an inherited disease termed anhidrotic ectodermal dysplasia with immunodeficiency (EDA-ID)[134,135]. In addition, ablation of the LUBAC component SHARPIN in mice results in severe skin lesions, inflammation and defects in secondary lymphoid organs[136].

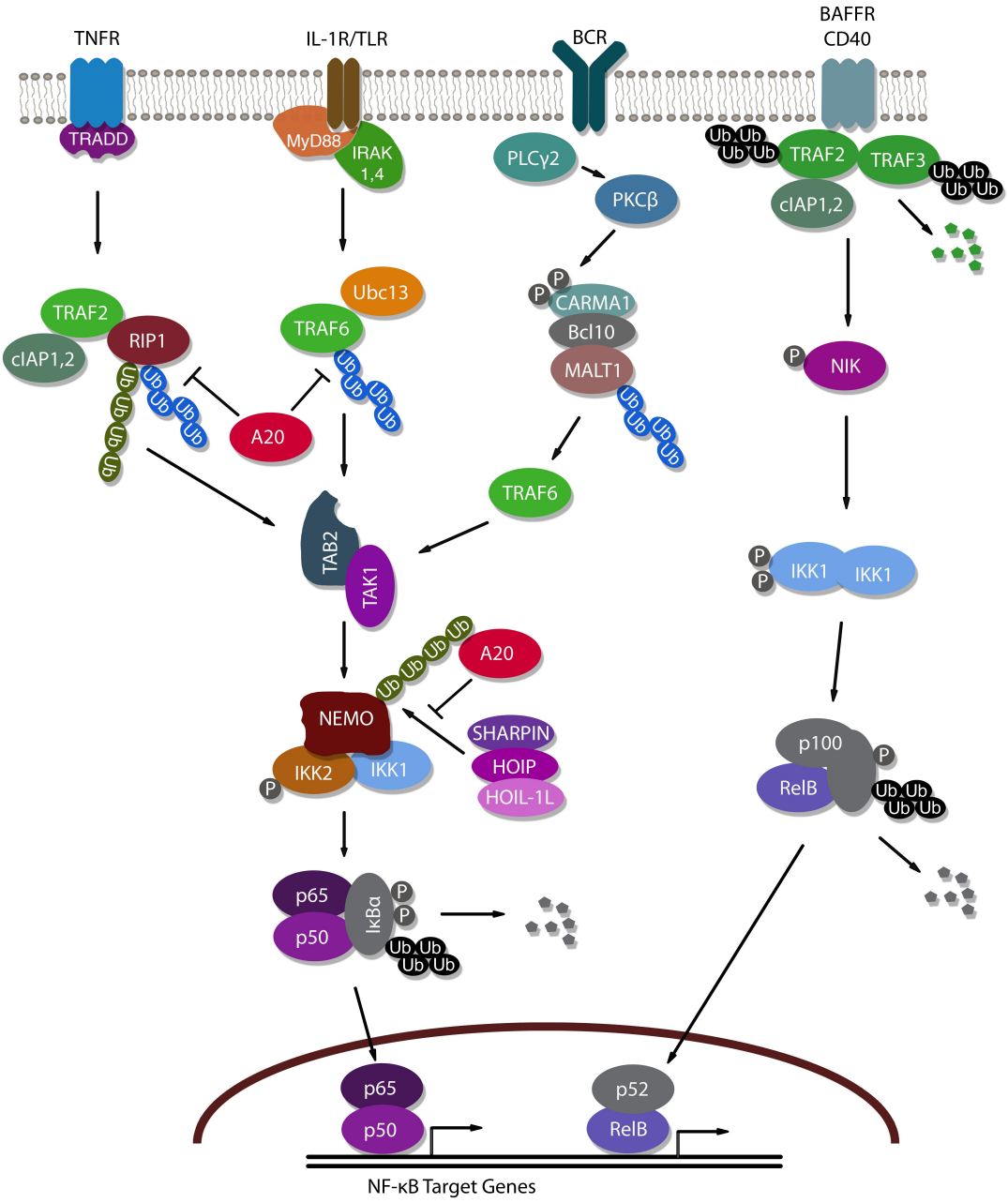

Figure 6: **A simplified scheme of the regulation of NF-κB signaling pathways through ubiquitylation.**
Upon receptor stimulation in canonical NF-κB pathways, proximal signaling events results in the non-proteolytic ubiquitination of signaling adaptor proteins including RIP1 and the family of TRAF E3 ligases. K63-linked (blue) or linear polyubiquitin chains (green) may serve as a scaffold for IKK activation by TAK1. In contrast, activation of the alternative NF-κB pathway requires cIAP1/2-mediated proteolytic K48-linked polyubiquitination (black) of TRAF2 and TRAF3, thereby allowing NIK stabilization and IKK1 activation.

4 A20, a central negative regulator of NF-κB activation

4.1 Cellular functions of the ubiquitin-editing enzyme A20

A20, also termed TNFα-induced protein 3 (TNFAIP3), is an inducible and cytoplasmic protein of 90 kDa, consisting of a N-terminal ovarian tumor (OTU) domain[137] and seven zinc finger (ZnF) motifs in the C-terminus (Fig. 7)[138]. A20 was proposed to act as an ubiquitin-editing enzyme with dual catalytic functions[139]. Due to its DUB function mediated by the OTU domain, A20 removes K63-linked polyubiquitin chains from specific substrates. In parallel, A20 can catalyze the conjugation of substrate proteins with K48-linked polyubiquitin chains. This E3 ligase function is mediated by its ZnF4 (Fig. 7)[140]. However, whether A20 directly or indirectly mediates these functions remains incompletely understood.

Via NF-κB sites in the A20 promoter, A20 expression is induced in a negative feedback loop by multiple inflammatory stimuli including TNFα, IL-1β, TLR ligands, NLR (nucleotide-binding oligomerization domain-like receptor) ligands and viral proteins such as human T lymphotropic virus (HTLV) 1 Tax and Epstein-Barr virus latent membrane protein 1 (LMP1)[141-145].

To date, four major cellular functions have been attributed to A20's ability to inhibit ubiquitin-dependent signal transduction: NF-κB-mediated inflammation; the antiviral response; programmed cell death and autophagy.

First, A20 functions as the key negative regulator of NF-κB activation in response to multiple NF-κB-activating stimuli (in detail under 4.2).

Second, A20 also controls TLR[146] and retinoic acid inducible gene 1 (RIG1)-mediated interferon signaling[147]. Antiviral type I interferons are essentially induced by two members of the interferon regulatory factor (IRF) family of transcription factors: IRF3 and IRF7. IRF3 activation requires the proximal adaptor TRIF- and TRAF3-mediated K63-linked polyubiquitination of the IKK-related kinases TBK1 and IKKε. These kinases then phosphorylate IRF3, thereby allowing IRF3 dimerization, nuclear translocation and binding to the IFNβ promoter[148]. Recently, it was reported that A20 and Tax1bp1 associate with TBK1/IKKε to block their K63-linked polyubiquitination, thereby terminating IRF3 signaling[149]. Interestingly, A20 does not require its DUB activity but rather its zinc finger motifs to disrupt K63-linked polyubiquitination of TBK1/IKKε[149]. In addition, A20 also negatively regulates IRF7-

mediated antiviral signaling. In contrast to IRF3 signaling, LMP1-induced IRF7 activation depends on TRAF6-mediated K63-linked polyubiquitination of IRF7, which is required for its phosphorylation[150]. A20 controls IRF7 activation by inhibiting TRAF6-dependent polyubiquitination of IRF7 through its DUB domain[151].

Third, in addition to its NF-κB and IRF3/IRF7 inhibitory functions, A20 blocks death receptor-mediated apoptosis[152,153]. Apoptotic cell death can be induced by the binding of members of the TNF superfamily to their cognate receptors such as Fas/CD95 or TNFR1[154]. Ligand binding triggers receptor trimerization and recruitment of the adaptor protein Fas-associated death domain protein (FADD) in Fas-mediated apoptosis and TRADD in TNFR1-induced cell death[154]. Subsequently, the initiator protease caspase 8 is recruited to the death receptor complex and activated through proximity-induced dimerization[154]. Activated caspase 8 cleaves and activates the downstream effector caspase 3 and 7, leading to apoptotic cell death[154]. Importantly, caspase 8 activation depends on Cullin 3 E3 ligase-mediated K63-linked polyubiquitination, which allows caspase 8 to interact with the ubiquitin-binding protein p62 (also known as sequestome-1)[155]. p62 further promotes caspase 8 aggregation and processing, leading to its full activation[155]. A20 prevents death receptor-induced apoptosis by blocking K63-linked polyubiquitination of caspase 8[155]. In the case of TNFα-induced signaling, recruitment of TRADD, TRAF2 and RIP1 to the TNFR1 can trigger both NF-κB-mediated survival and apoptotic cell death[154]. Normally, in the presence of pro-survival NF-κB signaling, apoptosis is repressed by NF-κB-induced anti-apoptotic proteins. In particular, the NF-κB target protein A20 disrupts the recruitment of TRADD and RIP1 to the receptor complex, thereby preventing cell death[156].

Fourth, A20 function is also involved in autophagy, a lysosome-dependent form of intracellular degradation, which plays a critical role in cellular processes such as starvation or immune responses against invading microbes[157]. In macrophages, autophagy can be triggered by LPS through TLR4 signaling[158,159]. TLR4 engagement recruits Beclin1, which is the mammalian homolog of yeast Atg6[160]. Beclin1 contributes to autophagosome formation, a process depending on TRAF6-mediated K63-linked polyubiquitination of Beclin1. To control TLR4-mediated autophagy, A20 counterregulates K63-linked polyubiquitination of Beclin1[161].

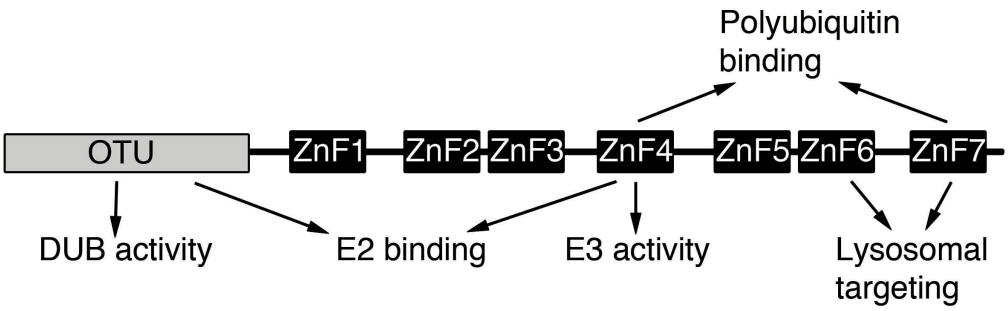

Figure 7: **Structural domains of A20 and theirs catalytic and non-catalytic functions.**
A20 consists of an ovarian tumor (OTU) domain and seven zinc finger motifs, mediating its ubiquitin-editing and non-catalytic functions.

4.2 Mechanisms of NF-κB inhibition by A20

Distinct molecular mechanisms have been put forward to explain the termination of NF-κB signaling by A20, which are both pathway- and most probably cell type-dependent. In particular, these different mechanisms largely rely on the dual ubiquitin-editing function of A20[139]. On the one hand, due to its DUB activity, which is mediated by its OTU domain, A20 removes K63-linked polyubiquitin chains from critical signaling molecules including RIP1, RIP2, TRAF6 and MALT1[139,143,162,163]. However, several studies have shown that *in vitro* the DUB domain of A20 does not have specificity for K63-linked polyubiquitin chains but hydrolyses K48-linked polyubiquitin chains[164-166]. Instead, A20 does not function as a processive DUB for K63-linked polyubiquitin chains but effectively cleaves entire K63-linked polyubiquitin chains from substrates such as TRAF6 (Fig. 6), thereby demonstrating specificity for particular polyubiquitinated subtrates[165]. The substrate specificity of A20 is most probably mediated through interaction with additional adaptor proteins. Indeed, Tax1-binding protein 1 (Tax1bp1) functions as an ubiquitin sensor and adaptor molecule to recruit A20 to K63-linked polyubiquitinated RIP1 and TRAF6[167,168]. In the absence of Tax1bp1, A20-mediated deubiquitination of RIP1 and TRAF6 and consequently inhibition of NF-κB activation is impaired[167,168].

On the other hand, A20 catalyzes the conjugation of K48-linked polyubiquitin chains onto RIP1 and the E2 enzymes Ubc13 and UbcH5c, resulting in the proteosomal degradation of RIP1, Ubc13 and UbcH5c[139,169]. This E3 ligase function of A20 is attributed to its ZnF4[140]. Similar to the substrate specificity for deubiquitination by A20, it was proposed that Tax1bp1, the E3 ligase Itch and the scaffold protein RNF11

are required for K48-linked polyubiquitination by A20[169-171]. Thus, together, they form a complex, termed A20 ubiquitin-editing complex.

Specifically in TNFR-mediated NF-κB signaling, A20 targets RIP1 in a sequential manner (Fig. 6). First, A20 is recruited via Tax1bp1 to K63-linked polyubiquitinated RIP1 and promotes RIP1 deubiquitination[139,167]. The deubiquitination then induces a conformational change of RIP1, thereby allowing K48-linked polyubiquitination of RIP1 by the A20 ubiquitin-editing complex followed by proteosomal degradation of RIP1[139,169]. In addition, A20 counteracts K63-linked polyubiquitination of RIP1 by inhibiting the E2-E3 complex formation between TRAF2, cIAP1/2 and Ubc13[169]. Disruption of E2-E3 association depends on ZnF4 and Cys103 in the OTU domain of A20[169]. Finally, the E2 enzyme Ubc13 is a target of K48-linked polyubiquination by the A20 ubiquitin-editing complex, resulting in complete termination of NF-κB signaling[169].

In a similar manner, A20 and Tax1bp1 deubiquitinate K63-linked polyubiquitinated TRAF6 during TLR-mediated NF-κB signaling (Fig. 6)[143,167]. However, A20 does not trigger TRAF6 proteosomal degradation, but disrupts TRAF6 binding to the E2 enzymes Ubc13 and UbcH5c[169]. Sequential proteosomal degradation of Ubc13 and UbcH5c, mediated by the A20 ubiquitin-editing complex, then effectively shuts down NF-κB signaling[169].

In contrast to other cell types, A20 is constitutively expressed in T cells, where A20 possibly functions both as a steady-state inhibitor and as a feedback regulator during T cell receptor (TCR)-mediated NF-κB signaling[172]. Similar to BCR-mediated NF-κB signaling, the CARMA1-Bcl10-MALT1 (CBM) complex plays a critical role during TCR-mediated NF-κB signaling. Upon CARMA1 phosphorylation, TRAF6 is recruited to the CBM complex to assemble K63-linked polyubiquitin chains onto MALT1 and Bcl10 (Fig. 6)[173-175]. Polyubiquitinated MALT1 functions as a scaffold molecule to bring the IKK complex and TAK1 into close proximity, thereby allowing IKK2 phosphorylation by TAK1[174]. A20, whose expression is enhanced upon TCR signaling, inhibits the scaffold function of MALT1 by removing K63-linked polyubiquitin chains from MALT1 in a negative feedback loop[163]. Interestingly, MALT1 does not only serve as a scaffold, but acts also as a paracaspase to cleave human A20 protein between its ZnF1 and ZnF2[176,177]. Proteolytic cleavage of A20 is required to allow optimal TCR-mediated NF-κB signaling. This suggests that the signal strength of TCR-mediated NF-κB activation is modulated by the opposing

mechanisms of induced expression of A20 and its cleavage by MALT1.

Due to the high similarity between TCR- and BCR-induced signal transduction mechanisms it is conceivable that A20 may also regulate BCR-mediated NF-κB signaling in this fashion.

Besides its ubiquitin-editing function, A20 can inhibit NF-κB signaling also through non-catalytic mechanisms. First, it was reported that A20 targets TRAF2 for lysosomal degradation, a mechanism that is mediated by ZnF6 and ZnF7[178]. Second, recently, it was shown that unanchored K63-linked polyubiquitin chains mediate A20 interaction with NEMO through its ZnF4 and ZnF7[179]. Therefore, A20 hinders structurally the formation of the IKK and TAK1 kinase complex and prevents IKK2 phosphorylation by TAK1[179]. Third, two recent studies demonstrated that *in vitro* A20 ZnF7 preferentially binds linear polyubiquitin chains[226,227], synthesized by the E3 ligase complex LUBAC. Thus, the A20 ZnF7 motif represents a novel linear ubiquitin-binding domain (LUBID)[226]. Upon stimulation with TNFα, A20 interacts with LUBAC and NEMO through linear polyubiquitin binding (Fig. 6)[226,227]. This interaction disrupts LUBAC binding to NEMO, thereby inhibiting TNF-induced NF-κB activation (Fig. 6)[226,227]. Interestingly, crystallization of A20 ZnF7 with linear diubiquitin identified the critical residues for the linear polyubiquitin interaction[227] and these residues were found mutated in human primary mediastinal B cell lymphoma[190]. Additional studies revealed that A20 containing these mutations in ZnF7 failed to bind linear di- and tetraubiquitin and was impaired in preventing LUBAC-mediated NF-κB activation[227].

4.3 CYLD: tumor suppressor and negative regulator of NF-κB signaling

In addition to A20, NF-κB signaling is also controlled by other DUBs such as CYLD, Cezanne and USP21[180-184]. In particular, several studies demonstrated that CYLD negatively regulates NF-κB signaling via its K63-linkage-specific DUB activity. CYLD, encoded by the cylindromatosis (*CYLD*) gene, is a 107 kDa ubiquitously expressed deubiquitinase of the USP family[185]. Originally, CYLD was identified as a tumor suppressor gene and mutations in this gene predispose patients to the development of benign tumors of hair follicle keratinocytes[186]. In mice, CYLD-deficiency causes the development of TPA-induced skin papillomas due to increased

tumor cell proliferation[187]. CYLD interacts with Bcl-3 and hydrolyses K63-linked polyubiquitin chains from Bcl-3 in TPA- or UV-treated keratinocytes[187]. Deubiquitination of Bcl-3 by CYLD prevents its nuclear translocation, where it interacts with p50 or p52 to drive the expression of cyclin D1[187]. Beside its critical role in cylindromatosis, CYLD also functions as a tumor suppressor in several other tumor types such as melanoma, lung cancer, prostate cancer, renal carcinoma and multiple myeloma[188,189].

Interestingly, over 60% of EBV-negative classical Hodgkin lymphoma (HL) cases contain mono- or bi-allelic losses of A20 function and 35% of classical HL cases display decreased CYLD copy numbers[190]. Strikingly, the HL cell line KM-H2 has completely lost both A20 and CYLD expression due to bi-allelic mutations in both genes[190], suggesting potential overlapping functions of both DUBs. Indeed, A20 and CYLD target the same set of signaling factors such as TRAF2, TRAF6, RIP1 and NEMO during the regulation of NF-κB signaling[191]. However, a key difference between A20 and CYLD is the specificity of CYLD to function as a processive DUB for K63-linked polyubiquitin chains[192], whereas A20 solely acts as a substrate-specific DUB for K63-linked polyubiquitin chains[165].

4.4 Physiological functions of A20

The NF-κB inhibitory and anti-apoptotic function of A20 was confirmed *in vivo* by the generation of constitutive A20-deficient mice. $A20^{-/-}$ mice display premature lethality due to severe multi-organ inflammation, tissue damage and cachexia[193]. In addition, $A20^{-/-}$ mice are hypersensitive to sublethal doses of TNFα and LPS[193]. In line with these data, A20-deficient thymocytes and murine embryonic fibroblasts (MEFs) are sensitized to TNF-mediated cell death[193]. Furthermore, A20-deficient MEFs show prolonged TNFα- and IL1β-mediated NF-κB signaling[193]. Subsequent studies revealed that the multi-organ inflammation is not mediated by lymphocytes[193] but myeloid cells and also occurs in a TNFR-independent manner[143]. However, disruption of TLR signals by ablation of the essential adaptor MyD88 rescued the spontaneous inflammation in A20/MyD88 double-deficient mice[194]. Similarly, the systemic inflammation and cachexia of A20-deficient mice were rescued by the eradication of commensal intestinal bacteria through treatment with broad-spectrum

antibiotics[194]. Thus, the spontaneous inflammation in A20-deficient mice is driven by myeloid cells exhibiting uncontrolled TLR-mediated NF-κB signaling in response to commensal flora.

4.5 Association of A20 with human diseases

Notably, the role of A20 as the central negative regulator of NF-κB activation is also reflected in the genetics of human diseases. Over the last few years, A20 has been strongly associated with both human inflammatory diseases and tumorigenesis.

4.5.1 Association of A20 polymorphisms with human autoimmune diseases

Genome-wide association studies (GWAS) and next-generation sequencing have provided valuable insights into the role of A20 polymorphisms in several human autoimmune diseases including systemic lupus erythematosus (SLE)[195-198], rheumatoid arthritis (RA)[197,199,200], psoriasis[197,201], coelic disease[202,203], Crohn's disease[197], multiple sclerosis[204], Sjögren's syndrome[197,205] and type 1 diabetes[206] (Table 1).

Most of the disease-related A20 single nucleotide polymorphisms (SNPs) are located outside of the A20 gene locus or in intronic sequences (summarized in [207]). However, human A20 is encoded by nine exons and two non-synonymous SNPs in exon 3 of the OTU domain functionally affect the DUB domain of A20: rs5029941/A125V and rs2230926/F127C[196,208]. Structural predictions using computer models suggest that SNP rs5029941/A125V may affect the conformation and thereby the catalytic activity of the DUB domain, whereas SNP rs2230926/F127C may influence the binding to A20 target proteins[208]. In addition, functional studies revealed that SNP rs5029941/A125V impairs A20-mediated deubiquitination[208], whereas the coding variant rs2230926/F127C causes reduced inhibition of TNF-mediated NF-κB activation[196]. Notably, SNP rs2230926/F127C, originally associated with SLE, was also identified as a genetic risk variant for Sjögren's syndrome, Crohn's disease, psoriasis and RA[197]. A recent sequencing effort to characterize A20 polymorphisms in the coding region identified in total 7 novel non-synonymous variants in exon 2, 3, 7, 8 and 9[197]. It is conceivable that these coding variants may cause reduced expression

or activity of A20 in the negative regulation of NF-κB activation.

Furthermore, a novel dinucleotide variant (TT>A) in the conserved regulatory region, 42kb downstream of the A20 promoter, was associated with SLE. This polymorphic dinucleotide reduced A20 mRNA and protein expression, possibly through altering NF-κB DNA binding to the A20 promoter[198].

Human autoimmune disease	Functionally impaired genetic variants of A20
Crohn's disease[197]	rs2230926/F127C
Coeliac disease[202,203]	
Multiple sclerosis[204]	
Rheumatoid arthritis[197,199,200]	rs2230926/F127C
Sjögren's syndrome[197,205]	rs2230926/F127C
Systemic lupus erythematosus[195-198]	rs5029941/A125V rs2230926/F127C Polymorphic dinucleotide/TT>A
Type 1 diabetes[206]	
Psoriasis[197,201]	rs2230926/F127C

Table 1: **Association of the A20 genomic locus with human autoimmune diseases**

4.5.2 Loss of A20 function in human lymphomas

Constitutive activation of NF-κB can promote proliferation and survival. Therefore, aberrant NF-κB activation is a hallmark of several human B cell lymphoma subtypes such as classical Hodgkin's lymphoma (cHL), diffuse large B cell lymphoma (DLBCL) and marginal zone lymphomas of mucosa-associated lymphoid tissue (MALT lymphoma)[209,210]. Over the last few years, genetic inactivation of A20 has been strongly associated with several human B cell lymphomas (in total about 40%) including cHL[190,211], DLBCL[211-213], follicular lymphoma (FL)[211], lymphoplasmacytic lymphoma[214], mantle cell lymphoma (MCL)[211,213], marginal zone B cell lymphoma (MZL)[211,213,215-220], primary mediastinal lymphoma (PMBL)[190] and Waldenström Macroglobulinemia (WM)[221] (see Table 2). Notably, A20 is the most commonly affected gene in DLBCL of the ABC subtype and lymphoplasmacytic lymphoma[212,214]. These findings indicate that A20 plays a role as a tumor suppressor in human B cell lymphoma.

In particular, A20 is inactivated by chromosomal deletion, promoter methylation and

mutations such as frame shift deletions/insertions or nonsense mutations, resulting in truncated A20 proteins that are functionally impaired or instable[211,212]. In line with these findings, reconstitution of wild-type but not mutant A20 in A20-deficient lymphoma cell lines induced apoptosis, growth arrest and suppressed NF-κB activation[190,211,213].

However, it remains controversial whether A20 acts as a classical tumor suppressor according to the Knudson's two-hit hypothesis[222]. Notably, besides homozygous loss of A20, mono-allelic inactivation was observed in a substantial proportion of ABC DLBCL patients (46% according to[213]; 23% according to[212]). These findings may suggest rather a haploinsufficient model of tumor suppression. In contrast, homozygous inactivation of A20 may be associated with a shorter survival rate in MALT lymphoma[217].

Recently, the role of A20 in tumor suppression was extended to Sézary syndrome (SS), a disseminated variant of primar cutaneous T cell lymphoma[223]. Mono- and bi-allelic deletions of A20 were found in 46% (6/13) of blood samples in SS-patients[223]. In addition, reconstitution of A20 in a SS cell line lacking A20 on both alleles suppresses cell proliferation[223].

Interestingly, the role of A20 in tumor suppression may be cell type-specific. In solid, non-lymphoid tumors, A20 is overexpressed in human breast carcinoma and glioma where A20 may function as an oncogene due to its anti-apoptotic function in these cell types[224,225].

Human B cell lymphoma	Frequency of A20 inactivation
Classical Hodgkin's lymphoma (cHL)[190,211]	33-44%
Diffuse large B cell lymphoma (DLBCL)[211-213]	38%
Follicular lymphoma (FL)[211]	26%
Lymphoplasmacytic lymphoma (w/o WM)[214]	46%
Mantle cell lymphoma (MCL)[211,213]	31%
Marginal zone B cell lymphoma (MZL)[211,213,215-220]	20%
Primary mediastinal B cell lymphoma (PMBL)[190]	36%
Waldenström Macroglobulinemia (WM)[221]	38%

Table 2: **Association of A20 with human B cell lymphoma**

Aim of the thesis

Over the last years, polymorphisms in the *TNFAIP3* gene locus, encoding the ubiquitin-editing enzyme A20, has been strongly associated with several human autoimmune diseases such as systemic lupus erythematosus, rheumatoid arthritis and Crohn's disease. In addition, loss of A20 function is a frequent event in human B cell lymphomas. Initial mouse studies revealed A20 as the central negative regulator of NF-κB signaling and NF-κB-mediated inflammation *in vivo*. However, the precise role of A20 in different cell types and its contribution to human autoimmune diseases was not known. In particular, given the critical role of B cells in autoimmune pathology and the strong implication of A20 inactivation in human B cell lymphomas, the role of A20 in B cells and in the prevention of B cell-mediated diseases awaited urgent clarification. In addition to A20, NF-κB activation is also controlled by other deubiquitinases such as CYLD. It is remarkable that A20 and CYLD share similar mechanisms and molecular targets in the negative regulation of NF-κB signaling, suggesting potential overlapping functions.
Therefore, we employed mouse genetics to address the following critical questions:

1. the role of A20 in B cell development, B cell immune responses and the prevention of autoimmunity (**Paper II**),
2. potential overlapping physiological functions of A20 and CYLD in B cell development and function (**Paper IV**),
3. the role of A20 in intestinal epithelial cells and its contribution to intestinal inflammation (**Paper I**),
4. the role of A20 in myeloid cells and its contribution to autoimmunity (**Paper III**).

Brief summaries of the publications

Paper I:

Vereecke et *al*., 2010. Enterocyte-specific A20 deficiency sensitizes to tumor necrosis factor-induced toxicity and experimental colitis. *Journal of Experimental Medicine* 207: 1513–1523.

Inflammatory bowel disease (IBD) encompasses a group of chronic inflammatory conditions of the gastrointestinal tract, such as Crohn's disease. IBD is thought to result from a dysregulated immune response directed against the commensal flora, leading to breakdown of the intestinal epithelial barrier. Recently, polymorphisms in the A20 gene locus have been associated with Crohn's disease. In line with human genetics, A20-deficient mice die prematurely due to severe inflammation in multiple organs including the intestine. A20, whose expression is regulated by NF-κB transcription factors, has been established as the key negative regulator of signaling leading to NF-κB activation. In parallel, A20 acts as an anti-apoptotic protein by preventing TNF-induced apoptosis. In contrast to many other cell types, NF-κB plays an anti-inflammatory role in intestinal epithelial cells (IECs). Since A20 blocks both TNF-induced apoptosis and NF-κB activation, it was not clear whether A20 deficiency in IECs would exacerbate or ameliorate intestinal inflammation. Therefore, to study whether A20 contribute to IBD, mice lacking A20 specifically in IECs were generated and evaluated in a model of dextran sodium sulphate (DSS)-induced colitis. A20 deficiency in IECs increased the susceptibility of mice to DSS-induced colitis and prevented the recovery from acute DSS-induced inflammation. In addition, mice lacking A20 in IECs are sensitized to TNF-induced apoptosis of A20-deficient IECs, leading to disruption of the intestinal epithelial barrier and infiltration of commensal bacteria that trigger a systemic inflammatory response. Taken together, A20 acts as a critical anti-apoptotic protein in the intestinal epithelium, thereby mediating the protective effect of NF-κB in intestinal epithelial cells. Thus, defects in A20 expression might contribute to inflammatory bowel disease in humans.

I contributed to this study by generating the antibody specifically recognizing mouse A20 protein. I also established the staining protocol to detect A20 protein by immunoblotting. In addition, I generated murine embryonic fibroblasts (MEFs) harboring conditional A20 alleles and A20-deficient MEFs by Cre protein transduction.

Paper II:

Chu et *al*., 2011. B cells lacking the tumor suppressor TNFAIP3/A20 display impaired differentiation and hyperactivation and cause inflammation and autoimmunity in aged mice. *Blood* 117: 2227–2236.

B cell homeostasis depends on B cell receptor (BCR) and BAFF receptor signaling during development and maintenance resulting in the activation of transcription factors such as NF-κB. The ubiquitin-editing enzyme A20 is essential to prevent prolonged NF-κB activation in response to different stimuli by controlling the ubiquitylation status of key signaling molecules such as TRAF6. Polymorphisms and mutations in the *A20* gene are linked to various human autoimmune conditions including type 1 diabetes, systemic lupus erythematosus, coeliac disease, Crohn's disease, psoriasis, multiple sclerosis and rheumatoid arthritis. Moreover, inactivation of A20 is a frequent event in human B cell lymphomas characterized by constitutive NF-κB activity. Therefore, we generated B cell-specific A20-deficient mice to study the role of A20 in B cell development and function and its contribution to prevent B cell-mediated autoimmunity. A20-deficient B cells accumulate during the transitional stage and show impaired development, function and/or localization of mature B cell subsets including marginal zone B cells, peritoneal B1 cells and bone marrow recirculating B cells. Moreover, loss of A20 in B cells lowers their activation threshold and enhances proliferation and survival in a gene-dose-dependent manner. The hyper-reactivity of A20-deficient B cells is also reflected in the enhanced formation of spontaneous germinal center in the gut-associated lymphoid tissue (GALT). Through the expression of pro-inflammatory cytokines, most notably IL-6, A20-deficient B cells trigger a progressive inflammatory reaction in naïve mice characterized by the expansion of myeloid cells, effector-type T and regulatory T cells. The chronic inflammation culminates in aged mice in an autoimmune syndrome defined by splenomegaly, plasma cell hyperplasia and the presence of class-switched, tissue-specific autoantibodies. Taken together, A20 is required for B cell homeostasis and to prevent B cell-mediated chronic inflammation and autoimmunity.

In this study, I performed the majority of the experiments and coordinated the work flow of all experiments. I received help from Christoph Vahl with T and myeloid cell analysis, Dilip Kumar with RT-PCR, Klaus Heger with IL-6 ELISA and Western blotting, Arianna Bertossi with cell cycle analysis, Miriam Reutelshöfer with kidney

and liver pathology and Brigitte Mack with immunohistochemical staining of the splenic marginal zone. Moreover, I wrote the paper.

Paper III:

Matmati et *al*., 2011. A20 (TNFAIP3) deficiency in myeloid cells triggers erosive polyarthritis resembling rheumatoid arthritis. *Nature Genetics* 43: 908–912.

Rheumatoid arthritis is an inflammatory autoimmune disease, which is characterized by chronic inflammation of the joints and progressive destruction of cartilage and bone. Increased NF-κB activation plays a key role in many autoimmune diseases including rheumatoid arthritis. Recently, polymorphisms in the *A20* gene were associated with several human autoimmune diseases such as systemic lupus erythematosus, coeliac disease, psoriasis and rheumatoid arthritis. A20 is involved in the negative feedback control of NF-κB signaling in response to multiple stimuli. In mice, constitutive A20 deficiency results in lethal multi-organ inflammation, which is driven by myeloid cells exhibiting uncontrolled TLR-mediated NF-κB signaling in response to commensal flora. Therefore, to address the myeloid cell-specific role of A20 in the etiology of autoimmune diseases, myeloid cell-specific A20-deficient mice were generated. Remarkably, A20 deficiency in myeloid cells results in spontaneous development of severe destructive polyarthritis with many hallmarks of human rheumatoid arthritis. Moreover, myeloid cell-specific A20-deficient mice have high levels of pro-inflammatory cytokines including TNF, IL-1β and IL-6 systemically and in local joint tissue. Although TNF plays a dominant role in the pathogenesis of rheumatoid arthritis, the polyarthritis in myeloid cell-specific A20-deficient mice does not depend on TNF, but is mediated by signaling via the TLR4/MyD88 axis and IL-6. In addition, systemic bone loss due to increased osteoclast differentiation is another feature of experimental and rheumatoid arthritis. In fact, A20 deficiency in myeloid cells is also associated with enhanced osteoclastogenesis, possibly driving the severe osteoporosis observed in these mice. In conclusion, these data support a critical, myeloid-specific role of A20 in the pathogenesis of rheumatoid arthritis.

I contributed to this study by demonstrating that A20 deficiency in B cells does not cause arthritis in mice and by generating control samples for Southern blotting.

Paper IV:

Chu et *al*., 2012. A20 and CYLD do not share significant overlapping functions during B cell development and activation. *Journal of Immunology.* Epub 2012 Sep 21.

The deubiquitinases A20 and CYLD are critical negative regulators of signaling events leading to the activation of NF-κB transcription factors. They share similar mechanisms by removing non-degradative K63-linked polyubiquitin chains from an overlapping set of substrates. In B cells, A20 deficiency results in hyperactivity, loss of immune homeostasis, inflammation, and autoimmunity. In contrast, the reported consequences of CYLD deficiency are controversial, ranging from an absence of effects to dramatic B cell hyperplasia. These differences could be due to varying compensation by A20. The aim of this study is to address potential overlapping physiological functions between A20 and CYLD in B cells. Therefore, we generated and characterized A20/CYLD double-deficient B cells. Interestingly, the combined loss of A20 and CYLD did not exacerbate the developmental defects and hyperresponsive activity of A20-deficient B cells. In addition, the extent of B cell activation after *in vitro* stimulation with anti-CD40, LPS, and CpG was comparable in B cells lacking A20/CYLD and A20 alone. However, in response to BCR cross-linking-induced proliferation, IL-6 production and NF-κB activation, we observed small but reproducible additive effects of the lack of A20 and CYLD. In conclusion, the lack of phenotypic effects in CYLD-deficient B cells is not due to compensation by A20. Therefore A20 and CYLD do not share significant functions during B cell development and activation.

In this study, I performed all *in vivo* and *in vitro* experiments, except for the CFSE labeling assay and the electrophoretic mobility shift assay, where I received help from Valeria Soberon and Laura Glockner. In addition, I analyzed all data presented in this study and wrote the paper.

Curriculum Vitae

Personal Details

Name	Yuanyuan Chu
Nationality	German
Date and place of birth	16.07.1982, Xian, China

Publications

Chu Y, Soberon V, Glockner L, Beyaert R, Massoumi R, van Loo G, Krappmann D and Schmidt-Supprian M, 2012. A20 and CYLD do not share significant overlapping functions during B cell dvelopment and activation. J Imm. Epub 2012 Sep 21.

Matmati M, Jacques P, Maelfait J, Verheugen E, Kool M, Sze M, Geboes L, Louagie E, Guire CM, Vereecke L, **Chu Y**, Boon L, Staelens S, Matthys P, Lambrecht BN, Schmidt-Supprian M, Pasparakis M, Elewaut D, Beyaert R, van Loo G, 2011. A20 (TNFAIP3) deficiency in myeloid cells triggers erosive polyarthritis resembling rheumatoid arthritis. Nat Genet 43: 908-912.

Chu Y, Vahl C, Kumar D, Heger K, Bertossi A, Wójtowicz E, Soberon V, Schenten D, Mack B, Reutelshöfer M, Beyaert R, Amann K, Van Loo G and Schmidt-Supprian M, 2011. B cells lacking the tumor suppressor TNFAIP3/A20 display impaired differentiation and hyperactivation and cause inflammation and autoimmunity in aged mice. Blood. 117(7): 2227-36. Epub 2010 Nov 18.

Vereecke, L, Sze M, MacGuire C, Rogiers B, **Chu Y**, Schmidt-Supprian M, Pasparakis M, Beyaert R and Van Loo G, 2010. Enterocyte-specific A20 deficiency sensitizes to tumor necrosis factor-induced toxicity and experimental colitis. J Exp Med 207(7): 1513-23.

Chu Y, Senghaas N, Koester RW, Wurst W, Kuehn R, 2008. Novel caspase-suicide proteins for tamoxifen-inducible apoptosis. Genesis. 46(10): 530-6.

References

1. Orkin, S. H. & Zon, L. I. Hematopoiesis: an evolving paradigm for stem cell biology. *Cell* **132**, 631–644 (2008).
2. Kondo, M. *et al.* Biology of hematopoietic stem cells and progenitors: implications for clinical application. *Annu Rev Immunol* **21**, 759–806 (2003).
3. Weissman, I. L. & Shizuru, J. A. The origins of the identification and isolation of hematopoietic stem cells, and their capability to induce donor-specific transplantation tolerance and treat autoimmune diseases. *Blood* **112**, 3543–3553 (2008).
4. Galli, S. J., Borregaard, N. & Wynn, T. A. Phenotypic and functional plasticity of cells of innate immunity: macrophages, mast cells and neutrophils. *Nat Immunol* **12**, 1035–1044 (2011).
5. Villadangos, J. A. & Schnorrer, P. Intrinsic and cooperative antigen-presenting functions of dendritic-cell subsets in vivo. *Nat Rev Immunol* **7**, 543–555 (2007).
6. Tonegawa, S. Somatic generation of antibody diversity. *Nature* **302**, 575–581 (1983).
7. Alt, F. W. *et al.* VDJ recombination. *Immunology today* **13**, 306 (1992).
8. Hardy, R. R. & Hayakawa, K. B cell development pathways. *Annu Rev Immunol* **19**, 595–621 (2001).
9. Nemazee, D. Receptor editing in lymphocyte development and central tolerance. *Nat Rev Immunol* **6**, 728–740 (2006).
10. Allman, D. & Pillai, S. Peripheral B cell subsets. *Curr Opin Immunol* **20**, 149–157 (2008).
11. Merrell, K. T. *et al.* Identification of Anergic B Cells within a Wild-Type Repertoire. *Immunity* **25**, 953–962 (2006).
12. Basten, A. & Silveira, P. A. B-cell tolerance: mechanisms and implications. *Curr Opin Immunol* **22**, 566–574 (2010).
13. Cariappa, A., Chase, C., Liu, H., Russell, P. & Pillai, S. Naive recirculating B cells mature simultaneously in the spleen and bone marrow. *Blood* **109**, 2339–2345 (2007).
14. Pillai, S. & Cariappa, A. The follicular versus marginal zone B lymphocyte cell fate decision. *Nat Rev Immunol* **9**, 767–777 (2009).
15. Pillai, S., Cariappa, A. & Moran, S. T. Marginal zone B cells. *Annu Rev Immunol* **23**, 161–196 (2005).
16. Cinamon, G., Zachariah, M. A., Lam, O. M., Foss, F. W. & Cyster, J. G. Follicular shuttling of marginal zone B cells facilitates antigen transport. *Nat Immunol* **9**, 54–62 (2008).
17. Baumgarth, N. The double life of a B-1 cell: self-reactivity selects for protective effector functions. *Nat Rev Immunol* **11**, 34–46 (2011).
18. Montecino-Rodriguez, E., Leathers, H. & Dorshkind, K. Identification of a B-1 B cell–specified progenitor. *Nat Immunol* **7**, 293–301 (2006).
19. MacLennan, I. C. & Gray, D. Antigen-driven selection of virgin and memory B cells. *Immunol Rev* **91**, 61–85 (1986).
20. Maclennan, I. C. M. *et al.* Extrafollicular antibody responses. *Immunol Rev* **194**, 8–18 (2003).

21. Vinuesa, C. G., Sanz, I. & Cook, M. C. Dysregulation of germinal centres in autoimmune disease. *Nat Rev Immunol* **9**, 845–857 (2009).
22. MacLennan, I. C. M. Germinal centers. *Annu Rev Immunol* **12**, 117–139 (1994).
23. Victora, G. D. & Nussenzweig, M. C. Germinal Centers. *Annu Rev Immunol* **30**, 429–457 (2012).
24. Allen, C. D. C., Okada, T. & Cyster, J. G. Germinal-center organization and cellular dynamics. *Immunity* **27**, 190–202 (2007).
25. Muramatsu, M. *et al.* Class switch recombination and hypermutation require activation-induced cytidine deaminase (AID), a potential RNA editing enzyme. *Cell* **102**, 553–563 (2000).
26. Rogozin, I. B., Pavlov, Y. I., Bebenek, K., Matsuda, T. & Kunkel, T. A. Somatic mutation hotspots correlate with DNA polymerase eta error spectrum. *Nat Immunol* **2**, 530–536 (2001).
27. Zeng, X. *et al.* DNA polymerase eta is an A-T mutator in somatic hypermutation of immunoglobulin variable genes. *Nat Immunol* **2**, 537–541 (2001).
28. Vinuesa, C. G., Linterman, M. A., Goodnow, C. C. & Randall, K. L. T cells and follicular dendritic cells in germinal center B-cell formation and selection. *Immunol Rev* **237**, 72–89 (2010).
29. Victora, G. D. *et al.* Germinal Center Dynamics Revealed by Multiphoton Microscopy with a Photoactivatable Fluorescent Reporter. *Cell* **143**, 592–605 (2010).
30. Kepler, T. B. & Perelson, A. S. Cyclic re-entry of germinal center B cells and the efficiency of affinity maturation. *Immunology today* **14**, 412–415 (1993).
31. Calame, K. L. Plasma cells: finding new light at the end of B cell development. *Nat Immunol* **2**, 1103–1108 (2001).
32. McHeyzer-Williams, L. J. & McHeyzer-Williams, M. G. Antigen-specific memory B cell development. *Annu Rev Immunol* **23**, 487–513 (2005).
33. Gatto, D., Paus, D., Basten, A., Mackay, C. R. & Brink, R. Guidance of B cells by the orphan G protein-coupled receptor EBI2 shapes humoral immune responses. *Immunity* **31**, 259–269 (2009).
34. Pereira, J. P., Kelly, L. M., Xu, Y. & Cyster, J. G. EBI2 mediates B cell segregation between the outer and centre follicle. *Nature* **460**, 1122–1126 (2009).
35. Green, J. A. *et al.* The sphingosine 1-phosphate receptor $S1P_2$ maintains the homeostasis of germinal center B cells and promotes niche confinement. *Nat Immunol* **12**, 672–680 (2011).
36. Allen, C. D. C. *et al.* Germinal center dark and light zone organization is mediated by CXCR4 and CXCR5. *Nat Immunol* **5**, 943–952 (2004).
37. Cyster, J. G. Homing of antibody secreting cells. *Immunol Rev* **194**, 48–60 (2003).
38. Maruyama, M., Lam, K. P. & Rajewsky, K. Memory B-cell persistence is independent of persisting immunizing antigen. *Nature* **407**, 636–642 (2000).
39. Zenewicz, L. A., Abraham, C., Flavell, R. A. & Cho, J. H. Unraveling the Genetics of Autoimmunity. *Cell* **140**, 791–797 (2010).
40. Manolio, T. A. *et al.* Finding the missing heritability of complex diseases.

Nature **461**, 747–753 (2009).
41. Lipsky, P. E. Systemic lupus erythematosus: an autoimmune disease of B cell hyperactivity. *Nat Immunol* **2**, 764–766 (2001).
42. Gürcan, H. M. *et al.* A review of the current use of rituximab in autoimmune diseases. *International Immunopharmacology* **9**, 10–25 (2009).
43. Yanaba, K. *et al.* B-lymphocyte contributions to human autoimmune disease. *Immunol Rev* **223**, 284–299 (2008).
44. Townsend, M. J., Monroe, J. G. & Chan, A. C. B-cell targeted therapies in human autoimmune diseases: an updated perspective. *Immunol Rev* **237**, 264–283 (2010).
45. Shoenfeld, Y. & Toubi, E. Protective autoantibodies: Role in homeostasis, clinical importance, and therapeutic potential. *Arthritis Rheum* **52**, 2599–2606 (2005).
46. Barr, T. A. *et al.* B cell depletion therapy ameliorates autoimmune disease through ablation of IL-6-producing B cells. *J Exp Med* **209**, 1001–1010 (2012).
47. Strasser, A. *et al.* Enforced BCL2 expression in B-lymphoid cells prolongs antibody responses and elicits autoimmune disease. *Proc Natl Acad Sci USA* **88**, 8661–8665 (1991).
48. Hao, Z. *et al.* Fas receptor expression in germinal-center B cells is essential for T and B lymphocyte homeostasis. *Immunity* **29**, 615–627 (2008).
49. Mackay, F. & Browning, J. L. BAFF: a fundamental survival factor for B cells. *Nat Rev Immunol* **2**, 465–475 (2002).
50. Thien, M. *et al.* Excess BAFF rescues self-reactive B cells from peripheral deletion and allows them to enter forbidden follicular and marginal zone niches. *Immunity* **20**, 785–798 (2004).
51. Grimaldi, C. M., Hicks, R. & Diamond, B. B cell selection and susceptibility to autoimmunity. *J Immunol* **174**, 1775–1781 (2005).
52. Vallabhapurapu, S. & Karin, M. Regulation and function of NF-kappaB transcription factors in the immune system. *Annu Rev Immunol* **27**, 693–733 (2009).
53. Ghosh, S. & Hayden, M. S. New regulators of NF-kappaB in inflammation. *Nat Rev Immunol* **8**, 837–848 (2008).
54. Hayden, M. S. & Ghosh, S. Shared principles in NF-kappaB signaling. *Cell* **132**, 344–362 (2008).
55. Baeuerle, P. A. & Baltimore, D. I kappa B: a specific inhibitor of the NF-kappa B transcription factor. *Science* **242**, 540 (1988).
56. Ghosh, S. & Karin, M. Missing pieces in the NF-kappaB puzzle. *Cell* **109 Suppl**, S81–96 (2002).
57. Kerr, L. D. *et al.* The proto-oncogene bcl-3 encodes an I kappa B protein. *Genes Dev* **6**, 2352–2363 (1992).
58. Yamazaki, S., Muta, T. & Takeshige, K. A novel IkappaB protein, IkappaB-zeta, induced by proinflammatory stimuli, negatively regulates nuclear factor-kappaB in the nuclei. *J Biol Chem* **276**, 27657–27662 (2001).
59. Bours, V. *et al.* The oncoprotein Bcl-3 directly transactivates through κB motifs via association with DNA-binding p50B homodimers. *Cell* **72**, 729–739 (1993).

60. Nolan, G. P. *et al.* The bcl-3 proto-oncogene encodes a nuclear I kappa B-like molecule that preferentially interacts with NF-kappa B p50 and p52 in a phosphorylation-dependent manner. *Mol Cell Biol* **13**, 3557–3566 (1993).
61. Westerheide, S. D., Mayo, M. W., Anest, V., Hanson, J. L. & Baldwin, A. S. The putative oncoprotein Bcl-3 induces cyclin D1 to stimulate G1 transition. *Mol Cell Biol* **21**, 8428–8436 (2001).
62. Musgrove, E. A., Caldon, C. E., Barraclough, J., Stone, A. & Sutherland, R. L. Cyclin D as a therapeutic target in cancer. *Nat Rev Genet* **11**, 558–572 (2011).
63. Yamamoto, M. *et al.* Regulation of Toll/IL-1-receptor-mediated gene expression by the inducible nuclear protein IκBζ. *Nature* **430**, 218–222 (2004).
64. Totzke, G. *et al.* A novel member of the IκB family, human IκB-ζ, inhibits transactivation of p65 and its DNA binding. *J Biol Chem* **281**, 12645–12654 (2006).
65. Zandi, E., Rothwarf, D. M., Delhase, M., Hayakawa, M. & Karin, M. The IκB kinase complex (IKK) contains two kinase subunits, IKKα and IKKβ, necessary for IκB phosphorylation and NF-κB activation. *Cell* **91**, 243–252 (1997).
66. Rothwarf, D. M., Zandi, E., Natoli, G. & Karin, M. IKK-γ is an essential regulatory subunit of the IκB kinase complex. *Nature* **395**, 297–300 (1998).
67. Chen, Z. J. Ubiquitination in signaling to and activation of IKK. *Immunol Rev* **246**, 95–106 (2012).
68. Xiao, G., Rabson, A. B., Young, W., Qing, G. & Qu, Z. Alternative pathways of NF-kappaB activation: a double-edged sword in health and disease. *Cytokine Growth Factor Rev* **17**, 281–293 (2006).
69. Dejardin, E. The alternative NF-kappaB pathway from biochemistry to biology: pitfalls and promises for future drug development. *Biochem Pharmacol* **72**, 1161–1179 (2006).
70. Sun, S.-C. Non-canonical NF-κB signaling pathway. *Cell Res* **21**, 71–85 (2010).
71. Ling, L., Cao, Z. & Goeddel, D. V. NF-κB-inducing kinase activates IKK-α by phosphorylation of Ser-176. *Proc Natl Acad Sci USA* **95**, 3792–3797 (1998).
72. Senftleben, U. *et al.* Activation by IKKalpha of a second, evolutionary conserved, NF-kappa B signaling pathway. *Science* **293**, 1495–1499 (2001).
73. Claudio, E., Brown, K., Park, S., Wang, H. & Siebenlist, U. BAFF-induced NEMO-independent processing of NF-kappa B2 in maturing B cells. *Nat Immunol* **3**, 958–965 (2002).
74. Hatada, E. N. *et al.* NF-κB1 p50 is required for BLyS attenuation of apoptosis but dispensable for processing of NF-κB2 p100 to p52 in quiescent mature B cells. *J Immunol* **171**, 761–768 (2003).
75. Gerondakis, S. *et al.* Unravelling the complexities of the NF-kappaB signalling pathway using mouse knockout and transgenic models. *Oncogene* **25**, 6781–6799 (2006).
76. Pasparakis, M., Schmidt-Supprian, M. & Rajewsky, K. IkappaB kinase

signaling is essential for maintenance of mature B cells. *J Exp Med* **196**, 743–752 (2002).
77. Schmidt-Supprian, M. *et al.* Mature T cells depend on signaling through the IKK complex. *Immunity* **19**, 377–389 (2003).
78. Siebenlist, U., Brown, K. & Claudio, E. Control of lymphocyte development by nuclear factor-kappaB. *Nat Rev Immunol* **5**, 435–445 (2005).
79. Sen, R. & Baltimore, D. Inducibility of K immunoglobulin enhancer-binding protein NF-KB by a posttranslational mechanism. *Cell* **47**, 921–928 (1986).
80. Derudder, E. *et al.* Development of immunoglobulin lambda-chain-positive B cells, but not editing of immunoglobulin kappa-chain, depends on NF-kappaB signals. *Nat Immunol* **10**, 647–654 (2009).
81. Verkoczy, L. *et al.* A Role for Nuclear Factor Kappa B/Rel Transcription Factors in the Regulation of the Recombinase Activator Genes. *Immunity* **22**, 519–531 (2005).
82. Cadera, E. J. *et al.* NF- B activity marks cells engaged in receptor editing. *J Exp Med* **206**, 1803–1816 (2009).
83. Gerondakis, S. & Siebenlist, U. Roles of the NF-kappaB pathway in lymphocyte development and function. *Cold Spring Harbor Perspectives in Biology* **2**, a000182 (2010).
84. Sasaki, Y. *et al.* Canonical NF-kappaB activity, dispensable for B cell development, replaces BAFF-receptor signals and promotes B cell proliferation upon activation. *Immunity* **24**, 729–739 (2006).
85. Hinz, M. *et al.* NF-kappaB function in growth control: regulation of cyclin D1 expression and G0/G1-to-S-phase transition. *Mol Cell Biol* **19**, 2690–2698 (1999).
86. McHeyzer-Williams, M. G. B cells as effectors. *Curr Opin Immunol* **15**, 354–361 (2003).
87. Shaffer, A. L. *et al.* Signatures of the immune response. *Immunity* **15**, 375–385 (2001).
88. Coussens, L. M. & Werb, Z. Inflammation and cancer. *Nature* **420**, 860–867 (2002).
89. Medzhitov, R. Inflammation 2010: New Adventures of an Old Flame. *Cell* **140**, 771–776 (2010).
90. Serhan, C. N. & Savill, J. Resolution of inflammation: the beginning programs the end. *Nat Immunol* **6**, 1191–1197 (2005).
91. Serhan, C. N. *et al.* Resolution of inflammation: state of the art, definitions and terms. *The FASEB Journal* **21**, 325–332 (2007).
92. Nathan, C. & Ding, A. Nonresolving Inflammation. *Cell* **140**, 871–882 (2010).
93. Epstein, F. H., Barnes, P. J. & Karin, M. Nuclear factor-κB—a pivotal transcription factor in chronic inflammatory diseases. *New England Journal of Medicine* **336**, 1066–1071 (1997).
94. Tak, P. P. & Firestein, G. S. NF-kappaB: a key role in inflammatory diseases. *J Clin Invest* **107**, 7–11 (2001).
95. Lawrence, T. The Nuclear Factor NF- B Pathway in Inflammation. *Cold Spring Harbor Perspectives in Biology* **1**, a001651–a001651 (2009).
96. Baker, R. G., Hayden, M. S. & Ghosh, S. NF-κB, Inflammation, and Metabolic Disease. *Cell Metabolism* **13**, 11–22 (2011).

97. Kaser, A., Zeissig, S. & Blumberg, R. S. Inflammatory bowel disease. *Annu Rev Immunol* **28**, 573–621 (2010).
98. Lizzul, P. F. *et al.* Differential expression of phosphorylated NF-κB/RelA in normal and psoriatic epidermis and downregulation of NF-κB in response to treatment with etanercept. *J Invest Dermatol* **124**, 1275–1283 (2005).
99. Greten, F. R. *et al.* IKKβ Links Inflammation and Tumorigenesis in a Mouse Model of Colitis-Associated Cancer. *Cell* **118**, 285–296 (2004).
100. Nenci, A. *et al.* Epithelial NEMO links innate immunity to chronic intestinal inflammation. *Nature* **446**, 557–561 (2007).
101. Pasparakis, M. *et al.* TNF-mediated inflammatory skin disease in mice with epidermis-specific deletion of IKK2. *Nature* **417**, 861–866 (2002).
102. Pasparakis, M. Regulation of tissue homeostasis by NF-kappaB signalling: implications for inflammatory diseases. *Nat Rev Immunol* **9**, 778–788 (2009).
103. Hershko, A. & Ciechanover, A. The ubiquitin system. *Annu Rev Biochem* **67**, 425–479 (1998).
104. Welchman, R. L., Gordon, C. & Mayer, R. J. Ubiquitin and ubiquitin-like proteins as multifunctional signals. *Nat Rev Mol Cell Biol* **6**, 599–609 (2005).
105. Liu, S. & Chen, Z. J. Expanding role of ubiquitination in NF-κB signaling. *Cell Res* **21**, 6–21 (2010).
106. Kerscher, O., Felberbaum, R. & Hochstrasser, M. Modification of proteins by ubiquitin and ubiquitin-like proteins. *Annu. Rev. Cell Dev. Biol.* **22**, 159–180 (2006).
107. Özkan, E., Yu, H. & Deisenhofer, J. Mechanistic insight into the allosteric activation of a ubiquitin-conjugating enzyme by RING-type ubiquitin ligases. *Proc Natl Acad Sci USA* **102**, 18890–18895 (2005).
108. Ikeda, F. & Dikic, I. Atypical ubiquitin chains: new molecular signals. 'Protein Modifications: Beyond the Usual Suspects' review series. *EMBO Rep* **9**, 536–542 (2008).
109. Hicke, L. A new ticket for entry into budding vesicles-ubiquitin. *Cell* **106**, 527–530 (2001).
110. Tokunaga, F. *et al.* Involvement of linear polyubiquitylation of NEMO in NF-kappaB activation. *Nat Cell Biol* **11**, 123–132 (2009).
111. Kim, H. T. *et al.* Certain pairs of ubiquitin-conjugating enzymes (E2s) and ubiquitin-protein ligases (E3s) synthesize nondegradable forked ubiquitin chains containing all possible isopeptide linkages. *J Biol Chem* **282**, 17375–17386 (2007).
112. Ye, Y. & Rape, M. Building ubiquitin chains: E2 enzymes at work. *Nat Rev Mol Cell Biol* **10**, 755–764 (2009).
113. Deng, L. *et al.* Activation of the IkappaB kinase complex by TRAF6 requires a dimeric ubiquitin-conjugating enzyme complex and a unique polyubiquitin chain. *Cell* **103**, 351–361 (2000).
114. Chen, Z. J. & Sun, L. J. Nonproteolytic functions of ubiquitin in cell signaling. *Mol Cell* **33**, 275–286 (2009).
115. Matsumoto, M. L. *et al.* K11-Linked Polyubiquitination in Cell Cycle Control Revealed by a K11 Linkage-Specific Antibody. *Mol Cell* **39**, 477–484 (2010).

116. Ashida, H. *et al.* A bacterial E3 ubiquitin ligase IpaH9.8 targets NEMO/IKKγ to dampen the host NF-κB-mediated inflammatory response. *Nat Cell Biol* **12**, 66–73 (2009).
117. Chastagner, P., Israël, A. & Brou, C. Itch/AIP4 mediates Deltex degradation through the formation of K29-linked polyubiquitin chains. *EMBO Rep* **7**, 1147–1153 (2006).
118. Malynn, B. A. & Ma, A. Ubiquitin Makes Its Mark on Immune Regulation. *Immunity* **33**, 843–852 (2010).
119. Kulathu, Y. & Komander, D. Atypical ubiquitylation — the unexplored world of polyubiquitin beyond Lys48 and Lys63 linkages. *Nat Rev Mol Cell Biol* **13**, 508–523 (2012).
120. Dynek, J. N. *et al.* c-IAP1 and UbcH5 promote K11-linked polyubiquitination of RIP1 in TNF signalling. *EMBO J* **29**, 4198–4209 (2010).
121. Ikeda, F. *et al.* SHARPIN forms a linear ubiquitin ligase complex regulating NF-κB activity and apoptosis. *Nature* **471**, 637–641 (2011).
122. Komander, D., Clague, M. J. & Urbé, S. Breaking the chains: structure and function of the deubiquitinases. *Nat Rev Mol Cell Biol* **10**, 550–563 (2009).
123. Fraile, J. M., Quesada, V., Rodríguez, D., Freije, J. M. P. & López-Otín, C. Deubiquitinases in cancer: new functions and therapeutic options. *Oncogene* **31**, 2373–2388 (2012).
124. Tokunaga, F. & Iwai, K. Linear ubiquitination: A novel NF-κB regulatory mechanism for inflammatory and immune responses by the LUBAC ubiquitin ligase complex [Review]. *Endocr. J.* **59**, 641–652 (2012).
125. Skaug, B., Jiang, X. & Chen, Z. J. The Role of Ubiquitin in NF-κB Regulatory Pathways. *Annu Rev Biochem* **78**, 769–796 (2009).
126. Xia, Z.-P. *et al.* Direct activation of protein kinases by unanchored polyubiquitin chains. *Nature* **461**, 114–119 (2009).
127. Kurosaki, T. Regulation of BCR signaling. *Mol Immunol* **48**, 1287–1291 (2011).
128. Kurosaki, T., Shinohara, H. & Baba, Y. B cell signaling and fate decision. *Annu Rev Immunol* **28**, 21–55 (2010).
129. Sun, S.-C. Controlling the fate of NIK: a central stage in noncanonical NF-kappaB signaling. *Sci Signal* **3**, pe18 (2010).
130. Vallabhapurapu, S. *et al.* Nonredundant and complementary functions of TRAF2 and TRAF3 in a ubiquitination cascade that activates NIK-dependent alternative NF-kappaB signaling. *Nat Immunol* **9**, 1364–1370 (2008).
131. Emmerich, C. H., Schmukle, A. C. & Walczak, H. The emerging role of linear ubiquitination in cell signaling. *Sci Signal* **4**, re5 (2011).
132. Iwai, K. Diverse ubiquitin signaling in NF-κB activation. *Trends in Cell Biology* **22**, 355–364 (2012).
133. Lo, Y.-C. *et al.* Structural basis for recognition of diubiquitins by NEMO. *Mol Cell* **33**, 602–615 (2009).
134. Döffinger, R. *et al.* X-linked anhidrotic ectodermal dysplasia with immunodeficiency is caused by impaired NF-kappaB signaling. *Nat Genet* **27**, 277–285 (2001).
135. Rahighi, S. *et al.* Specific recognition of linear ubiquitin chains by NEMO

is important for NF-kappaB activation. *Cell* **136**, 1098–1109 (2009).
136. Gerlach, B. *et al.* Linear ubiquitination prevents inflammation and regulates immune signalling. *Nature* **471**, 591–596 (2011).
137. Makarova, K. S., Aravind, L. & Koonin, E. V. A novel superfamily of predicted cysteine proteases from eukaryotes, viruses and Chlamydia pneumoniae. *Trends Biochem Sci* **25**, 50–52 (2000).
138. Opipari, A. W., Boguski, M. S. & Dixit, V. M. The A20 cDNA induced by tumor necrosis factor alpha encodes a novel type of zinc finger protein. *J Biol Chem* **265**, 14705–14708 (1990).
139. Wertz, I. E. *et al.* De-ubiquitination and ubiquitin ligase domains of A20 downregulate NF-κB signalling. *Nature* **430**, 694–699 (2004).
140. Bosanac, I. *et al.* Ubiquitin binding to A20 ZnF4 is required for modulation of NF-κB signaling. *Mol Cell* **40**, 548–557 (2010).
141. Dixit, V. M. *et al.* Tumor necrosis factor-alpha induction of novel gene products in human endothelial cells including a macrophage-specific chemotaxin. *J Biol Chem* **265**, 2973 (1990).
142. Jäättelä, M., Mouritzen, H., Elling, F. & Bastholm, L. A20 zinc finger protein inhibits TNF and IL-1 signaling. *J Immunol* **156**, 1166 (1996).
143. Boone, D. L. *et al.* The ubiquitin-modifying enzyme A20 is required for termination of Toll-like receptor responses. *Nat Immunol* **5**, 1052–1060 (2004).
144. Laherty, C. D., Perkins, N. D. & Dixit, V. M. Human T cell leukemia virus type I Tax and phorbol 12-myristate 13-acetate induce expression of the A20 zinc finger protein by distinct mechanisms involving nuclear factor kappa B. *J Biol Chem* **268**, 5032–5039 (1993).
145. Laherty, C. D., Hu, H. M., Opipari, A. W., Wang, F. & Dixit, V. M. The Epstein-Barr virus LMP1 gene product induces A20 zinc finger protein expression by activating nuclear factor kappa B. *J Biol Chem* **267**, 24157–24160 (1992).
146. Saitoh, T. *et al.* A20 is a negative regulator of IFN regulatory factor 3 signaling. *J Immunol* **174**, 1507–1512 (2005).
147. Lin, R. *et al.* Negative regulation of the retinoic acid-inducible gene I-induced antiviral state by the ubiquitin-editing protein A20. *J Biol Chem* **281**, 2095–2103 (2006).
148. Honda, K. & Taniguchi, T. IRFs: master regulators of signalling by Toll-like receptors and cytosolic pattern-recognition receptors. *Nat Rev Immunol* **6**, 644–658 (2006).
149. Parvatiyar, K., Barber, G. N. & Harhaj, E. W. TAX1BP1 and A20 inhibit antiviral signaling by targeting TBK1-IKKi kinases. *J Biol Chem* **285**, 14999–15009 (2010).
150. Ning, S., Campos, A. D., Darnay, B. G., Bentz, G. L. & Pagano, J. S. TRAF6 and the three C-terminal lysine sites on IRF7 are required for its ubiquitination-mediated activation by the tumor necrosis factor receptor family member latent membrane protein 1. *Mol Cell Biol* **28**, 6536–6546 (2008).
151. Ning, S. & Pagano, J. S. The A20 deubiquitinase activity negatively regulates LMP1 activation of IRF7. *Journal of Virology* (2010).doi:10.1128/JVI.00364-10
152. Opipari, A. W., Hu, H. M., Yabkowitz, R. & Dixit, V. M. The A20 zinc finger

protein protects cells from tumor necrosis factor cytotoxicity. *J Biol Chem* **267**, 12424–12427 (1992).
153. Daniel, S. *et al.* A20 protects endothelial cells from TNF-, Fas-, and NK-mediated cell death by inhibiting caspase 8 activation. *Blood* **104**, 2376–2384 (2004).
154. Vucic, D., Dixit, V. M. & Wertz, I. E. Ubiquitylation in apoptosis: a post-translational modification at the edge of life and death. *Nat Rev Mol Cell Biol* **12**, 439–452 (2011).
155. Jin, Z. *et al.* Cullin3-based polyubiquitination and p62-dependent aggregation of caspase-8 mediate extrinsic apoptosis signaling. *Cell* **137**, 721–735 (2009).
156. He, K. L. & Ting, A. T. A20 Inhibits Tumor Necrosis Factor (TNF) Alpha-Induced Apoptosis by Disrupting Recruitment of TRADD and RIP to the TNF Receptor 1 Complex in Jurkat T Cells. *Mol Cell Biol* **22**, 6034–6045 (2002).
157. Kundu, M. & Thompson, C. B. Autophagy: Basic Principles and Relevance to Disease. *Annu. Rev. Pathol. Mech. Dis.* **3**, 427–455 (2008).
158. Xu, Y. *et al.* Toll-like Receptor 4 Is a Sensor for Autophagy Associated with Innate Immunity. *Immunity* **27**, 135–144 (2007).
159. Shi, C.-S. & Kehrl, J. H. MyD88 and Trif target Beclin 1 to trigger autophagy in macrophages. *J Biol Chem* **283**, 33175–33182 (2008).
160. Xie, Z. & Klionsky, D. J. Autophagosome formation: core machinery and adaptations. *Nat Cell Biol* **9**, 1102–1109 (2007).
161. Shi, C.-S. & Kehrl, J. H. TRAF6 and A20 regulate lysine 63-linked ubiquitination of Beclin-1 to control TLR4-induced autophagy. *Sci Signal* **3**, ra42 (2010).
162. Hitotsumatsu, O. *et al.* The ubiquitin-editing enzyme A20 restricts nucleotide-binding oligomerization domain containing 2-triggered signals. *Immunity* **28**, 381–390 (2008).
163. Düwel, M. *et al.* A20 negatively regulates T cell receptor signaling to NF-kappaB by cleaving Malt1 ubiquitin chains. *The Journal of Immunology* **182**, 7718–7728 (2009).
164. Evans, P. C. *et al.* Zinc-finger protein A20, a regulator of inflammation and cell survival, has de-ubiquitinating activity. *Biochem J* **378**, 727–734 (2004).
165. Lin, S.-C. *et al.* Molecular basis for the unique deubiquitinating activity of the NF-kappaB inhibitor A20. *Journal of Molecular Biology* **376**, 526–540 (2008).
166. Komander, D. & Barford, D. Structure of the A20 OTU domain and mechanistic insights into deubiquitination. *Biochem J* **409**, 77–85 (2008).
167. Shembade, N., Harhaj, N. S., Liebl, D. J. & Harhaj, E. W. Essential role for TAX1BP1 in the termination of TNF-alpha-, IL-1- and LPS-mediated NF-kappaB and JNK signaling. *EMBO J* **26**, 3910–3922 (2007).
168. Iha, H. *et al.* Inflammatory cardiac valvulitis in TAX1BP1-deficient mice through selective NF-κB activation. *EMBO J* **27**, 629–641 (2008).
169. Shembade, N., Ma, A. & Harhaj, E. W. Inhibition of NF-kappaB signaling by A20 through disruption of ubiquitin enzyme complexes. *Science* **327**, 1135–1139 (2010).
170. Shembade, N. *et al.* The E3 ligase Itch negatively regulates inflammatory

signaling pathways by controlling the function of the ubiquitin-editing enzyme A20. *Nat Immunol* **9**, 254–262 (2008).
171. Shembade, N. D., Parvatiyar, K., Harhaj, N. S. & Harhaj, E. W. The ubiquitin-editing enzyme A20 requires RNF11 to downregulate NF-kappaB signalling. *EMBO J* **28**, 513–522 (2009).
172. Tewari, M. *et al.* Lymphoid expression and regulation of A20, an inhibitor of programmed cell death. *J Immunol* **154**, 1699–1706 (1995).
173. Matsumoto, R. *et al.* Phosphorylation of CARMA1 Plays a Critical Role in T Cell Receptor-Mediated NF-κB Activation. *Immunity* **23**, 575–585 (2005).
174. Oeckinghaus, A. *et al.* Malt1 ubiquitination triggers NF-κB signaling upon T-cell activation. *EMBO J* **26**, 4634–4645 (2007).
175. Sun, L., Deng, L., Ea, C.-K., Xia, Z.-P. & Chen, Z. J. The TRAF6 ubiquitin ligase and TAK1 kinase mediate IKK activation by BCL10 and MALT1 in T lymphocytes. *Mol Cell* **14**, 289–301 (2004).
176. Coornaert, B. *et al.* T cell antigen receptor stimulation induces MALT1 paracaspase-mediated cleavage of the NF-kappaB inhibitor A20. *Nat Immunol* **9**, 263–271 (2008).
177. Rebeaud, F. *et al.* The proteolytic activity of the paracaspase MALT1 is key in T cell activation. *Nat Immunol* **9**, 272–281 (2008).
178. Li, L. *et al.* Localization of A20 to a lysosome-associated compartment and its role in NFkappaB signaling. *Biochim Biophys Acta* **1783**, 1140–1149 (2008).
179. Skaug, B. *et al.* Direct, Noncatalytic Mechanism of IKK Inhibition by A20. *Mol Cell* **44**, 559–571 (2011).
180. Brummelkamp, T. R., Nijman, S. M. B., Dirac, A. M. G. & Bernards, R. Loss of the cylindromatosis tumour suppressor inhibits apoptosis by activating NF-kappaB. *Nature* **424**, 797–801 (2003).
181. Kovalenko, A. *et al.* The tumour suppressor CYLD negatively regulates NF-kappaB signalling by deubiquitination. *Nature* **424**, 801–805 (2003).
182. Trompouki, E. *et al.* CYLD is a deubiquitinating enzyme that negatively regulates NF-kappaB activation by TNFR family members. *Nature* **424**, 793–796 (2003).
183. Enesa, K. *et al.* NF-kappaB suppression by the deubiquitinating enzyme Cezanne: a novel negative feedback loop in pro-inflammatory signaling. *J Biol Chem* **283**, 7036–7045 (2008).
184. Xu, G. *et al.* Ubiquitin-specific peptidase 21 inhibits tumor necrosis factor alpha-induced nuclear factor kappaB activation via binding to and deubiquitinating receptor-interacting protein 1. *J Biol Chem* **285**, 969–978 (2010).
185. Massoumi, R. Ubiquitin chain cleavage: CYLD at work. *Trends Biochem Sci* **35**, 392–399 (2010).
186. Bignell, G. R. *et al.* Identification of the familial cylindromatosis tumour-suppressor gene. *Nat Genet* **25**, 160–165 (2000).
187. Massoumi, R., Chmielarska, K., Hennecke, K., Pfeifer, A. & Fässler, R. Cyld inhibits tumor cell proliferation by blocking Bcl-3-dependent NF-kappaB signaling. *Cell* **125**, 665–677 (2006).
188. Massoumi, R. *et al.* Down-regulation of CYLD expression by Snail promotes tumor progression in malignant melanoma. *J Exp Med* **206**, 221–232 (2009).

189. Massoumi, R. CYLD: a deubiquitination enzyme with multiple roles in cancer. *Future Oncology* **7**, 285–297 (2011).
190. Schmitz, R. *et al.* TNFAIP3 (A20) is a tumor suppressor gene in Hodgkin lymphoma and primary mediastinal B cell lymphoma. *J Exp Med* **206**, 981–989 (2009).
191. Harhaj, E. W. & Dixit, V. M. Deubiquitinases in the regulation of NF-κB signaling. *Cell Res* **21**, 22–39 (2011).
192. Komander, D. *et al.* The Structure of the CYLD USP Domain Explains Its Specificity for Lys63-Linked Polyubiquitin and Reveals a B Box Module. *Mol Cell* **29**, 451–464 (2008).
193. Lee, E. G. *et al.* Failure to regulate TNF-induced NF-kappaB and cell death responses in A20-deficient mice. *Science* **289**, 2350–2354 (2000).
194. Turer, E. E. *et al.* Homeostatic MyD88-dependent signals cause lethal inflamMation in the absence of A20. *J Exp Med* **205**, 451–464 (2008).
195. Graham, R. R. *et al.* Genetic variants near TNFAIP3 on 6q23 are associated with systemic lupus erythematosus. *Nat Genet* **40**, 1059–1061 (2008).
196. Musone, S. L. *et al.* Multiple polymorphisms in the TNFAIP3 region are independently associated with systemic lupus erythematosus. *Nat Genet* **40**, 1062–1064 (2008).
197. Musone, S. L. *et al.* Sequencing of TNFAIP3 and association of variants with multiple autoimmune diseases. *Genes Immun* **12**, 176–182 (2011).
198. Adrianto, I. *et al.* Association of a functional variant downstream of TNFAIP3 with systemic lupus erythematosus. *Nat Genet* **43**, 253–258 (2011).
199. Thomson, W. *et al.* Rheumatoid arthritis association at 6q23. *Nat Genet* **39**, 1431–1433 (2007).
200. Plenge, R. M. *et al.* Two independent alleles at 6q23 associated with risk of rheumatoid arthritis. *Nat Genet* **39**, 1477–1482 (2007).
201. Nair, R. P. *et al.* Genome-wide scan reveals association of psoriasis with IL-23 and NF-kappaB pathways. *Nat Genet* **41**, 199–204 (2009).
202. Trynka, G. *et al.* Coeliac disease-associated risk variants in TNFAIP3 and REL implicate altered NF-kappaB signalling. *Gut* **58**, 1078–1083 (2009).
203. Coenen, M. J. H. *et al.* Common and different genetic background for rheumatoid arthritis and coeliac disease. *Hum Mol Genet* **18**, 4195–4203 (2009).
204. De Jager, P. L. *et al.* Meta-analysis of genome scans and replication identify CD6, IRF8 and TNFRSF1A as new multiple sclerosis susceptibility loci. *Nat Genet* **41**, 776–782 (2009).
205. Sisto, M. *et al.* A failure of TNFAIP3 negative regulation maintains sustained NF-κB activation in Sjögren's syndrome. *Histochem Cell Biol* **135**, 615–625 (2011).
206. Fung, E. Y. M. G. *et al.* Analysis of 17 autoimmune disease-associated variants in type 1 diabetes identifies 6q23/TNFAIP3 as a susceptibility locus. *Genes Immun* **10**, 188–191 (2009).
207. Vereecke, L., Beyaert, R. & van Loo, G. Genetic relationships between A20/TNFAIP3, chronic inflammation and autoimmune disease. *Biochem. Soc. Trans.* **39**, 1086–1091 (2011).
208. Lodolce, J. P. *et al.* African-derived genetic polymorphisms in TNFAIP3

mediate risk for autoimmunity. *The Journal of Immunology* **184**, 7001–7009 (2010).
209. Jost, P. J. & Ruland, J. Aberrant NF-kappaB signaling in lymphoma: mechanisms, consequences, and therapeutic implications. *Blood* **109**, 2700–2707 (2007).
210. Staudt, L. M. Oncogenic activation of NF-kappaB. *Cold Spring Harbor Perspectives in Biology* **2**, a000109 (2010).
211. Kato, M. *et al.* Frequent inactivation of A20 in B-cell lymphomas. *Nature* **459**, 712–716 (2009).
212. Compagno, M. *et al.* Mutations of multiple genes cause deregulation of NF-kappaB in diffuse large B-cell lymphoma. *Nature* **459**, 717–721 (2009).
213. Honma, K. *et al.* TNFAIP3/A20 functions as a novel tumor suppressor gene in several subtypes of non-Hodgkin lymphomas. *Blood* **114**, 2467–2475 (2009).
214. Braggio, E. *et al.* Genomic analysis of marginal zone and lymphoplasmacytic lymphomas identified common and disease-specific abnormalities. *Mod Pathol* **25**, 651–660 (2012).
215. Honma, K. *et al.* TNFAIP3is the target gene of chromosome band 6q23.3-q24.1 loss in ocular adnexal marginal zone B cell lymphoma. *Genes Chromosomes Cancer* **47**, 1–7 (2008).
216. Novak, U. *et al.* The NF- B negative regulator TNFAIP3 (A20) is inactivated by somatic mutations and genomic deletions in marginal zone lymphomas. *Blood* **113**, 4918–4921 (2009).
217. Chanudet, E. *et al.* A20 is targeted by promoter methylation, deletion and inactivating mutation in MALT lymphoma. *Leukemia* **24**, 483–487 (2010).
218. Rinaldi, A. *et al.* Genome-wide DNA profiling of marginal zone lymphomas identifies subtype-specific lesions with an impact on the clinical outcome. *Blood* **117**, 1595–1604 (2011).
219. Yan, Q. *et al.* BCR and TLR signaling pathways are recurrently targeted by genetic changes in splenic marginal zone lymphomas. *Haematologica* **97**, 595–598 (2012).
220. Rossi, D. *et al.* The coding genome of splenic marginal zone lymphoma: activation of NOTCH2 and other pathways regulating marginal zone development. *J Exp Med* **209**, 1537–1551 (2012).
221. Braggio, E. *et al.* Identification of Copy Number Abnormalities and Inactivating Mutations in Two Negative Regulators of Nuclear Factor- B Signaling Pathways in Waldenstrom's Macroglobulinemia. *Cancer Res* **69**, 3579–3588 (2009).
222. Knudson, A. G. Mutation and cancer: statistical study of retinoblastoma. *Proc Natl Acad Sci USA* **68**, 820 (1971).
223. Braun, F. C. M. *et al.* Tumor suppressor TNFAIP3 (A20) is frequently deleted in Sézary syndrome. *Leukemia* **25**, 1494–1501 (2011).
224. Vendrell, J. A. *et al.* A20/TNFAIP3, a new estrogen-regulated gene that confers tamoxifen resistance in breast cancer cells. *Oncogene* **26**, 4656–4667 (2007).
225. Guo, Q. *et al.* A20 is overexpressed in glioma cells and may serve as a potential therapeutic target. *Expert Opin. Ther. Targets* **13**, 733–741

(2009).
226. Verhelst, K. *et al.* A20 inhibits LUBAC-mediated NF-κB activation by binding linear polyubiquitin chains via its zinc finger 7. *EMBO J* **31**, 3845–3855 (2012).
227. Tokunaga, F. *et al.* Specific recognition of linear polyubiquitin by A20 zinc finger 7 is involved in NF-κB regulation. *EMBO J* **31**, 3856–3870 (2012).

Supplements

In the following, papers I, II, III and IV are reprinted.

Paper I

Enterocyte-specific A20 deficiency sensitizes to tumor necrosis factor–induced toxicity and experimental colitis

Lars Vereecke,[1,2] Mozes Sze,[1,2] Conor Mc Guire,[1,2] Brecht Rogiers,[1,2] Yuanyuan Chu,[3] Marc Schmidt-Supprian,[3] Manolis Pasparakis,[4] Rudi Beyaert,[1,2] and Geert van Loo[1,2]

[1]Department for Molecular Biomedical Research, VIB, B-9052 Ghent, Belgium
[2]Department of Biomedical Molecular Biology, Ghent University, B-9052 Ghent, Belgium
[3]Max Planck Institute of Biochemistry, D-82152 Martinsried, Germany
[4]Institute for Genetics, University of Cologne, D-50674 Cologne, Germany

A20 **is a nuclear factor κB (NF-κB) target gene that encodes a ubiquitin-editing enzyme that is essential for the termination of NF-κB activation after tumor necrosis factor (TNF) or microbial product stimulation and for the prevention of TNF-induced apoptosis. Mice lacking A20 succumb to inflammation in several organs, including the intestine, and A20 mutations have been associated with Crohn's disease. However, ablation of NF-κB activity, specifically in intestinal epithelial cells (IECs), promotes intestinal inflammation. As A20 deficiency sensitizes cells to TNF-induced apoptosis yet also promotes NF-κB activity, it is not clear if A20 deficiency in IECs would exacerbate or ameliorate intestinal inflammation. We generated mice lacking A20 specifically in IECs. These mice did not show spontaneous intestinal inflammation but exhibited increased susceptibility to experimental colitis, and their IECs were hypersensitive to TNF-induced apoptosis. The resulting TNF-driven breakdown of the intestinal barrier permitted commensal bacterial infiltration and led to systemic inflammation. These studies define A20 as a major antiapoptotic protein in the intestinal epithelium and further indicate that defects in A20 might contribute to inflammatory bowel disease in humans.**

CORRESPONDENCE
Geert van Loo:
geert.vanloo@dmbr.vib-UGent.be
OR
Rudi Beyaert:
rudi.beyaert@dmbr.vib-UGent.be

Abbreviations used: $A20^{IEC-KO}$, IEC-specific A20 knockout; CD, Crohn's disease; DSS, dextran sodium sulphate; ES, embryonic stem; IBD, inflammatory bowel disease; IEC, intestinal epithelial cell; IKK, IκB kinase; MEF, mouse embryonic fibroblast; NEMO, NF-κB essential modulator; NLR, NOD-like receptor; TLR, toll-like receptor; TNFR, TNF receptor.

Inflammatory bowel disease (IBD) and, in particular, Crohn's disease (CD), is thought to result from a dysregulated interaction between the host immune system and normal luminal microflora (Rakoff-Nahoum et al., 2006; Artis, 2008; Round and Mazmanian, 2009). Furthermore, epidemiological and linkage studies suggest a genetic predisposition and the involvement of environmental factors (Podolsky, 2002). The aberrant immune response in IBD is most likely facilitated by defects in both the barrier function of the intestinal epithelium and the mucosal immune system. Recognition of commensal bacterial products by toll-like receptors (TLRs) and NOD-like receptors (NLRs) leads to the production of a mix of inflammatory cytokines and chemokines by immune cells and surface epithelial cells (Rakoff-Nahoum et al., 2004; Baumgart and Carding, 2007). In this context, the transcription factor NF-κB, which is activated by TLRs, NLRs, and cytokine receptors, such as TNF and IL-1, plays a critical role. On the one hand, NF-κB regulates the expression of various cytokines and other modulators of the inflammatory processes in IBD. On the other hand, NF-κB enhances the survival of cells through the regulation of antiapoptotic genes. A tight regulation of the NF-κB signaling pathway and the genes induced is thus an absolute requirement. Recently, significant progress has been made in our understanding of the mechanisms that control the dynamics of NF-κB activation, and several autoregulatory feedback loops terminating the NF-κB response have been described (Renner and Schmitz, 2009). In this context, the NF-κB–responsive and ubiquitin-editing protein A20 (also referred to as TNF-α–induced protein 3 or TNFAIP3) has been described as a central gatekeeper in inflammation and immunity (Coornaert et al., 2009).

R. Beyaert and G. van Loo contributed equally to this paper.

The Rockefeller University Press $30.00
J. Exp. Med.
www.jem.org/cgi/doi/10.1084/jem.20092474

The Journal of Experimental Medicine

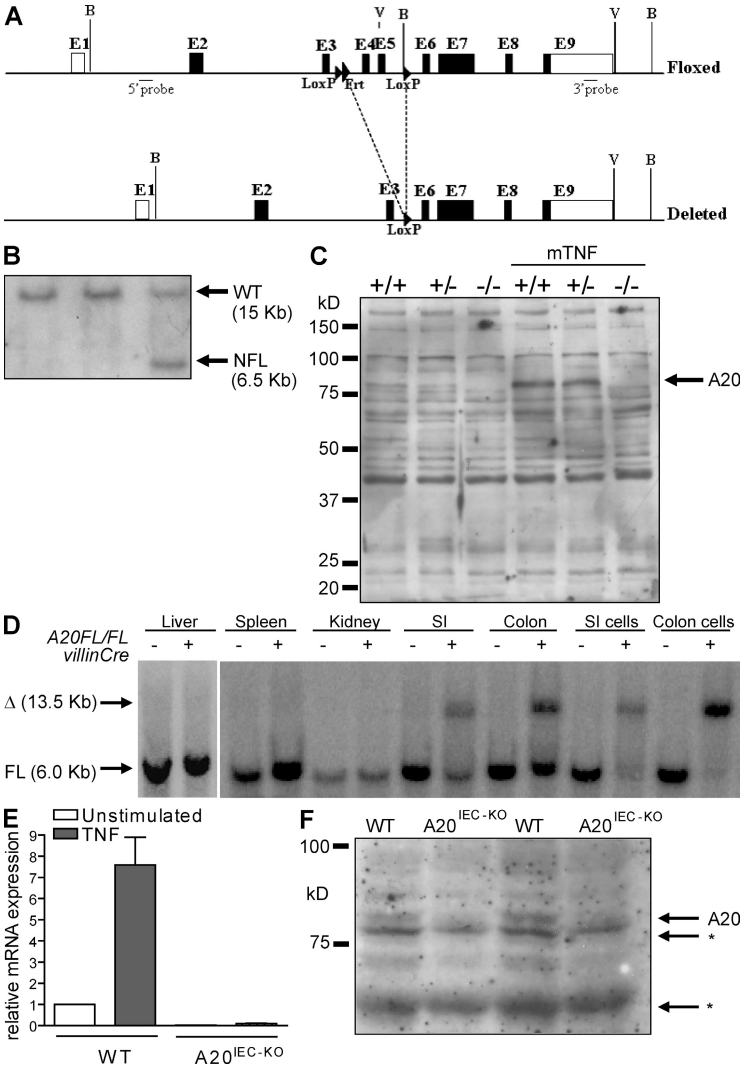

Figure 1. Generation and molecular analysis of A20^{IEC-KO} mice. (A) Targeting scheme. The diagram shows the loxP-flanked (floxed) and deleted A20 alleles. The boxes indicate exons 1–9 (E1–E9). Restriction enzyme sites and the location of the probe used for Southern blot analysis are depicted. B, BamH1; V, EcoRV. LoxP and Frt sites are indicated by arrowheads. (B) Southern blot analysis on DNA from WT (+/+) and homologous recombinant (NFL/+) ES cells. (C) Western blot analysis for A20 expression in WT (+/+), heterozygous (+/−), and A20 knockout (−/−) primary MEFs either stimulated or not for 5 h with recombinant mouse TNF. (D) DNA isolated from various tissues of a *A20$^{FL/FL}$/Villin-Cre^{+}* mouse and a control littermate (*A20$^{FL/FL}$/Villin-Cre^{-}*) was subjected to Southern blot analysis. Δ, deleted allele; FL, floxed allele; SI, small intestine. (E) Quantitative PCR measurement of A20 mRNA expression in purified IECs from A20^{IEC-KO} ($n = 2$) and control WT littermate mice ($n = 2$) 0 or 30 min after mouse TNF injection. Error bars represent SEM. (F) Western blot analysis for A20 expression in colonic epithelial cells from two individual A20^{IEC-KO} and control WT littermate mice. *, unspecific. Data are representative of two independent experiments.

A20 is essential for the termination of NF-κB signaling in response to TNF and microbial products such as LPS and muramyl dipeptide (Boone et al., 2004; Hitotsumatsu et al., 2008), which trigger TLR4 and NOD2 (nucleotide-binding oligomerization domain-containing 2) receptors, respectively. Moreover, A20 also negatively regulates TNF-induced apoptosis (Opipari et al., 1992; Lee et al., 2000). Mice deficient for A20 are hypersensitive to TNF and die prematurely as a result of severe multiorgan inflammation and cachexia (Lee et al., 2000). Interestingly, *A20* has recently been identified as a susceptibility locus for multiple immunopathologies (Vereecke et al., 2009). More specifically related to IBD, a recent genome-wide association study for seven major common diseases, undertaken in the British population by the Wellcome Trust Case Control Consortium (2007), identified *A20* as a CD susceptibility gene. An earlier independent study on IBD-affected pairs of multiple families also associated mutations in a region of human chromosome 6q, containing the *A20* locus, with the IBD phenotype (Barmada et al., 2004). Finally, mucosal biopsies from CD patients confirmed a consistent down-regulation of mucosal A20 expression in CD patients, which may hamper their ability to regulate pathological NF-κB activation induced by acute inflammatory responses (Arsenescu et al., 2008). Interestingly, single nucleotide polymorphisms in the *A20* region on 6q23.3 were recently also identified as a disease risk factor in celiac disease (Trynka et al., 2009). These studies, as well as the fact that mice genetically deficient in A20 develop multiorgan inflammation including severe intestinal inflammation (Lee et al., 2000), indicate that defective A20 expression or activity could be a risk factor for IBD. Previous studies showed that transfer of A20-deficient myeloid cells in WT irradiated mice elicits the spontaneous inflammatory phenotype as seen in full A20 knockout mice (Turer et al., 2008). These data indicate that A20 expression in myeloid cells plays a key role in restricting proinflammatory signaling. However, whether A20 also has a role in stromal cells such as the intestinal epithelium remains unknown. There is multiple evidence that epithelial NF-κB preserves the integrity of the gut epithelial barrier and maintains immune homeostasis in the gut (Ben-Neriah and Schmidt-Supprian, 2007; Artis, 2008; Pasparakis, 2008). Epithelial-specific NF-κB deficiency in mice through conditional ablation of NF-κB essential modulator (NEMO) or both IκB kinase (IKK) 1 and IKK2 spontaneously led to enterocyte apoptosis and massive intestinal inflammation (Nenci et al., 2007). Similarly, mice with specific deletion of RelA in intestinal epithelial cells (IECs) exhibit increased susceptibility to chemically induced colitis (Steinbrecher et al., 2008). An important step in the inflammatory process in these NF-κB–deficient mice involves the sensitization of NF-κB–deficient epithelial cells to TNF-induced apoptosis, compromising epithelial integrity and allowing bacterial translocation into the mucosa, thus leading to recruitment of inflammatory immune cells and chronic inflammation (Nenci et al., 2007). The identity of

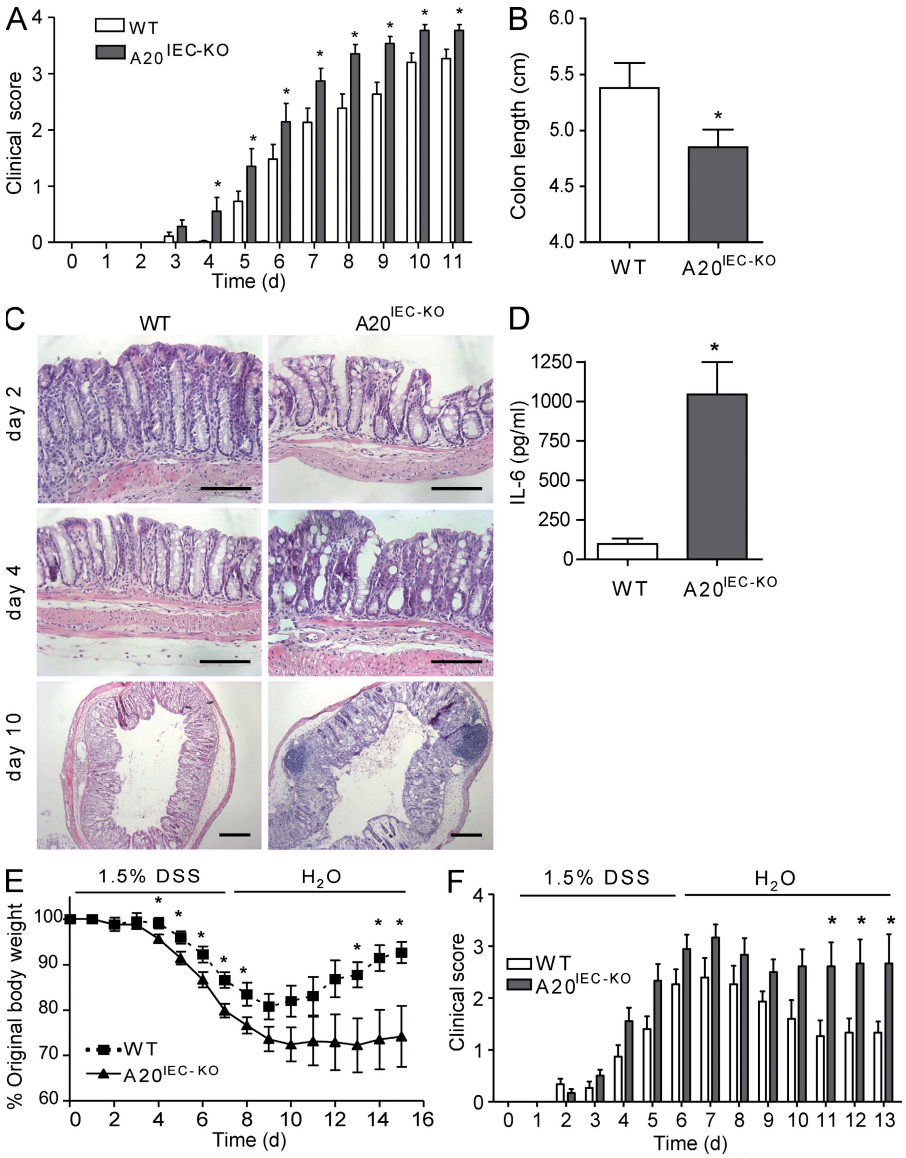

Figure 2. Enterocyte expression of A20 is required for recovery of mice from acute DSS-induced inflammation. (A) Clinical score of $A20^{IEC\text{-}KO}$ mice ($n = 18$) and control littermates (WT, $n = 20$) treated with 1.5% DSS. (B) Colon length of $A20^{IEC\text{-}KO}$ mice ($n = 18$) and control littermates (WT, $n = 20$) after 10 d of 1.5% DSS treatment. (C) Hematoxylin and eosin (H&E) histology on DSS-treated $A20^{IEC\text{-}KO}$ mice and control littermates (WT). Bars: (days 2 and 4) 100 µm; (day 10) 250 µm. (D) Serum IL-6 levels after 1.5% DSS treatment for 4 d. (E and F) Clinical score and body weight of $A20^{IEC\text{-}KO}$ mice ($n = 6$) and control littermates (WT, $n = 5$) treated for 6 d with 1.5% DSS followed by normal drinking water. Data in A–D are representative of three independent experiments. Experiments in E and F were performed two times. Error bars represent SEM. *, $P < 0.05$.

the NF-κB–regulated genes that control enterocyte survival in intestinal immune homeostasis or in a proinflammatory environment remains unknown. *A20* is an NF-κB–dependent gene that is naturally expressed in mouse enterocytes as soon as the gut gets colonized by bacteria, a process which is initiated right after birth (Wang et al., 2009). We might, therefore, expect an important role for A20 in establishing NF-κB–mediated tolerance and epithelial protection against environmental and proinflammatory signals. However, the dual antiapoptotic and NF-κB–inhibitory function of A20 imposes a real conundrum. On the one hand, A20 deficiency in the gut would increase the susceptibility of enterocytes to apoptosis, leading to the translocation of commensal bacteria and intestinal inflammation. On the other hand, and consistent with the previously reported key role of NF-κB in maintaining immune homeostasis in the gut (Ben-Neriah and Schmidt-Supprian, 2007; Nenci et al., 2007; Pasparakis, 2008; Steinbrecher et al., 2008), excessive NF-κB activation in A20-deficient enterocytes can be expected to be protective.

To study the role of A20 expression in IECs in intestinal immunity under normal and proinflammatory conditions, we generated A20 conditional knockout mice that are specifically deficient for A20 in IECs. IEC-specific A20 knockout ($A20^{IEC\text{-}KO}$) mice show increased susceptibility to dextran sodium sulphate (DSS)–induced colitis associated with increased sensitivity of IECs to apoptosis. $A20^{IEC\text{-}KO}$ mice are also hypersensitive to normally sublethal doses of TNF, leading to enterocyte apoptosis and disintegration of the intestinal barrier. As a result, infiltrating commensal bacteria initiate a systemic inflammatory response leading to death. These data indicate that A20 expression in the intestinal epithelium is a crucial antiapoptotic factor that mediates the protective effect of NF-κB in IEC and determines susceptibility to IBD.

RESULTS

Generation and phenotypic analysis of $A20^{IEC\text{-}KO}$ mice

We generated mice carrying a conditional A20 allele in which exons IV and V of the mouse A20 gene are flanked by LoxP sites (Fig. 1 A). This conditional A20 allele allows the tissue-specific inactivation of A20 through expression of Cre recombinase, as removal of exons IV and V results in an out-of-frame transcript. Correctly targeted homologous recombinant embryonic stem (ES) cell clones were identified by Southern blotting and used to generate chimeric mice that transmitted the targeted allele to their offspring (Fig. 1 B). Mice homozygous for the LoxP-flanked A20 allele ($A20^{FL/FL}$)

express normal levels of A20 and develop normally (Fig. S1). Deletion of the LoxP-flanked A20 alleles through expression of the Cre recombinase leads to a loss of A20 protein, as shown in mouse embryonic fibroblasts (MEFs; Fig. 1 C). Moreover, no alternative or shorter A20 protein can be detected in $A20^{-/-}$ MEFs. To study the role of A20 in physiological maintenance of the IEC layer as well as its response to intestinal inflammation, we crossed the $A20^{FL/FL}$ mice with a transgenic mouse line that expresses Cre under the control of the IEC-specific villin gene regulatory sequences (villin-Cre). The villin-Cre transgenic line targets all epithelial cell lineages of the distal small intestine, cecum, and colon, and expression mediates efficient Cre-mediated recombination in IECs starting before birth (Madison et al., 2002). $A20^{IEC\text{-}KO}$ ($A20^{FL/FL}$/villin-Cre, $A20^{IEC\text{-}KO}$) mice were born showing normal Mendelian segregation and reached adulthood without any evidence of intestinal defects. To verify the tissue specificity of the $A20^{IEC\text{-}KO}$, we performed Southern blot analysis of DNA isolated from various tissues of a $A20^{IEC\text{-}KO}$ mouse, showing efficient Cre-mediated recombination in intestinal tissue (colon and small intestine) and in purified IECs isolated from colon and small intestine (Fig. 1 D). Recombination was not detected in any other tested tissues. In addition, quantitative real-time PCR on IEC mRNA and immunoblot analysis of IEC protein extracts revealed ablation of A20 in $A20^{IEC\text{-}KO}$ cells (Fig. 1, E and F).

A20 expression in IEC determines the susceptibility to experimental colitis

$A20^{IEC\text{-}KO}$ mice look healthy, and phenotypic analysis of $A20^{IEC\text{-}KO}$ mice up to the age of 12 mo revealed no pathological signs in the intestine. To further investigate whether A20 expression determines the susceptibility to IBD, $A20^{IEC\text{-}KO}$ mice and control littermates were evaluated in an established model of DSS-induced colitis. Mice were subjected to 1.5% DSS in drinking water for 9 d and monitored daily for clinical pathology based on loss in body weight, stool consistency, and presence of fecal blood. Compared with control mice, $A20^{IEC\text{-}KO}$ mice show increased susceptibility to DSS-induced colitis and develop more severe colitis symptoms, like gross rectal bleeding and diarrhea (Fig. 2 A). Colon shortening, a typical clinical feature of colonic inflammation, is much more pronounced in $A20^{IEC\text{-}KO}$ mice 10 d after DSS treatment (Fig. 2 B). Histological examination of the distal colon reveals increased mucosal damage, crypt loss, and immune cell infiltration in DSS-treated $A20^{IEC\text{-}KO}$ mice compared with control littermates (Fig. 2 C). Inflammation was further assessed by quantifying the presence of IL-6 in serum. In contrast to untreated mice, which do not show inflammatory cytokine expression (not depicted), IL-6 was found to be significantly

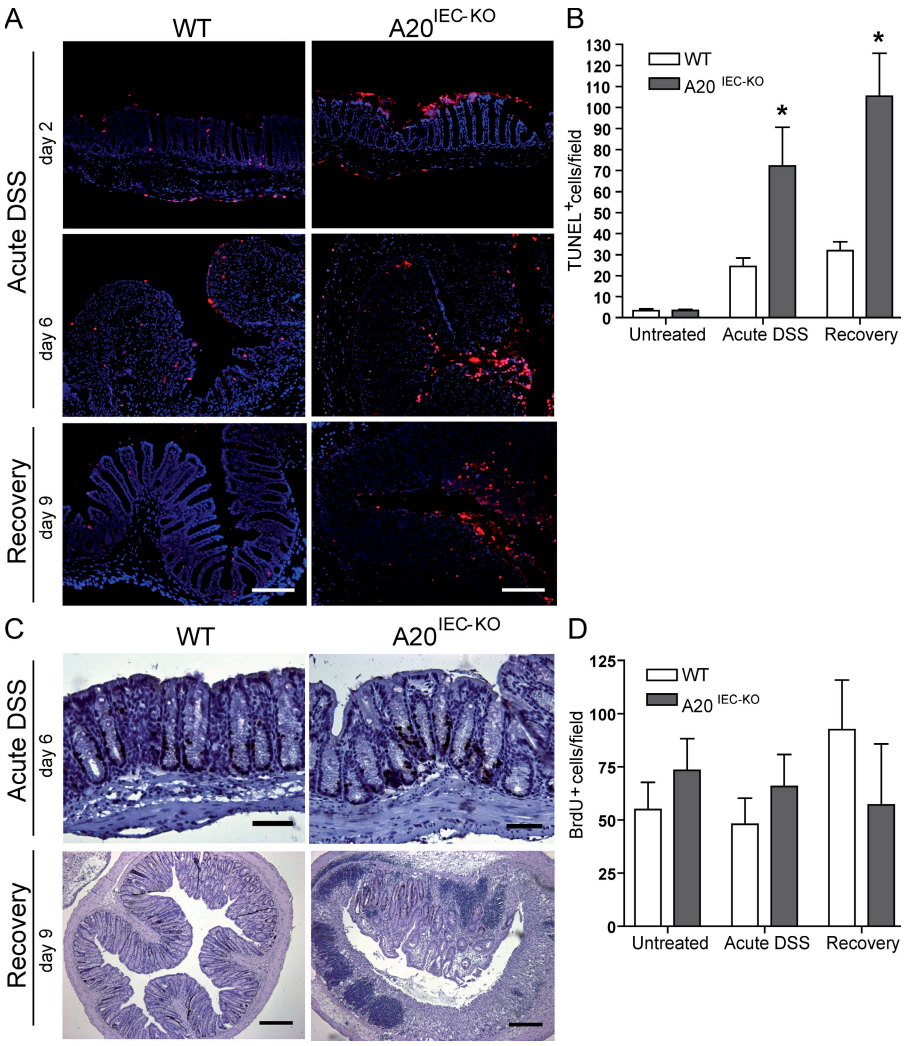

Figure 3. A20 deficiency sensitizes IECs to DSS-induced apoptosis. (A) TUNEL staining on distal colon sections of $A20^{IEC\text{-}KO}$ mice and control littermates (WT) after 2 and 6 d of 1.5% DSS treatment, and after 9 d during recovery (6 d of 1.5% DSS followed by normal drinking water). Bars, 150 µm. (B) Quantification of the number of TUNEL-positive cells/field from untreated and DSS-treated mice. Error bars represent SEM. *, $P < 0.05$. (C) Detection of BrdU incorporation on distal colon sections of $A20^{IEC\text{-}KO}$ mice and control littermates (WT) after 6 d of 1.5% DSS treatment, and after 9 d during recovery (6 d of 1.5% DSS followed by normal drinking water). Bars: (day 4) 50 µm; (day 9) 250 µm. (D) Quantification of the number of BrdU-positive cells/field from untreated and DSS-treated mice. Error bars represent SEM. Data are representative of three independent experiments.

higher in A20$^{IEC\text{-}KO}$ mice then in controls after DSS treatment (Fig. 2 D).

To evaluate the ability of A20$^{IEC\text{-}KO}$ mice to recover from DSS-induced epithelial damage, mice were put on 1.5% DSS for 6 d and were then put back on regular drinking water. Control mice display maximal clinical colitis on day 7, after which they recover and gain up to 90% of their original body weight (Fig. 2, E and F). A20$^{IEC\text{-}KO}$ mice, however, are unable to cope with the initial DSS challenge and do not recover. All A20$^{IEC\text{-}KO}$ mice continue to display severe signs of clinical colitis, they do not gain weight, and many of them (66%) die around day 12–13 after treatment (Fig. 2, E and F). The increased and sustained pathological response in A20$^{IEC\text{-}KO}$ mice indicates an essential role for A20 in the termination of intestinal inflammation and the recovery from intestinal epithelial damage.

A20 protects IECs from apoptosis in experimental colitis

A20 has a dual NF-κB inhibitory and antiapoptotic effect (Coornaert et al., 2009). The increased susceptibility of A20$^{IEC\text{-}KO}$ mice to DSS-induced colitis may therefore be explained by increased IEC apoptosis, allowing infiltration of commensal bacteria into the submucosa and the activation of several immune cells that built up a proinflammatory environment, leading to a further breakdown of the epithelial barrier. Therefore, we determined apoptosis in the intestinal epithelium of A20$^{IEC\text{-}KO}$ and control littermate mice after DSS challenge by TUNEL staining. Compared with controls, A20$^{IEC\text{-}KO}$ epithelium already showed much more TUNEL-positive cells after the start of DSS treatment (days 2–6) (Fig. 3, A and B), which is likely an underestimation because of the significant loss of IECs in A20$^{IEC\text{-}KO}$ mice as a result of excessive mucosal damage. This difference in epithelial cell apoptosis between A20$^{IEC\text{-}KO}$ and control littermate mice is even more pronounced during the recovery phase after putting mice back on regular drinking water (day 9; Fig. 3, A and B). Although IECs from A20$^{IEC\text{-}KO}$ mice are highly sensitive to apoptosis when exposed to DSS, the expression of different pro- or antiapoptotic genes (Bax, PUMA, Bcl2, BclXL, and XIAP) was not significantly changed in A20-deficient IECs compared with DSS-challenged control IECs (unpublished data).

Next to increased apoptosis, A20-deficient IECs may have an impaired capacity to restore the epithelial barrier after DSS-induced epithelial erosion as the result of a decreased proliferative response. However, similar numbers of BrdU-labeled cells were found in A20$^{IEC\text{-}KO}$ and control epithelial cell layers of DSS-treated animals during acute DSS treatment (Fig. 3, C and D), excluding a difference in proliferation in the absence of A20. During recovery (after putting mice back on regular drinking water, day 9), however, a slight difference in the numbers of BrdU-labeled cells between both groups is observed (Fig. 3, C and D). This difference most probably results from the excessive mucosal damage and the significant loss of IECs in A20$^{IEC\text{-}KO}$ mice. Indeed, mucosal areas with modest damage display similar numbers of BrdU-labeled cells compared with control areas.

MyD88 deficiency exacerbates, whereas TNF receptor (TNFR) 1 deficiency reduces experimental colitis in A20$^{IEC\text{-}KO}$ mice

Because TLRs expressed on IECs are essential as sensors of commensal bacteria establishing intestinal homeostasis (Rakoff-Nahoum et al., 2004), A20 could be involved in this regulation in addition to its role as a protective factor against IEC apoptosis. To explore this possibility, we also analyzed the sensitivity of A20$^{IEC\text{-}KO}$ mice to DSS-induced colitis in a MyD88-deficient background. As expected, double A20$^{IEC\text{-}KO}$MyD88-deficient mice are much more sensitive to DSS-induced colitis compared with control A20$^{IEC\text{-}KO}$MyD88 heterozygous mice (Fig. 4 A). These results suggest that, in addition to enhanced IEC apoptosis in the absence of A20, a defective TLR-mediated bacterial recognition in the absence of MyD88 contributes to DSS-induced intestinal inflammation and that both signals are happening in concert in conditions of A20 deficiency in IECs.

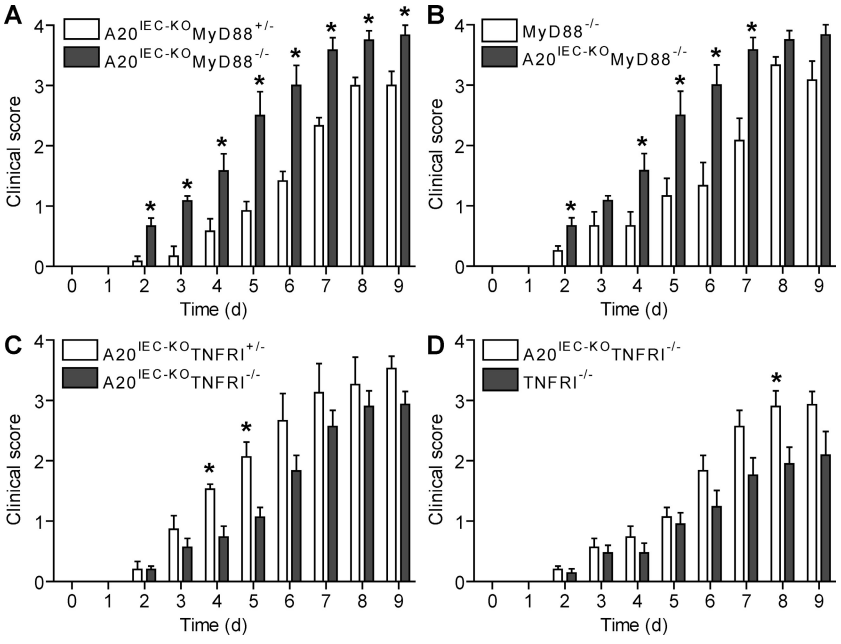

Figure 4. MyD88 deficiency sensitizes and TNFR1 deficiency reduces experimental colitis in A20$^{IEC\text{-}KO}$ mice. (A) Clinical score of A20$^{IEC\text{-}KO}$MyD88-deficient mice (n = 4) and control A20$^{IEC\text{-}KO}$MyD88 heterozygous mice (n = 4) treated with 1.5% DSS. (B) Clinical score of double A20$^{IEC\text{-}KO}$MyD88-deficient mice (n = 4) and single MyD88 knockout mice (n = 4) treated with 1.5% DSS. (C) Clinical score of A20$^{IEC\text{-}KO}$TNFR1-deficient mice (n = 10) and control A20$^{IEC\text{-}KO}$TNFR1 heterozygous mice (n = 5) treated with 1.5% DSS. (D) Clinical score of double A20$^{IEC\text{-}KO}$TNFR1-deficient mice (n = 10) and single TNFR1 knockout mice (n = 7) treated with 1.5% DSS. Error bars represent SEM. *, $P < 0.05$. Data are representative of two independent experiments.

This is also strengthened by the fact that double A20^{IEC-KO}-MyD88-deficient mice are much more sensitive to DSS-induced inflammation than single MyD88-deficient mice (Fig. 4 B). Overall, it can be concluded from these results that both MyD88 and A20 play a nonredundant protective role in intestinal immune homeostasis.

TNF is one of the major proinflammatory cytokines contributing to the pathogenesis of CD in humans and experimental colitis in mice, and TNF-blocking agents have shown clinical efficiency in both patients and mice (Neurath et al., 1997; Targan et al., 1997). To investigate whether TNF signaling contributes to the development of colitis in DSS-treated A20^{IEC-KO} mice, we crossed them onto a TNFR1-deficient background. Double A20^{IEC-KO}TNFR1-deficient mice and control A20^{IEC-KO}TNFR1 heterozygous mice were subjected to DSS and monitored for clinical pathology. Compared with control mice, A20^{IEC-KO}TNFR1-deficient mice develop less severe colitis symptoms (Fig. 4 C), demonstrating that A20 restricts harmful TNFR1 signaling which contributes to disease pathogenesis in this model. Compared with TNFRI-deficient mice, double A20^{IEC-KO}TNFRI-deficient mice are more sensitive to DSS-induced colitis (Fig. 4 D), further suggesting that A20 also restricts the role of other receptors than TNFRI, such as TLRs and NLRs, in DSS-induced colitis. We can conclude that A20 acts as a major protective NF-κB response gene in the intestinal epithelium by restricting both proinflammatory and proapoptotic signaling pathways induced by TLR-MyD88 and TNFRI, respectively.

A20 deficiency in IEC increases TNF-induced damage of the intestinal epithelium and lethality

TNF may contribute to disease pathology by activating NF-κB and inflammation, as well as by inducing apoptosis of IECs, which causes loss of epithelial barrier integrity. Besides its well documented NF-κB inhibitory function, A20 also inhibits TNF-induced apoptosis (Opipari et al., 1992; Lee et al., 2000; Coornaert et al., 2009). We therefore evaluated the effect of A20 deficiency in IECs on TNF-induced pathology. For this, we injected A20^{IEC-KO} mice and control littermates with a normally sublethal dose of mouse TNF. In contrast to control mice, which all resist such a sublethal dose of TNF and only show a modest drop in body temperature 6–8 h after injection, A20^{IEC-KO} mice display typical symptoms associated with TNF toxicity, including hypothermia and severe diarrhea, already starting 2 h after injection. 5 h after TNF administration, all A20^{IEC-KO} mice showed a severe drop in body temperature (Fig. 5 A), and they died between 5 and 9 h after injection, whereas all control mice survived (Fig. 5 B). We further assessed inflammation in A20^{IEC-KO} mice by quantifying proinflammatory cytokine and chemokine production after TNF injection. A20^{IEC-KO} mice had higher levels of IL-6 and MCP-1 in circulation after TNF challenge than control littermate mice (Fig. 5 C). TNF toxicity in A20^{IEC-KO} mice involves TNFR1 signaling, as injecting human TNF, which only binds mouse TNFR1 and not mouse TNFR2 (Lewis et al., 1991), similarly induced lethality in A20^{IEC-KO} mice (Fig. 5 D).

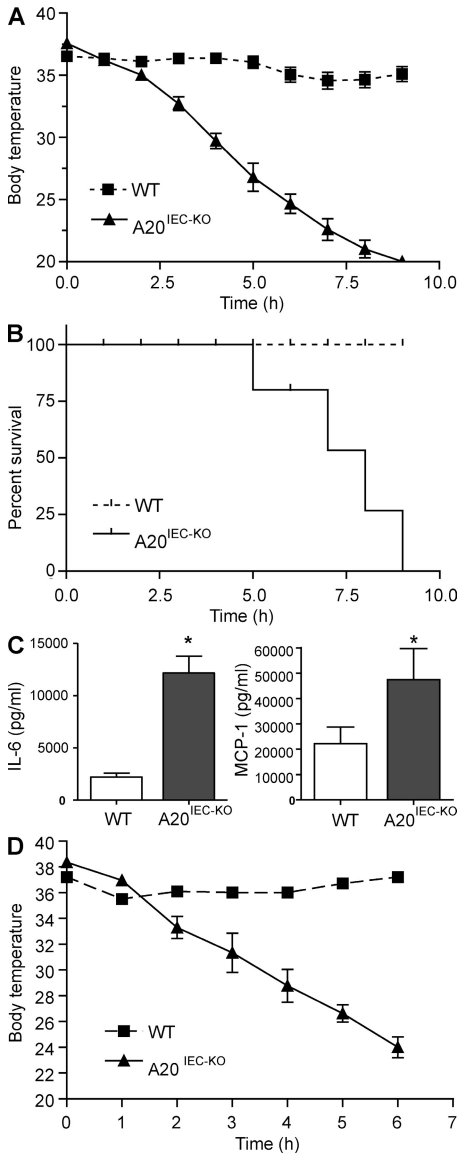

Figure 5. A20 deficiency in IECs sensitizes mice to TNF-induced toxicity. (A and B) Mice were injected i.p. with 5 µg of recombinant mouse TNF. Body temperature (A) and survival (B) of A20^{IEC-KO} mice (n = 8) and littermate control mice (WT; n = 6). (C) Serum IL-6 and MCP-1 levels 4 h after mouse TNF injection. (D) Body temperature of A20^{IEC-KO} mice (n = 6) and control littermate mice (n = 6) after injection with 50 µg of recombinant human TNF. Data are representative of three independent experiments. Error bars represent SEM. *, $P < 0.05$.

To investigate the TNF-induced tissue damage in A20^{IEC-KO} mice, parts of the intestine from control and A20^{IEC-KO} mice were removed and stained with hematoxylin/eosin for histological examination. Treatment with TNF resulted in severe damage of the jejunum and ileum of A20^{IEC-KO} mice, showing extensive epithelial destruction and a nearly complete loss of crypt-villus structure, which is in contrast to control littermates which maintain tissue integrity (Fig. 6 A). To investigate TNF-induced apoptosis at the cellular level, intestinal tissue sections were analyzed by TUNEL assay. In control mice

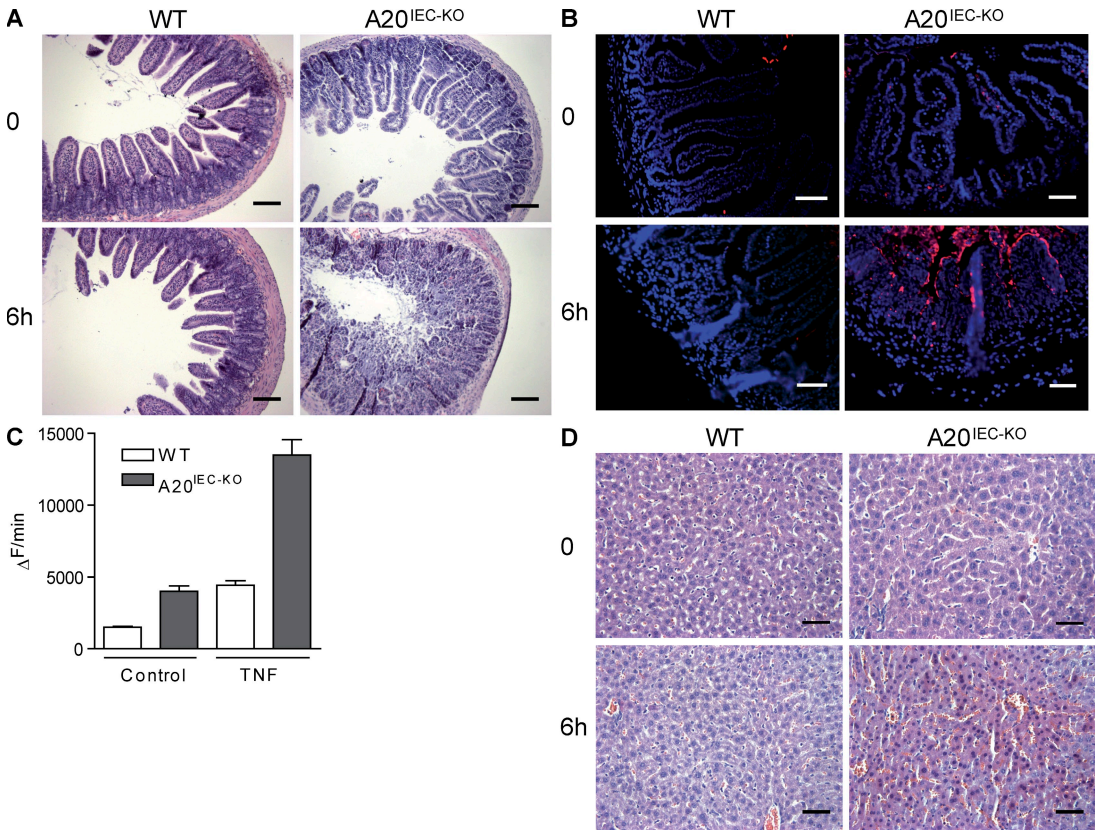

Figure 6. A20 deficiency in IECs sensitizes to TNF-induced damage of the small intestine and liver. (A) H&E histology on a section of the small intestine from A20^{IEC-KO} mice and control littermates (WT) 0 and 6 h after mouse TNF injection. Bars, 100 µm. (B) TUNEL staining on sections from small intestine 0 and 6 h after mouse TNF injection, staining apoptotic cells in red. Bars, 50 µm. (C) Caspase activity assayed on tissue homogenates of terminal ileum of A20^{IEC-KO} mice and WT littermates at 0 (control) and 90 min after mouse TNF injection. Error bars represent SEM. (D) H&E histology on liver samples from control (WT) and A20^{IEC-KO} mice 0 and 6 h after mouse TNF injection. Bars, 50 µm. Data are representative of two independent experiments.

treated with TNF, TUNEL staining was completely absent. In contrast, TNF-challenged A20^{IEC-KO} mice showed massive positive TUNEL staining, mainly at the epithelial cells lining the villi (Fig. 6 B; Fig. S2 A). Moreover, numerous apoptotic cells could be detected in the intestinal lumen. In contrast to the enhanced sensitivity of A20-deficient IECs to apoptosis, no differences in epithelial cell proliferation could be observed between A20^{IEC-KO} and control littermate mice (Fig. S2 B). To confirm IEC apoptosis in TNF-treated A20^{IEC-KO} mice, intestinal tissue homogenates were made and the extent of apoptosis was assessed by measuring caspase activity. PBS-injected A20^{IEC-KO} mice already show higher caspase activity then control littermates (Fig. 6 C). Moreover, the effect of TNF was much more pronounced in A20^{IEC-KO} mice, which is in agreement with the increase in apoptosis as observed in the TUNEL assay. Finally, to analyze whether A20 deficiency in the intestinal epithelium also induced histopathological changes in other tissues, we examined the liver of TNF-treated control and A20^{IEC-KO} mice. Interestingly, TNF-treated A20^{IEC-KO} mice not only show increased damage of the intestinal tissue but also of the liver (Fig. 6 D and Fig. S3), although A20^{IEC-KO} mice express normal A20 levels in this tissue (Fig. S4). This demonstrates that specific A20 deficiency in the intestine can also affect the systemic effects of TNF on other tissues.

Commensal intestinal microbes contribute to TNF-induced lethality in A20^{IEC-KO} mice

As TNF induces massive epithelial destruction in A20^{IEC-KO} mice, infiltration of commensal bacteria may contribute to the lethal inflammatory shock observed in these mice. To determine to what extent commensal intestinal microbes contribute to epithelial damage and lethality in A20^{IEC-KO} mice, we treated these mice for 2 wk with a mix of broad-spectrum antibiotics (ciprofloxacin, ampicillin, metronidazole, and vancomycin), which has been shown to substantially reduce the numbers of commensal bacteria in the intestine (unpublished data). Interestingly, antibiotics treatment completely protected A20^{IEC-KO} mice against the lethal effect of TNF up to 8 h after TNF injection (Fig. 7 A). A20^{IEC-KO} mice that are rescued from TNF-induced lethality by antibiotics still show massive epithelial destruction in the small intestine (Fig. 7 B), although epithelial damage is less severe than in TNF-treated mice that did not receive antibiotics (not depicted). This suggests that a mucosal cytokine burst initiated by bacterial infiltration contributes to further epithelial damage

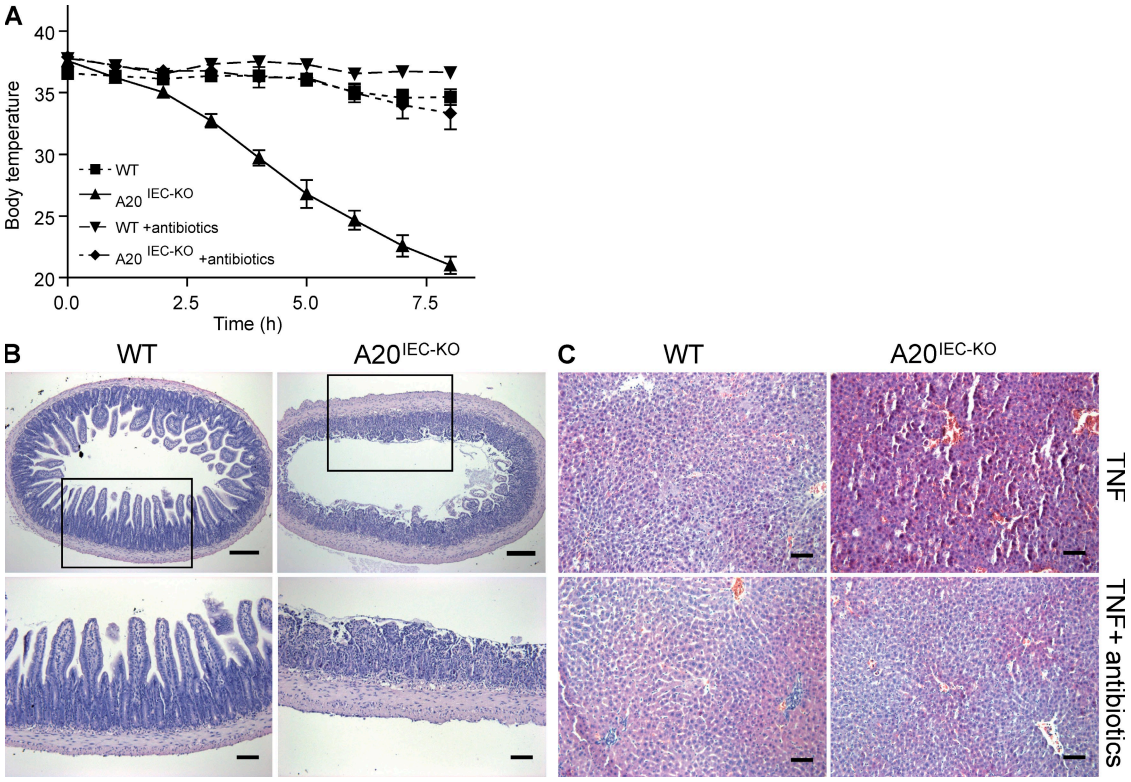

Figure 7. Commensal intestinal microbes contribute to TNF-induced toxicity in A20^{IEC-KO} mice. (A) Body temperature after mouse TNF challenge of A20^{IEC-KO} mice and control littermate mice (WT) either untreated (IEC-KO, $n = 6$; WT, $n = 5$) or treated (IEC-KO, $n = 6$; WT, $n = 8$) with broad-spectrum antibiotics. (B) H&E histology on sections from distal ileum 0 and 7 h after i.p. injection of mouse TNF in control (WT) and A20^{IEC-KO} mice treated with antibiotics. Bottom images are magnifications of rectangles in top images. Bars: (top) 100 µm; (bottom) 75 µm. (C) H&E histology on liver samples 0 and 7 h after TNF injection in control (WT) and A20^{IEC-KO} mice either untreated or treated with antibiotics. Bars, 75 µm. Data are representative of two independent experiments. Error bars represent SEM.

in the absence of A20. However, although intestinal epithelial damage in A20^{IEC-KO} mice is only slightly reduced by antibiotics treatment, TNF-induced liver damage is completely prevented (Fig. 7 C). Collectively, these data suggest that infiltration of commensal bacteria as a result of the TNF-mediated destruction of the epithelial barrier in A20^{IEC-KO} mice initiates a systemic inflammatory response, causing dramatic body temperature loss, severe liver damage, and cardiovascular collapse causing lethality.

DISCUSSION

In this paper, we have shown that the NF-κB–regulated gene *A20* is a major protective factor in the intestinal epithelium. Specific deletion of A20 in enterocytes increased the susceptibility of mice to DSS-induced colitis and prevented the recovery from acute DSS-induced inflammation. We also demonstrated that A20 deficiency in enterocytes renders mice sensitive to TNF-induced lethal inflammation. TNF-induced lethality was mediated by an apoptotic effect of TNF on A20-deficient cells, leading to disruption of the epithelial barrier and infiltration of commensal bacteria that initiate a systemic inflammatory response.

A20 is well documented as an NF-κB–responsive gene that plays a key role in the negative feedback regulation of NF-κB signaling (Coornaert et al., 2009). However, A20 is also recognized as a strong antiapoptotic factor (Opipari et al., 1992; Lee et al., 2000). This may seem contradictory, as NF-κB is important for cytoprotection by inducing the expression of antiapoptotic genes and cell cycle regulators (Luo et al., 2005). NF-κB inhibition is therefore often sensitizing toward cell death. Because enterocytes from A20^{IEC-KO} mice are highly sensitive to TNF-induced apoptosis, the antiapoptotic effect of A20 seems to be dominant to the cell death–sensitizing effect of NF-κB inhibition. Moreover, this would suggest that the antiapoptotic function of A20 is sufficient for its protective effect against sublethal TNF doses. We cannot exclude, however, that an additional antiinflammatory effect of NF-κB inhibition by A20 also contributes to its protective function. The hypersensitivity of A20^{IEC-KO} mice to DSS-induced acute colitis is consistent with the important role of NF-κB in IBD. It was previously reported that defective NF-κB activity in intestinal epithelium as a result of enterocyte-specific ablation of the regulatory subunit of the IKK complex NEMO, as well as of enterocyte-specific RelA deficiency, causes spontaneous colitis (Nenci et al., 2007; Steinbrecher et al., 2008). It can be hypothesized that this phenotype is partly caused by the defective NF-κB–dependent expression of A20. However, in contrast to NEMO- or RelA-deficient mice, A20^{IEC-KO} mice do not

develop spontaneous intestinal inflammation, at least at young age, indicating that enterocyte A20 expression is dispensable for normal intestinal immune homeostasis.

TNF is one of the major proinflammatory cytokines contributing to the malignancy of IBD, and TNF blockade is an effective therapy for IBD patients (Targan et al., 1997). By inducing enterocyte apoptosis, aberrant TNF production may cause loss of epithelial barrier integrity, which is considered an early step in the pathogenesis of IBD. Our data show that in the absence of A20, enterocytes become hypersensitive to TNF-induced apoptosis, compromising epithelial integrity. Interestingly, A20 deficiency not only sensitizes mice to mouse TNF but also to human TNF, which is hardly toxic in WT mice (Ameloot et al., 2002). Therefore, our $A20^{IEC\text{-}KO}$ mice may be a useful tool to study human TNF-targeting therapeutic strategies. Moreover, although mouse TNF binds both TNFR1 and TNFR2, human TNF only binds TNFR1 (Lewis et al., 1991), demonstrating that intestinal damage in $A20^{IEC\text{-}KO}$ mice is mediated by TNFR1. The exact molecular mechanism by which A20 prevents TNF-induced apoptosis is still unclear. The ubiquitin-editing function of A20 has been shown to be responsible for its NF-κB inhibitory properties (Wertz et al., 2004; Heyninck and Beyaert, 2005), and several NF-κB signaling proteins can be deubiquitinated by A20 (Coornaert et al., 2009). Death receptor ligation was recently shown to induce polyubiquitination of the apoptosis signaling protein caspase-8, which led to the binding of the ubiquitin-binding protein p62/sequestosome-1, caspase-8 aggregation, and commitment to cell death (Jin et al., 2009). Interestingly, caspase-8 polyubiquitination could be reversed by A20, suggesting a possible anti-apoptotic mechanism.

TNF-induced disruption of the intestinal epithelial barrier can be expected to allow mucosal infiltration of commensal bacteria, resulting in immune cell recruitment and activation. This would then result in the expression of several proinflammatory mediators, including TNF, which imposes further epithelial damage and complete epithelial barrier destruction. Ultimately, this allows bacteria to get in circulation and induce a systemic inflammatory response syndrome that is characterized by liver damage, severe hypotension, and death. The fact that we could inhibit TNF-induced lethality and liver damage in $A20^{IEC\text{-}KO}$ mice with antibiotics confirms a key role for commensal bacteria in TNF toxicity. It should be mentioned that treatment with antibiotics only slightly decreased TNF-induced intestinal epithelial damage in $A20^{IEC\text{-}KO}$ mice, demonstrating that bacteria themselves are not responsible for enterocyte apoptosis. Previous studies showed that transfer of A20-deficient myeloid cells in irradiated WT mice induces multiorgan inflammation, as seen in full A20 knockout mice (Turer et al., 2008). These myeloid cell–transplanted mice are also completely protected with antibiotics or when bred onto a MyD88-negative background, demonstrating that A20 expression in myeloid cells is critical in restricting homeostatic TLR-mediated immune responses to intestinal commensal bacteria (Turer et al., 2008). Our data show that A20 also has a prominent role in stromal cells such as the intestinal epithelium. However, A20's primary function here is not to restrict MyD88-dependent proinflammatory signaling because these mice do not develop spontaneous inflammation in response to commensal bacteria but, rather, to control a cellular protection system once local intestinal inflammation is initiated. In such inflammatory conditions, A20 ensures maintenance of the epithelial barrier integrity by protecting cells from TNF-induced apoptosis.

In conclusion, because unrestrained activation of the immune system directed against the intestinal commensal microflora resulting in uncontrolled proinflammatory cytokine production is believed to play a key role in the development and progression of IBD (Round and Mazmanian, 2009), the present study further demonstrates that defects in the NF-κB–dependent expression and function of A20 might play an important role in the development and progression of IBD. Although A20 expression in enterocytes is largely dispensable for normal intestinal tissue homeostasis, A20 has an essential protective role in conditions of intestinal injury and inflammation. These data also further support recent genome-wide association studies that identified *A20* as a susceptibility locus for CD (Wellcome Trust Case Control Consortium, 2007; Arsenescu et al., 2008; Trynka et al., 2009) and other autoimmune diseases (Vereecke et al., 2009), implicating A20 as an interesting therapeutic target.

MATERIALS AND METHODS

Generation of IEC-specific knockout mice. To generate a conditional *A20* allele, we prepared a targeting vector to flank exons IV and V of *A20* with two LoxP sites. An Frt site-flanked cassette, containing a neo gene, was placed into the third intron of the *A20* gene. A 4.0-kb fragment was used as 5′ homology region, a 2-kb fragment was placed between the two LoxP sites, and a 4.0-kb fragment was used as 3′ homology region. The targeting vector was linearized and transfected into Bruce-4 ES cells derived from C57BL/6 mice (Köntgen and Stewart, 1993) as previously described (Schmidt-Supprian et al., 2000). The targeted ES cell clone was injected into 3.5-d blastocysts and transferred to the uteri of pseudopregnant foster mothers. Male chimeras were mated with C57BL/6 females to obtain germline transmission of the *A20* floxed allele (still containing the neomycine selection cassette; $A20^{NFL}$). The Frt-flanked neomycin cassette was removed by crossing $A20^{NFL}$ mice with an Flp-deleter strain (Rodríguez et al., 2000) generating an *A20* floxed allele ($A20^{FL}$). $A20^{+/-}$ mice were generated by crossing chimeras transmitting the $A20^{NFL}$ genotype with Cre-deleter mice. MEFs were prepared from embryonic day 13.5 $A20^{+/+}$, $A20^{+/-}$, and $A20^{-/-}$ embryos. $A20^{FL/FL}$ mice were crossed to Villin-Cre transgenic mice (Madison et al., 2002; gift from D. Gumucio and B. Madison, University of Michigan Medical School, Ann Arbor, MI) to generate $A20^{IEC\text{-}KO}$. All experiments were performed on mice backcrossed into the C57BL/6 genetic background for at least five generations. Mice were housed in individually ventilated cages at the VIB Department of Molecular Biomedical Research in either specific pathogen-free or conventional animal facilities. All experiments on mice were conducted according to institutional, national, and European animal regulations. Animal protocols were approved by the ethics committee of Ghent University.

Southern and Western blot analysis. For ES cell selection, 10 μg of genomic DNA was digested with BamHI to differentiate between 15.0- and 6.5-kb fragments for the WT and $A20^{NFL}$ alleles, respectively. To differentiate between $A20^{FL}$ and $A20^{IEC\text{-}KO}$ alleles, genomic DNA was digested with BamHI yielding 6.5- and 13.5-kb fragments, respectively. DNA was separated on agarose gels and transferred to nitrocellulose. Hybridization was performed with ^{32}P-labeled probe. Protein lysates were prepared from MEF,

liver, or IEC samples, separated by SDS-PAGE (PAGE), transferred to nitrocellulose, and analyzed by immunoblotting. A20 was detected with rabbit polyclonal anti-A20 as primary antibody and anti–rabbit Ig-HRP (GE Healthcare) as secondary antibody. For the generation of anti-A20, rabbits were immunized with purified A20 OTU domain (gift from D. Komander, Medical Research Council Laboratory of Molecular Biology, Cambridge, England, UK) protein in TiterMax Gold and subsequently boosted five times with A20 OTU domain protein in Freund's adjuvant.

Proliferation and apoptosis assays. Proliferation was analyzed by microscopy after i.p. injection of 1 mg BrdU 2 h before sacrifice, using a BrdU in situ detection kit (BD). Apoptosis was analyzed by fluorescence microscopy using an in situ cell death detection kit (Roche). Five random optical fields were taken, and the results are presented as mean ± SEM. Caspase activity was measured by incubation of 25 µg of tissue homogenate with 50 µM acetyl-Asp-Glu-Val-Asp-aminomethylcoumarin (Peptide Institute, Osaka, Japan) in 150 µl of cell-free system buffer (10 mM Hepes–NaOH, pH 7.4, 220 mM mannitol, 68 mM sucrose, 2 mM NaCl, 2.5 mM KH_2PO_4, 0.5 mM EGTA, 2 mM $MgCl_2$, 5 mM pyruvate, 0.1 mM PMSF, and 1 mM dithiothreitol). The release of fluorescent 7-amino-4-methylcoumarin was measured for 50 min at 2-min intervals by fluorospectrometry at 360 nm excitation and 480 nm emission wavelength, and the maximal rate of increase in fluorescence was calculated (Δfluorescence/min; Cytofluor; PerSeptive Biosystems).

In vivo TNF toxicity. Mice were injected i.p. with a sublethal dose of mouse or human TNF (5 µg of mouse [m] TNF/20-g mouse; 50 µg of human [h] TNF/20-g mouse). *E. coli*–derived recombinant mTNF had a specific activity of 9.46×10^7 IU/mg, and hTNF had a specific activity of 3×10^7 IU/mg. Both were produced and purified to homogeneity in our laboratory, and endotoxin levels did not exceed 1 ng/mg of protein. Body temperature and survival were monitored every hour, and blood was collected by retroorbital bleeding for cytokine analysis. In a separate experiment, mice were euthanized after 2 and 4 h for histological analysis and caspase activity assays.

Depletion of commensal intestinal bacteria. For antibiotic-mediated depletion of commensal bacteria, mice were treated with 200 mg/liter ciprofloxacin (Sigma-Aldrich), 1 g/liter ampicillin (Sigma-Aldrich), 1 g/liter metronidazole (Sigma-Aldrich), and 500 mg/liter vancomycin (Labconsult) in drinking water. After 2 wk, the presence of colonic microflora was determined by culturing fecal samples in both brain heart infusion (BD) and thioglycollate medium (Sigma-Aldrich).

Induction of DSS-induced colitis and clinical score. Female 8–12-wk-old $A20^{IEC\text{-}KO}$ and littermate WT controls were used in DSS-induced colitis experiments. Acute colitis was induced by addition of 1.5% DSS (36–50 kD; MP Biomedicals) to the drinking water for 9 or 6 d followed by regular distilled water. Body weight, occult or gross blood lost per rectum, and stool consistency were determined daily during the colitis experiment. Fecal blood was determined using Hemoccult SENSA (Beckman Coulter) analysis. The baseline clinical score was determined on day 0. In brief, no weight loss was scored as 0, weight loss of 1–5% from baseline as 1, 5–10% as 2, 10–20% as 3, and >20% as 4. For bleeding, a score of 0 was assigned for no blood, 2 for positive hemoccult, and 4 for gross bleeding. For stool consistency, a score of 0 was assigned for well-formed pellets, pasty and semiformed stools were scored as 2, and liquid stools as 4. These scores were added together and divided by three, resulting in a total clinical score ranging from 0 (healthy) to 4 (maximal colitis). To eliminate any diagnostic bias, mice were scored blindly.

Histological scoring. Postmortem, the entire colon was removed from cecum to anus, and the colon length was measured as a marker for inflammation.

Isolation of IECs. IECs were isolated as previously described (Nenci et al., 2007). In brief, small intestines or colons were dissected and flushed with a solution containing 154 mM NaCl and 1 mM DTT to remove fecal contents. The intestinal segments were ligated, filled with PBS, and incubated in PBS at 37°C. After 15 min, PBS was substituted with PBS supplemented with 1.5 mM EDTA and 0.5 mM DTT. After 30 min at 37°C, one ligature was removed and contents were collected. These recovered cells were washed twice in PBS by centrifugation at 1,300 rpm for 5 min and were used for preparation of RNA or protein extracts.

Quantitative real-time PCR. Total RNA was isolated from purified IECs using the Aurum Total RNA Mini kit (Bio-Rad Laboratories) before cDNA synthesis using the iScript cDNA synthesis kit (Bio-Rad Laboratories) according to the manufacturer's instructions. 10 ng cDNA was used for quantitative PCR in a total volume of 10 µl with LightCycler 480 SYBR Green I Master Mix (Roche) and specific primers on a LightCycler 480 (Roche). Real-time PCR reactions were performed in triplicates. The following mouse-specific primers were used: A20 forward, 5′-AAACCAATGGTGATGGAAACTG-3′; A20 reverse, 5′-GTTGTCCCATTCGTCATTCC-3′; ubiquitin forward, 5′-AGGTCAAACAGGAAGACAGACGTA-3′; and ubiquitin reverse, 5′-TCACACCCAAGAACAAGCACA-3′.

Statistics. Results are expressed as the mean ± SEM. Statistical significance between experimental groups was assessed using an unpaired two-sample Student's *t* test.

Online supplemental material. Fig. S1 shows normal A20 expression in $A20^{FL}$ mice. Fig. S2 shows the number of apoptotic IECs and the number of proliferating IECs after TNF treatment. Fig. S3 shows AST and ALT levels in serum after TNF treatment. Fig. S4 shows normal A20 expression in liver from $A20^{IEC\text{-}KO}$ mice.

We are grateful to Dr. Deborah Gumucio and Dr. Blair Madison for donating the Villin-Cre transgenic mouse, and to David Komander for kindly providing purified A20 OTU domain. We thank Tino Hochepied for transgenic services, and Pieter Rottiers, Janneke Samsom, Anje Cauwels, Claude Libert, and Filip Van Hauwermeiren for helpful discussions and suggestions. We are grateful to Dimitri Huyghebaert, Laetitia Bellen, and Carine Van Laere for animal care.

L. Vereecke is a PhD fellow with the Instituut voor Innovatie door Wetenschap en Technologie (IWT), C. Mc Guire is a PhD fellow with the Fonds voor Wetenschappelijk Onderzoek-Vlaanderen (FWO), and G. van Loo is a postdoctoral researcher with the FWO. G. van Loo is also supported by a Marie Curie Reintegration Grant from the sixth EU Framework Program (FP6-ERG-2005-031063) and an FWO Odysseus Grant. Work in the authors' laboratory is further supported by research grants from the Interuniversity Attraction Poles program (IAP6/18), the FWO, the Belgian Foundation against Cancer, the Strategic Basis Research program of the IWT, the Centrum voor Gezwelziekten, and the Concerted Research Actions (GOA) and Group-ID MRP of the Ghent University.

The authors declare no competing financial interests.

Submitted: 19 November 2009
Accepted: 5 May 2010

REFERENCES

Ameloot, P., N. Takahashi, B. Everaerdt, J. Hostens, H.P. Eugster, W. Fiers, and P. Brouckaert. 2002. Bioavailability of recombinant tumor necrosis factor determines its lethality in mice. *Eur. J. Immunol.* 32:2759–2765. doi:10.1002/1521-4141(2002010)32:10<2759::AID-IMMU2759>3.0.CO;2-L

Arsenescu, R., M.E. Bruno, E.W. Rogier, A.T. Stefka, A.E. McMahan, T.B. Wright, M.S. Nasser, W.J. de Villiers, and C.S. Kaetzel. 2008. Signature biomarkers in Crohn's disease: toward a molecular classification. *Mucosal Immunol.* 1:399–411. doi:10.1038/mi.2008.32

Artis, D. 2008. Epithelial-cell recognition of commensal bacteria and maintenance of immune homeostasis in the gut. *Nat. Rev. Immunol.* 8:411–420. doi:10.1038/nri2316

Barmada, M.M., S.R. Brant, D.L. Nicolae, J.P. Achkar, C.I. Panhuysen, T.M. Bayless, J.H. Cho, and R.H. Duerr. 2004. A genome scan in 260 inflammatory bowel disease-affected relative pairs. *Inflamm. Bowel Dis.* 10:15–22. doi:10.1097/00054725-200401000-00002

Baumgart, D.C., and S.R. Carding. 2007. Inflammatory bowel disease: cause and immunobiology. *Lancet*. 369:1627–1640. doi:10.1016/S0140-6736(07)60750-8

Ben-Neriah, Y., and M. Schmidt-Supprian. 2007. Epithelial NF-kappaB maintains host gut microflora homeostasis. *Nat. Immunol*. 8:479–481. doi:10.1038/ni0507-479

Boone, D.L., E.E. Turer, E.G. Lee, R.C. Ahmad, M.T. Wheeler, C. Tsui, P. Hurley, M. Chien, S. Chai, O. Hitotsumatsu, et al. 2004. The ubiquitin-modifying enzyme A20 is required for termination of Toll-like receptor responses. *Nat. Immunol*. 5:1052–1060. doi:10.1038/ni1110

Coornaert, B., I. Carpentier, and R. Beyaert. 2009. A20: central gatekeeper in inflammation and immunity. *J. Biol. Chem*. 284:8217–8221. doi:10.1074/jbc.R800032200

Heyninck, K., and R. Beyaert. 2005. A20 inhibits NF-kappaB activation by dual ubiquitin-editing functions. *Trends Biochem. Sci*. 30:1–4. doi:10.1016/j.tibs.2004.11.001

Hitotsumatsu, O., R.C. Ahmad, R. Tavares, M. Wang, D. Philpott, E.E. Turer, B.L. Lee, N. Shiffin, R. Advincula, B.A. Malynn, et al. 2008. The ubiquitin-editing enzyme A20 restricts nucleotide-binding oligomerization domain containing 2-triggered signals. *Immunity*. 28:381–390. doi:10.1016/j.immuni.2008.02.002

Jin, Z., Y. Li, R. Pitti, D. Lawrence, V.C. Pham, J.R. Lill, and A. Ashkenazi. 2009. Cullin3-based polyubiquitination and p62-dependent aggregation of caspase-8 mediate extrinsic apoptosis signaling. *Cell*. 137:721–735. doi:10.1016/j.cell.2009.03.015

Köntgen, F., and C.L. Stewart. 1993. Simple screening procedure to detect gene targeting events in embryonic stem cells. *Methods Enzymol*. 225:878–890. doi:10.1016/0076-6879(93)25055-7

Lee, E.G., D.L. Boone, S. Chai, S.L. Libby, M. Chien, J.P. Lodolce, and A. Ma. 2000. Failure to regulate TNF-induced NF-kappaB and cell death responses in A20-deficient mice. *Science*. 289:2350–2354. doi:10.1126/science.289.5488.2350

Lewis, M., L.A. Tartaglia, A. Lee, G.L. Bennett, G.C. Rice, G.H. Wong, E.Y. Chen, and D.V. Goeddel. 1991. Cloning and expression of cDNAs for two distinct murine tumor necrosis factor receptors demonstrate one receptor is species specific. *Proc. Natl. Acad. Sci. USA*. 88:2830–2834. doi:10.1073/pnas.88.7.2830

Luo, J.L., H. Kamata, and M. Karin. 2005. The anti-death machinery in IKK/NF-kappaB signaling. *J. Clin. Immunol*. 25:541–550. doi:10.1007/s10875-005-8217-6

Madison, B.B., L. Dunbar, X.T. Qiao, K. Braunstein, E. Braunstein, and D.L. Gumucio. 2002. Cis elements of the villin gene control expression in restricted domains of the vertical (crypt) and horizontal (duodenum, cecum) axes of the intestine. *J. Biol. Chem*. 277:33275–33283. doi:10.1074/jbc.M204935200

Nenci, A., C. Becker, A. Wullaert, R. Gareus, G. van Loo, S. Danese, M. Huth, A. Nikolaev, C. Neufert, B. Madison, et al. 2007. Epithelial NEMO links innate immunity to chronic intestinal inflammation. *Nature*. 446:557–561. doi:10.1038/nature05698

Neurath, M.F., I. Fuss, M. Pasparakis, L. Alexopoulou, S. Haralambous, K.H. Meyer zum Büschenfelde, W. Strober, and G. Kollias. 1997. Predominant pathogenic role of tumor necrosis factor in experimental colitis in mice. *Eur. J. Immunol*. 27:1743–1750. doi:10.1002/eji.1830270722

Opipari, A.W. Jr., H.M. Hu, R. Yabkowitz, and V.M. Dixit. 1992. The A20 zinc finger protein protects cells from tumor necrosis factor cytotoxicity. *J. Biol. Chem*. 267:12424–12427.

Pasparakis, M. 2008. IKK/NF-kappaB signaling in intestinal epithelial cells controls immune homeostasis in the gut. *Mucosal Immunol*. 1:S54–S57. doi:10.1038/mi.2008.53

Podolsky, D.K. 2002. Inflammatory bowel disease. *N. Engl. J. Med*. 347:417–429. doi:10.1056/NEJMra020831

Rakoff-Nahoum, S., J. Paglino, F. Eslami-Varzaneh, S. Edberg, and R. Medzhitov. 2004. Recognition of commensal microflora by toll-like receptors is required for intestinal homeostasis. *Cell*. 118:229–241. doi:10.1016/j.cell.2004.07.002

Rakoff-Nahoum, S., L. Hao, and R. Medzhitov. 2006. Role of toll-like receptors in spontaneous commensal-dependent colitis. *Immunity*. 25:319–329. doi:10.1016/j.immuni.2006.06.010

Renner, F., and M.L. Schmitz. 2009. Autoregulatory feedback loops terminating the NF-kappaB response. *Trends Biochem. Sci*. 34:128–135. doi:10.1016/j.tibs.2008.12.003

Rodríguez, C.I., F. Buchholz, J. Galloway, R. Sequerra, J. Kasper, R. Ayala, A.F. Stewart, and S.M. Dymecki. 2000. High-efficiency deleter mice show that FLPe is an alternative to Cre-loxP. *Nat. Genet*. 25:139–140. doi:10.1038/75973

Round, J.L., and S.K. Mazmanian. 2009. The gut microbiota shapes intestinal immune responses during health and disease. *Nat. Rev. Immunol*. 9:313–323. doi:10.1038/nri2515

Schmidt-Supprian, M., W. Bloch, G. Courtois, K. Addicks, A. Israël, K. Rajewsky, and M. Pasparakis. 2000. NEMO/IKK gamma-deficient mice model incontinentia pigmenti. *Mol. Cell*. 5:981–992. doi:10.1016/S1097-2765(00)80263-4

Steinbrecher, K.A., E. Harmel-Laws, R. Sitcheran, and A.S. Baldwin. 2008. Loss of epithelial RelA results in deregulated intestinal proliferative/apoptotic homeostasis and susceptibility to inflammation. *J. Immunol*. 180:2588–2599.

Targan, S.R., S.B. Hanauer, S.J. van Deventer, L. Mayer, D.H. Present, T. Braakman, K.L. DeWoody, T.F. Schaible, and P.J. Rutgeerts. 1997. A short-term study of chimeric monoclonal antibody cA2 to tumor necrosis factor alpha for Crohn's disease. Crohn's Disease cA2 Study Group. *N. Engl. J. Med*. 337:1029–1035. doi:10.1056/NEJM199710093371502

Trynka, G., A. Zhernakova, J. Romanos, L. Franke, K.A. Hunt, G. Turner, M. Bruinenberg, G.A. Heap, M. Platteel, A.W. Ryan, et al. 2009. Coeliac disease-associated risk variants in TNFAIP3 and REL implicate altered NF-kappaB signalling. *Gut*. 58:1078–1083. doi:10.1136/gut.2008.169052

Turer, E.E., R.M. Tavares, E. Mortier, O. Hitotsumatsu, R. Advincula, B. Lee, N. Shifrin, B.A. Malynn, and A. Ma. 2008. Homeostatic MyD88-dependent signals cause lethal inflamMation in the absence of A20. *J. Exp. Med*. 205:451–464. doi:10.1084/jem.20071108

Vereecke, L., R. Beyaert, and G. van Loo. 2009. The ubiquitin-editing enzyme A20 (TNFAIP3) is a central regulator of immunopathology. *Trends Immunol*. 30:383–391. doi:10.1016/j.it.2009.05.007

Wang, J., Y. Ouyang, Y. Guner, H.R. Ford, and A.V. Grishin. 2009. Ubiquitin-editing enzyme A20 promotes tolerance to lipopolysaccharide in enterocytes. *J. Immunol*. 183:1384–1392. doi:10.4049/jimmunol.0803987

Wellcome Trust Case Control Consortium. 2007. Genome-wide association study of 14,000 cases of seven common diseases and 3,000 shared controls. *Nature*. 447:661–678. doi:10.1038/nature05911

Wertz, I.E., K.M. O'Rourke, H. Zhou, M. Eby, L. Aravind, S. Seshagiri, P. Wu, C. Wiesmann, R. Baker, D.L. Boone, et al. 2004. De-ubiquitination and ubiquitin ligase domains of A20 downregulate NF-kappaB signalling. *Nature*. 430:694–699. doi:10.1038/nature02794

Published June 7, 2010

JEM

SUPPLEMENTAL MATERIAL

Vereecke et al., http://www.jem.org/cgi/content/full/jem.20092474/DC1

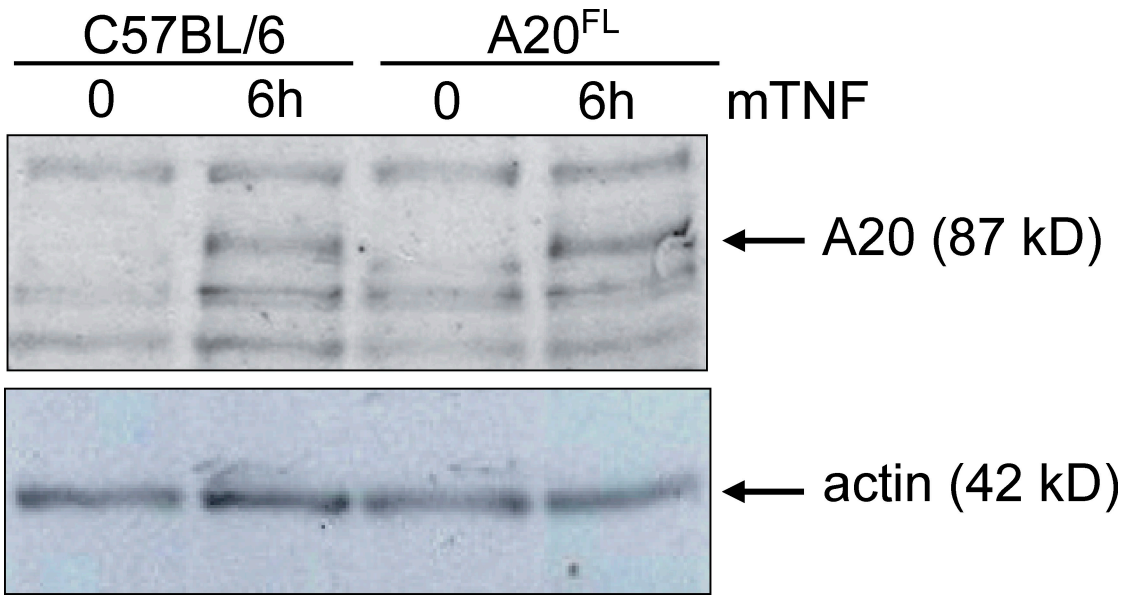

Figure S1. A20^{FL} mice express normal levels of A20. Western blot analysis for A20 expression in liver from a C57BL/6 WT and A20$^{FL/FL}$ mouse, 0 or 6 h after TNF injection. Data are representative of two independent experiments.

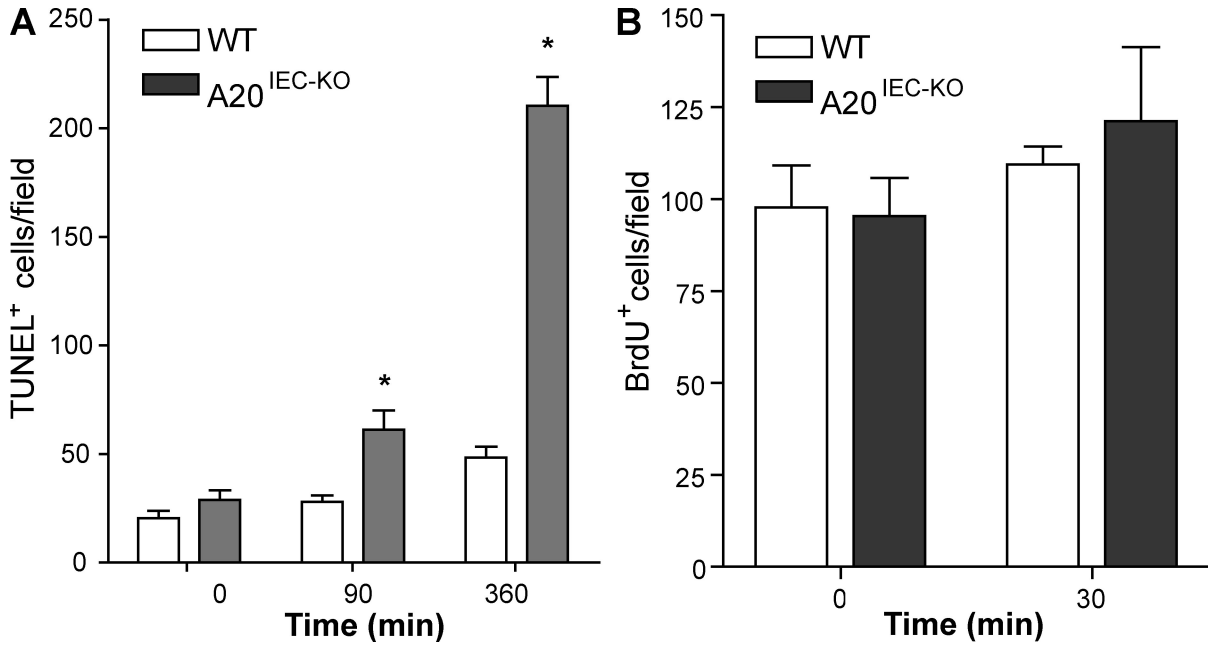

Figure S2. A20 deficiency in IECs sensitizes to TNF-induced damage. (A) Quantification of the number of TUNEL-positive cells/field from untreated and TNF-treated mice. Error bars represent SEM. *, $P < 0.05$. (B) Quantification of the number of BrdU-positive cells/field from untreated and TNF-treated mice. Data are representative of three independent experiments. Error bars represent SEM.

Published June 7, 2010

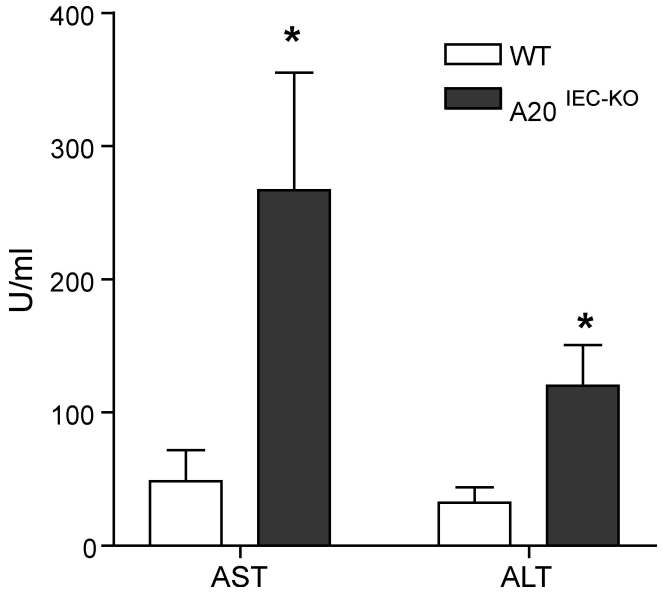

Figure S3. A20 deficiency in IECs sensitizes to TNF-induced liver damage. Serum from A20^{IEC-KO} (n = 9) and control WT littermate mice (n = 7) was collected 4 h after TNF injection and levels of AST and ALT enzymes were measured. Data are representative of two independent experiments. Error bars represent SEM. *, $P < 0.05$.

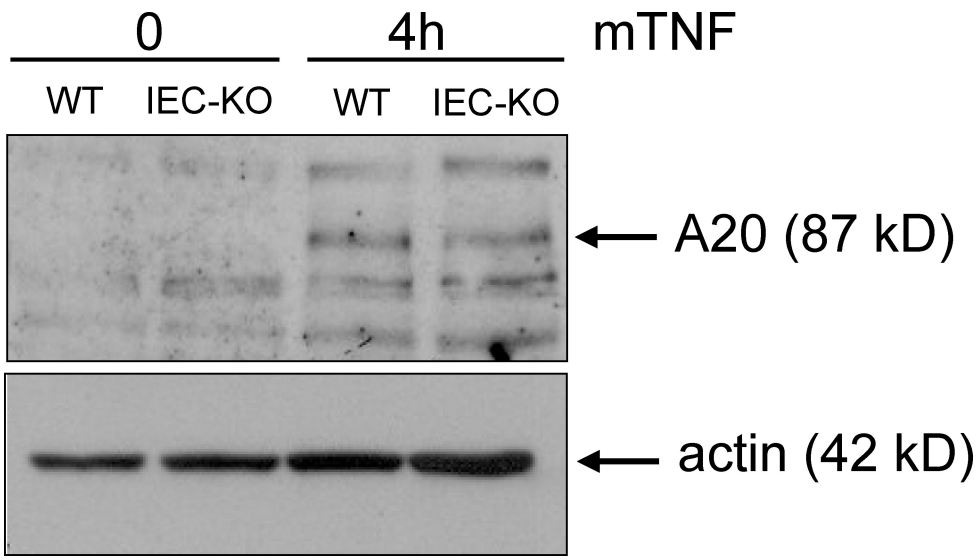

Figure S4. A20^{IEC-KO} mice express normal levels of A20 in liver. Western blot analysis for A20 expression in liver from A20^{IEC-KO} and control WT littermate mouse, 0 or 4 h after TNF injection. Data are representative of two independent experiments.

SUPPLEMENTAL MATERIAL

Vereecke et al., http://www.jem.org/cgi/content/full/jem.20092474/DC1

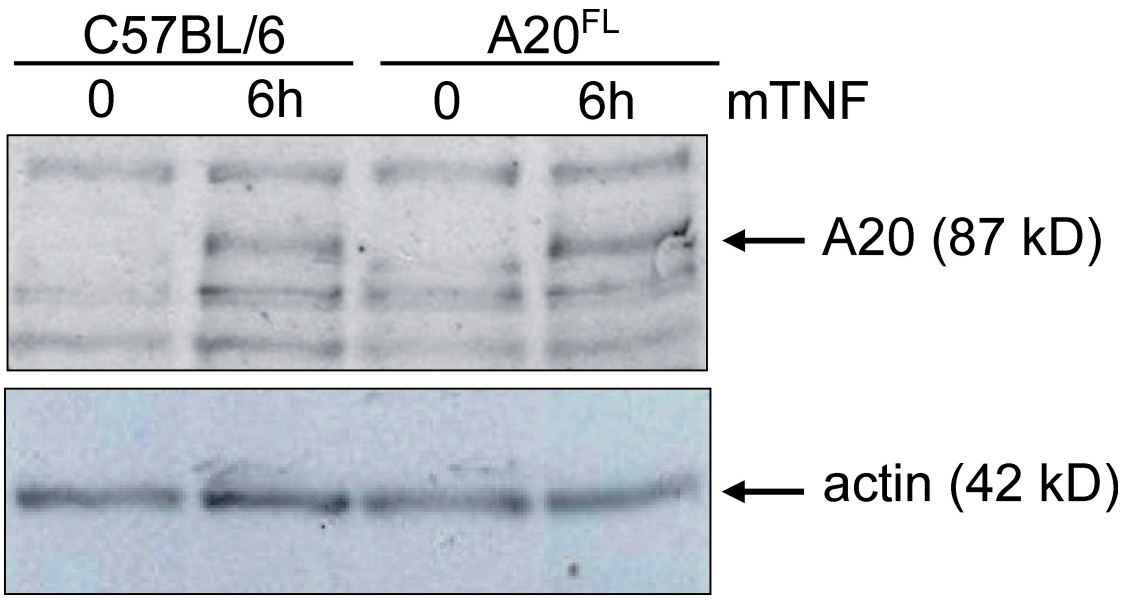

Figure S1. A20^{FL} mice express normal levels of A20. Western blot analysis for A20 expression in liver from a C57BL/6 WT and A20$^{FL/FL}$ mouse, 0 or 6 h after TNF injection. Data are representative of two independent experiments.

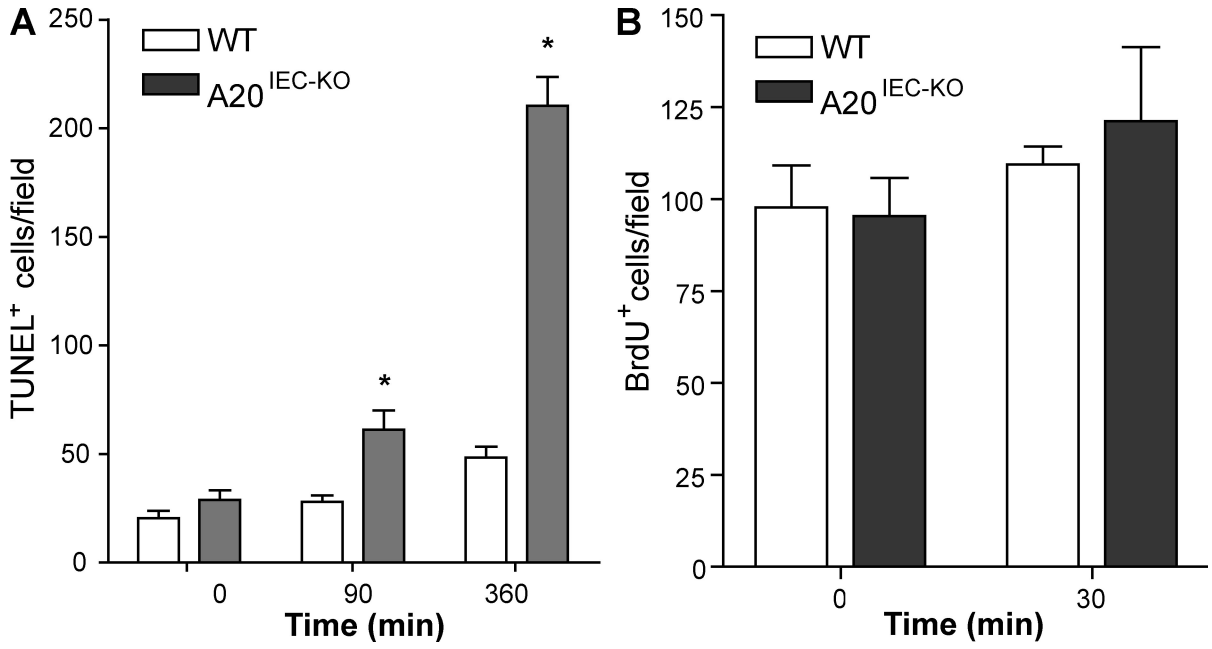

Figure S2. A20 deficiency in IECs sensitizes to TNF-induced damage. (A) Quantification of the number of TUNEL-positive cells/field from untreated and TNF-treated mice. Error bars represent SEM. *, $P < 0.05$. (B) Quantification of the number of BrdU-positive cells/field from untreated and TNF-treated mice. Data are representative of three independent experiments. Error bars represent SEM.

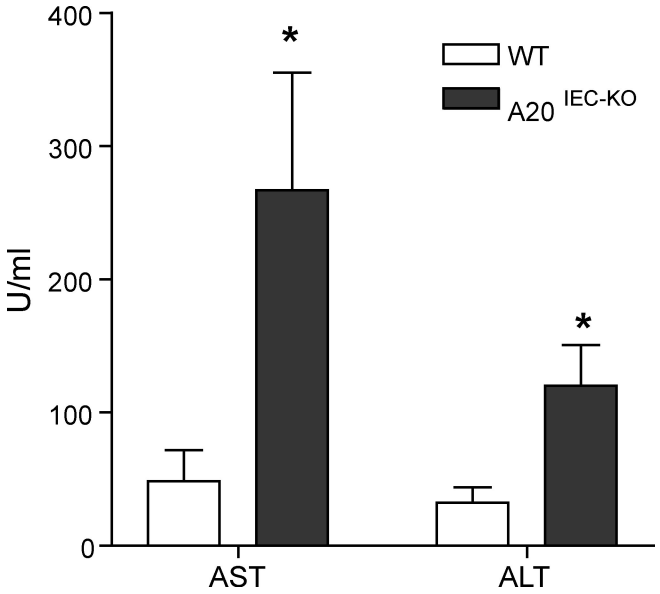

Figure S3. A20 deficiency in IECs sensitizes to TNF-induced liver damage. Serum from A20^{IEC-KO} (n = 9) and control WT littermate mice (n = 7) was collected 4 h after TNF injection and levels of AST and ALT enzymes were measured. Data are representative of two independent experiments. Error bars represent SEM. *, P < 0.05.

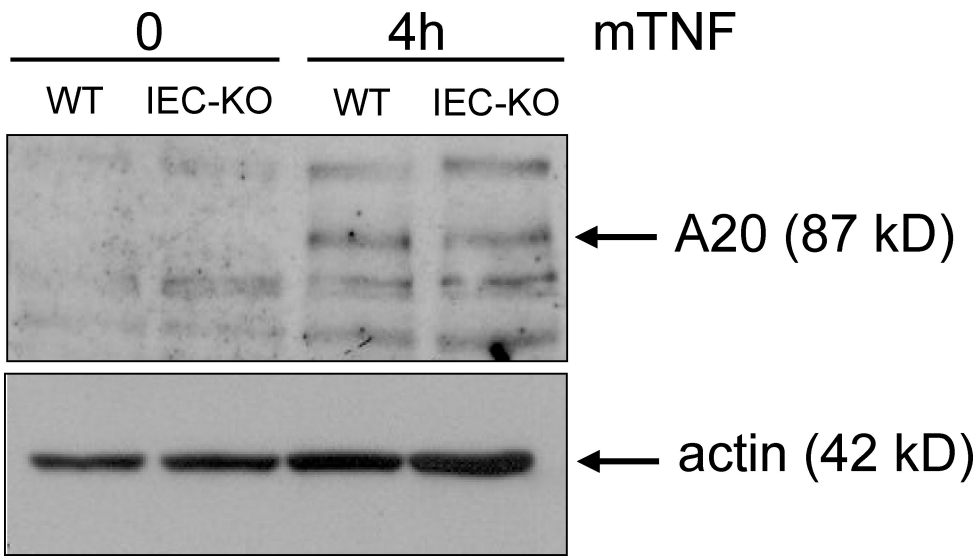

Figure S4. A20^{IEC-KO} mice express normal levels of A20 in liver. Western blot analysis for A20 expression in liver from A20^{IEC-KO} and control WT littermate mouse, 0 or 4 h after TNF injection. Data are representative of two independent experiments.

Paper II

blood

2011 117: 2227-2236
Prepublished online Nov 18, 2010;
doi:10.1182/blood-2010-09-306019

B cells lacking the tumor suppressor TNFAIP3/A20 display impaired differentiation and hyperactivation and cause inflammation and autoimmunity in aged mice

Yuanyuan Chu, J. Christoph Vahl, Dilip Kumar, Klaus Heger, Arianna Bertossi, Edyta Wójtowicz, Valeria Soberon, Dominik Schenten, Brigitte Mack, Miriam Reutelshöfer, Rudi Beyaert, Kerstin Amann, Geert van Loo and Marc Schmidt-Supprian

Blood (print ISSN 0006-4971, online ISSN 1528-0020), is published weekly by the American Society of Hematology, 2021 L St, NW, Suite 900, Washington DC 20036.

B cells lacking the tumor suppressor TNFAIP3/A20 display impaired differentiation and hyperactivation and cause inflammation and autoimmunity in aged mice

Yuanyuan Chu,[1] J. Christoph Vahl,[1] Dilip Kumar,[1] Klaus Heger,[1] Arianna Bertossi,[1] Edyta Wójtowicz,[1] Valeria Soberon,[1] Dominik Schenten,[2] Brigitte Mack,[3] Miriam Reutelshöfer,[4] Rudi Beyaert,[5] Kerstin Amann,[4] Geert van Loo,[5] and Marc Schmidt-Supprian[1]

[1]Max Planck Institute of Biochemistry, Martinsried, Germany; [2]Yale University School of Medicine, New Haven, CT; [3]Department of Otorhinolaryngology, Head and Neck Surgery, Grosshadern Medical Center, Ludwig-Maximilians-University of Munich, Munich, Germany; [4]Universitätsklinikum Erlangen, Pathologisches Institut, Abt Nephropathologie, Erlangen, Germany; and [5]Department for Molecular Biomedical Research, VIB and Department of Biomedical Molecular Biology, Ghent University, Ghent, Belgium

The ubiquitin-editing enzyme A20/*TNFAIP3* is essential for controlling signals inducing the activation of nuclear factor-κB transcription factors. Polymorphisms and mutations in the *TNFAIP3* gene are linked to various human autoimmune conditions, and inactivation of A20 is a frequent event in human B-cell lymphomas characterized by constitutive nuclear factor-κB activity. Through B cell-specific ablation in the mouse, we show here that A20 is required for the normal differentiation of the marginal zone B and B1 cell subsets. However, loss of A20 in B cells lowers their activation threshold and enhances proliferation and survival in a gene-dose–dependent fashion. Through the expression of proinflammatory cytokines, most notably interleukin-6, A20-deficient B cells trigger a progressive inflammatory reaction in naive mice characterized by the expansion of myeloid cells, effector-type T cells, and regulatory T cells. This culminates in old mice in an autoimmune syndrome characterized by splenomegaly, plasma cell hyperplasia, and the presence of class-switched, tissue-specific autoantibodies. (*Blood*. 2011;117(7):2227-2236)

Introduction

B cells play essential roles during protective immune responses to invading pathogens. On encounter of foreign antigen and with cognate T-cell help, B lymphocytes proliferate and form distinct histologic structures, termed germinal center (GC). In the GC, they undergo somatic hypermutation and class-switch recombination. During somatic hypermutation, they introduce random mutations into their immunoglobulin variable regions while they exchange the heavy chain constant region during class-switch recombination to allow for different effector functions. After a selection process by antigen, B cells differentiate into memory B cells and plasma cells (PCs), which secrete antibodies.[1] The deregulation of this process is heavily implicated in human disease. Production of class-switched antibodies against self-antigens causes or contributes to various autoimmune syndromes and unrestrained B-cell proliferation and survival can result in lymphomas.[1,2] It is thought that the majority of human lymphomas derive from the GC, probably because the DNA damage inherent to the GC reaction facilitates mutations and chromosomal translocations.[1,3]

Recently, the ubiquitin-editing enzyme A20, encoded by the tumor necrosis factor-α-inducible gene 3 (*TNFAIP3*), has been associated with both autoimmunity and lymphomagenesis. Polymorphisms and mutations in or near the *TNFAIP3* genomic locus have been linked with various human autoimmune syndromes with a strong humoral component, such as systemic lupus erythematosus (SLE),[4,5] rheumatoid arthritis,[6,7] and celiac disease.[8] Loss of A20 function through mutations, chromosomal deletions, and/or promoter methylation is a frequent event in several human lymphomas,[9-12] all of which are characterized by constitutive activation of nuclear factor-κB (NF-κB).[13] These factors regulate a plethora of genes encoding for proinflammatory mediators, antiapoptotic proteins, cell adhesion molecules and, for negative feedback control, inhibitory proteins, such as p100, IκBα, and A20.[14,15]

During the transmission of NF-κB activating signals from cell-surface receptors such as the B-cell receptor (BCR), CD40, or Toll-like receptors (TLRs), signal transduction occurs via the attachment of polyubiquitin chains to key proteins, including MALT1 or TRAF6. Polyubiquitin chains, linked via K63 or linear assembly, serve to recruit different kinase complexes. In the case of canonical NF-κB, induced proximity allows the upstream kinase TAK1 to phosphorylate its target IKK2, which then effects NF-κB activation. A20, whose transcription is induced by NF-κB, dampens signaling through 2 main activities. First, as deubiquitinase A20 removes K63-linked polyubiquitin chains from essential signaling intermediates, such as TRAF6. Second, A20 induces, in concert with other proteins, degradation of some of its molecular targets, through addition of K48-linked ubiquitin chains.[14,16] Degradation of RIP1 limits TNF-induced signaling,[14] whereas degradation of the K63-chain-specific E2 ligases Ubc13/UbcH5c generally affects the assembly of K63-linked polyubiquitin chains.[17]

Submitted September 8, 2010; accepted October 28, 2010. Prepublished online as *Blood* First Edition paper, November 18, 2010; DOI 10.1182/blood-2010-09-306019.

An Inside *Blood* analysis of this article appears at the front of this issue.

The online version of this article contains a data supplement.

The publication costs of this article were defrayed in part by page charge payment. Therefore, and solely to indicate this fact, this article is hereby marked "advertisement" in accordance with 18 USC section 1734.

To date, the main molecular action of A20 is to prevent prolonged NF-κB activation in response to stimulation of TNF-R, TLR-, or NOD-like receptors and the TCR.[14,16] Signal containment by A20 is crucial for immune homeostasis because A20-deficient mice die early on due to an uncontrolled inflammatory disease. The inflammation is triggered via MyD88-dependent TLRs by the commensal intestinal flora.[18] To study the cell-type-specific and cell-intrinsic roles of A20 in the mouse, we recently generated a conditional *Tnfaip3* allele ($A20^F$).[19] Given the implication of A20/TNFAIP3 in B-cell lymphomas and autoimmune diseases, we used B lineage-specific ablation of A20 to study its role in B-cell development, function, and disease.

Methods

Genetically modified mice

All mice described in this study are published and were originally generated using C57BL/6 ES cells, or backcrossed to C57BL/6 at least 6 times. Mice were housed in the specific pathogen-free animal facility of the Max Planck Institute. All animal procedures were approved by the Regierung of Oberbayern.

Flow cytometry

Single-cell suspensions were prepared[20] and stained with monoclonal antibodies: AA4.1(AA4.1), B220(RA3-6B2), CD1d(1B1), CD19(eBio1D3), CD22(2D6), CD23(B3B4), CD25(PC61.5), CD3(17A2), CD38(90) CD4(RM4-5), CD44(IM7), CD5(53-7.3), CD62L(MEL-14), CD69(H1.2F3), CD8(53-6.7), FoxP3(FJK-16s), GR-1(RB6-8C5), IgD(11-26), IgM(II/41), IL-10(JES5-16E3), IL-17A(eBio17B7), IL-4(11B11), IL-6(MP5-20F3), INF-γ(XMG1.2), Mac-1(M1/70), TCR-β(H57-597), TNF-α(MP6-XT22), CD95(15A7), CD21(7G6), CD86(GL-1), CD80(16-10A1), c-kit(2B8) (eBioscience), Ly-6G(1A8), Siglec-F(E50-2440), CD138(281-2) (BD Biosciences), and PNA (Vector Laboratories).

For intranuclear FoxP3 stainings (eBioscience) according to the manufacturer's instructions, dead cells were excluded with ethidium monoazide bromide. Samples were acquired on FACSCalibur and FACSCantoII (BD Biosciences) machines and analyzed with FlowJo software (TreeStar). For intracellular cytokine stainings, cells were stimulated for 5 hours at 37°C with 10nM phorbol myristate acetate (Calbiochem), 1mM ionomycin (Calbiochem), and 10nM brefeldin-A (Applichem). Cells were treated with Fc-block (eBioscience), and washed and surface-stained before fixation with 2% paraformaldehyde and permeabilization with 0.5% saponin. For in vitro culture, cells were purified by MACS (Miltenyi Biotec; > 85%-90% pure). Final concentrations of the activating stimuli: 2.5 μg/mL αCD40 (HM40–3, eBioscience), 10 μg/mL αIgM (Jackson ImmunoResearch Laboratories), 0.1μM CpG (InvivoGen), 20 μg/mL lipopolysaccharide (LPS; Sigma-Aldrich), and 4 ng/mL IL-4 (R&D Systems). Enzyme-linked immunosorbent assays were conducted using antibody pairs to IL-6 (BD Biosciences) and TNF (BD Biosciences). Cell-cycle analyses by propidium iodide (PI) and carboxyfluorescin diacetate succimidyl ester (CFDASE) were conducted as described.[20]

Real-time PCR

RNA was isolated (QIAGEN RNeasy Mini Kit) and reverse transcribed (Promega) for quantitative real-time polymerase chain reaction (PCR) using probes and primers from the Universal Probe Library (Roche Diagnostics) according to the manufacturer's instructions.

Biochemistry

B-cell whole-cell, cytoplasmic, and nuclear lysates were essentially prepared as published.[20] PVDF membranes were blotted with the following antibodies: p-IκBα, p-ERK, ERK, p-JNK, JNK, p-Akt, Akt, p-p38, p38, p100/p52 (Cell Signaling); IκBα, PLCγ2, RelB, RelA, c-Rel, Lamin B (Santa Cruz Biotechnology); tubulin (Upstate Biotechnology); p105/50 (Abcam); and A20.[19]

Immunofluorescence and immunohistochemistry

For immunofluorescence stainings, frozen 10-μm sections were thawed, air-dried, methanol-fixed, and stained for 1 hour at room temperature in a humidified chamber with B220-fluorescein isothiocyanate (eBioscience), biotinylated rat anti-CD3 (BD Biosciences), biotinylated rat anti-CD138 (BD Biosciences), and rabbit anti–laminin (gift from Michael Sixt) followed by Cy3-streptavidin and Cy5-conjugated anti–rabbit antibodies (Jackson ImmunoResearch). Immunohistochemically, MZB cells were identified by anti-CD1d (eBioscience) and metallophilic macrophages by anti-MOMA1 (Serotec). Detection of IgG immune complexes in paraformaldehyde-fixed kidney sections was performed using peroxidase-labeled anti–mouse IgG antibodies and 3-amino-9-ethylcarbazole staining (Vector Laboratories). For the detection of tissue-specific autoantibodies, frozen sections from organs of $Rag2^{-/-}$ mice were incubated with sera of aged and control mice and an anti–mouse IgG-Cy3 conjugate (Jackson ImmunoResearch Laboratories).

Images were acquired on a Zeiss Axiophot microscope (10×/0.3 or 20×/0.75 objectives; Carl Zeiss) using a Zeiss AxioCamMRm camera (Carl Zeiss) for monochromatic pictures and a Zeiss AxioCamMRC5 for RGB pictures. The following software programs were employed: Axiovision release 4.8 (Carl Zeiss), Photoshop CS4 and Illustrator CS4 (Adobe Systems).

Immunizations, ELISA

Mice were immunized intraperitoneally with 10 μg NP-Ficoll (Biosearch Technologies) and bled by the tail vein. Serum immunoglobulin concentrations and NP-specific antibodies were determined by ELISA.[21] The detection of antinuclear and anticardiolipin autoantibodies was performed using ELISA kits (Varelisa). Rheumatoid factor: ELISA plates were coated with rabbit IgG (Jackson ImmunoResearch Laboratories).

Results

Loss of A20 leads to defects in the generation and/or localization of mature B-cell subsets

To inactivate A20 specifically in B lineage cells at different developmental time points and to distinguish the specific effects of A20 ablation from potential artifacts inherent to individual cre-transgenic strains,[22] we initially investigated the consequences of CD19cre- and Mb1cre-mediated ablation of A20 in parallel (supplemental Figure 1A, available on the *Blood* Web site; see the Supplemental Materials link at the top of the online article). Because we did not observe any significant differences between $CD19cre/A20^{F/F}$ and $Mb1cre/A20^{F/F}$ mice in our experiments, we refer to them collectively as $B^{A20-/-}$ mice ($B^{A20+/-}$ for heterozygous deletion). Most of the experiments presented here were conducted using CD19cre. Efficient loss of the NF-κB–inducible A20 protein in B cells of these mice was confirmed by Western blot in both resting conditions and after treatment with LPS (Figure 1A).

Loss of A20 does not affect early B-cell development in the bone marrow, except for a minor increase in immature B cells. In contrast, the number of mature recirculating B cells is significantly reduced (supplemental Figure 1C-E). $B^{A20-/-}$ mice have enlarged spleens, coinciding with a minor increase in total B-cell numbers (supplemental Figure 1B; Figure 1B), suggesting that other cell types are also expanded. Mature follicular B-cell numbers are unaffected by A20 deficiency, but immature transitional B cells accumulate (Figure 1C-D) without any apparent block within the transitional compartment (supplemental Figure 2A). The numbers of marginal zone B (MZB) cells, defined by CD1d and CD21 expression (Figure 1C), are elevated because of an expansion of $CD23^+$ MZB precursor cells (Figure 1E; supplemental Figure 2B).

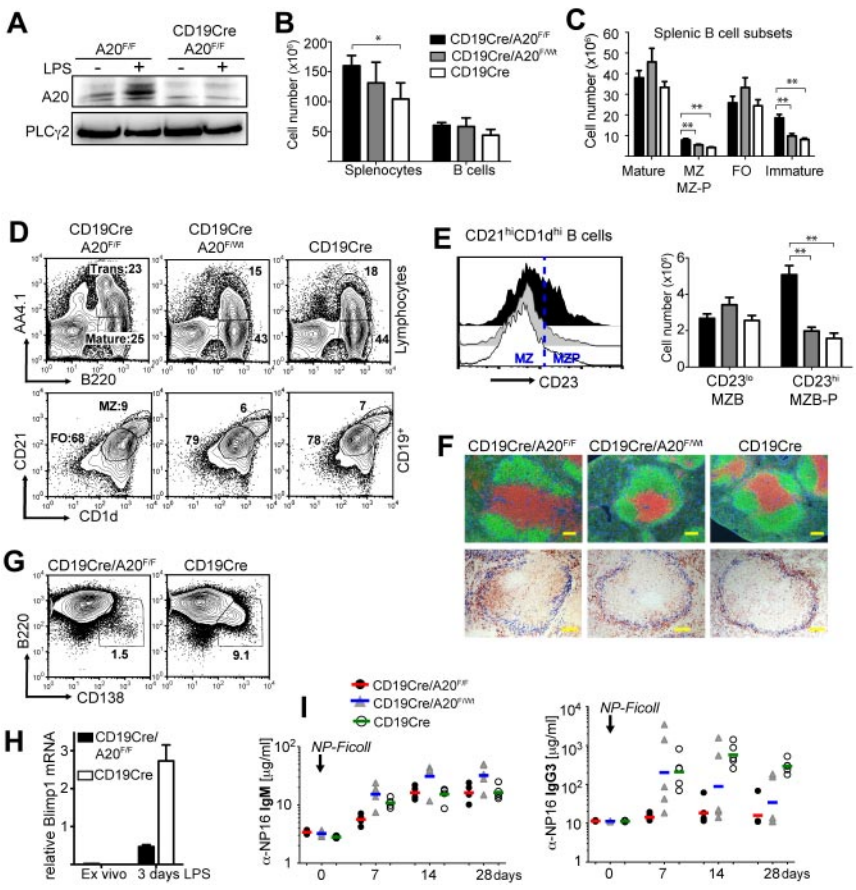

Figure 1. Conditional knockout of A20 in B cells induces severe defects in B-cell development and differentiation. (A) A20 protein expression in CD43-depleted B cells after 4-hour culture with or without 10 μg/mL LPS. (B-E) Absolute cell numbers were calculated from 5 to 7 age-matched mice per genotype. Data are mean ± SD. (B) Absolute splenocyte and B-cell numbers of the indicated genotypes. (C) Absolute cell numbers of splenic mature (B220^{+}AA4.1^{-}), marginal zone/marginal zone precursor (MZ; MZ-P: B220^{+}CD1d^{high}CD21^{high}), follicular (B220^{+}AA4.1^{-}CD1d^{-}CD23^{+}), and transitional (B220^{+}AA4.1^{+}) B cells. (D) Representative proportions of transitional (Trans: B220^{+}AA4.1^{+}) and mature (B220^{+}AA4.1^{-}) B cells of total lymphocytes (top panels) and of follicular (FO: CD1d^{int}CD21^{int}) and marginal zone/marginal zone precursor (MZ: CD1d^{high}CD21^{high}) B cells of CD19^{+} B cells (bottom panels) in the spleen. (E) CD23 expression on B220^{+}CD1d^{hi}CD21^{hi} B cells (left panel). Absolute cell numbers of marginal zone (B220^{+}CD1d^{hi}CD21^{hi}CD23^{lo}) and marginal zone precursor (B220^{+}CD1d^{hi}CD21^{hi}CD23^{hi}) B cells (right panel). (F) Top panels: Immunofluorescence of spleen sections: green represents αB220, B cells; red, αCD3, T cells; and blue, laminin. Bottom panels: Immunohistochemistry of spleen sections: blue represents MOMA-1, metallophilic macrophages; and brown, CD1d-expressing cells. Bar represents 100 μm. (G) Proportions of B220^{lo}CD138^{hi} plasma blasts in splenic B cells 3 days after LPS treatment. (H) Blimp1 mRNA expression relative to porphobilinogen deaminase was determined by real-time PCR in splenic B cells 3 days after LPS treatment. (I) Antigen-specific IgM and IgG3 serum titers in response to T-independent immunizations with 10 μg NP-Ficoll determined by ELISA. Lines represent geometric means for 5 mice per experimental group. *$P < .05$ (1-way analysis of variance). **$P < .001$ (1-way analysis of variance).

Inspection of the splenic follicular organization by immunofluorescence revealed normal B- and T-cell compartments in B$^{A20-/-}$ spleens (Figure 1F). However, in B$^{A20-/-}$ spleen sections, CD1d-expressing MZB cells are mostly located inside the follicle, whose border is defined by MOMA-1-expressing metallophilic macrophages located adjacent to the marginal sinus. In contrast, on B$^{A20+/-}$ and control spleen sections, CD1d-expressing cells are properly located in the marginal zone (Figure 1F). Immunofluorescent detection of laminin and B cells indicates that the B$^{A20-/-}$ splenic marginal zone is essentially devoid of B cells (supplemental Figure 2B), further demonstrating that A20-deficient MZB cells are not at their proper location. To test MZB cell function, we treated splenocyte cultures with LPS for 3 days and monitored the differentiation of short-lived plasma cells. At early times after activation of splenic B cells by LPS MZB cells, and to much lesser extent follicular B cells, differentiate into short-lived plasma cells.[23] As opposed to control B cells, A20-deficient splenic B cells show a profound defect in their ability to differentiate into Blimp1-expressing plasmablasts after LPS stimulation in vitro (Figure 1G-H), indicating the absence or paucity of functional MZB cells. Further underscoring this notion, B$^{A20-/-}$ mice display a significant reduction in the production of class-switched, antigen-specific IgG3 after immunizations with the TI-II antigen NP-Ficoll (Figure 1I), a response exquisitely dependent on the presence of MZB cells.[24] These results are in line with a significant reduction of total IgG3 serum levels in naive B$^{A20-/-}$ mice. IgG1 levels are also lower in these mice, whereas IgG2c and IgG2b levels are unchanged and IgM and IgA serum levels are strongly elevated (Figure 2A; supplemental Table 1). Supporting a role for A20 in B-cell differentiation and/or proper localization, peritoneal B1, especially B1a cells, are reduced in B$^{A20-/-}$ mice (Figure 2B; supplemental Figure 2E). In addition, thymic B cells are reduced in B$^{A20-/-}$ mice, although they appear elevated in B$^{A20+/-}$ mice (supplemental Figure 2D). Together, our results uncover several surprising deficiencies in the generation, differentiation, and/or maintenance of mature B-cell subsets in absence of A20. The affected subsets include MZB and B1 cells, which are thought to mediate the innate functions of the B lineage.[25]

A20-deficiency enhances GC B-cell formation in gut-associated lymphoid tissues

Given A20's role as negative regulator of NF-κB signaling, we expected A20-deficient B cells to be hyper-reactive to stimulation. We did not observe significant spontaneous GC formation in the spleens of the mice analyzed, indicating that spontaneous B-cell activation, if present in these mice, is not strong enough to induce GCs. In naive mice, gut-associated lymphoid tissue (GALT) is the place where B cells are constantly triggered by bacterial antigens to enter the GC.[26] The percentages and, to a lesser extent, absolute cell numbers of GC B cells in mesenteric lymph nodes and Peyer patches are increased in B$^{A20-/-}$ and B$^{A20+/-}$ mice (Figure 2C; and data not shown). This shows that, during B-cell activation by bacterial antigens in the GALT, strong hemizygous effects of A20 deficiency become apparent.

B cell–specific lack of A20 induces the spontaneous expansion of regulatory T, effector-type T, and myeloid cells

The increase in transitional and MZB precursor cell numbers is not sufficient to explain the higher splenocyte numbers in young B$^{A20-/-}$ mice (Figure 1B). Further detailed analyses showed that

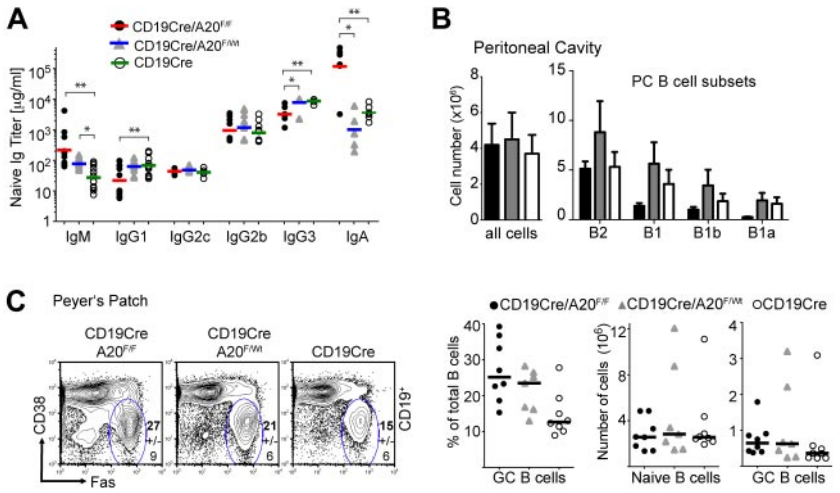

Figure 2. A20-deficiency impairs B1 cell generation but enhances GC formation in the GALT. (A) Titers of immunoglobulin isotypes were determined by ELISA; n = 6 to 12 per genotype. (B) Absolute cell numbers of B-cell subsets in the peritoneal cavity: B2 ($CD19^{+}B220^{+}$), B1 ($CD19^{high}B220^{low}$), B1a ($CD19^{high}B220^{low}CD5^{+}$), and B1b ($CD19^{high}B220^{low}CD5^{-}$) cell numbers were calculated from 5 to 7 age-matched mice per genotype. Data are mean ± SD. (C) Left panel: Proportions of GC ($CD19^{+}PNA^{hi}Fas^{hi}CD38^{lo}$) of total B cells in Peyer patches. Data are mean ± SD of 8 mice per genotype. Right panel: Proportions of GC B cells depicted as individual data points (left chart), absolute cell numbers for naive B cells (mantle zone B cells: $CD19^{+}PNA^{-}$ $Fas^{-}CD38^{hi}$; middle chart), and GC B cells (right chart). Bars represent medians of 8 mice per group (same as in the left panel). $^{*}P < .05$ (1-way analysis of variance). $^{**}P < .001$ (1-way analysis of variance).

homozygous and heterozygous ablation of A20 in B cells induces elevated numbers of T and myeloid cells. The sizes of many splenic T-cell compartments are increased in $B^{A20-/-}$ mice, especially the regulatory (Figure 3A-B), memory-type and effector-type CD4 (Figure 3B), and effector-type CD8 T cells (Figure 3C). Similar effects on T cells were observed in the lymph nodes (data not shown). The analysis of ex vivo T-cell cytokine production by intracellular staining revealed comparable proportions of IL-17–, interferon-γ– and TNF-producing cells between $B^{A20-/-}$ and control mice (Figure 3E). We were unable to detect any IL-4-producing cells (not shown). These analyses suggest the absence of detectable T-cell differentiation into specific T-helper lineages. The cell numbers of all splenic myeloid subsets analyzed were higher in $B^{A20-/-}$ compared with control mice, with significant increases in dendritic cells and eosinophils (Figure 3D). Importantly, heterozygous loss of A20 in B cells induces an intermediate phenotype (Figures 3A-D) in most aspects of this immune deregulation. $B^{A20+/-}$ mice contain even higher proportions of splenic regulatory and effector T cells than $B^{A20-/-}$ mice (Figure 3A). However, the higher absolute cell numbers of total CD4 T cells in $B^{A20-/-}$ mice leads to the greatest absolute cell numbers also in these subsets (Figure 3B). $B^{A20-/-}$ and $B^{A20+/-}$ mice contain elevated proportions of IL-10–producing B cells (supplemental Figure 2C), excluding the possibility that absence of this immune-regulatory B-cell subset[27] causes the perturbation in immune homeostasis. To validate that CD19cre mediates inactivation of A20 alleles only in B cells, we performed PCR on DNA purified from splenic cell subsets of $B^{A20-/-}$ mice. The purified T cells, dendritic cells, macrophages, and granulocytes contain less than 0.2% A20-knockout cells, which could be contaminating B cells (supplemental Figure 3). Our findings therefore indicate that the absence or gene-dose reduction of A20, specifically in B cells, induces an immune deregulation reminiscent of sterile inflammation, possibly held in check by regulatory lymphocyte subsets.

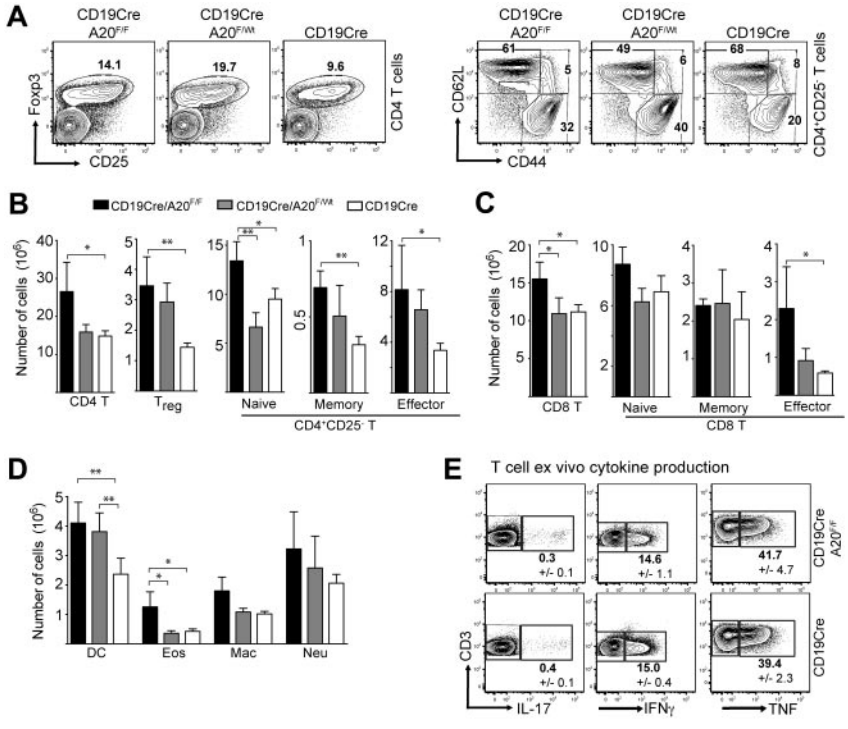

Figure 3. Ablation of A20 in the B-lineage has B cell-extrinsic effects on immune homeostasis. (A) Dot-plots showing percentages of $CD4^{+}Foxp3^{+}$ regulatory T cells and $CD4^{+}CD25^{-}$ T cells (naïve indicates $CD44^{int}CD62L^{hi}$; memory, $CD44^{hi}CD62L^{hi}$; and effector, $CD44^{hi}CD62L^{lo}$) in the spleen. Numbers indicate the mean of 4 to 6 mice for each genotype. (B-D) Absolute cell numbers of CD4 T (B), CD8 T (C), and myeloid cell (D) subsets in $B^{A20-/-}$, $B^{A20+/-}$, and CD19cre mice (n = 6 per group; 8-12 weeks old). Data are mean ± SD. Treg indicates $Foxp3^{+}$; naive, $CD44^{int}CD62L^{hi}$; memory, $CD44^{hi}CD62L^{hi}$; effector/memory, $CD44^{hi}CD62L^{lo}$; DC, dendritic cell ($CD11c^{+}$); Eos, eosinophils ($Gr1^{int}SiglecF^{+}$); Mac, macrophages ($Mac1^{+}Gr1^{lo}$); and Neu, neutrophils ($Gr1^{hi}Ly6G^{+}$). (E) Intracellular cytokine staining of ex vivo isolated splenocytes (gated on T cells). Numbers represent mean plus or minus SD of 3 mice per genotype. $^{*}P < .05$ (1-way analysis of variance). $^{**}P < .001$ (1-way analysis of variance).

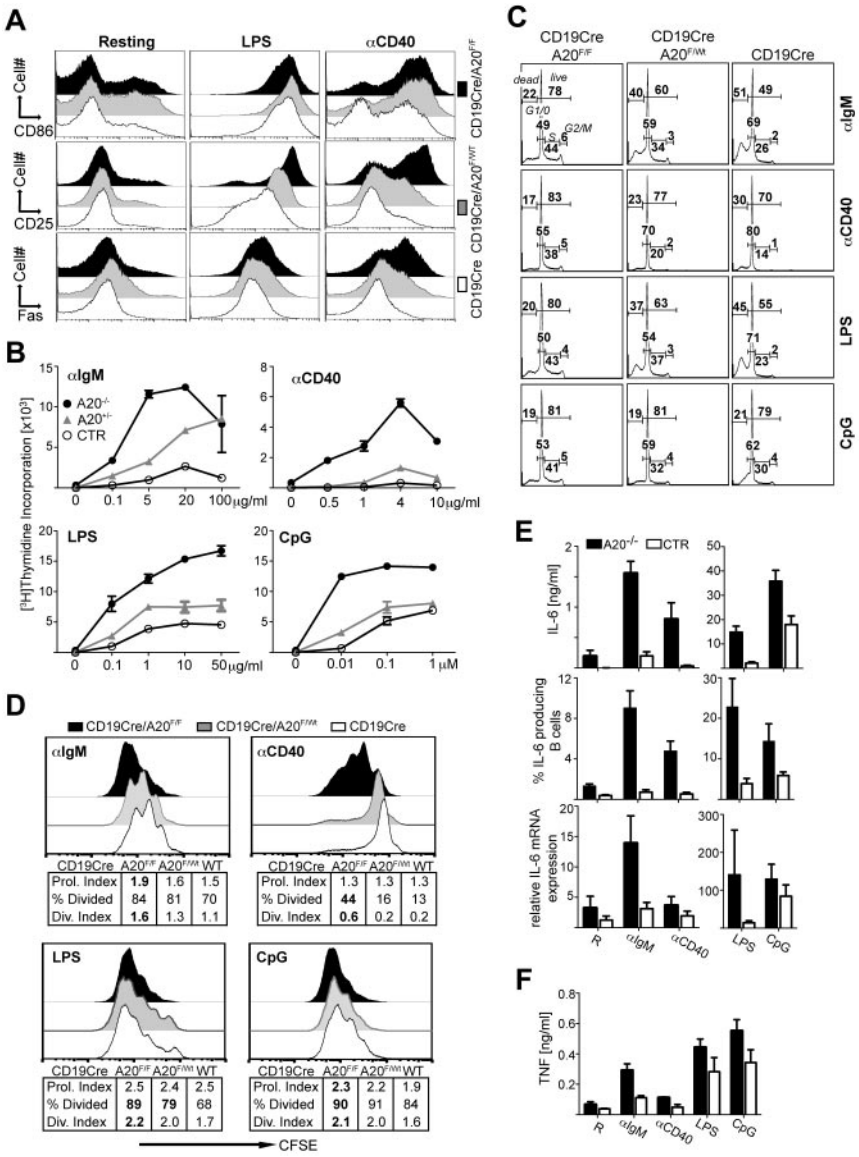

Figure 4. A20-deficiency amplifies B-cell responses. (A) Expression levels of the respective B-cell activation marker after overnight stimulation with LPS or αCD40. The dot-plots are representative of 3 to 6 independent experiments. (B) [^{3}H]Thymidine incorporation during a 10-hour pulse 48 hours after stimulation of B-cell cultures with αIgM, αCD40, LPS, or CpG. Data are mean ± SD of triplicate measurements. The experiment was repeated with similar results. (C) Cell cycle profile analysis by propidium iodide staining of B cells 2 days after stimulation with the indicated mitogens. Percentages of dead (sub G_0) and live cells are indicated at the top of each histogram. The distribution within the cell cycle was calculated with the FlowJo software Version 8.7.3 using the Watson model (values do not add up to 100%). Data are means of 2 independent experiments. (D) Assessment of proliferation by the carboxyfluorescein succinimidyl ester dilution assay: histograms represent carboxyfluorescein succinimidyl ester intensities 3 days after stimulation. The tables under each histogram show the proliferation index (Prol. Index: average number of divisions of the proliferating cells), the percentage of dividing cells (% Divided: the proportion of cells that initially started to divide), and the division index (Div. Index: average number of divisions of all cells); values were calculated with the FlowJo software. Data represent the means of 5 independent experiments, and bold values are significantly different ($P < .05$) from wild-type according to 1-way analysis of variance analysis. (E) Evaluation of IL-6 production in overnight activated B cells by ELISA (top panels), intracellular FACS (middle panels), and real-time PCR (bottom panels). For intracellular FACS, B cells were stimulated for 3 days. cDNA was quantified relative to porphobilinogen deaminase. Data are mean ± SD of 3 independent experiments. (F) Quantification of TNF production by overnight-stimulated B cells via ELISA. Data are mean ± SD of 3 independent experiments.

A20 regulates B-cell responses in vitro in a gene-dose–dependent fashion

Our observations of enhanced GC B-cell formation in the GALT in B$^{A20-/-}$ and B$^{A20+/-}$ mice suggested the possibility that their B cells are more easily activated in this context. To analyze this in more detail, we first quantified the relative A20 mRNA expression at different time points after activation with αIgM, αCD40, LPS, CpG DNA, and TNF. All these stimuli induced a strong increase in A20 mRNA, peaking at approximately 1 hour (supplemental Figure 4A), prompting us to test the in vitro responses of purified A20-deficient and A20$^{+/-}$ B cells to these mitogens. B cells up-regulate certain cell surface molecules (activation markers) upon activation, among them B7.1/CD80, B7.2/CD86, MHC II, CD25, and Fas. The expression of these markers was already slightly higher in unstimulated B cells purified from B$^{A20-/-}$ and B$^{A20+/-}$ mice compared with control B cells (Figure 4A; supplemental 4B). This is probably because of the latent immune activation we observed in these mice. Upon activation with the indicated mitogens, A20-deficient B cells produced higher surface levels of many activation markers (Figure 4A; supplemental Figure 3B). B cells carrying one functional A20 allele showed an intermediate phenotype regarding expression of these activation markers (Figure 4A). We then monitored αIgM-, αCD40-, LPS-, and CpG DNA-induced proliferation by 3 assays: Both [^{3}H]thymidine incorporation (Figure 4B) and cell cycle analysis (Figure 4C) showed increased proliferative activity in the A20-deficient B-cell cultures in response to all stimuli, and quantification of live cells revealed increased survival after all stimuli, except for CpG DNA (Figure 4C). By CFSE dilution assay (Figure 4D), we determined that the absence of A20 increased the proportion of B cells that initially start to divide (% divided) in response to αCD40 and LPS. Only CpG DNA and BCR crosslinking enhanced the proliferation of dividing A20-deficient B cells (Proliferation Index; Figure 4D). Combination of stimuli, such as LPS and αIgM, or the addition of IL-4, did not yield additive effects (supplemental Figure 4C). In all stimulations, the magnitude of the A20$^{+/-}$ B-cell response was in between A20$^{-/-}$ and control B cells (Figure 4B-D). Taken together, our studies show that reduction of A20 function magnifies B-cell responses through 3 mechanisms, depending on the activating stimulus: lowering the threshold for initial activation (αCD40, LPS), protecting activated B cells against apoptosis (αIgM, αCD40, LPS), and enhancing the proliferation of cells that were activated to divide (αIgM, CpG).

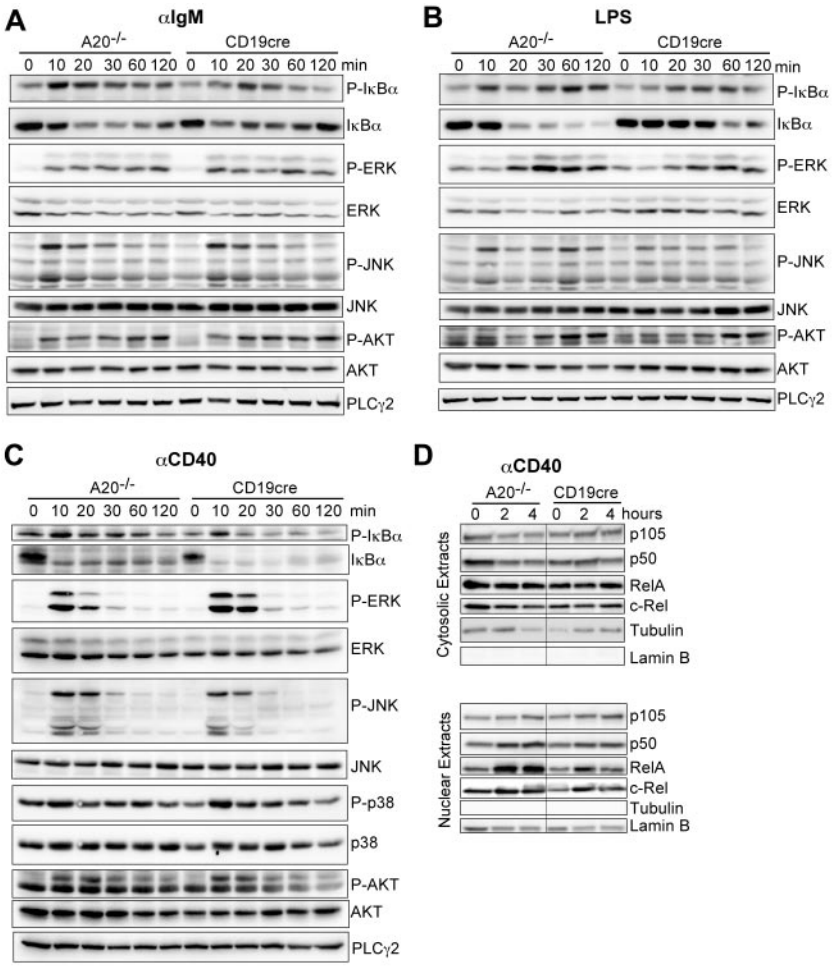

Figure 5. A20 controls canonical NF-κB activation in response to B-cell mitogens. (A-C) Western blot of whole cell lysates stimulated for the indicated time points with (A) 10 μg/mL αIgM, (B) 20 μg/mL LPS, and (C) 10 μg/mL αCD40. (D) Western blots on cytoplasmic and nuclear extracts after stimulation with αCD40. Results are representative of 2 or 3 independent experiments.

A20-deficient B cells exhibit spontaneous IL-6 secretion and highly elevated IL-6 secretion on activation

In light of the T effector and myeloid cell expansion, we wondered whether the higher excitability of A20-deficient B cells leads to secretion of proinflammatory cytokines, which in turn affect the differentiation and expansion of immune cells. IL-6 is a pleiotropic cytokine with inflammatory activity, and its levels are up-regulated in various autoimmune diseases, such as rheumatoid arthritis and SLE.[28] Activated A20-deficient B cells produced dramatically more IL-6 mRNA and protein than control B cells in response to all mitogens (Figure 4E). We could again detect an intermediate phenotype in $A20^{+/-}$ B cells (supplemental Figure 4D). Indeed, A20-deficient B cells spontaneously produced and released IL-6 into the cell culture medium in the absence of stimulation in comparable amounts to the IL-6 secretion in αIgM-stimulated control B cells (Figure 4E). A20-deficient B cells also produced slightly more TNF in response to all stimuli (Figure 4F). In accord with these findings, we detected more IL-6 and TNF-producing cells in ex vivo isolated A20-deficient compared with control B cells (supplemental Figure 4E). The evaluation of IL-6 production in immune cell subsets of 3- to 4-month-old $B^{A20-/-}$ mice by intracellular flow cytometry and real-time PCR revealed that, in addition to B cells, dendritic cells and, to a lesser extent, macrophages also produce IL-6 (supplemental Figure 5). This suggests that secondary activation of myeloid cells by A20-deficient B cells exacerbates the immune deregulation in $B^{A20-/-}$ mice.

A20 negatively regulates canonical NF-κB, but not MAPK or AKT activation, in response to engagement of the BCR, CD40, and TLRs

We established that A20 is a gene-dose–dependent negative regulator of B-cell activation in response to triggering of the BCR, CD40, and TLRs. A20 was reported to limit the activation of canonical NF-κB in response to various stimuli in other cell types.[14,16] Therefore, we wanted to confirm that the hyper-reactivity of A20-deficient B cells also correlates with enhanced canonical NF-κB activity in response to the stimuli used in our study. Indeed, the absence of A20 selectively enhances the activation of the canonical NF-κB pathway, evidenced by prolonged increased IκBα phosphorylation and degradation (Figure 5A-C). The activation of MAPK pathways or AKT phosphorylation was unaltered in response to αIgM, LPS, and αCD40 (Figure 5A-C). The increased IκBα phosphorylation correlated well with an increase in nuclear translocation of p50 and RelA 2 and 4 hours after activation with αCD40 (Figure 5D). We detected elevated expression of p100 and RelB, substrates of the alternative NF-κB pathway and transcriptional targets of canonical NF-κB in whole cell extracts of A20-deficient B cells (data not shown) in accord with the higher canonical NF-κB activity in these cells. Taken together, although we do not rule out that A20 has additional functions, we demonstrate that deficiency for A20 in B cells strongly enhances activation of the canonical NF-κB pathway in response to BCR cross-linking (antigen), T-cell costimulation (αCD40), and microbial components (TLRs).

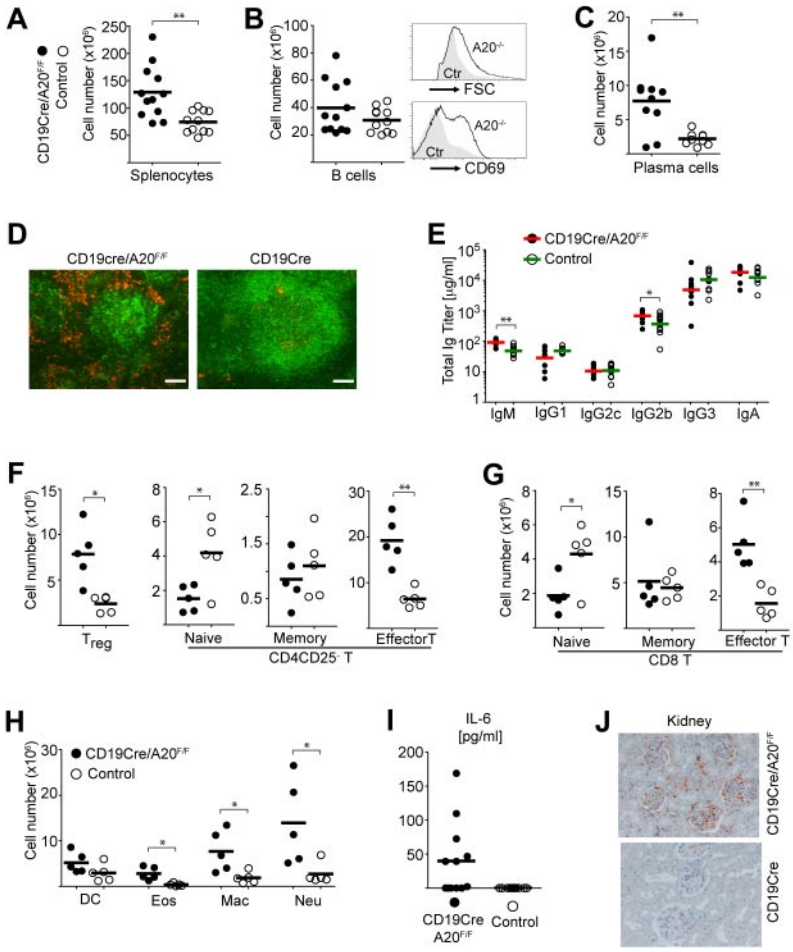

Figure 6. Splenomegaly and plasma cell hyperplasia in old B$^{A20-/-}$ mice. Cohort description: age range, 60 to 85 weeks; mean age of experimental group, 68 weeks; mean age of control group, 66 weeks. (A) Absolute cell numbers of splenocytes (n(B$^{A20-/-}$) = 10, n(control) = 9). (B) Left panel: Absolute cell numbers of B cells (CD19^{+}; n(B$^{A20-/-}$) = 12, n(control) = 11). Right panel: Representative size and CD69 expression of splenic B220^{+} B cells. (C) Absolute cell numbers of splenic plasma cells (B220^{lo}CD138^{hi}; n(B$^{A20-/-}$) = 10, n(control) = 9). (D) Representative immunofluorescence analysis of plasma cells in the spleen, plasma cells (red represents αCD138), B cells (green represents αB220). Bar represents 100 μm. (E) Titers of immunoglobulin isotypes in aged mice were determined by ELISA; n(B$^{A20-/-}$) = 12, n(control) = 11. (F-H) Absolute splenic cell numbers for the following cellular subsets: CD4 T cells. (F) Treg (CD4^{+}CD25^{+}); CD4^{+} naive (CD25^{-}CD44^{int}CD62L^{hi}), memory-type (CD25^{-}CD44^{hi}CD62L^{hi}), and effector T (CD4^{+}CD44^{hi}CD62L^{lo}); CD8-T cells. (G) Naive (CD44^{int}CD62L^{hi}), memory-type (CD44^{hi}CD62L^{hi}), and effector T (CD44^{hi}CD62L^{lo}); myeloid cells (H): DC indicates dendritic cell (CD11c^{+}); Eos, eosinophils (Gr1^{int}SiglecF^{+}); Mac, macrophages (Mac1^{+}Gr1^{lo}); and Neu, neutrophils (Gr1^{hi}Ly6G^{+}). n(B$^{A20-/-}$) = 5, n(control) = 5. (I) Serum IL-6 (pg/mL) in aged mice was measured by ELISA; n(B$^{A20-/-}$) = 12, n(control) = 11. (J) Representative stainings of IgG immune complexes in kidneys of B$^{A20-/-}$ and control mice. Original magnification × 20. *$P < .05$ (1-way analysis of variance). **$P < .001$ (1-way analysis of variance).

Loss of A20 in B cells leads to autoimmune pathology in old mice

To assess the impact of the chronic proinflammatory state induced by B cell-specific loss of A20 in old age, we aged a cohort of B$^{A20-/-}$ and control mice. Histologic analysis of organs from 20-week-old B$^{A20-/-}$ mice did not yield any signs of inflammation (not shown). B$^{A20-/-}$ mice, more than one year old, on the contrary, were characterized by splenomegaly (Figure 6A; supplemental Figure 6A-B). Although total B-cell numbers were not significantly elevated in old B$^{A20-/-}$ compared with control mice, all A20$^{-/-}$ B cells appeared activated, as judged by the larger cell size and elevated levels of the activation marker CD69 (Figure 6B). In addition, we observed a marked expansion of PCs in the spleen (Figure 6C; supplemental Figure 6C), but not in the bone marrow (data not shown). Immunofluorescence analysis of the enlarged spleens revealed a diffuse pattern of PCs surrounding altered and disrupted B-cell follicles (Figure 6D). Analysis of the serum isotype titers in aged B$^{A20-/-}$ mice revealed higher IgM titers compared with controls, as seen in young mice. However, in contrast to the latter, in old B$^{A20-/-}$ mice the levels of the pathogenic IgG2b isotype[29] are elevated (Figure 6E; supplemental Table 2). The increase of effector and regulatory T cells, already apparent in young B$^{A20-/-}$ mice, has further expanded in old mice, at the expense of the respective naive compartments (Figure 6F-G). In addition, the expansion of myeloid cell subsets was much more pronounced (Figure 6H). The progressive nature of the inflammation in the B$^{A20-/-}$ mice is also reflected in elevated levels of serum IL-6 in aged B$^{A20-/-}$ mice (Figure 6I), which could not be detected in the 20-week-old B$^{A20-/-}$ mice (not shown). Histologic analysis of organs from aged mice revealed inflammatory infiltrates in the liver and kidney of most of the old B$^{A20-/-}$ mice (supplemental Figure 6D). Examinations of the renal pathology revealed no extensive glomerular damage but clear IgG immune complex depositions in aged B$^{A20-/-}$ mice (Figure 6J).

Given this finding, we tested the sera of all old B$^{A20-/-}$ and control mice for indicators of self-recognition. Class-switched antibodies against nuclear self-antigens (ANAs) are the most common autoantibodies observed in autoimmune conditions in mice and humans.[30] Sera from B$^{A20-/-}$ mice did not contain significantly higher ANA levels than sera from the controls, and we also did not detect enhanced reactivity to endogenous red blood cells (Figure 7A). In addition, we observed increased levels of rheumatoid factor of the IgM isotype in some B$^{A20-/-}$ mice, but not of the IgG isotype (Figure 7A). However, we detected significantly elevated amounts of anticardiolipin IgG antibodies in aged B$^{A20-/-}$ mice (Figure 7A), demonstrating systemic class-switched autoimmune reactivity. To evaluate whether antiphospholipid antibodies are already detectable in younger mice, we screened the sera of 3-month-old mice. We detected elevated anticardiolipin IgG antibodies in sera from B$^{A20-/-}$ mice (and B$^{A20+/-}$ mice) compared with control sera, but the differences were not statistically significant (Figure 7C).

To screen for further autoreactivity against potentially tissue-specific self-antigens, we incubated organ sections of Rag2$^{-/-}$ mice with the sera of the aged mice. We detected autoreactive class-switched IgG antibodies in the sera of B$^{A20-/-}$, but not of

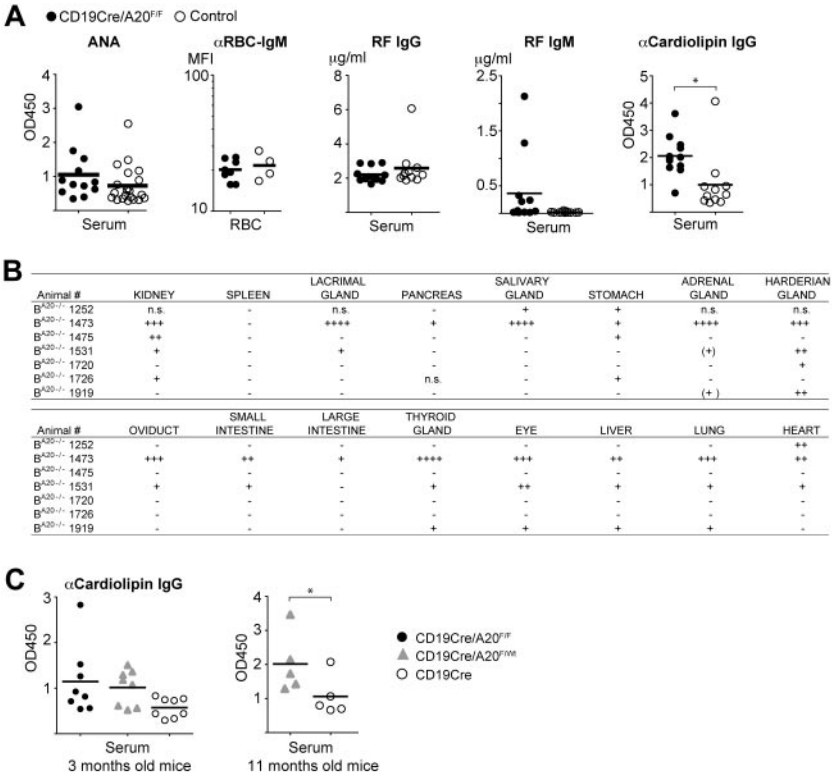

Figure 7. Autoimmune manifestations in old $B^{A20-/-}$ mice. (A) Analysis of autoantibodies in aged mice. ANA indicates that antinuclear IgG antibodies were detected by ELISA, n($B^{A20-/-}$) = 12, n(control) = 21; αRBC-IgM, antierythrocyte IgM was detected by FACS and represented as mean fluorescence intensity, n($B^{A20-/-}$) = 8, n(control) = 4. IgG and IgM rheumatoid factor (RF) was measured by ELISA; n($B^{A20-/-}$) = 12, n(control) = 11. α-Cardiolipin IgG antibodies were detected by ELISA; n($B^{A20-/-}$) = 12, n(control) = 11. *$P < .05$ (2-tailed unpaired Student t test). **$P < .001$ (2-tailed unpaired Student t test). (B) Table depicting the self-reactivity of sera from individual $B^{A20-/-}$ mice against the indicated organs from $Rag2^{-/-}$ mice. +, ++, and +++ indicate the severity of autoreactivity; and n.s., not screened. (C) Levels of α-cardiolipin IgG autoantibodies in 3-month-old mice (left panel; n = 8 per genotype) and in 11-month-old mice (right panel; n = 5 per genotype) were detected by ELISA. *$P < .05$ (1-tailed unpaired Student t test).

Animal #	KIDNEY	SPLEEN	LACRIMAL GLAND	PANCREAS	SALIVARY GLAND	STOMACH	ADRENAL GLAND	HARDERIAN GLAND
$B^{A20-/-}$ 1252	n.s.	-	n.s.	-	+	+	n.s.	n.s.
$B^{A20-/-}$ 1473	+++	-	++++	+	++++	+	++++	+++
$B^{A20-/-}$ 1475	++	-	-	-	-	+	-	-
$B^{A20-/-}$ 1531	+	-	+	-	-	-	(+)	++
$B^{A20-/-}$ 1720	-	-	-	-	-	-	-	+
$B^{A20-/-}$ 1726	+	-	-	n.s.	-	+	-	-
$B^{A20-/-}$ 1919	-	-	-	-	-	-	(+)	++

Animal #	OVIDUCT	SMALL INTESTINE	LARGE INTESTINE	THYROID GLAND	EYE	LIVER	LUNG	HEART
$B^{A20-/-}$ 1252	-	-	-	-	-	-	-	++
$B^{A20-/-}$ 1473	+++	++	+	++++	+++	++	+++	++
$B^{A20-/-}$ 1475	-	-	-	-	-	-	-	-
$B^{A20-/-}$ 1531	+	+	-	+	++	+	+	+
$B^{A20-/-}$ 1720	-	-	-	-	-	-	-	-
$B^{A20-/-}$ 1726	-	-	-	-	-	-	-	-
$B^{A20-/-}$ 1919	-	-	-	+	+	+	+	-

control mice, directed predominantly against kidney, harderian gland, stomach, thyroid gland, eye, liver, and lung (Figure 7B; supplemental Figure 6E). Pancreas, salivary, lacrimal, and adrenal glands were also recognized by sera from few $B^{A20-/-}$ mice but with a lower penetrance compared with the organs mentioned earlier (Figure 7B). Notably, the kidney was recognized by autoantibodies in the sera of the majority of $B^{A20-/-}$ mice. Therefore, we conclude that A20-deficient B cells induce chronic progressive inflammation, which results in significant autoimmune manifestations and pathologic alterations in old mice.

Discussion

The prevalent inactivation of the ubiquitin-editing enzyme A20 in human B-cell lymphoma and the linkage of polymorphisms in the A20/*TNFAIP3* gene to human autoimmune diseases raise the question of its function in the B-lineage, especially during B-cell activation.

The major molecular function of A20 uncovered to date is the negative regulation of canonical NF-κB activation.[14] We confirm that, also in B cells, A20 limits activation of this signaling pathway by all relevant physiologic inducers. Constitutive activation of canonical NF-κB in B cells induces B-cell hyperplasia, especially pronounced in MZB cells.[20] In contrast, we uncovered that A20 activity is required for the correct localization of MZB cells and for MZB cell function. Therefore, we conclude that proper differentiation of A20-deficient MZB cells does not take place. In addition, A20 is needed for the generation or cellular maintenance of peritoneal B1, bone marrow recirculating and thymic B cells, either directly or by mediating their correct localization. Reduced cellular maintenance could be caused by lower sensitivity to survival signals available in naive mice, but also by increased terminal differentiation because of their hyperactivatable state. The elevated IgA serum levels could be a consequence of the enhanced GC reactivity in the GALT of $B^{A20-/-}$ mice. Another possible explanation is that the lower levels of B1a cells could, at least in part, be caused by their enhanced differentiation to IgA-producing plasma cells in response to inducing signals, such as IL-15,[31] a cytokine known to induce NF-κB activation. This phenomenon could also contribute to the elevated IgM levels. Because B1 cells are thought to be the main source of naturally occurring autoantibodies in naive mice,[32] this could signify that also natural autoantibody IgM titers, which are not pathogenic but rather play a protective role, are enhanced in the $B^{A20-/-}$ mice. The accumulation of A20-deficient precursor populations (transitional B cells and MZB cell precursors) points to blocks in development, although we cannot exclude a role for impaired negative selection.

Taken together, our data on B-cell development and in vitro activation studies suggest the following: A20 activity is required to limit acute B-cell activation induced by stimuli connected to invasion by pathogens. Its absence reduces the activation threshold and enhances survival and proliferation in response to such stimuli. On the other side, the absence of A20 does not render B cells more responsive to maintenance signals required for mature resting cells.

Increased B cell–mediated IL-6 secretion resulting from sporadic local activation and, at least in the case of A20 deficiency, spontaneous production and release of IL-6 is a probable underlying cause of the effector T-cell differentiation and myeloid cell hyperplasia that we observed in $B^{A20-/-}$ and $B^{A20+/-}$ mice. Subsequent cytokine secretion by activated myeloid cells most probably amplifies this response. Indeed, Tsantikos et al recently showed that effector T-cell activation, myeloid cell expansion, and the development of autoimmune disease in Lyn-deficient mice, which strikingly resemble $B^{A20-/-}$ and $B^{A20+/-}$ mice in this regard, are entirely dependent on the secretion of IL-6.[33] Interestingly, the authors also observed expansion of $CD4^+CD25^+$ T cells but did not investigate whether they represent activated or regulatory

T cells.[33] The enhanced numbers of Tregs we observe in the B$^{A20-/-}$ and B$^{A20+/-}$ mice appear paradoxical in the context of elevated IL-6 levels.[34] We suggest that they expand and/or are induced in reaction to the IL-6-driven inflammation. However, the presence of IL-6 increases the resistance of effector T cells to suppression by regulatory T cells,[35] both systemically and locally. Expansion of Tregs has also been observed in the BWF1 mouse model for human SLE.[36] Whether, and to what extent, an expanded Treg population serves to keep the sterile inflammation in check is an intriguing question to be tested in future studies.

While this manuscript was in preparation, a study by Tavares et al on the same topic was published.[37] The authors also found a convincing gene-dose–dependent effect of A20 ablation on B-cell activation. They detected elevated levels of antibodies in the serum of CD19cre/A20$^{F/F}$ mice that recognize self-antigens on a protein array. However, in their approach, anti–mouse Ig was used to detect autoantibodies, which also recognizes IgM. Indeed, both studies find highly elevated titers of IgM in naive B$^{A20-/-}$ mice (in our case, a 10-fold difference in the geometric mean). Naturally occurring autoantibodies are mostly of the IgM isotype.[38,39] Therefore, the increased recognition of self observed by Tavares et al[37] could reflect, at least to some degree, this increase in natural autoantibodies. This possibility is substantiated by the fact that only IgM$^+$ dsDNA-recognizing plasma cells were detected and that IgM immune complex deposits were revealed in naive 6-month-old mice, in the absence of any sign of pathology.[37] Given that the role of IgM autoantibodies is also discussed as being protective,[38,39] it is unclear whether the autoreactivity observed in younger mice contributes to the development of, or helps to prevent, disease.

We observed significant autoreactivity of class-switched antibodies only in old mice, together with autoimmune pathology and inflammation. The chronic inflammation induced by the A20-deficient B cells perhaps contributes to a progressive break in B-cell tolerance resulting in the production of class-switched, autoreactive antibodies. The immune senescence of old age might also contribute to this break in tolerance.[32] The inflammatory microenvironment in the spleen, and potentially in other affected organs, together with the elevated presence of the pleiotropic cytokine IL-6, may serve as a niche for the (autoreactive) plasma cells. However, we do not detect significant levels of IgG ANAs, the hallmark of SLE.[30] Instead, we observe general IgG autoreactivity to cardiolipin, a common autoantigen in autoimmune disease[30,40] in old B$^{A20-/-}$ mice. The presence of tissue-specific class-switched autoantibodies strongly underscores the loss of tolerance. Some pathologic features of the old B$^{A20-/-}$ mice are reminiscent of human Castleman disease, namely, massive infiltrations of plasma cells and the elevated presence of IL-6.[28,41] It is indeed possible that the disturbed B-cell development, including the elevated levels of naturally occurring auto-IgM, are preventing a more severe syndrome. Heterozygous B$^{A20+/-}$ mice display inflammation and B-cell hyper-reactivity, but no developmental defects. Therefore, they might represent a good tool for modeling the reduced expression or function of A20 that should underlie the link between mutations and polymorphisms in A20/*TNFAIP3* and human autoimmune disease. Indeed, initial analyses revealed elevated class-switched antibodies against cardiolipin in a cohort of 11-month-old B$^{A20+/-}$ mice (Figure 7C).

We demonstrate here that selective loss of A20 in B cells is sufficient to cause an inflammatory syndrome with autoimmune manifestations in old mice. This condition is characterized by a progressive chronic inflammation, elevated levels of IL-6, dramatic plasma cell expansion, and the presence of class-switched systemic and tissue-specifc autoantibodies. The exquisite dose effects of monoallelic loss of A20 make it a prime target for deregulation by proinflammatory miRNAs and oncomirs in disease contexts. Our results demonstrate that B-cell hyper-reactivity caused by reduced A20 function can contribute to the observed link between inherited genetic mutations or polymorphisms in A20/*TNFAIP3* and various human autoimmune diseases.

Acknowledgments

The authors thank Reinhard Fässler for support; Julia Knogler and Barbara Habermehl for technical assistance; Reinhard Voll and Michael Sixt for advice; Guru Krishnamoorthy for help with thymidine incorporation assays; Ludger Klein for tissues of Rag2$^{-/-}$ mice; Claudia Uthoff-Hachenberg for ELISA reagents; and Michael Sixt, Charo Robles, Vigo Heissmeyer, Stefano Casola, Sergei Koralov, Manu Derudder, and Dinis Calado for critical reading of the manuscript.

This work was supported by the Deutsche Forschungsgemeinschaft (SFB684) and an Emmy Noether grant (M.S.-S.). J.C.V. and K.H. received PhD stipends from the Ernst Schering Foundation and the Boehringer Ingelheim Fonds, respectively. G.v.L. is a FWO postdoctoral researcher with an Odysseus Grant, K.A. was supported by the IZKF Erlangen (project A31) and D.S. by the Cancer Research Institute.

Authorship

Contribution: Y.C. and M.S.-S. designed and performed research, analyzed data, and wrote the paper; J.C.V., D.K., K.H., A.B., E.W., V.S., B.M., and M.R. performed research; D.S. and K.A. analyzed data; and R.B. and G.v.L. contributed new reagents.

Conflict-of-interest disclosure: The authors declare no competing financial interests.

Correspondence: Marc Schmidt-Supprian, Max Planck Institute of Biochemistry, Am Klopferspitz 18, D-82152 Martinsried, Germany; e-mail: supprian@biochem.mpg.de.

References

1. Klein U, Dalla-Favera R. Germinal centres: role in B-cell physiology and malignancy. *Nat Rev Immunol.* 2008;8(1):22-33.
2. Goodnow CC. Multistep pathogenesis of autoimmune disease. *Cell.* 2007;130(1):25-35.
3. Kuppers R. Mechanisms of B-cell lymphoma pathogenesis. *Nat Rev Cancer.* 2005;5(4):251-262.
4. Graham RR, Cotsapas C, Davies L, et al. Genetic variants near TNFAIP3 on 6q23 are associated with systemic lupus erythematosus. *Nat Genet.* 2008;40(9):1059-1061.
5. Musone SL, Taylor KE, Lu TT, et al. Multiple polymorphisms in the TNFAIP3 region are independently associated with systemic lupus erythematosus. *Nat Genet.* 2008;40(9):1062-1064.
6. Plenge RM, Cotsapas C, Davies L, et al. Two independent alleles at 6q23 associated with risk of rheumatoid arthritis. *Nat Genet.* 2007;39(12):1477-1482.
7. Thomson W, Barton A, Ke X, et al. Rheumatoid arthritis association at 6q23. *Nat Genet.* 2007;39(12):1431-1433.
8. Trynka G, Zhernakova A, Romanos J, et al. Coeliac disease-associated risk variants in TNFAIP3 and REL implicate altered NF-kappaB signalling. *Gut.* 2009;58(8):1078-1083.
9. Schmitz R, Hansmann ML, Bohle V, et al. TNFAIP3 (A20) is a tumor suppressor gene in Hodgkin lymphoma and primary mediastinal B cell lymphoma. *J Exp Med.* 2009;206(5):981-989.
10. Chanudet E, Huang Y, Ichimura K, et al. A20 is targeted by promoter methylation, deletion and inactivating mutation in MALT lymphoma. *Leukemia.* 2010;24(2):483-487.

11. Honma K, Tsuzuki S, Nakagawa M, et al. TNFAIP3 is the target gene of chromosome band 6q23.3-q24.1 loss in ocular adnexal marginal zone B cell lymphoma. *Genes Chromosomes Cancer.* 2008;47(1):1-7.
12. Novak U, Rinaldi A, Kwee I, et al. The NF-κB negative regulator TNFAIP3 (A20) is inactivated by somatic mutations and genomic deletions in marginal zone lymphomas. *Blood.* 2009;113(20): 4918-4921.
13. Packham G. The role of NF-kappaB in lymphoid malignancies. *Br J Haematol.* 2008;143(1):3-15.
14. Hymowitz SG, Wertz IE. A20: from ubiquitin editing to tumour suppression. *Nat Rev Cancer.* 2010;10(5):332-341.
15. Karin M, Cao Y, Greten FR, Li ZW. NF-kappaB in cancer: from innocent bystander to major culprit. *Nat Rev Cancer.* 2002;2(4):301-310.
16. Vereecke L, Beyaert R, van Loo G. The ubiquitin-editing enzyme A20 (TNFAIP3) is a central regulator of immunopathology. *Trends Immunol.* 2009; 30(8):383-391.
17. Shembade N, Ma A, Harhaj EW. Inhibition of NF-kappaB signaling by A20 through disruption of ubiquitin enzyme complexes. *Science.* 2010; 327(5969):1135-1139.
18. Turer EE, Tavares RM, Mortier E, et al. Homeostatic MyD88-dependent signals cause lethal inflammation in the absence of A20. *J Exp Med.* 2008;205(2):451-464.
19. Vereecke L, Sze M, Guire CM, et al. Enterocyte-specific A20 deficiency sensitizes to tumor necrosis factor-induced toxicity and experimental colitis. *J Exp Med.* 2010;207(7):1513-1523.
20. Sasaki Y, Derudder E, Hobeika E, et al. Canonical NF-kappaB activity, dispensable for B cell development, replaces BAFF-receptor signals and promotes B-cell proliferation upon activation. *Immunity.* 2006;24(6):729-739.
21. Schmidt-Supprian M, Tian J, Ji H, et al. I kappa B kinase 2 deficiency in T cells leads to defects in priming, B cell help, germinal center reactions, and homeostatic expansion. *J Immunol.* 2004; 173(3):1612-1619.
22. Schmidt-Supprian M, Rajewsky K. Vagaries of conditional gene targeting. *Nat Immunol.* 2007; 8(7):665-668.
23. Fairfax KA, Kallies A, Nutt SL, Tarlinton DM. Plasma cell development: from B-cell subsets to long-term survival niches. *Semin Immunol.* 2008; 20(1):49-58.
24. Guinamard R, Okigaki M, Schlessinger J, Ravetch JV. Absence of marginal zone B cells in Pyk-2-deficient mice defines their role in the humoral response. *Nat Immunol.* 2000;1(1):31-36.
25. Allman D, Pillai S. Peripheral B-cell subsets. *Curr Opin Immunol.* 2008;20(2):149-157.
26. Casola S, Rajewsky K. B cell recruitment and selection in mouse GALT germinal centers. *Curr Top Microbiol Immunol.* 2006;308:155-171.
27. Bouaziz JD, Yanaba K, Tedder TF. Regulatory B cells as inhibitors of immune responses and inflammation. *Immunol Rev.* 2008;224:201-214.
28. Nishimoto N, Kishimoto T. Inhibition of IL-6 for the treatment of inflammatory diseases. *Curr Opin Pharmacol.* 2004;4(4):386-391.
29. Ehlers M, Fukuyama H, McGaha TL, Aderem A, Ravetch JV. TLR9/MyD88 signaling is required for class switching to pathogenic IgG2a and 2b autoantibodies in SLE. *J Exp Med.* 2006;203(3): 553-561.
30. Vinuesa CG, Sanz I, Cook MC. Dysregulation of germinal centres in autoimmune disease. *Nat Rev Immunol.* 2009;9(12):845-857.
31. Hiroi T, Yanagita M, Ohta N, Sakaue G, Kiyono H. IL-15 and IL-15 receptor selectively regulate differentiation of common mucosal immune system-independent B-1 cells for IgA responses. *J Immunol.* 2000;165(8):4329-4337.
32. Cancro MP, Hao Y, Scholz JL, et al. B cells and aging: molecules and mechanisms. *Trends Immunol.* 2009;30(7):313-318.
33. Tsantikos E, Oracki SA, Quilici C, Anderson GP, Tarlinton DM, Hibbs ML. Autoimmune disease in Lyn-deficient mice is dependent on an inflammatory environment established by IL-6. *J Immunol.* 2010;184(3):1348-1360.
34. Kimura A, Kishimoto T. IL-6: regulator of Treg/Th17 balance. *Eur J Immunol.* 2010;40(7):1830-1835.
35. Pasare C, Medzhitov R. Toll pathway-dependent blockade of CD4+CD25+ T cell-mediated suppression by dendritic cells. *Science.* 2003; 299(5609):1033-1036.
36. Abe J, Ueha S, Suzuki J, Tokano Y, Matsushima K, Ishikawa S. Increased Foxp3(+) CD4(+) regulatory T cells with intact suppressive activity but altered cellular localization in murine lupus. *Am J Pathol.* 2008;173(6):1682-1692.
37. Tavares RM, Turer EE, Liu CL, et al. The ubiquitin modifying enzyme A20 restricts B cell survival and prevents autoimmunity. *Immunity.* 2010; 33(2):181-191.
38. Shoenfeld Y, Toubi E. Protective autoantibodies: role in homeostasis, clinical importance, and therapeutic potential. *Arthritis Rheum.* 2005; 52(9):2599-2606.
39. Witte T. IgM antibodies against dsDNA in SLE. *Clin Rev Allergy Immunol.* 2008;34(3):345-347.
40. Font J, Cervera R, Lopez-Soto A, et al. Anticardiolipin antibodies in patients with autoimmune diseases: isotype distribution and clinical associations. *Clin Rheumatol.* 1989;8(4):475-483.
41. Kishimoto T. IL-6: from its discovery to clinical applications. *Int Immunol.* 2010;22(5):347-352.

Cell purification and flow cytometry
The purification of lymphocyte and leukocyte subsets was achieved by a two step procedure. Splenic cell suspensions were first separated into CD43-expressing and CD43-negative fractions by MACS (Miltenyi). The CD43-negative fraction was stained with antibodies against B220 (eBioscience) and CD19 (eBioscience) and $B220^{+}CD19^{+}$ B cells were purified using a FACSAria (BD). The CD43-positive fraction was stained with antibodies against B220, TCRβ, CD11c, Gr-1 and Mac1 (all eBioscience). The following subsets were purified by FACS: T cells ($B220^{-}TCR\beta^{+}$), dendritic cells ($B220^{-}TCR\beta^{-}CD11c^{+}$), granulocytes ($B220^{-}TCR\beta^{-}CD11c^{-}Gr1^{+}Mac1^{lo}$) and macrophages ($B220^{-}TCR\beta^{-}CD11c^{-}Gr1^{lo}Mac1^{hi}$). All cell populations were over 99% pure.

For intracellular ex vivo IL-6 stainings of lymphocytes and leukocyte subsets, cells were stimulated for 5 h at 37°C with 10 nM brefeldin-A (Applichem).

PCR to identify A20 knock-out cells
PCR was performed using the primers a (CATTTAACCCTTCTGAGTTTCCA), b (CCGGGCTTTAACCACTCTC), c (CCACCCCTATTACTACGTGACC) and the following touchdown program: (1) 95°C 3min, (2) 95°C 30s, (3) 65°C 45s, (4) 72°C 60s, while steps (2)–(4) are repeated 10 times, the annealing temperature is decreased by 1°C/cycle, until 55°C is reached; (5) 95°C 30s, (6) 55°C 45s, (7) 72°C 60s, (5)–(7) are repeated 20 times; (8) 72°C 5min, (9) 4°C 15min. The PCR was conducted with either all three primers or only two (b, c) to specifically amplify the A20-knockout allele. PCR was performed on DNA isolated from the purified cell subsets. To estimate the sensitivity of the PCR for the knockout allele, we diluted DNA from CD19cre/$A20^{F/F}$ B cells at different ratios in DNA from $A20^{F/F}$ macrophages.

Immunohistochemistry
Spleen, kidney, liver were fixed in 4% PFA, processed, and embedded in paraffin. 2-µm sections for PAS stainings were prepared according to routine protocols. For the detection of tissue-specific autoantibodies, frozen sections from organs of *Rag2*$^{-/-}$ mice were incubated with sera of aged and control mice and an anti–mouse IgG–Cy3 conjugate (Jackson ImmunoResearch).

Table S1. Immunoglobulin titers in young mice

IgM			IgG1			IgG2c			IgG2b			IgG3			IgA		
KO	**Het**	**WT**	**KO**	**Het**	**WT**	**KO**	**Het**	**WT**	**KO**	**Het**	**WT**	**KO**	**Het**	**WT**	**KO**	**Het**	**WT**
841	150	31	66	81	178	56	71	59	3493	1178	981	2959	10141	9547	480439	1923	3237
131	70	71	33	72	80	32	47	46	1588	4593	3269	1177	9541	9553	285393	6048	8266
4220	121	81	97	82	66	42	41	46	2886	4480	2141	5473	10099	8299	124031	1923	5450
581	71	41	96	94	198	39	49	37	2815	3059	1301	2389	9961	6361	137648	327	3593
581	50	21	70	61	194	45	45	41	2123	4868	965	3235	2287	9421	351497	753	1733
201	90	90	53	122	115	52	44	25	544	1874	896	7495	9829	9787	3237	194	2628
63	75	14	6	66	31				482	479	467						
73	79	12	6	30	60				446	470	469						
172	63	8	10	63	25				483	478	449						
85	49	20	7	28	29				485	455	464						
70	52	54	10	49	54				455	485	414						
69	116	10	8	71	32				494	488	442						
216	***77***	***28***	***22***	***63***	***68***	***44***	***49***	***41***	***957***	***1187***	***796***	***3214***	***7762***	***8734***	***117737***	***1012***	***3655***

Numbers represent individual values (μg/ml) as determined by ELISA. Geometric means are shown in bold and italics in the last row.
KO = CD19cre/A20$^{F/F}$, Het = CD19cre/A20$^{F/Wt}$, WT = A × CD19cre; B × other.

Table S2. Immunoglobulin titers in old mice

IgM		IgG1		IgG2c		IgG2b		IgG3		IgA	
KO	WT	KO	WT	KO	WT	KO	WT	KO	WT	KO	WT
95	36	16	56	17	10	1085	346	7912	9512	26417	24875
97	40	36	43	10	18	991	552	5752	23912	21417	8208
116	37	64	73	14	17	956	239	38552	5192	4750	18625
59	59	69	58	14	7	615	385	2952	16472	24750	16958
80	28	50	56	9	7	249	506	5432	20952	23083	10708
57	70	37	41	8	7	403	266	1752	2312	23917	10292
124	38	48	41	19	19	828	737	312	4632	23917	19875
122	60	6	46	11	17	920	917	7512	9832	18917	3208
104	87	16	43	6	16	544	616	4232	19752	28917	26542
107	53	33	42	6	11	781	196	10472	20232	23917	8208
82	49	10	39	13	13	928	648	6552	10712	16417	
95		37		9	4	598	54	5192		8083	
92	***48***	***28***	***48***	***10***	***11***	***689***	***371***	***4861***	***10568***	***18419***	***12573***

Numbers represent individual values (μg/ml) as determined by ELISA. Geometric means are shown in bold and italics in the last row.
KO = CD19cre/A20$^{F/F}$, WT = A × CD19cre; B × other.

Figure S1. Loss of A20 B-lineage cells leads to decreased numbers of recirculating B cells in the bone marrow

(A) Scheme of B cell development and developmental time-frame (depicted as arrow), during which Mb1cre and CD19cre mouse strains express the cre recombinase. CD19cre induces partial recombination in preB and immature B cells: dotted line. (B) Representative spleen sizes of 8–12-week-old age-matched mice. (C) Representative dotplots showing proportions of pre/pro ($B220^+IgM^-$), immature ($B220^{lo}IgM^+$) and mature/recirculating ($B220^{hi}IgM^+$) B cells of lymphocytes (upper panels) and pro (proB: $CD25^-$c-Kit^+) and pre (preB: $CD25^+$c-Kit^-) B cells of $B220^+IgM^-$ cells (lower panels) in the bone marrow. (D) Absolute cell numbers of lymphocyte subsets in the bone marrow: total bone marrow cells, B cells ($B220^+$), proB, preB, immature B and recirculating B cells (defined as in C). Values represent means and s.d. calculated from 5–6 mice per genotype. (E) Effects of Mb1cre-mediated ablation of A20 on B-lineage cells in the bone marrow: upper two sets of panels as in (C), lower panels: percentages of large ($B220^{hi}IgM^+CD25^+$c-Kit^-FSC^{hi}) preB of total preB cells. * = $p < 0.05$; ** = $p < 0.001$; one-way anova

Figure S2. Loss of A20 B-lineage cells leads to an accumulation of transitional B cells in the spleen

(A) Representative dotplots showing proportions (left) and bar charts with absolute cell numbers (right) of $B220^+AA4.1^+$ transitional B cell subsets in the spleen: $IgM^{hi}CD23^-$ T1, $IgM^{hi}CD23^+$ T2 and $IgM^{lo}CD23^+$ T3 (anergic). Values represent means and s.d. calculated from 5–6 mice per genotype. (B) Upper panels: representative dotplots showing proportions of $CD19^+CD21^{hi}CD1d^{hi}$ B cells in the spleen: $CD23^{lo}$ MZ and $CD23^{hi}$ MZ precursor B cells. Values represent means and s.d. calculated from 5–6 mice per genotype. Lower panels: immunofluorescence of spleen sections demonstrating the marginal sinus (depicted as dotted yellow line) as border between the marginal and follicular zone: green = αB220, B cells; red = αCD3, T cells; blue = laminin. Magnification: 20×. (C) Representative dotplots showing proportions of IL-10 producing B cells ($B220^+IL10^+$) after 5h stimulation with PMA/ionomycin/BFA/LPS. Values represent means and s.d. of 3 mice per genotype. (D) Representative dotplots showing proportions of B cells in the thymus ($B220^+TCR\beta^-$). Values represent means and s.d. of 3 mice per genotype. (E) Representative dotplots showing proportions of B cell subsets in the peritoneal cavity (absolute cell numbers are shown in Fig. 2B): $B220^{hi}CD19^+$ B2 and $B220^{lo}CD19^{hi}$ B1 cells of total lymphocytes (upper panels) and $CD43^{lo}CD5^-$ B1b and $CD43^+CD5^+$ B1a cells of B1 cells (lower panels). * = $p < 0.05$; ** = $p < 0.001$; one-way anova

Figure S3. Fidelity of CD19cre for specific recombination of conditional A20 alleles only in B cells

(A) Scheme of the conditional A20 allele before (upper panel) and after (lower panel) cre-mediated recombination. The location of the primers (a–c) employed for the genotyping PCR are shown and the length of the respective PCR amplification products. Squares indicate exons (E3–E7) and triangles loxP sites. (B) Upper panels: representative PCR results for two PCR reactions on DNA from purified splenic cell subsets: the three primer PCR (a, b, c) amplifies A20 loxP-flanked and knockout alleles,

whereas the two primer PCR (a, c) amplifies only DNA from A20-knockout alleles. Splenic cell subsets (T cells = $B220^{-}TCR\beta^{+}$, dendritic cells/DC = $B220^{-}TCR\beta^{-}CD11c^{+}$, macrophages/Mac = $B220^{-}TCR\beta^{-}CD11c^{-}Gr1^{lo}Mac1^{hi}$ and granulocytes/Gr = $B220^{-}TCR\beta^{-}CD11c^{-}Gr1^{+}Mac1^{lo}$) were MACS purified followed by cell sorting and were over 99% pure. Identical results were obtained for all the cellular subsets sorted from three individual CD19cre/$A20^{F/F}$ mice. Lower panels: evaluation of the sensitivity of the two PCRs. A20-knockout cells were diluted at different ratios with $A20^{F/F}$ cells. The PCRs are able to amplify the knockout allele at a dilution of 1 to 500. The amplification product for the knockout allele that could be observed with the DNA from purified T cells, DCs, macrophages and granulocyte was weaker than the amplification product from the 1:500 A20-knockout to $A20^{F/F}$ dilution in all cases. This band therefore represents most likely the presence of less than 0.2% contaminating B cells in the respective purified cell-type. However, this analysis does not allow us to rule out the presence of less than 0.2% A20-knockout cells within each cell-type.

Figure S4. A20 regulates B cell activation in a dose-dependent fashion
(A) Realtime PCR quantifying the amount of A20 mRNA relative to PBGD mRNA in wild-type B cells stimulated with the indicated mitogens for 1, 4 and 12 h. Means and s.d. of triplicate measurements are shown. (B) Expression levels of the B cell activation marker after o/n stimulation with αIgM, LPS, CpG or αCD40. The dotplots are representative of 3 independent experiments. (C) Assessment of proliferation by the CFSE dilution assay: histograms show CFSE intensities 3 days after stimulation with the indicated mitogens. The table depicts the proliferation index (Proliferation index: average number of divisions of the proliferating cells), the percentage of dividing cells (% Divided: the proportion of cells that initially started to divide) and the division index (Div. Index: average number of divisions of all cells). Numbers represent the means of 3 to 4 (αCD40/IL-4) independent experiments. (D) IL-6 levels were measured in the supernatant after o/n stimulation with αIgM, LPS, CpG or αCD40. (E) Representative dotplots showing proportions of TNFα- or IL-6–producing B cells ($B220^{+}$ $TNF\alpha^{+}$ or $B220^{+}$ $IL\text{-}6^{+}$) after 5h stimulation with PMA/ionomycin/BFA. Values represent means and s.d. of 3 mice per genotype.

Figure S5. IL-6 producing cell-types in CD19cre/$A20^{F/F}$ mice
(A) Realtime PCR analysis of IL-6 expression in FACS-purified splenic cell subsets of CD19cre/$A20^{F/F}$ and CD19cre control mice. Splenic cell subsets (T cells = $B220^{-}TCR\beta^{+}$, dendritic cells/DC = $B220^{-}TCR\beta^{-}CD11c^{+}$, macrophages/Mac = $B220^{-}TCR\beta^{-}CD11c^{-}Gr1^{lo}Mac1^{hi}$ and granulocytes/Gr = $B220^{-}TCR\beta^{-}CD11c^{-}Gr1^{+}Mac1^{lo}$) were MACS purified followed by cell sorting and were over 99% pure. IL6 cDNA was quantified relative to PBGD. Values represent means and s.d. of 3 independent experiments. (B) Proportions of IL-6 expressing cells of individual immune cell subsets in the spleen of CD19cre/$A20^{F/F}$ and CD19cre control mice identified by intracellular FACS. Values represent means and s.d. of 3 independent experiments.

Figure S6. Chronic inflammation and autoreactivity in aged $B^{A20-/-}$ mice
(A) Representative spleen size of old CD19cre/$A20^{F/F}$ and age-matched CD19cre control mice. (B) Spleen weight (n($B^{A20-/-}$) = 10, n(control) = 9). (C) Representative dotplot showing proportions of plasma cells ($B220^{lo}CD138^{hi}$), mean and s.d. for n = 9 mice per genotype are shown. (D) Representative PAS stainings of liver and kidney sections from aged mice. Magnification: 10×. (E) Representative immunofluorescence staining of tissue-specific IgG autoantibodies directed against kidney, harderian gland, stomach and lacrimal gland. Staining was performed by incubating sera from aged mice on sections of tissues isolated from $Rag2^{-/-}$ mice. Magnification: 20×.

Fig. S1

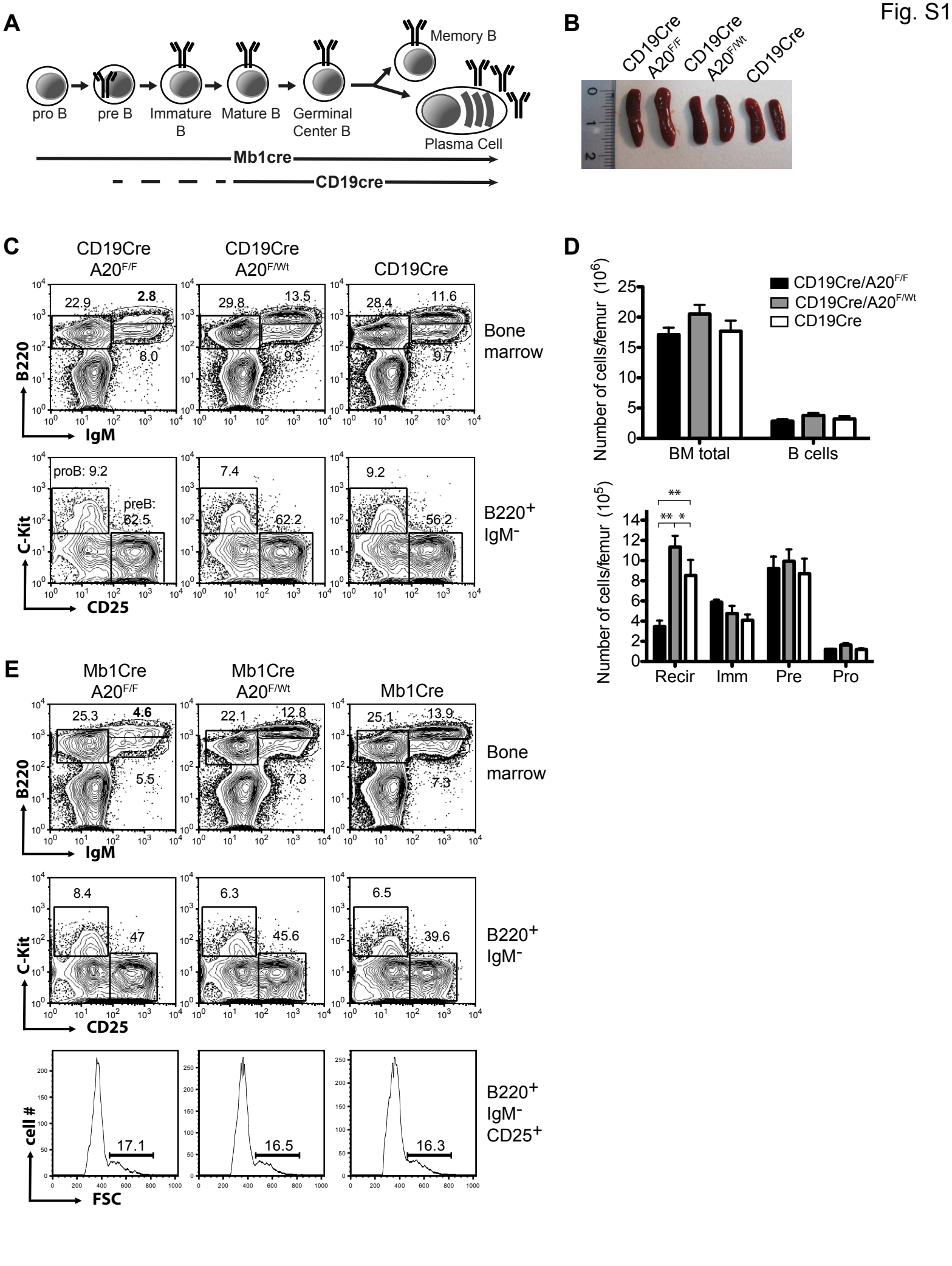
A
pro B
pre B
Immature B
Mature B
Germinal Center B
Memory B
Plasma Cell
Mb1cre
CD19cre
B
CD19Cre A20F/F
CD19Cre A20F/Wt
CD19Cre
C
CD19Cre A20F/F
CD19Cre A20F/Wt
CD19Cre
22.9
2.8
8.0
29.8
13.5
9.3
28.4
11.6
9.7
Bone marrow
B220
IgM
proB: 9.2
preB: 62.5
7.4
62.2
9.2
56.2
B220+ IgM-
C-Kit
CD25
D
CD19Cre/A20F/F
CD19Cre/A20F/Wt
CD19Cre
Number of cells/femur (10^6)
BM total
B cells
Number of cells/femur (10^5)
Recir
Imm
Pre
Pro
E
Mb1Cre A20F/F
Mb1Cre A20F/Wt
Mb1Cre
25.3
4.6
5.5
22.1
12.8
7.3
25.1
13.9
7.3
Bone marrow
8.4
47
6.3
45.6
6.5
39.6
B220+ IgM-
17.1
16.5
16.3
B220+ IgM- CD25+
cell #
FSC

A

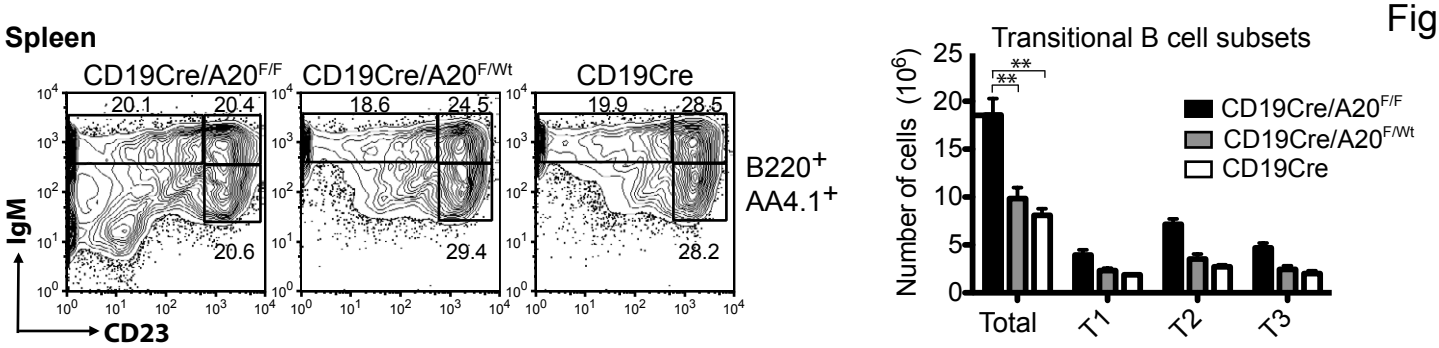
Spleen
CD19Cre/A20F/F
CD19Cre/A20F/Wt
CD19Cre
20.1
20.4
20.6
18.6
24.5
29.4
19.9
28.5
28.2
IgM
CD23
B220+
AA4.1+
Transitional B cell subsets
Number of cells (10^6)
**
**
CD19Cre/A20F/F
CD19Cre/A20F/Wt
CD19Cre
Total
T1
T2
T3

B

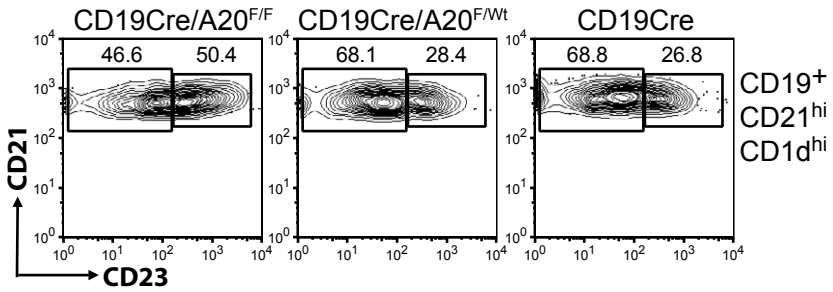
Spleen
CD19Cre/A20F/F
CD19Cre/A20F/Wt
CD19Cre
46.6
50.4
68.1
28.4
68.8
26.8
CD21
CD23
CD19+
CD21hi
CD1dhi

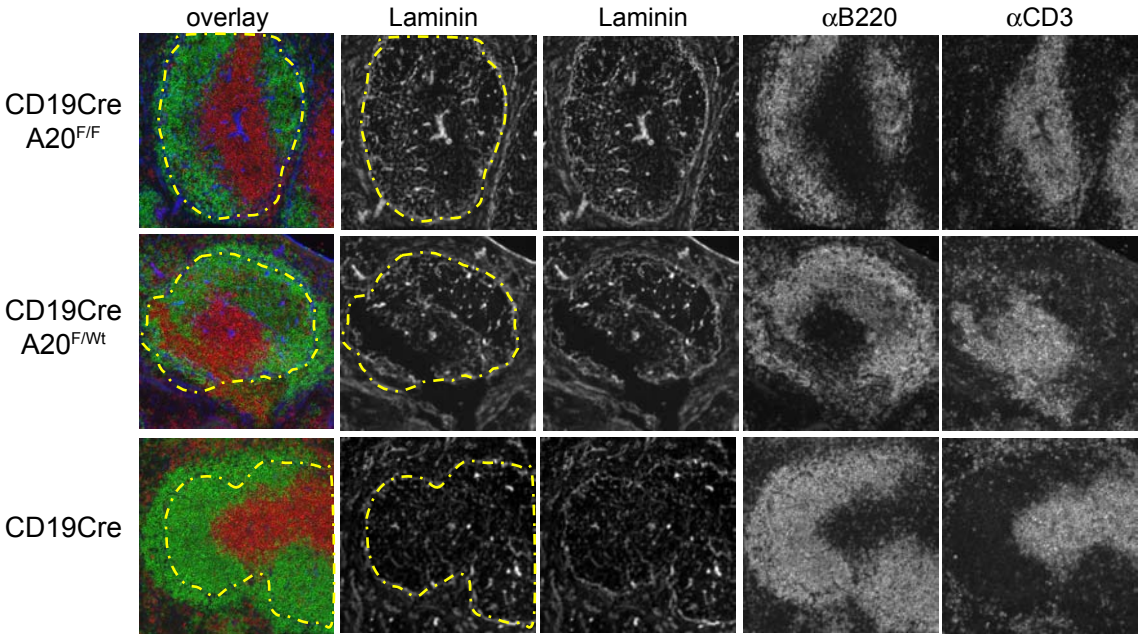
overlay
Laminin
Laminin
αB220
αCD3
CD19Cre
A20F/F
CD19Cre
A20F/Wt
CD19Cre

C

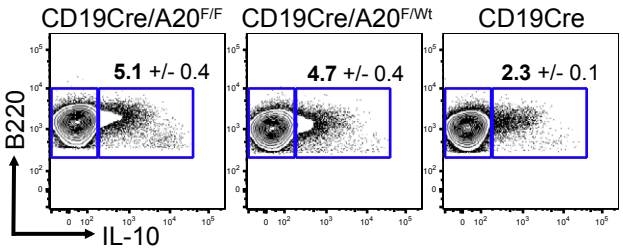
Spleen
CD19Cre/A20F/F
CD19Cre/A20F/Wt
CD19Cre
5.1 +/- 0.4
4.7 +/- 0.4
2.3 +/- 0.1
B220
IL-10

D

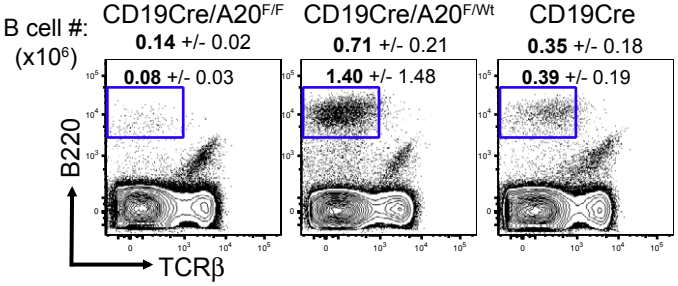
Thymus
B cell #:
(x10^6)
CD19Cre/A20F/F
CD19Cre/A20F/Wt
CD19Cre
0.14 +/- 0.02
0.71 +/- 0.21
0.35 +/- 0.18
0.08 +/- 0.03
1.40 +/- 1.48
0.39 +/- 0.19
B220
TCRβ

E

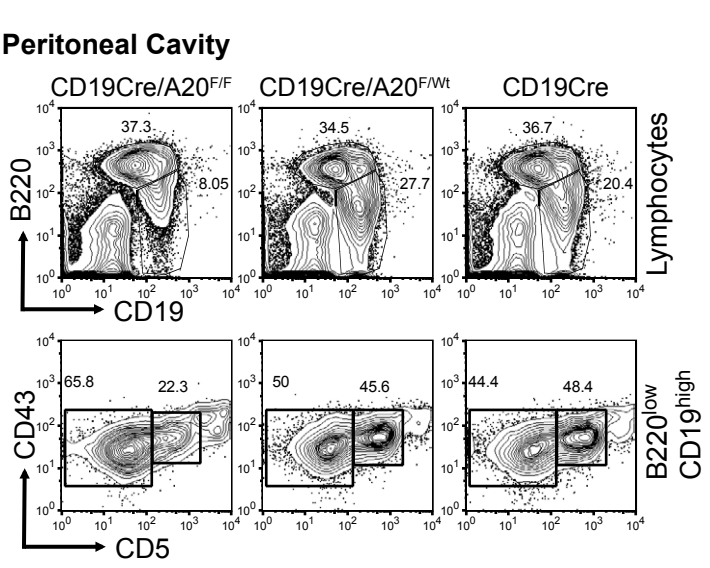
Peritoneal Cavity
CD19Cre/A20F/F
CD19Cre/A20F/Wt
CD19Cre
37.3
8.05
34.5
27.7
36.7
20.4
B220
CD19
Lymphocytes
65.8
22.3
50
45.6
44.4
48.4
CD43
CD5
B220low
CD19high

Fig. S3

A

loxP-flanked A20 allele

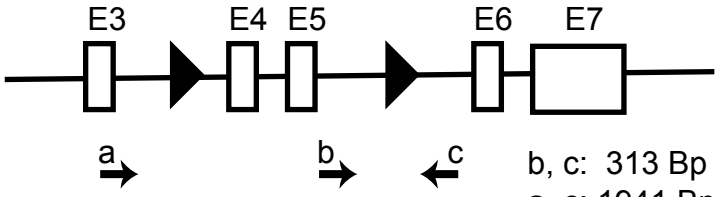

b, c: 313 Bp
a, c: 1941 Bp, not amplified

A20-knockout allele

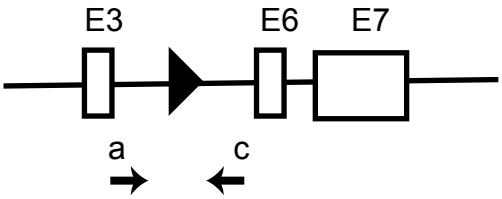

a, c: 210 Bp

B

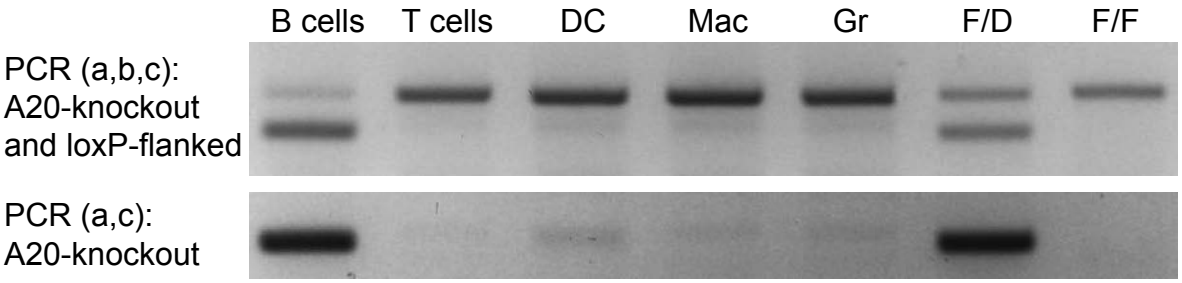

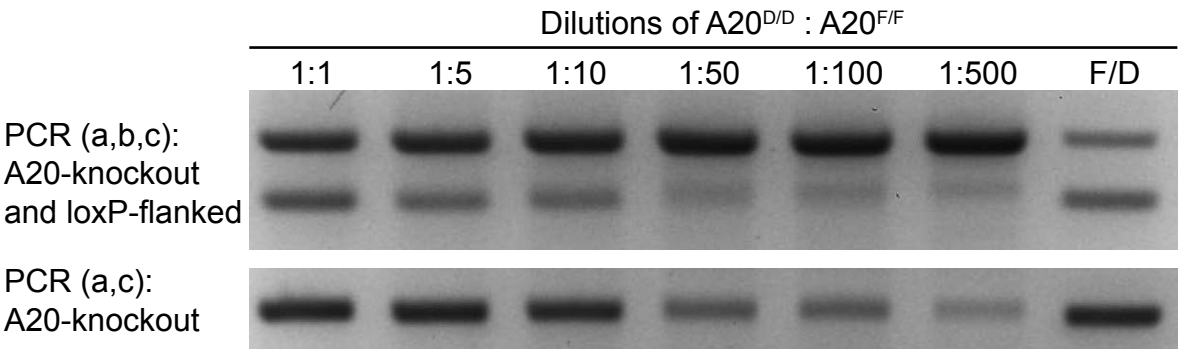

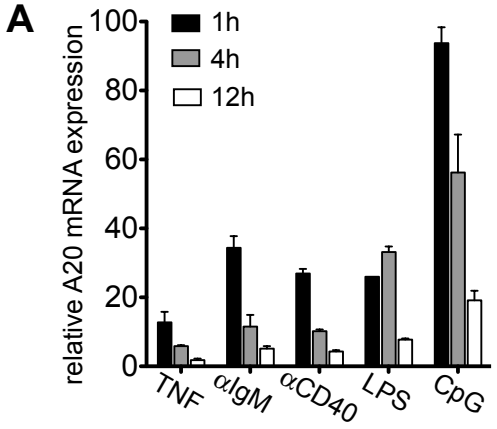

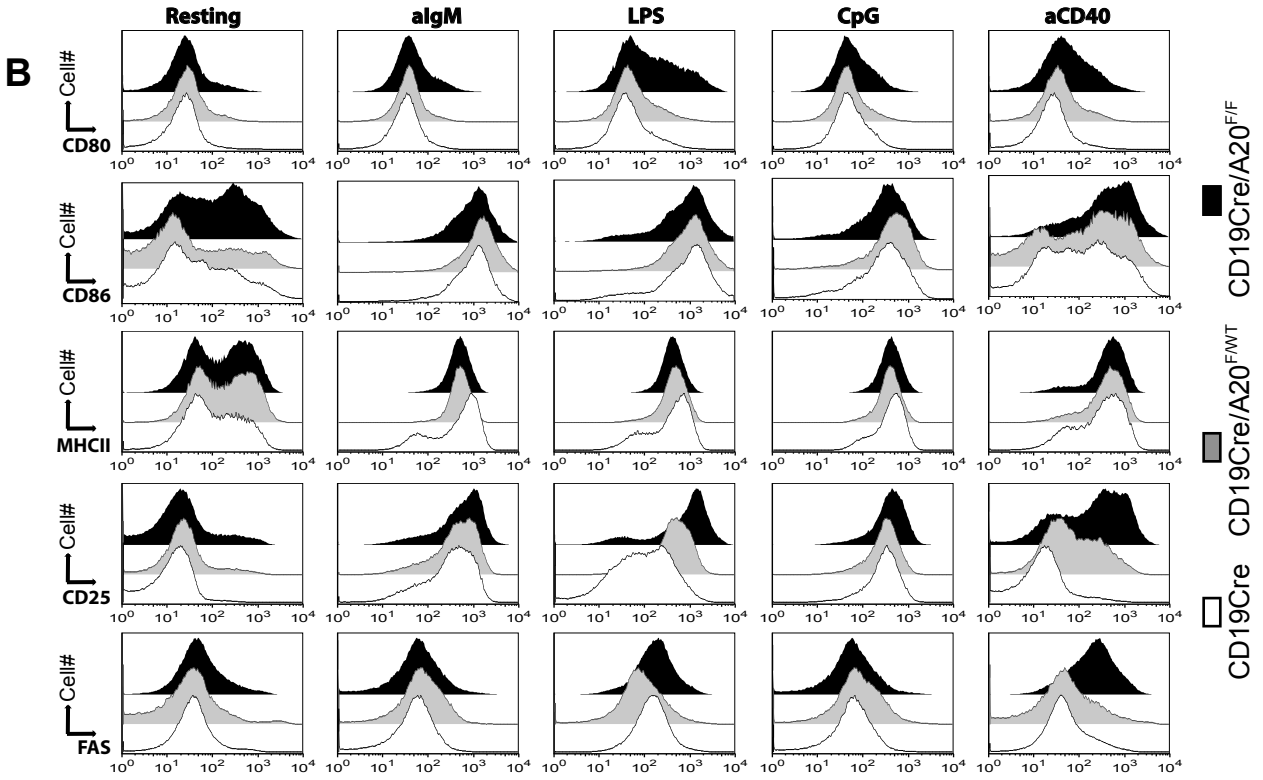

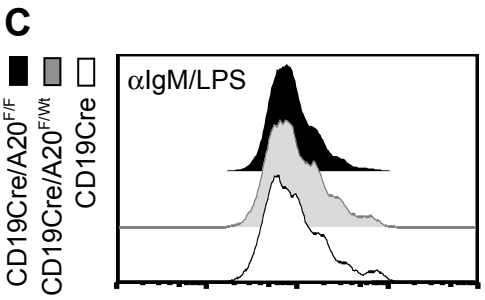

		CD19Cre	A20F/F	A20F/Wt	WT
αIgM/IL-4	Prol. Index	1.9	1.6	1.5
	% Divided	90	94	92
	Div. Index	1.9	1.7	1.7
αCD40/IL-4	Prol. Index	1.4	1.2	1.2
	% Divided	66	24	34
	Div. Index	0.9	0.3	0.4
LPS/IL-4	Prol. Index	2.2	2.1	2.2
	% Divided	86	76	70
	Div. Index	1.9	1.6	1.5
αIgM/LPS	Prol. Index	2.2	2.3	2.4
	% Divided	89	95	94
	Div. Index	2.0	2.2	2.2

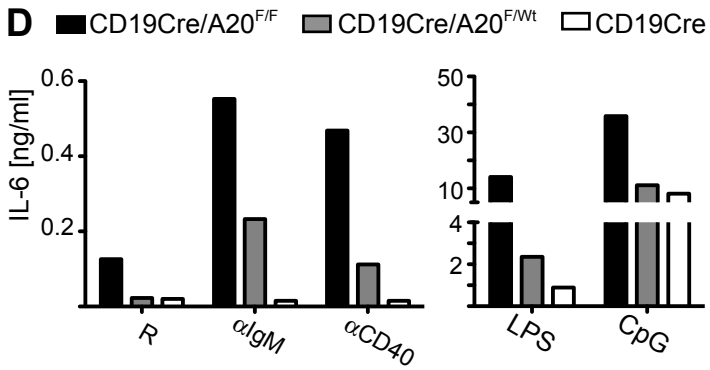

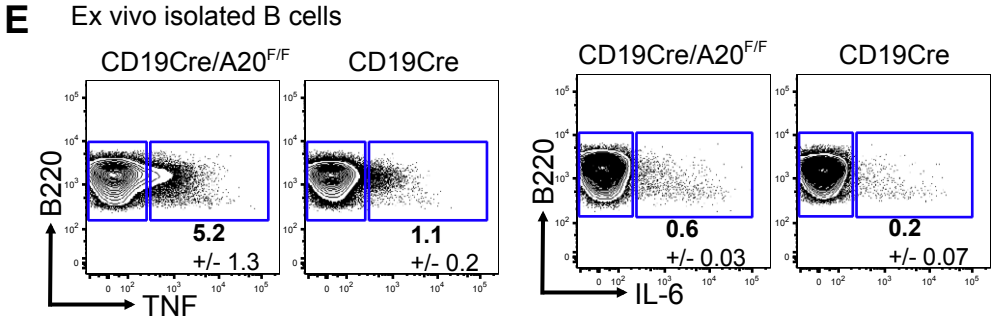

Fig. S5

A

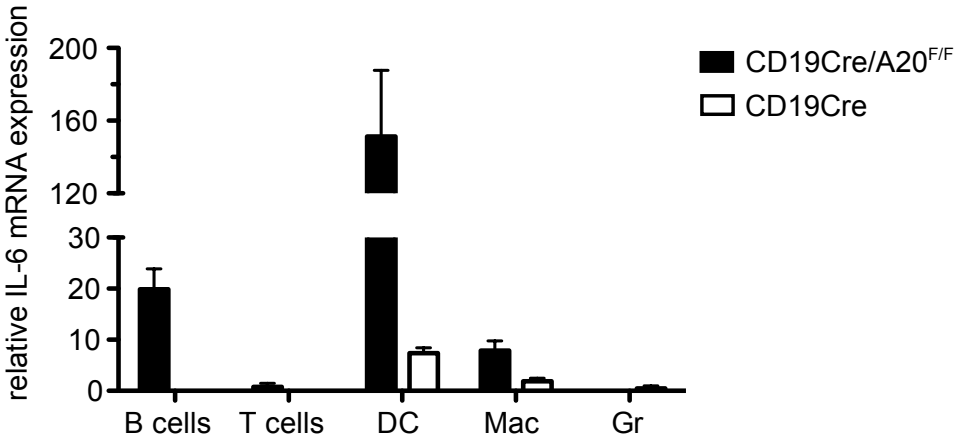
relative IL-6 mRNA expression
200
160
120
30
20
10
0
B cells
T cells
DC
Mac
Gr
CD19Cre/A20F/F
CD19Cre

B

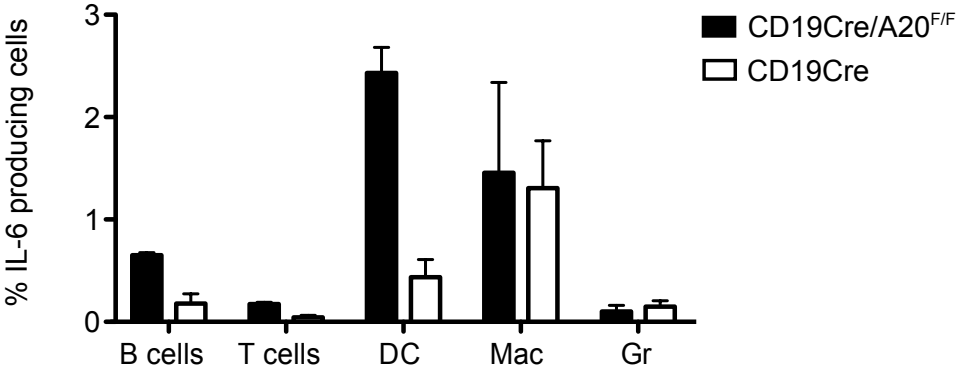
% IL-6 producing cells
3
2
1
0
B cells
T cells
DC
Mac
Gr
CD19Cre/A20F/F
CD19Cre

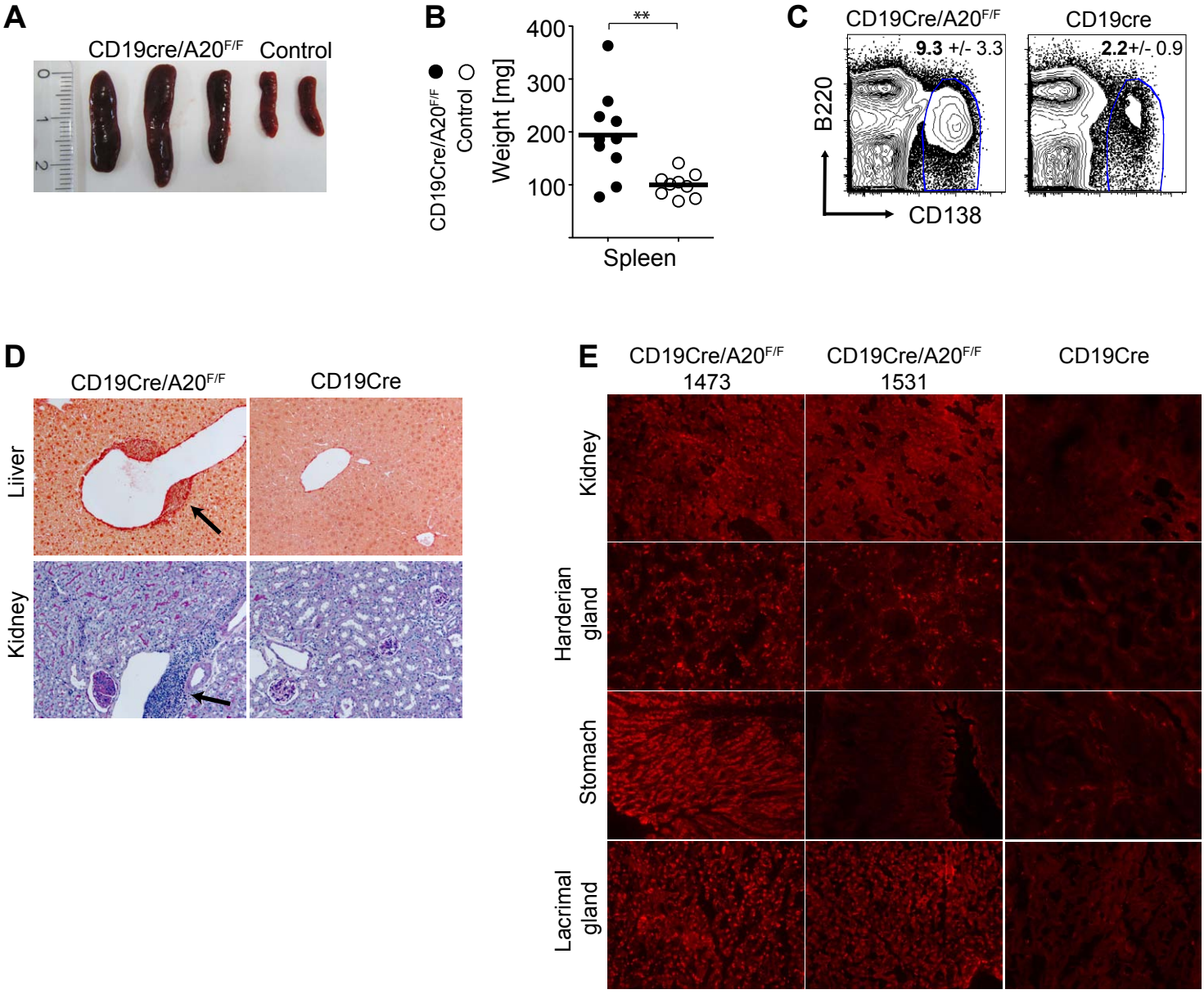
A
CD19cre/A20F/F
Control
B
CD19Cre/A20F/F
Control
Weight [mg]
400
300
200
100
**
Spleen
C
CD19Cre/A20F/F
CD19cre
9.3 +/- 3.3
2.2+/-. 0.9
B220
CD138
D
CD19Cre/A20F/F
CD19Cre
Liiver
Kidney
E
CD19Cre/A20F/F
1473
CD19Cre/A20F/F
1531
CD19Cre
Kidney
Harderian gland
Stomach
Lacrimal gland

Paper III

nature genetics

A20 (TNFAIP3) deficiency in myeloid cells triggers erosive polyarthritis resembling rheumatoid arthritis

Mourad Matmati[1,2,11], Peggy Jacques[3,11], Jonathan Maelfait[1,2], Eveline Verheugen[3], Mirjam Kool[1,4], Mozes Sze[1,2], Lies Geboes[5], Els Louagie[3], Conor Mc Guire[1,2], Lars Vereecke[1,2], Yuanyuan Chu[6], Louis Boon[7], Steven Staelens[8,9], Patrick Matthys[5], Bart N Lambrecht[4], Marc Schmidt-Supprian[6], Manolis Pasparakis[10], Dirk Elewaut[3,12], Rudi Beyaert[1,2,12] & Geert van Loo[1,2,12]

A20 (TNFAIP3) is a protein that is involved in the negative feedback regulation of NF-κB signaling in response to specific proinflammatory stimuli in different cell types and has been suggested as a susceptibility gene for rheumatoid arthritis. To define the contribution of A20 to rheumatoid arthritis pathology, we generated myeloid-specific A20-deficient mice and show that specific ablation of *Tnfaip3* in myeloid cells results in spontaneous development of a severe destructive polyarthritis with many features of rheumatoid arthritis. Myeloid-A20–deficient mice have high levels of inflammatory cytokines in their serum, consistent with a sustained NF-κB activation and higher TNF production by macrophages. Destructive polyarthritis in myeloid A20 knockout mice was TLR4-MyD88 and IL-6 dependent but was TNF independent. Myeloid A20 deficiency also promoted osteoclastogenesis in mice. Together, these observations indicate a critical and cell-specific function for A20 in the etiology of rheumatoid arthritis, supporting the idea of developing A20 modulatory drugs as cell-targeted therapies.

Rheumatoid arthritis is an inflammatory autoimmune disease affecting about 1% of the adult population. It is characterized by chronic inflammation of the joints associated with progressive destruction of cartilage and bone. The etiology of rheumatoid arthritis is still not understood, but it is well accepted that activation of nuclear factor-κB (NF-κB)-dependent gene expression plays a key role in the development of rheumatoid arthritis and many other autoimmune diseases. A20 (also known as TNFAIP3) is a deubiquitinating protein that negatively regulates NF-κB–dependent gene expression in response to different immune-activating stimuli, including tumor necrosis factor (TNF), interleukin-1 (IL-1) and antigens, and in response to triggering of Toll-like receptors (TLRs) and nucleotide-binding oligomerization domain containing 2 (NOD2) receptor[1]. A20 is believed to inhibit NF-κB function by deubiquitinating specific NF-κB signaling molecules, such as RIP1, RIP2, TRAF6 and MALT1 (refs. 2–5), which disrupts specific protein-protein interactions. A20-deficient mice spontaneously develop multiorgan inflammation and cachexia and die within 2 weeks of birth, illustrating the potent anti-inflammatory function of this molecule[6]. More recently, several SNPs in the human *TNFAIP3* locus were shown to be associated with increased susceptibility to type 1 diabetes, systemic lupus erythematosus, celiac disease, Crohn's disease, psoriasis, multiple sclerosis and rheumatoid arthritis[7], suggesting that defects in A20 expression or activity could be involved in the development of specific autoimmune diseases. However, the relative contribution of A20 expression in different cell types to the pathophysiology of disease development is still unknown.

To address the cell-type–specific role of A20 in the etiology of autoimmune disease in general and rheumatoid arthritis in particular, we generated A20 conditional knockout mice in which exon 4 and 5 of *Tnfaip3* are flanked by LoxP consensus sites[8]. We crossed mice containing a conditional *Tnfaip3* allele[8] with LysM-Cre[9] transgenic mice to generate mice deficient in A20 in their myeloid cells (**Supplementary Fig. 1**). In contrast to the previously described cachexia and premature death of mice deficient in A20 either completely[6] or in hematopoietic cells [10], mice deficient in A20 in myeloid cells did not develop cachexia or die prematurely. However, myeloid-A20–deficient mice developed swelling and redness of the front and hind paws at 8–12 weeks of age, with the incidence reaching 100% in all mice at the age of 20 weeks (**Fig. 1a–c**). Histological analysis of the ankle joints of these mice showed marked synovial and periarticular inflammation, with infiltration by mononuclear cells, and massive cartilage and bone destruction (**Fig. 1a** and **Supplementary Fig. 2**).

[1]Department for Molecular Biomedical Research, Unit of Molecular Signal Transduction in Inflammation, Vlaams Instituut voor Biotechnologie (VIB), Ghent, Belgium. [2]Department of Biomedical Molecular Biology, Ghent University, Ghent, Belgium. [3]Department of Rheumatology, Laboratory for Molecular Immunology and Inflammation, Ghent University Hospital, Ghent, Belgium. [4]Department of Respiratory Diseases, Laboratory of Immunoregulation and Mucosal Immunology, Ghent University Hospital, Ghent, Belgium. [5]Rega Institute, Leuven University, Leuven, Belgium. [6]Max Planck Institute of Biochemistry, Martinsried, Germany. [7]Bioceros, Utrecht, The Netherlands. [8]Medical Image and Signal Processing, Ghent University and Institute for Broadband Technology, Ghent, Belgium. [9]Molecular Imaging Center Antwerp, Antwerp University, Antwerp, Belgium. [10]Institute for Genetics, Centre for Molecular Medicine (CMMC) and Cologne Excellence Cluster on Cellular Stress Responses in Aging-Associated Diseases (CECAD), University of Cologne, Cologne, Germany. [11]These authors contributed equally to this work. [12]These authors jointly directed this work. Correspondence should be addressed to G.v.L. (geert.vanloo@dmbr.ugent.be), R.B. (rudi.beyaert@dmbr.ugent.be) or D.E. (dirk.elewaut@ugent.be).

Received 22 April; accepted 29 June; published online 14 August 2011; doi:10.1038/ng.874

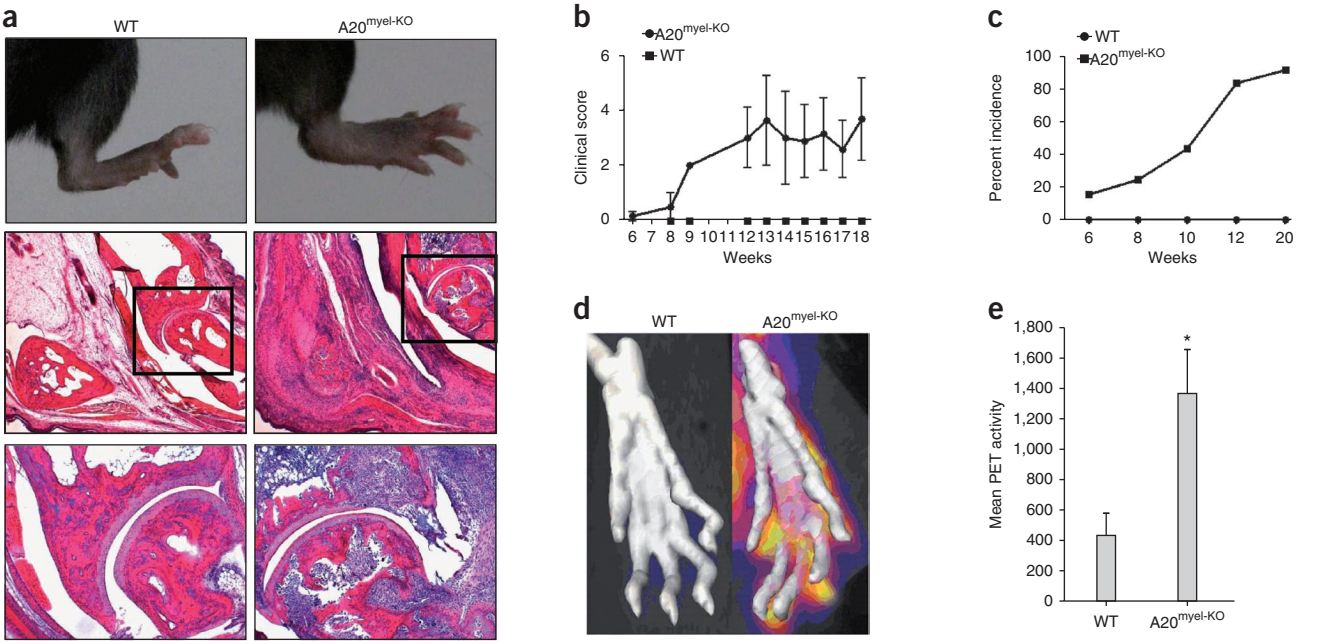

Figure 1 A20$^{myel\text{-}KO}$ mice develop spontaneous destructive arthritis. (**a**) Pictures of ankles of A20$^{myel\text{-}KO}$ and control littermate (WT) mice at the age of 13 weeks (top). Histological section of ankle joints stained with haematoxylin and eosin; magnification, 40× (middle). The detail of the ankle joint region illustrates the infiltration of mononuclear cells, cartilage destruction and bone erosion in A20$^{myel\text{-}KO}$ mice; magnification, 100× (bottom). (**b**) We clinically scored A20$^{myel\text{-}KO}$ mice ($n = 6$) and control littermates (WT, $n = 6$) twice a week for development of peripheral arthritis. (**c**) The cumulative incidence of arthritis in A20$^{myel\text{-}KO}$ ($n = 6$) and control (WT, $n = 6$) littermate mice. (**d**) Illustration of fluorodeoxyglucose (FDG) positron emission tomography (PET) activation in an A20$^{myel\text{-}KO}$ mouse and a control (WT) littermate. (**e**) The mean PET activity in hind paws from A20$^{myel\text{-}KO}$ mice ($n = 5$) and control (WT, $n = 5$) littermates normalized for injected activity. Results are shown as mean ± s.d. $^*P = 0.004$.

Inflammation started in the posterior part of the ankle and gradually spread out to the tibiotalar joint and tarsal joints. Erosions are an early manifestation of the disease, eventually leading to a complete destruction of the joints. The wrists of the mice were also affected. However, we could detect only minor inflammatory changes in the fingers and toes, and no signs of arthritis were evident in the knees and hips. This was confirmed by *in vivo* positron emission tomography–computed tomography (PET-CT) analysis, which showed pronounced inflammation in the paws of myeloid-A20–deficient mice (**Fig. 1d**,**e**). These mice had elevated levels of serum antibodies against type II collagen, suggesting the development of autoimmunity (**Supplementary Fig. 3**). Similar features characterize rheumatoid arthritis in humans. Neither the incidence nor the severity of arthritis was substantially different between male and female mice (data not shown). Notably, an analysis of skin, liver, intestine and lungs of myeloid-A20–deficient mice did not reveal signs of inflammation (**Supplementary Fig. 4** and data not shown).

Myeloid-A20–deficient mice had high serum levels of the inflammatory and rheumatoid arthritis–associated cytokines TNF, IL-1β, IL-6 and MCP-1 (**Fig. 2a**) as well as high levels of TNF, IL-1β, IL-6 and IL-23 locally in joint tissue (**Fig. 2b**). In line with the *in vivo* observations, cultured peritoneal macrophages from myeloid-A20–deficient mice, in contrast to wild-type macrophages, constitutively produced substantial amounts of TNF and IL-6 (**Fig. 2c**,**d**). Consistent with the essential role of A20 as a negative feedback regulator of inducible NF-κB–dependent gene expression, cultured A20-deficient macrophages showed sustained degradation of the NF-κB inhibitory molecule IκBα (**Fig. 2e**) and markedly higher TNF production in response to lipopolysaccharide (LPS) than wild-type cells (**Fig. 2f**). Myeloid cells of the monocyte and macrophage lineage are considered the main producers of cytokines such as TNF, IL-1β and IL-6, and so they are probably also responsible for the augmented levels of these cytokines in the serum of myeloid-A20–deficient mice. TNF, IL-1β and IL-6 have all been implicated in the pathophysiology of rheumatoid arthritis, and anti-TNF biological agents are presently the anti-cytokine therapy of choice for rheumatoid arthritis[11].

Because of the dominant role of TNF in the pathogenesis of rheumatoid arthritis, we crossed the myeloid A20 knockout mice (A20$^{myel\text{-}KO}$) into a TNFR1-deficient genetic background (TNFR1^{KO})[12]. Notably, double homozygous A20$^{myel\text{-}KO}$ TNFR1^{KO} mice still developed rheumatoid arthritis–like pathology (**Fig. 3a**), indicating that the destructive arthritis seen in myeloid A20 knockout mice is not dependent on TNFR1-dependent signaling. Similarly, systemic treatment of myeloid A20 knockout mice with TNF-neutralizing antibodies did not suppress the arthritis-like pathology, confirming the genetic approach using TNFR1-deficient mice. In contrast, significant protection could be obtained upon therapeutic treatment with IL-6–neutralizing antibodies (**Supplementary Fig. 5**), indicating an important role of IL-6 in disease progression. Also Toll-like receptor 4 (TLR4) has been suggested to be an important player in rheumatoid arthritis[13,14]. We therefore tested the importance of TLR4-MyD88 for the arthritis phenotype by applying TLR4-neutralizing *Rhodobacter sphaeroides* LPS (LPS-Rs) to myeloid A20 knockout mice or by crossing the myeloid A20 knockout mice into a MyD88-deficient genetic background (MyD88^{KO})[15]. Systemic administration of LPS-Rs almost completely neutralized the rheumatoid arthritis–like phenotype in myeloid A20 knockout mice (**Fig. 3b**). Moreover, double homozygous A20$^{myel\text{-}KO}$ MyD88^{KO} mice developed normally, showing no macroscopic and only minor histopathological signs of rheumatoid arthritis–like pathology (**Fig. 3c**). Together, these

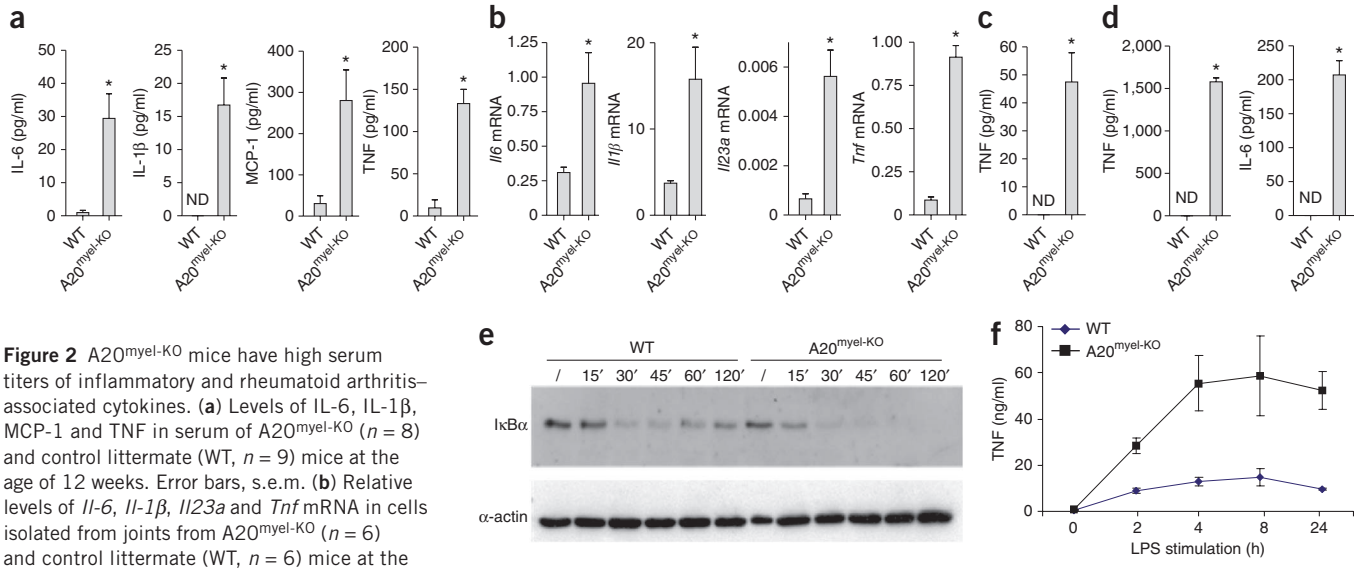

Figure 2 A20$^{myel\text{-}KO}$ mice have high serum titers of inflammatory and rheumatoid arthritis–associated cytokines. (**a**) Levels of IL-6, IL-1β, MCP-1 and TNF in serum of A20$^{myel\text{-}KO}$ ($n = 8$) and control littermate (WT, $n = 9$) mice at the age of 12 weeks. Error bars, s.e.m. (**b**) Relative levels of *Il-6*, *Il-1β*, *Il23a* and *Tnf* mRNA in cells isolated from joints from A20$^{myel\text{-}KO}$ ($n = 6$) and control littermate (WT, $n = 6$) mice at the age of 12 weeks. (**c**) TNF secretion by resident peritoneal macrophages after 24 h of rest ($n = 4$). (**d**) TNF and IL-6 secretion by thioglycollate-induced peritoneal macrophages after 24 h of rest ($n = 4$). (**e**) Immunoblot analysis for IκBα in extracts of peritoneal macrophages incubated with 100 ng/ml LPS for the indicated durations; we used anti-actin as a loading control. (**f**) Kinetics of TNF secretion by A20$^{myel\text{-}KO}$ ($n = 4$) and control (WT, $n = 4$) peritoneal macrophages after stimulation with LPS for the indicated durations. ND, not detectable. Error bars, s.e.m. $^*P < 0.05$.

data suggest a crucial contribution of a TLR4-dependent signaling pathway in the development of rheumatoid arthritis–like pathology in myeloid A20 knockout mice. As the intestinal flora is thought to play an important role in regulating immune responses and because LPS from intestinal bacteria may be crucially involved in autoimmune joint inflammation[16–19], we treated myeloid A20 knockout mice with a mix of broad spectrum antibiotics (ciprofloxacin, ampicillin, metronidazole and vancomycin), which has previously been shown to substantially reduce the numbers of commensal bacteria in the intestine[8]. However, we observed no differences in the clinical manifestation of arthritis in myeloid A20 knockout mice either treated or not treated with antibiotics, making the involvement of the commensal microbial flora in the arthritic phenotype unlikely (**Supplementary Fig. 6**).

A20 deficiency in myeloid cells could be instrumental in overcoming immune tolerance to joint-specific antigens and the induction of adaptive immune responses against them. Flow cytometric analysis of the inguinal lymph nodes and splenocytes of myeloid-A20–deficient mice showed a higher percentage of T helper 17 (Th17) cells, memory CD4$^+$ cells and CD8$^+$ T cells, all of which are key players in the development of rheumatoid arthritis pathology[20] (**Supplementary Fig. 7**). Moreover, Th17 cells were identified as an osteoclastogenic T-helper–cell subset that links T cell activation and bone resorption[21]. To evaluate whether T and B lymphocytes are involved in the development of arthritic pathology in myeloid A20 knockout mice, these mice were bred into a RAG2-deficient background (RAG2^{KO}) lacking functional T and B cells[22]. Double homozygous A20$^{myel\text{-}KO}$ RAG2^{KO} mice still developed rheumatoid arthritis–like pathology (**Fig. 3d**), indicating that T and B cells are not essential for the development of the destructive arthritis seen in myeloid A20 knockout mice.

Upon analysis of secondary lymphoid organs, we noticed that the spleen and axillary and inguinal lymph nodes were markedly larger in myeloid-A20–deficient mice than in littermate controls. Similar to the reduced development of arthritis in A20$^{myel\text{-}KO}$ mice in the absence of MyD88 (A20$^{myel\text{-}KO}$ MyD88^{KO} mice), splenomegaly was also markedly reduced in A20$^{myel\text{-}KO}$ MyD88^{KO} mice compared to A20$^{myel\text{-}KO}$ mice (**Supplementary Fig. 8**). As the axillary and inguinal lymph nodes are responsible for draining the joints, their enlargement is in line with intense inflammation at these sites. The fraction of CD11b$^+$Gr1$^+$ myeloid cells in the spleen, which include granulocytes and activated monocytes, was sixfold higher in myeloid-A20–deficient animals than in littermate controls (**Fig. 4a**). In line with the extramedullary expansion of myeloid cells and the myeloid origin of osteoclasts, CD115$^+$CD117$^+$ osteoclast precursors were also increased in the spleen of A20-deficient mice compared to wild-type animals (**Fig. 4b**).

Differentiation and activation of osteoclasts requires the TNF superfamily member RANK ligand (RANKL), which is pivotal to systemic bone loss in experimental and human rheumatoid arthritis[20,23]. Although TNF promotes osteoclastogenesis in mice, its effect is RANK dependent[24]. Incubation of wild-type and A20-deficient blood leukocytes with RANKL and macrophage colony-stimulating factor (M-CSF) resulted in a substantial increase in the number of tartrate-resistant acid phosphatase (TRAP)-positive osteoclasts in A20-deficient conditions (**Fig. 4c**). Osteoclasts derived from blood leukocyte cultures of A20-deficient mice were also markedly larger and contained substantially more nuclei than osteoclasts derived from wild-type mice. *In vitro* osteoclast activity, determined by measuring the amount of calcium phosphate resorption in a pit-forming assay, was much higher in the absence of A20 (**Fig. 4d**). *In vivo*, we detected TRAP-positive multinucleated osteoclasts at the bone-erosive front between the inflammatory infiltrate and the outer bone surface in histological sections of ankle joints of myeloid-A20–deficient animals but not in sections from control littermates (data not shown). The expansion of peripheral osteoclast precursors and the increased osteoclast differentiation in the absence of A20 probably contributes to the severe osteoporosis in myeloid-A20–deficient mice.

NF-κB–dependent gene expression in several cell types is known to contribute to the development and progression of autoimmune diseases. Understanding the mechanisms that negatively regulate NF-κB activation is therefore of great importance. We show that myeloid-cell–specific deletion of the NF-κB inhibitor protein A20 in mice results in spontaneous development of an erosive polyarthritis with many hallmarks of rheumatoid arthritis, providing a new mouse

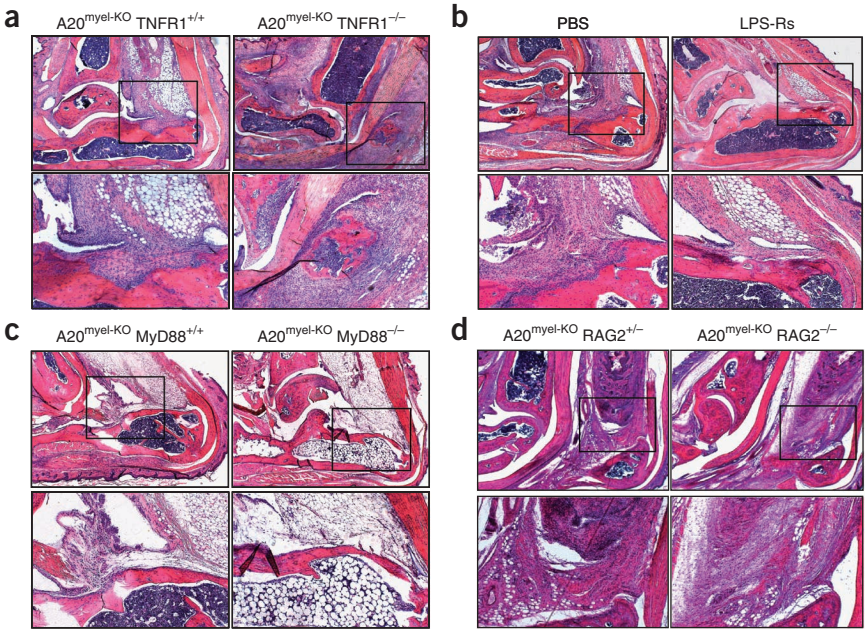

Figure 3 The development of arthritis in A20$^{myel\text{-}KO}$ mice crucially depends on a TLR4-dependent signaling pathway. (**a**) Histological section of an ankle joint of a 25-week-old A20$^{myel\text{-}KO}$ (TNFR1$^{+/+}$) mouse and a double homozygous A20$^{myel\text{-}KO}$ TNFR1$^{-/-}$ littermate mouse stained with haematoxylin and eosin; magnification, 40× (top). Detail of the ankle joint region illustrates the infiltration of mononuclear cells, cartilage destruction and bone erosion in double homozygous A20$^{myel\text{-}KO}$ TNFR1$^{-/-}$ mice; magnification, 100× (bottom). (**b**) Histological section of an ankle joint of a 25-week-old A20$^{myel\text{-}KO}$ mouse after systemic administration of LPS-Rs or phosphate-buffered saline (PBS) control; magnification, 40× (top); detail magnification, 100× (bottom). (**c**) Histological section of an ankle joint of a 25-week-old A20$^{myel\text{-}KO}$ (MyD88$^{+/+}$) mouse and a double homozygous A20$^{myel\text{-}KO}$ MyD88$^{-/-}$ littermate mouse; magnification, 40× (top); detail magnification, 100× (bottom). (**d**) Histological section of an ankle joint of a 20-week-old A20$^{myel\text{-}KO}$ (RAG2$^{+/-}$) mouse and a double homozygous A20$^{myel\text{-}KO}$ RAG2$^{-/-}$ littermate mouse; magnification, 40× (top); detail magnification, 100× (bottom). Each picture is representative of at least four mice.

model of human rheumatoid arthritis. Although we detected high levels of circulating TNF in serum and in joint tissue, the rheumatoid arthritis–like phenotype is not dependent on TNF-dependent signaling but does require TLR4-MyD88–induced signaling and IL-6. This is therapeutically very important in view of the fact that up to 30% of rheumatoid arthritis patients fail to respond to anti-TNF treatment, which is a major problem in the clinic[25]. Together, our data show that A20 has a cell-specific anti-inflammatory function in the pathophysiology of rheumatoid arthritis, and it also provides the new concept that myeloid-specific ablation of an intracellular signaling protein may lead to the development of a rheumatoid arthritis phenotype. Our findings also fortify previous genome-wide association studies indicating that *TNFAIP3* is a susceptibility locus for rheumatoid arthritis in humans[26,27]. Given the importance of proinflammatory gene expression by myeloid cells in innate and adaptive immune responses, it is remarkable that the inflammatory phenotype of myeloid-A20–deficient mice is restricted to the joints. We anticipate that factors other than systemic immune elements might contribute to the rheumatoid arthritis phenotype in myeloid-A20–deficient mice, such as local physical stress and tissue damage resulting in, for example, the release of endogenous TLR ligands in the joints[13]. Most importantly, the cell-specific function of A20 and the specific development of a rheumatoid arthritis–like pathology without any other notable tissue damage in myeloid-A20–deficient

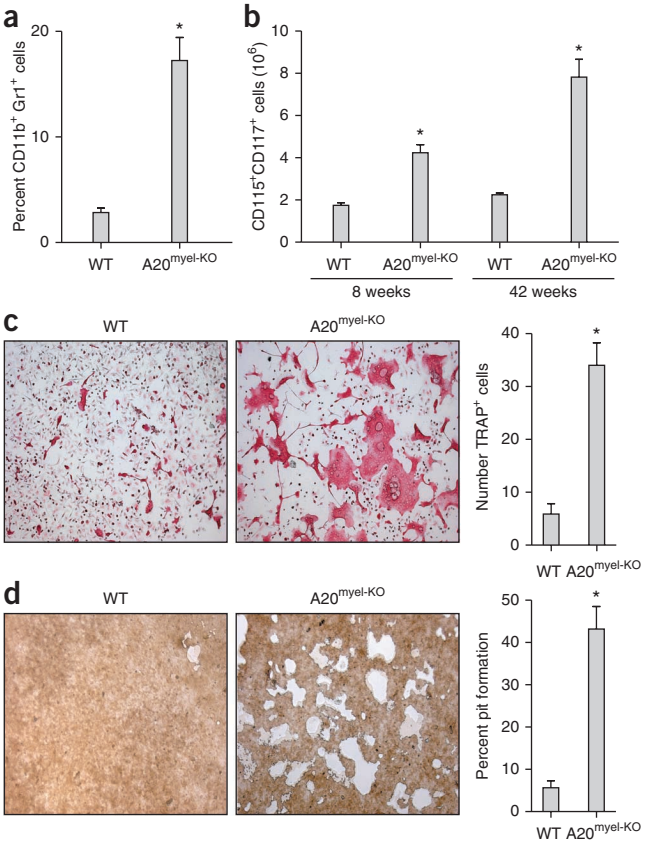

Figure 4 Increased osteoclastogenesis from blood leukocytes of A20$^{myel\text{-}KO}$ mice. (**a**) Percentage of CD11b^{+}Gr1^{+} splenocytes of A20$^{myel\text{-}KO}$ mice ($n = 5$) and control littermates (WT, $n = 5$) as assessed by flow cytometry and gated on living cells. (**b**) Absolute numbers of CD115^{+}CD117^{+} splenocytes within the CD3^{-}CD45R^{-}CD11b^{+} cell population of A20$^{myel\text{-}KO}$ mice ($n = 5$) and control littermates (WT, $n = 4$) at the ages of 8 and 42 weeks. (**c**,**d**) We cultured blood leukocytes of A20$^{myel\text{-}KO}$ ($n = 6$) and control mice (WT, $n = 6$) for 6 days in chamber slides (**c**) or on quartz substrates coated with a calcium phosphate film (**d**) in the presence of M-CSF (20 ng/ml) and RANKL (100 ng/ml). (**c**) After incubation, cultures were fixed and stained for TRAP. We counted TRAP^{+} multinucleated cells (three or more nuclei) in each cup. Error bars represent the mean ± s.e.m. Representative pictures of TRAP-stained blood leukocyte cultures of both groups are shown. (**d**) We removed the cells and assayed resorption of the film by light microscopy. Error bars represent the mean of 10 cups ± s.e.m. Representative pictures of resorption pits are shown. $^{*}P < 0.05$.

mice indicate that modulation of A20 might become an important option for targeted therapy of rheumatoid arthritis.

METHODS

Methods and any associated references are available in the online version of the paper at http://www.nature.com/naturegenetics/.

Note: Supplementary information is available on the Nature Genetics website.

ACKNOWLEDGMENTS

We are grateful to I. Förster for donating the LysM-Cre transgenic mice. We thank H. Heremans for providing us with the IL-6 and control antibodies. We thank T. Hochepied for transgenic services, P. Bogaert and E. Parthoens for technical help, A. Bredan for critical reading of the manuscript and D. Huyghebaert and L. Bellen for animal care. L.V. and J.M. are PhD fellows with the Instituut voor Innovatie door Wetenschap en Technologie (IWT), and J.M. is also supported by an Emmanuel van der Schueren award. C.M.G., L.G. and P.J. are PhD fellows with the Fonds voor Wetenschappelijk Onderzoek-Vlaanderen (FWO). G.v.L. is supported, as a postdoctoral researcher, by the FWO, by an FWO Odysseus Grant and by the Charcot Foundation. M.K. is supported by an Intra European fellowship from the Marie Curie Actions. M.P. is supported by an FP7 EC program grant Masterswitch (EC-223404). B.N.L. is supported by an FWO Odysseus grant, a European Research Council Starting grant and the Group-ID Multidisciplinary Research Partnership grant of Ghent University. Work in the lab of R.B. and G.v.L. is further supported by research grants from the Interuniversity Attraction Poles program (IAP6/18), the FWO, the Belgian Foundation against Cancer, the Strategic Basis Research program of the IWT, the Centrum voor Gezwelziekten, the Hercules Foundation, and the Concerted Research Actions (GOA) and Group-ID MRP of Ghent University.

AUTHOR CONTRIBUTIONS

M.M., P.J., J.M., E.V., M.K., M.S., L.G., E.L., C.M.G., L.V., S.S. and G.v.L. performed the experiments. M.M., P.J., C.M.G., S.S., P.M., B.N.L., M.P., D.E., R.B. and G.v.L. analyzed the data. Y.C., L.B., P.M., M.S.-S. and M.P. provided materials. D.E., R.B. and G.v.L. provided ideas and coordinated the project. R.B. and G.v.L. wrote the manuscript.

COMPETING FINANCIAL INTERESTS

The authors declare no competing financial interests.

Published online at http://www.nature.com/naturegenetics/.
Reprints and permissions information is available online at http://www.nature.com/reprints/index.html.

1. Coornaert, B., Carpentier, I. & Beyaert, R. A20: central gatekeeper in inflammation and immunity. *J. Biol. Chem.* **284**, 8217–8221 (2009).
2. Wertz, I.E. *et al.* De-ubiquitination and ubiquitin ligase domains of A20 downregulate NF-κB signalling. *Nature* **430**, 694–699 (2004).
3. Boone, D.L. *et al.* The ubiquitin-modifying enzyme A20 is required for termination of Toll-like receptor responses. *Nat. Immunol.* **5**, 1052–1060 (2004).
4. Hitotsumatsu, O. *et al.* The ubiquitin-editing enzyme A20 restricts nucleotide-binding oligomerization domain containing 2-triggered signals. *Immunity* **28**, 381–390 (2008).
5. Düwel, M. *et al.* A20 negatively regulates T cell receptor signaling to NF-κB by cleaving Malt1 ubiquitin chains. *J. Immunol.* **182**, 7718–7728 (2009).
6. Lee, E.G. *et al.* Failure to regulate TNF-induced NF-κB and cell death responses in A20-deficient mice. *Science* **289**, 2350–2354 (2000).
7. Vereecke, L., Beyaert, R. & van Loo, G. The ubiquitin-editing enzyme A20 (TNFAIP3) is a central regulator of immunopathology. *Trends Immunol.* **30**, 383–391 (2009).
8. Vereecke, L. *et al.* Enterocyte-specific A20 deficiency sensitizes to tumor necrosis factor-induced toxicity and experimental colitis. *J. Exp. Med.* **207**, 1513–1523 (2010).
9. Clausen, B.E., Burkhardt, C., Reith, W., Renkawitz, R. & Forster, I. Conditional gene targeting in macrophages and granulocytes using LysMcre mice. *Transgenic Res.* **8**, 265–277 (1999).
10. Turer, E.E. *et al.* Homeostatic MyD88-dependent signals cause lethal inflamMation in the absence of A20. *J. Exp. Med.* **205**, 451–464 (2008).
11. Taylor, P.C. & Feldmann, M. Anti-TNF biologic agents: still the therapy of choice for rheumatoid arthritis. *Nat. Rev. Rheumatol.* **5**, 578–582 (2009).
12. Rothe, J. *et al.* Mice lacking the tumour necrosis factor receptor 1 are resistant to TNF-mediated toxicity but highly susceptible to infection by *Listeria monocytogenes*. *Nature* **364**, 798–802 (1993).
13. Huang, Q.Q. & Pope, R.M. The role of Toll-like receptors in rheumatoid arthritis. *Curr. Rheumatol. Rep.* **11**, 357–364 (2009).
14. Hennessy, E.J., Parker, A.E. & O'Neill, L.A. Targeting Toll-like receptors: emerging therapeutics? *Nat. Rev. Drug Discov.* **9**, 293–307 (2010).
15. Adachi, O. *et al.* Targeted disruption of the MyD88 gene results in loss of IL-1– and IL-18–mediated function. *Immunity* **9**, 143–150 (1998).
16. Aoki, S. *et al.* Role of enteric bacteria in the pathogenesis of rheumatoid arthritis: evidence for antibodies to enterobacterial common antigens in rheumatoid sera and synovial fluids. *Ann. Rheum. Dis.* **55**, 363–369 (1996).
17. Yoshino, S., Sasatomi, E., Mori, Y. & Sagai, M. Oral administration of lipopolysaccharide exacerbates collagen-induced arthritis in mice. *J. Immunol.* **163**, 3417–3422 (1999).
18. Nieuwenhuis, E.E. *et al.* Oral antibiotics as a novel therapy for arthritis: evidence for a beneficial effect of intestinal *Escherichia coli*. *Arthritis Rheum.* **43**, 2583–2589 (2000).
19. Vaahtovuo, J., Munukka, E., Korkeamaki, M., Luukkainen, R. & Toivanen, P. Fecal microbiota in early rheumatoid arthritis. *J. Rheumatol.* **35**, 1500–1505 (2008).
20. McInnes, I.B. & Schett, G. Cytokines in the pathogenesis of rheumatoid arthritis. *Nat. Rev. Immunol.* **7**, 429–442 (2007).
21. Sato, K. *et al.* Th17 functions as an osteoclastogenic helper T cell subset that links T cell activation and bone destruction. *J. Exp. Med.* **203**, 2673–2682 (2006).
22. Shinkai, Y. *et al.* RAG-2-deficient mice lack mature lymphocytes owing to inability to initiate V(D)J rearrangement. *Cell* **68**, 855–867 (1992).
23. Wada, T., Nakashima, T., Hiroshi, N. & Penninger, J.M. RANKL-RANK signaling in osteoclastogenesis and bone disease. *Trends Mol. Med.* **12**, 17–25 (2006).
24. Li, J. *et al.* RANK is the intrinsic hematopoietic cell surface receptor that controls osteoclastogenesis and regulation of bone mass and calcium metabolism. *Proc. Natl. Acad. Sci. USA* **97**, 1566–1571 (2000).
25. Criscione, L.G. & St. Clair, E.W. Tumor necrosis factor-α antagonists for the treatment of rheumatic diseases. *Curr. Opin. Rheumatol.* **14**, 204–211 (2002).
26. Plenge, R.M. *et al.* Two independent alleles at 6q23 associated with risk of rheumatoid arthritis. *Nat. Genet.* **39**, 1477–1482 (2007).
27. Thomson, W. *et al.* Rheumatoid arthritis association at 6q23. *Nat. Genet.* **39**, 1431–1433 (2007).

ONLINE METHODS

Generation of tissue-specific A20-deficient mice. Conditional A20 *Tnfaip3* knockout mice, in which exons 4 and 5 of *Tnfaip3* are flanked by two LoxP sites, were generated as previously described[8]. $A20^{NFL}$ mice, still containing the neomycin selection cassette, were crossed to a Flp-deleter strain[28] to remove the Frt-flanked neomycin cassette generating a *Tnfaip3* floxed allele ($A20^{FL}$) (**Supplementary Fig. 1**). $A20^{FL/FL}$ mice were crossed with LysM-Cre transgenic mice[9] to generate a myeloid-specific A20 knockout mouse ($A20^{myel\text{-}KO}$). Experiments were performed on mice backcrossed into the C57BL/6 genetic background for at least three generations. Mice were housed in individually ventilated cages in the specific pathogen-free animal facility of the Department for Molecular Biomedical Research (VIB and Ghent University). All experiments on mice were performed according to institutional, national and European animal regulations.

Clinical score. Mice were scored twice a week for development of peripheral arthritis. A score ranging from 0 to 3 was assigned to each paw, with 0 being normal, 0.5 being swelling of one or more toes, 1 being mild swelling of the wrist and/or ankle or carpus and/or tarsus, 2 being moderate swelling of the wrist and/or ankle or carpus and/or tarsus or mild swelling of both, and 3 being severe swelling of the entire paw.

Antibody treatment. Twenty-week-old $A20^{myel\text{-}KO}$ mice showing clear clinical rheumatoid arthritis pathology were treated by intraperitoneal injection every 4 days with neutralizing TNF antibodies[29] (MP6-XT22 MAb, 20 mg/kg body weight), IL-6 antibodies[30] (20F3 MAb, 10 mg/kg body weight) and isotype control antibodies, and clinical pathology was scored as described.

Histology. Total ankle joints were dissected, fixed in phosphate-buffered formalin (pH 7.4), decalcified in 5% buffered formic acid and embedded in paraffin wax. Ankle joint sections were stained with hematoxylin and eosin. Except for B220 detection, proteolytic-enzyme–induced epitope retrieval was performed on deparaffinized and hydrated sections of decalcified ankles by a 15 min incubation at 37 °C 0.05% pepsin (Sigma) in 0.02N HCl, or 0.004% proteinase K (Sigma), 0.1% $CaCl_2$ in TE (Tris and EDTA) pH 8 for CD3 and F4/80 detection, respectively. After a 20-min block in PBS containing 5% BSA and 2% serum of the species of the second antibody, primary antibody was applied overnight at 4 °C in the same solution. The primary antibodies rat anti-mouse B220 (BD Pharmingen), rabbit anti-human CD3 (Dako) and rat anti-mouse F4/80 (eBioscience) were followed by a 30 min incubation with the secondary antibodies Alexa Fluor 546 goat anti-rat IgG (Invitrogen), DyLight 649 donkey anti-rabbit IgG (Jackson ImmunoResearch) or biotin-SP donkey anti-rat IgG (Jackson ImmunoResearch) in PBS, respectively. Alexa Fluor 647 conjugated streptavidin (Invitrogen) was applied for 30 min in PBS as a third step to detect F4/80. Cell nuclei were counterstained by mounting with ProLong Gold anti-fade reagent with DAPI (Invitrogen). Microscopy was performed using a TCS SP5 confocal microscope (Leica).

PET-CT. Mice were injected with 0.5 mCi fluorodeoxyglucose (FDG) 1 hour before the start of each PET-CT scan. Scans were performed using the Gamma Medica Ideas labPET 8 (GMI) microPET device, which consists of $2 \times 2 \times 10$ mm^3 LYSO/LGSO scintillators in an 8-pixel, quad-APD detector module arrangement. Twenty-minute scans were performed in two bed positions and afterwards statically reconstructed on a $0.5 \times 0.5 \times 1.175$ mm voxel grid by 60 iterations of maximum likelihood expectation maximization. A μCT scan of the animal was also acquired with the same multimodal scanner in fly mode acquiring 512 projections (2×2 rebinning) with the 50-μm focal spot size tube set to 70 kV and 145 μA and the magnification at 1.3 (field of view = 91.08 mm). A general purpose reconstruction mode was used in a 512×512 matrix of 150-μm pixel size. The resultant image was then fused with the μPET scan. Based on the CT, regions of interest were defined on a slice-by-slice basis delineating the hind paws of the animals. The mean voxel value of the FDG PET activation in these regions of interest was a posteriori corrected for injected activity to deliver a quantitative measure of inflammation.

Depletion of commensal intestinal bacteria. Mice were treated with ciprofloxacin (200 mg/l; Sigma-Aldrich), ampicillin (1 g/l; Sigma-Aldrich), metronidazole (1 g/l; Sigma-Aldrich) and vancomycin (500 mg/l; Labconsult) in drinking water. Every 2 weeks, the presence of colonic microflora was determined by culturing fecal samples in both 'brain heart infusion' (BD) and thioglycollate medium (Sigma-Aldrich).

Protein blot analysis. Peritoneal macrophages were lysed in E1A lysis buffer (250 mM NaCl, 50 mM Tris pH 7.4, 0.1% NP-40) containing a complete protease inhibitor cocktail (1:25) (Roche). Supernatants were separated by sodium dodecyl sulfate polyacrylamide gel electrophoresis (SDS-PAGE), transferred to nitrocellulose membranes and immunodetected with IκBα (Santa Cruz Biotechnology, Inc.), mouse A20 (Santa Cruz Biotechnology, Inc.) and actin (MP Biomedicals) antibodies.

Isolation of peritoneal macrophages. Mice were injected intraperitoneally with 1 ml of thioglycollate broth. After four days, mice were killed by cervical dislocation and macrophages were washed from the peritoneal cavity with 10 ml of ice-cold sterile PBS and centrifuged at 106*g* for 5 min. The pellet was resuspended in RPMI 1640 medium (Invitrogen) supplemented with 10% (v/v) heat-inactivated FCS (FCS), 1% penicillin streptavidin, 2% L-glutamate and 2% Na-pyruvate.

Quantification of cytokines. Cytokines in serum and supernatants were quantified by the Cytometric Bead Array Mouse Inflammation Kit (BD Biosciences) on a FACS Calibur cytometer equipped with CellQuest Pro and CBA software (BD Biosciences). A Bio-plex Pro kit was used for the mouse cytokines IL-6, IL-1β and MCP-1 (Bio-Rad) on the Bio-plex 200 system (Bio-Rad). Enzyme-linked immunosorbent assay (ELISA) was used for mouse TNF (eBioscience).

Isolation of cells from joint tissue and quantitative real-time PCR. Ankle joints were isolated from the hind legs, and joints were cut in two through the joint space. Dissected joints were incubated in RPMI 1640 containing 10% FCS, 1% Glutamine, 1% peniclin streptavidin and 10mg/ml collagenase D (Roche) for 90 min at 37 °C to release synovial cells. Total RNA was purified from joint cells using the TRIzol reagent (Invitrogen). RNA samples (1 μg) were treated with DNase I, Amp Grade (Invitrogen) before complementary DNA (cDNA) synthesis using the iScript cDNA synthesis kit (Bio-Rad) according to the manufacturer's instructions. Ten nanograms of cDNA was used for quantitative PCR in a total volume of 10μl with LightCycler 480 SYBR Green I Master Mix (Roche) and specific primers on a LightCycler 480 (Roche). Real-time PCR reactions were performed in triplicates. The primer sequences used are listed in **Supplementary Table 1**.

Flow cytometry. All flow cytometric analyses were performed on a FACS Calibur (BD Biosciences). Cell suspensions were prepared from total spleens and/or inguinal lymph nodes. Red blood cells were lysed by incubation with ACK lysis buffer (BioWhittaker). Total cell suspensions were pre-incubated with purified rat anti-mouse CD16/CD32 (mouse Fc block; BD Biosciences, Pharmingen). Subsequently, cells were incubated with anti–CD11b-PerCp Cy5.5 and anti–Gr1-FITC (BD Biosciences), anti–CD4-FITC or anti–CD8α-FITC (BD biosciences) with anti–CD44-APC and anti–CD62L-PE (eBioscience). To assess the amount of osteoclast precursors, splenocytes were incubated with anti–CD11b-PerCp Cy5.5 (BD Biosciences), anti–CD3-V500, anti–CD45R-PECy7, CD117-APC and CD115-PE (all from eBioscience). To analyze Th17 cells, splenocytes and inguinal lymph node cells were incubated with 10 ng/ml phorbol-12-myristate-13-acetate (PMA) and 250 ng/ml ionomycin for 8 hours. Four hours before assessment, cells were incubated with 5 μg/ml Brefeldin A, fixed, permeabilized with a fixation and permeabilization kit (eBioscience) and incubated with anti–IL-17-PerCP-Cy5.5 (eBioscience) and anti–CD4-FITC.

***In vitro* induction of osteoclast formation and TRAP staining.** *In vitro* osteoclastogenesis assay of blood cells was performed as described[31]. Briefly, blood cells (2.5×10^4) in a volume of 400 μl were seeded in chamber slides (Lab-Tek Brand Products, Nalge Nunc International) and incubated for 6 days with 20 ng/ml M-CSF and 100 ng/ml RANKL (R&D Systems). On day 3, the media and stimuli were replaced. On day 6, media were removed and cells were stained for the presence of TRAP. Briefly, cells were fixed with 3.7% formaldehyde in Ca^{2+}- and Mg^{2+}-free PBS for 10 min and subsequently for 1 min with

doi:10.1038/ng.874

a 1:1 (v/v) solution of ethanol and acetone. Cells were incubated for 10 min with a staining solution (0.01% naphthol AS-MX phosphate (Sigma-Aldrich), 50 mM tartrate and 0.06% fast red violet LB salt (Sigma-Aldrich) in 0.1 M acetate buffer pH 5.0) and washed with distilled water. Staining solutions were freshly prepared before use. $TRAP^+$ multinucleated cells (three or more nuclei) were defined as osteoclasts.

Pit-forming assay. Suspensions of blood leukocytes were obtained as described above, washed twice with ice-cold PBS, and resuspended in α-modified minimal essential medium containing 10% FCS (Gibco). Cells (10^6) were cultured for 6 days with M-CSF (20 ng/ml) and RANKL (100 ng/ml) (both from R&D Systems) on transparent quartz slides coated with a calcium phosphate film (BioCoat Osteologic Discs; BD Biosciences Pharmingen). On day 3, media and stimuli were replaced, and on day 6, cells were removed and resorption of the film was assessed by light microscopy. In each well, the percentage of resorption pits was determined in eight different regions.

Statistical analyses. Values in the graphs indicate group means ± s.d. or s.e.m., as indicated in the legends. Comparisons between groups were performed by two-tailed paired or unpaired Student's *t*-test. Multigroup comparisons were performed by one-way analysis of variance with post-hoc Bonferroni correction. $P < 0.05$ was considered to indicate statistical significance.

28. Rodríguez, C.I. *et al.* High-efficiency deleter mice show that FLPe is an alternative to Cre-loxP. *Nat. Genet.* **25**, 139–140 (2000).
29. Onizawa, M. *et al.* Signaling pathway via TNF-α/NF-κB in intestinal epithelial cells may be directly involved in colitis-associated carcinogenesis. *Am. J. Physiol. Gastrointest. Liver Physiol.* **296**, G850–G859 (2009).
30. Starnes, H.F. *et al.* Anti-IL-6 monoclonal antibodies protect against lethal *Escherichia coli* infection and lethal tumor necrosis factor-α challenge in mice. *J. Immunol.* **145**, 4185–4191 (1990).
31. Geboes, L. *et al.* Freund's complete adjuvant induces arthritis in mice lacking a functional interferon-γ receptor by triggering tumor necrosis factor α-driven osteoclastogenesis. *Arthritis Rheum.* **56**, 2595–2607 (2007).

Supplementary Information

A20 (TNFAIP3) deficiency in myeloid cells triggers erosive polyarthritis resembling rheumatoid arthritis

Mourad Matmati[1,2]*, Peggy Jacques[3]*, Jonathan Maelfait[1,2], Eveline Verheugen[3], Mirjam Kool[1,4], Mozes Sze[1,2], Lies Geboes[5], Els Louagie[3], Conor Mc Guire[1,2], Lars Vereecke[1,2], Yuanyuan Chu[6], Louis Boon[7], Steven Staelens[8], Patrick Matthys[5], Bart N. Lambrecht[4], Marc Schmidt-Supprian[6], Manolis Pasparakis[9], Dirk Elewaut[3+], Rudi Beyaert[1,2+] and Geert van Loo[1,2+]

[1]Department for Molecular Biomedical Research, Unit of Molecular Signal Transduction in Inflammation, VIB, B-9052 Ghent, Belgium.
[2]Department of Biomedical Molecular Biology, Ghent University, B-9052 Ghent, Belgium.
[3]Department of Rheumatology, Laboratory for Molecular Immunology and Inflammation, Ghent University Hospital, B-9000 Ghent, Belgium.
[4]Department of Respiratory Diseases, Laboratory of Immunoregulation and Mucosal Immunology, Ghent University Hospital, B-9000 Ghent, Belgium.
[5]Rega Institute, Leuven University, B-3000 Leuven, Belgium.
[6]Max Planck Institute of Biochemistry, D-82152 Martinsried, Germany.
[7]Bioceros BV, N-3584 Utrecht, The Netherlands.
[8]Medical Image and Signal Processing, Ghent University– IBBT, B-9000 Ghent, and Molecular Imaging Center Antwerp, Antwerp University, B-2610 Antwerp, Belgium.
[9]Institute for Genetics, Centre for Molecular Medicine (CMMC), and Cologne Excellence Cluster on Cellular Stress Responses in Aging-Associated Diseases (CECAD), University of Cologne, D-50674 Cologne, Germany.
*These authors contributed equally
[+]These authors share senior authorship

Address correspondence to: geert.vanloo@dmbr.ugent.be or rudi.beyaert@dmbr.ugent.be or dirk.elewaut@ugent.be

Nature Genetics: doi:10.1038/ng.874

Supplementary Table

Supplementary Table 1 Primer sequences of mouse-specific cytokines for qPCR

TNF forward	ACCCTGGTATGAGCCCATATAC
TNF reverse	ACACCCATTCCCTTCACAGAG
IL-1β forward	CACCTCACAAGCAGAGCACAAG
IL-1β reverse	GCATTAGAAACAGTCCAGCCCATAC
IL-6 forward	GAGGATACCACTCCCAACAGACC
IL-6 reverse	AAGTGCATCATCGTTGTTCATACA
IL-23 forward	GCACCAGCGGGACATATGA
IL-23 reverse	CCTTGTGGGTCACAACCATCT

Nature Genetics: doi:10.1038/ng.874

Supplementary Figures

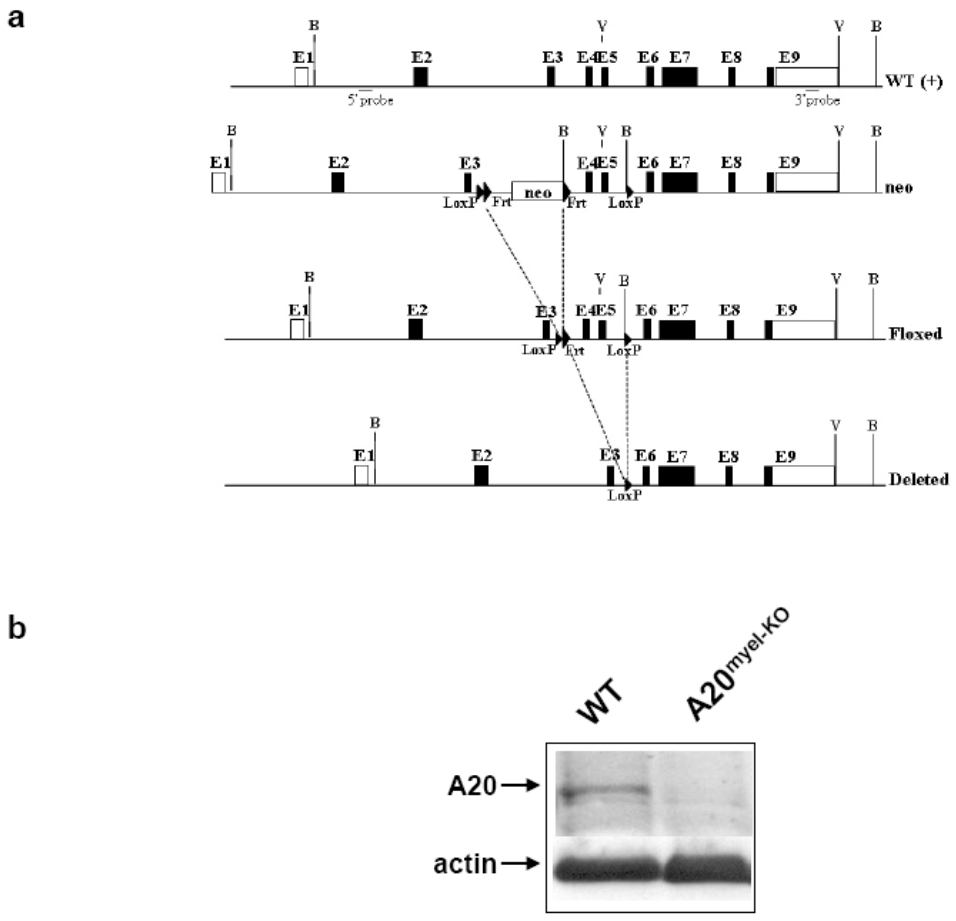

Supplementary Figure 1 Generation of myeloid-specific A20 knockout mice. **(a)** Targeting scheme. Diagram showing the wild-type *Tnfaip3* genomic locus (WT), the neomycin-resistance-containing (neo) allele, the LoxP-flanked (Floxed) allele, and the deleted A20 allele. Boxes indicate exons 1 to 9 (E1–E9). Restriction enzyme sites and the location of the probe used for Southern blot analysis are depicted. B, *Bam*H1; V, *Eco*RV. LoxP and Frt sites are indicated by arrowheads. **(b)** Western blot analysis for A20 expression in BMDMs, derived from WT mice and $A20^{myel\text{-}KO}$ mice.

Nature Genetics: doi:10.1038/ng.874

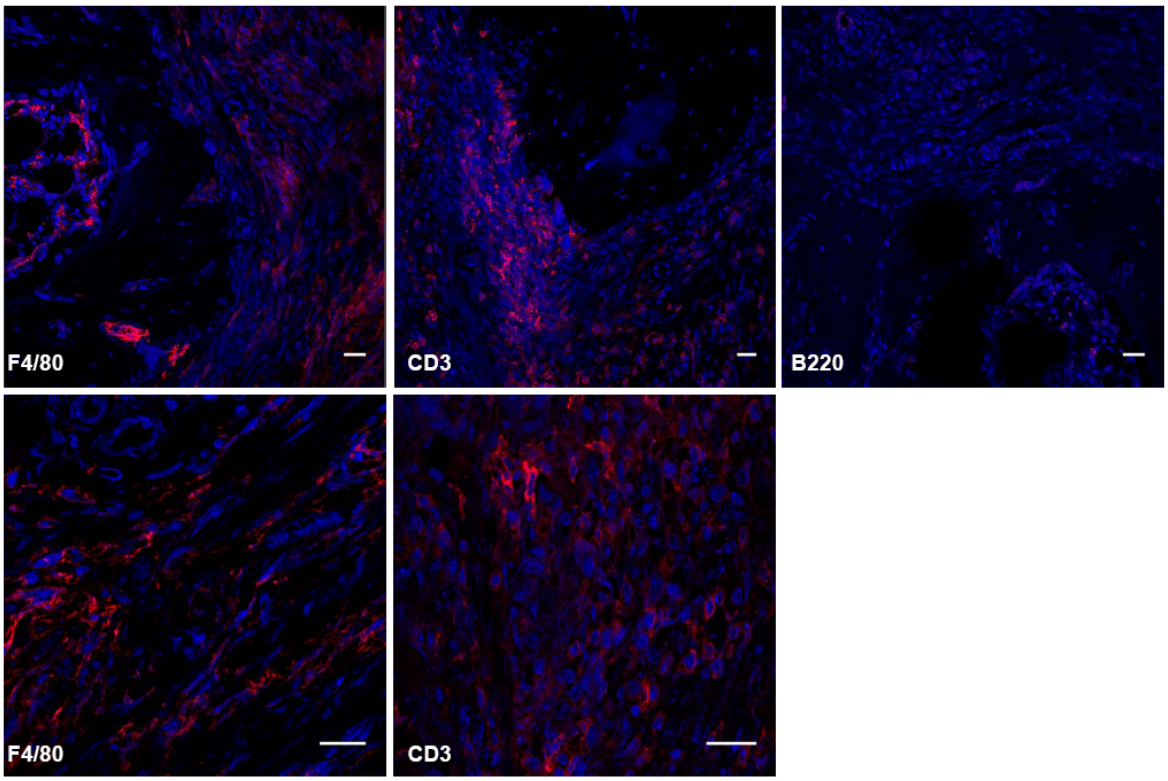

Supplementary Figure 2 Immune cell infiltration in joints from A20$^{myel\text{-}KO}$ mice. Immunohistological section of ankle joints stained with anti-F4/80 (macrophages), anti-CD3 (T cells), and anti-B220 (B cells) antibodies. Detail magnification (lower); scale bars = 20µm.

Nature Genetics: doi:10.1038/ng.874

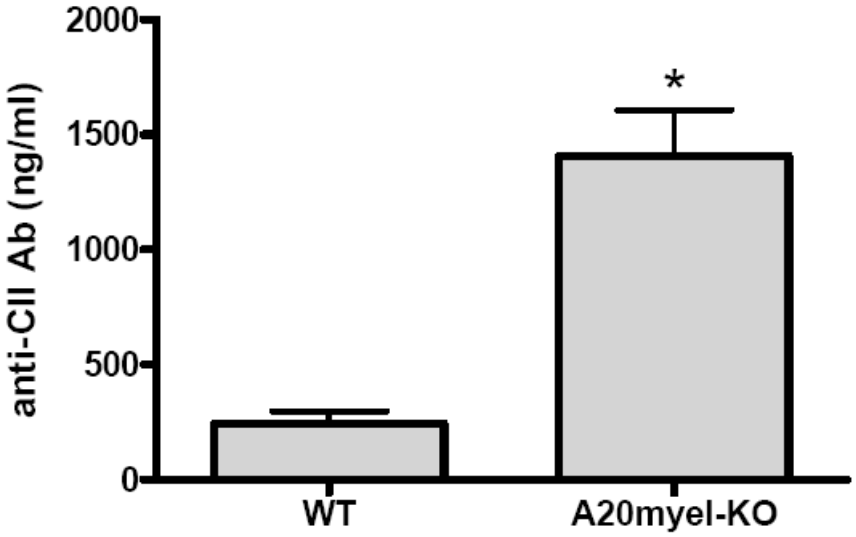

Supplementary Figure 3 Antibody production in A20$^{myel\text{-}KO}$ mice. Serum levels of IgG autoantibodies specific for collagen type II in A20$^{myel\text{-}KO}$ mice (n=9) and control littermates (WT, n=6). * $p < 0.05$.

Nature Genetics: doi:10.1038/ng.874

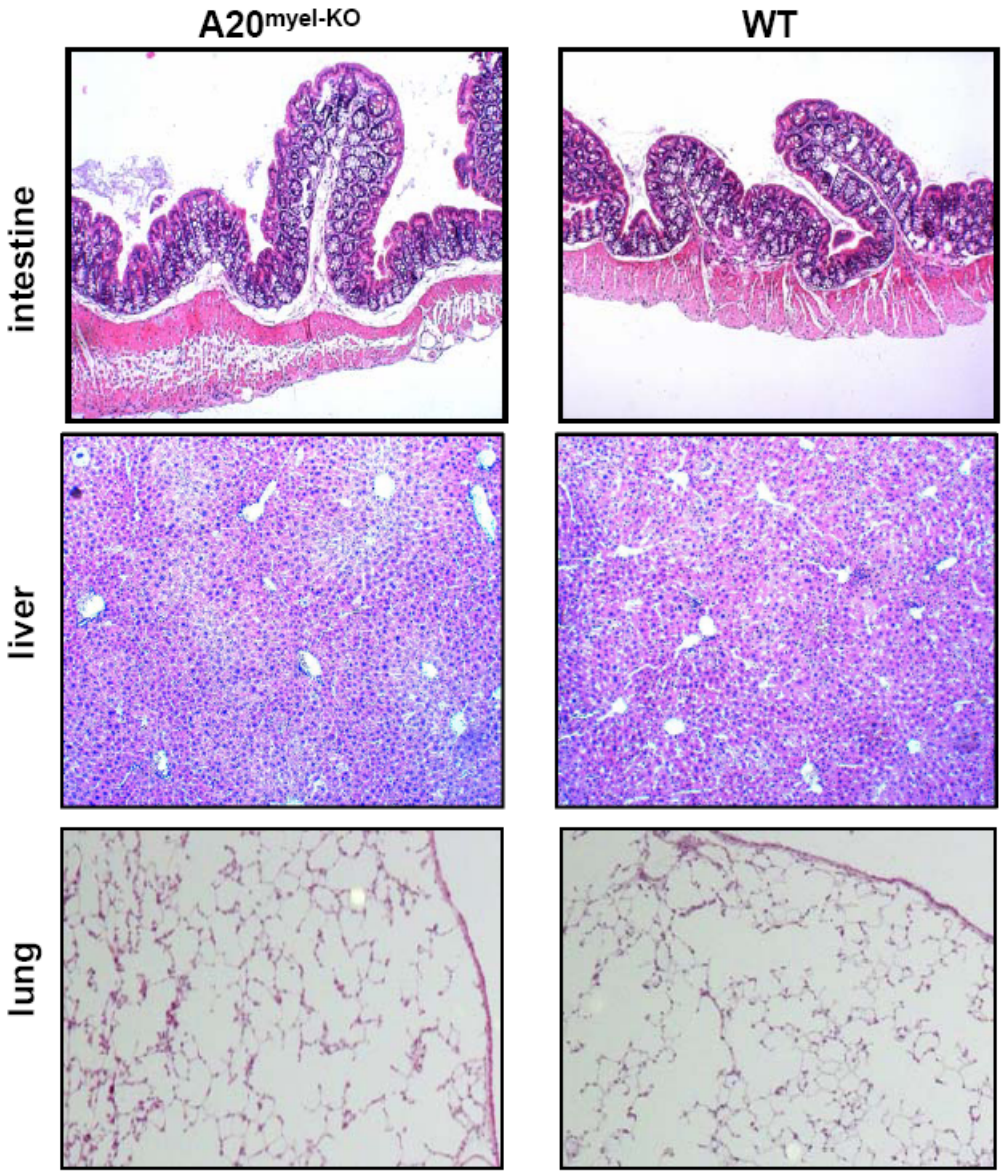

Supplementary Figure 4 A20$^{myel\text{-}KO}$ mice do not develop multi-organ inflammation. H&E staining of histological sections of intestine, liver and lung tissue from A20$^{myel\text{-}KO}$ and littermate control (WT) mice.

Nature Genetics: doi:10.1038/ng.874

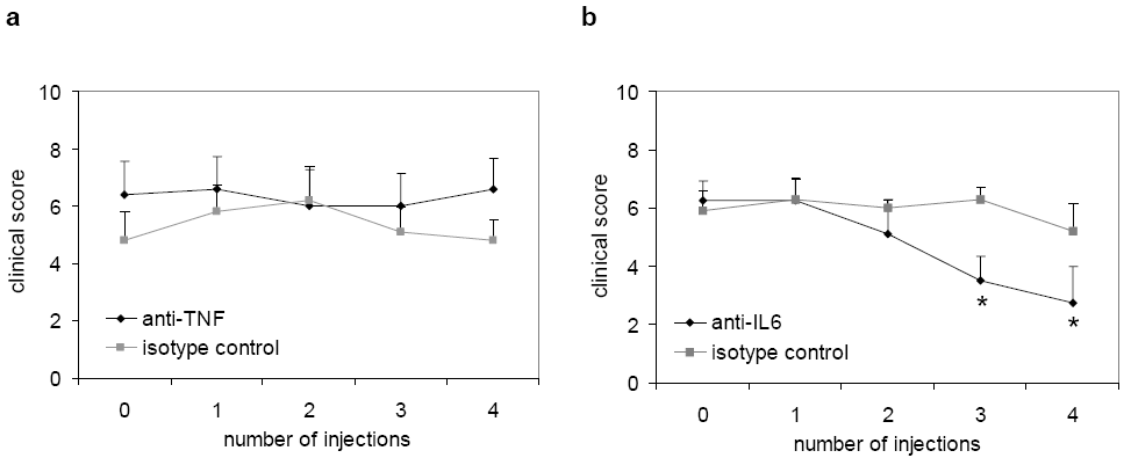

Supplementary Figure 5 Systemic anti-IL-6 treatment suppresses disease progression in A20$^{myel\text{-}KO}$ mice, in contrast to anti-TNF treatment. **(a)** 20-week-old A20$^{myel\text{-}KO}$ mice showing arthritis-like pathology were treated with neutralizing anti-TNF antibodies (n=5) or isotype control antibodies (n=5) and clinically scored for disease regression. **(b)** 20-week-old A20$^{myel\text{-}KO}$ mice showing arthritis-like pathology were treated with neutralizing anti-IL-6 antibodies (n=5) or isotype control antibodies (n=5) and clinically scored for disease regression. * $p < 0.05$ compared to start of therapeutic treatment.

Nature Genetics: doi:10.1038/ng.874

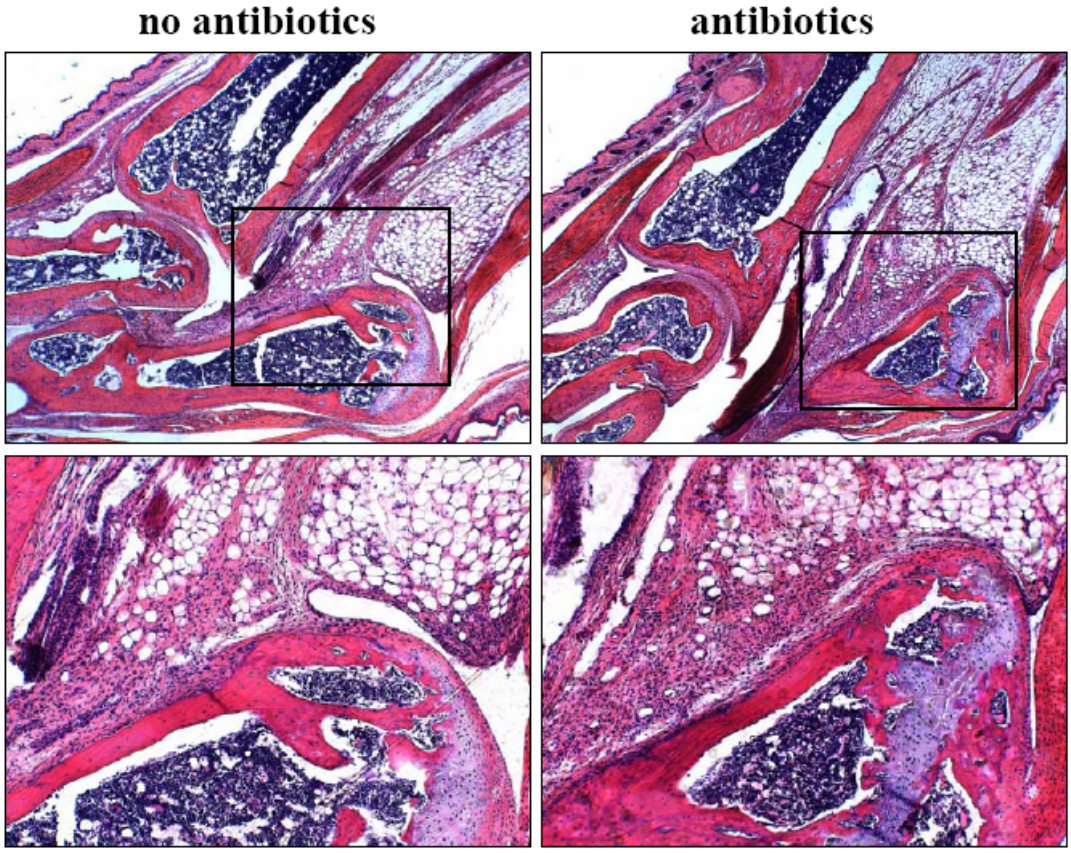

Supplementary Figure 6 Antibiotic treatment does not protect A20$^{myel\text{-}KO}$ mice from arthritis development. Histological section of ankle joint of 25 weeks old A20$^{myel\text{-}KO}$ mouse either or not treated with broad-spectrum antibiotics; magnification 40x (upper); detail magnification 100x (lower). Each picture is representative of at least four mice.

Nature Genetics: doi:10.1038/ng.874

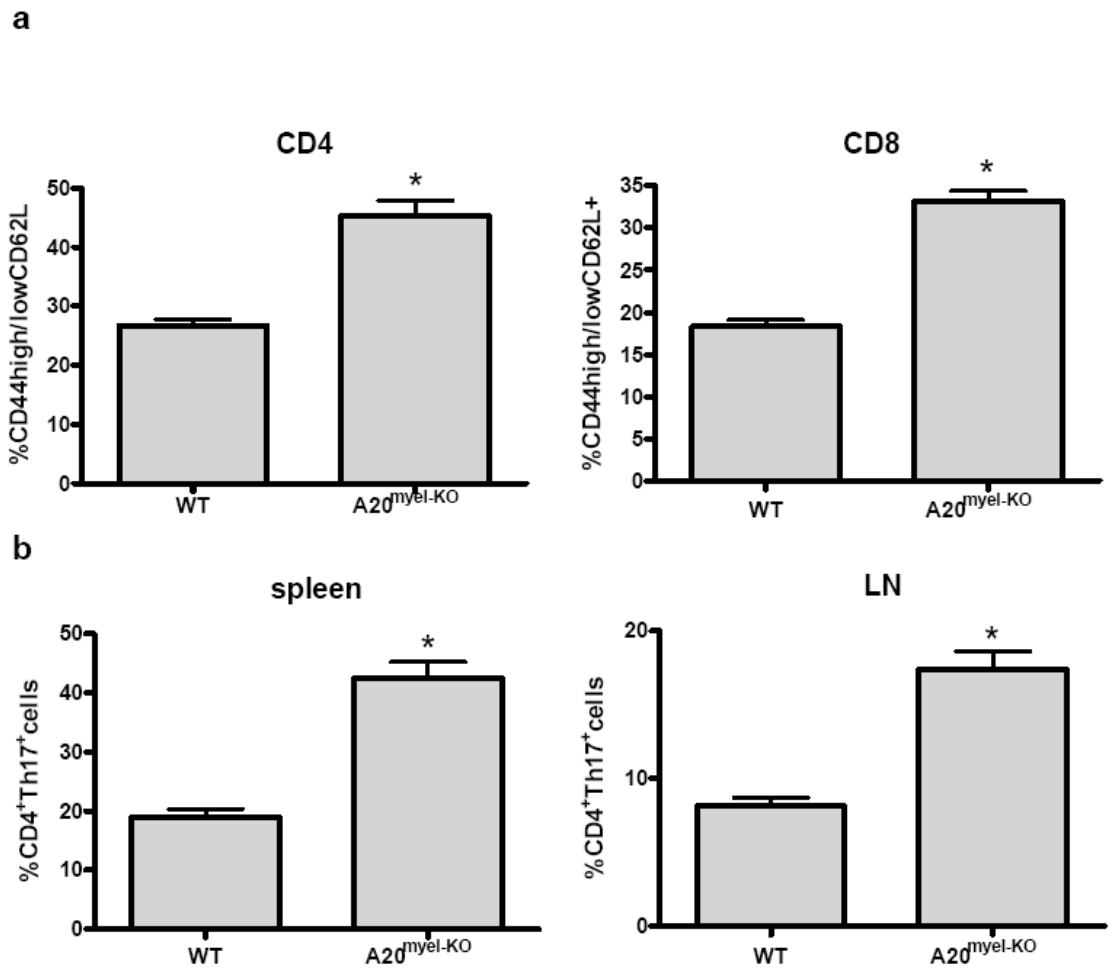

Supplementary Figure 7 Induction of the adaptive immune system in A20$^{myelo\text{-}KO}$ mice. **(a)** Percentages of CD4$^+$ and CD8$^+$ memory cells in the lymphocyte gate of A20$^{myel\text{-}KO}$ (n=6) and WT littermates (n=5) as assessed by flow cytometry. **(b)** Percentages of Th17 positive CD4$^+$ T cells in the inguinal lymph node and spleen from A20$^{myel\text{-}KO}$ mice (n=6) and WT littermates (n=5) as assessed by flow cytometry. * $p < 0.05$.

Nature Genetics: doi:10.1038/ng.874

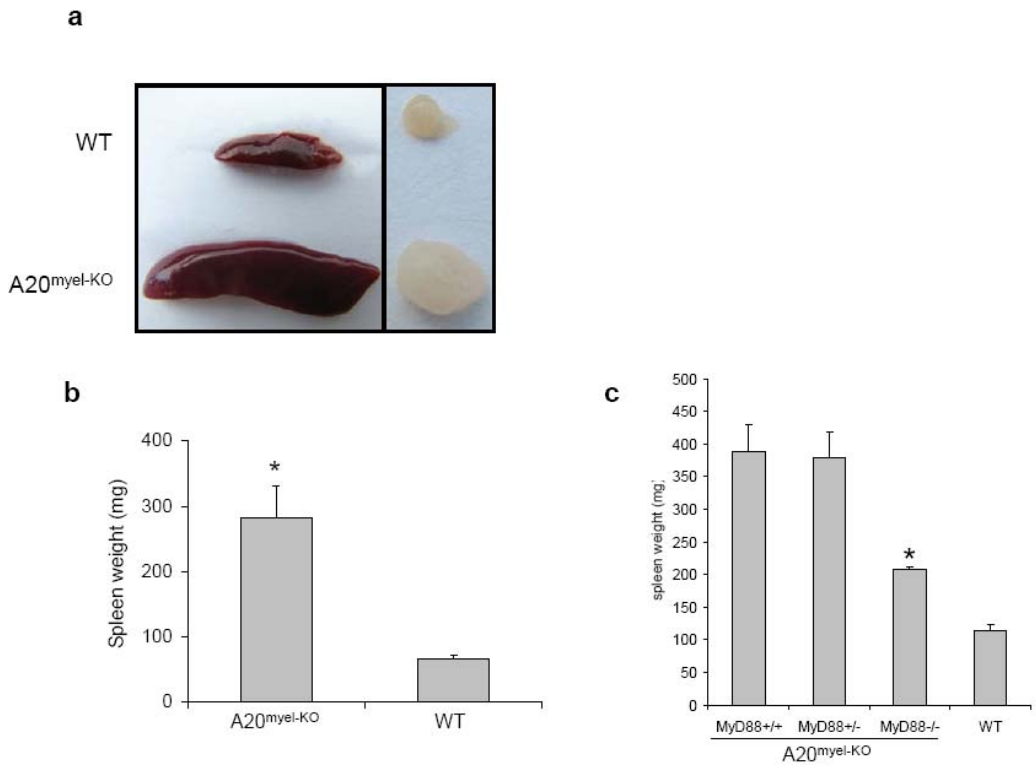

Supplementary Figure 8 A20$^{myel\text{-}KO}$ mice have splenomegaly and enlargement of inguinal and axillary lymph nodes. **(a)** Splenomegaly and enlargement of inguinal lymph nodes in A20$^{myel\text{-}KO}$ mice. (**b)** Spleen weight of 12-week-old A20$^{myel\text{-}KO}$ (n=10) and WT mice (n=10). (**c**) Spleen weight of 20-week-old A20$^{myel\text{-}KO}$/MyD88$^{+/+}$(n=6), A20$^{myel\text{-}KO}$/MyD88$^{+/-}$(n=8), A20$^{myel\text{-}KO}$/MyD88$^{-/-}$ (n=6) and WT mice (n=6). Bars represent averages ± SEM. * $p < 0.05$.

Nature Genetics: doi:10.1038/ng.874

Paper IV

A20 and CYLD Do Not Share Significant Overlapping Functions during B Cell Development and Activation

Yuanyuan Chu, Valeria Soberon, Laura Glockner, Rudi Beyaert, Ramin Massoumi, Geert van Loo, Daniel Krappmann and Marc Schmidt-Supprian

J Immunol published online 21 September 2012
http://www.jimmunol.org/content/early/2012/09/21/jimmunol.1200396

The Journal of Immunology is published twice each month by The American Association of Immunologists, Inc., 9650 Rockville Pike, Bethesda, MD 20814-3994.

Print ISSN: 0022-1767 Online ISSN: 1550-6606.

Published September 21, 2012, doi:10.4049/jimmunol.1200396

A20 and CYLD Do Not Share Significant Overlapping Functions during B Cell Development and Activation

Yuanyuan Chu,* Valeria Soberon,*,[1] Laura Glockner,[†,1] Rudi Beyaert,[‡,§] Ramin Massoumi,[¶] Geert van Loo,[‡,§] Daniel Krappmann,[†] and Marc Schmidt-Supprian*

The ubiquitin-editing enzyme A20 (TNFAIP3) and the deubiquitinase CYLD are central negative regulators of NF-κB signaling. Both can act by removing nonproteolytic K63-linked polyubiquitin chains from an overlapping set of signaling molecules. In B cells, A20 deficiency results in hyperactivity, loss of immune homeostasis, inflammation, and autoimmunity. The reported consequences of CYLD deficiency are controversial, ranging from an absence of effects to dramatic B cell hyperplasia. These differences could be due to varying compensation for the loss of CYLD function by A20. Therefore, to explore potential overlapping physiological functions between A20 and CYLD, we generated and characterized A20/CYLD double-deficient B cells. Interestingly, the lack of both A20 and CYLD did not exacerbate the developmental defects and hyperresponsive activity of A20-deficient B cells. In addition, the extent of B cell activation after in vitro stimulation with anti-CD40, LPS, and CpG was comparable in B cells lacking A20/CYLD and A20 alone. However, in response to BCR cross-linking, we observed small but reproducible additive effects of the lack of A20 and CYLD. Taken together, our results demonstrate that A20 and CYLD do not share significant functions during B cell development and activation. *The Journal of Immunology*, **2012, 189: 000–000.**

The NF-κB pathway plays an important role in many physiological processes including innate and adaptive immunity, cell survival, and proliferation. NF-κB–activating signals can be delivered from immune cell-surface receptors such as TNFR, BCR, CD40, and TLRs. Tight control of these signals is required to maintain immune cell homeostasis and prevent persistent activation of NF-κB, which may lead to chronic inflammation, autoimmunity, and tumorigenesis.

The modification of key signaling molecules such as RIP1, TNFR-associated factor (TRAF) 6, or MALT1 with polyubiquitin chains has emerged as an essential regulatory mechanism of NF-κB activation. Linkage with polyubiquitin chains via lysine 48 (K48) results in proteosomal degradation of the target protein. In contrast, nondegradative and regulatory functions are mediated through K63 and linear polyubiquitin chains that serve as scaffold molecules to recruit different kinase complexes. Ubiquitination is reversible and counterregulated by deubiquitinating enzymes (summarized in Refs. 1, 2). Several deubiquitinases (DUBs) have been reported to negatively regulate NF-κB. Among them are A20, CYLD, Cezanne, and USP21 (3–6).

A20, encoded by the TNF-α–inducible gene 3 (Tnfaip3), is a ubiquitin-modifying enzyme that negatively regulates K63-linked ubiquitination events and induces protein degradation via K48-linked polyubiquitin chains. Gene inactivation studies in mice established A20 as the central negative regulator of multiple NF-κB–activating signaling pathways. Lack of signal containment in A20-deficient mice results in severe inflammation and lethality that is triggered by MyD88-dependent TLR signaling initiated by the commensal flora (7, 8). Cell type-specific deletion of A20 in immune cells and other tissues like intestinal epithelial cells and skin further confirmed its crucial role in the maintenance of tissue homeostasis and to prevent inflammatory diseases including autoimmunity (9–15). In B cells, loss of A20 causes hyperreactivity, general immune activation, and the production of autoantibodies (10, 11, 16).

In line with these studies, polymorphisms and mutations in the A20 gene locus are strongly associated with human autoimmune diseases (17–21). In contrast, CYLD mutations predispose to familial cylindromatosis, which is characterized by the development of benign tumors of skin appendages (22).

Using murine knockout (KO) models, the DUB CYLD was reported to be involved in a wide range of physiological processes including immune cell function, osteoclastogenesis, spermatogenesis, and tumorigenesis (23). The consensus mechanism of these functions is CYLD's specificity for removing K63-linked polyubiquitin chains from substrates, thereby controlling different pathways like NF-κB, MAPK, and Wnt signaling (24–28). Most of the known molecular targets of CYLD's DUB activity are involved in NF-κB signaling pathways.

Studies using a number of independently generated CYLD-deficient mice came to different conclusions regarding the cell type-specific roles of CYLD in the negative regulation of NF-κB. In particular, the role of CYLD in B cell function is controversial.

*Max Planck Institute of Biochemistry, 82152 Martinsried, Germany; [†]Research Unit Cellular Signal Integration, Institute of Molecular Toxicology and Pharmacology, Helmholtz Center Munich–German Research Center for Environmental Health, 85764 Neuherberg, Germany; [‡]Department for Molecular Biomedical Research, Flanders Institute for Biotechnology, Ghent University, B-9052 Ghent, Belgium; [§]Department of Biomedical Molecular Biology, Ghent University, B-9052 Ghent, Belgium; and [¶]Department of Laboratory Medicine, Lund University, 20502 Malmö, Sweden

[1]V.S. and L.G. contributed equally to this work.

Received for publication January 31, 2012. Accepted for publication August 31, 2012.

This work was supported by the Deutsche Forschungsgemeinschaft through Grant SFB684 and an Emmy Noether grant (to M.S.-S.). G.v.L. was supported by the Ghent Researchers on Unfolded Proteins in Inflammatory Disease Multidisciplinary Research Partnership of Ghent University.

Address correspondence and reprint requests to Dr. Marc Schmidt-Supprian, Max Planck Institute of Biochemistry, Am Klopferspitz 18, 82152 Martinsried, Germany. E-mail address: supprian@biochem.mpg.de

The online version of this article contains supplemental material.

Abbreviations used in this article: DUB, deubiquitinase; GC, germinal center; HL, Hodgkin lymphoma; KO, knockout; mLN, mesenteric lymph node; MZP, marginal zone precursor; TRAF, TNFR-associated factor.

Jin and colleagues (29) found massive hyperplasia and expansion of marginal zone B cells in CYLD-deficient mice and increased responses of CYLD-deficient B cells in response to activation. Similar effects were caused by the expression of a truncated CYLD lacking exons 7 and 8 (30). However, in another study, CYLD deficiency did not affect peripheral B cell numbers, but increased NF-κB activation after stimulation (31). In accordance, B cells developed normally in CYLD-deficient mice employed in the current study (32). The lack of a B cell phenotype in our CYLD-deficient mouse model suggested the possibility of compensatory mechanisms by redundant proteins. It is, for example, conceivable that dysregulation of B cell homeostasis is caused by truncated CYLD rather than through the absence of full-length CYLD. Truncated forms of CYLD could exert dominant-negative functions by interfering with the action of redundant proteins.

As mentioned above, genetic studies in both human (17, 19, 21, 22) and mice (23, 33) have revealed different consequences of lack of A20 or CYLD function. Interestingly, however, >60% of EBV-negative classical Hodgkin lymphoma (HL) cases contain mono- or biallelic losses of A20 function, and 35% of classical HL cases display decreased CYLD copy numbers (34). Strikingly, the HL line KM-H2 has completely lost both A20 and CYLD expression due to biallelic mutations in both genes (34). In addition, it is remarkable that both A20 and CYLD share a set of signaling factors such as TRAF2, TRAF6, RIP1, and NF-κB essential modulator as molecular targets (4, 5). Therefore, A20 represents a valid candidate protein that could compensate for the loss of CYLD function in B cells. To test this hypothesis, we generated A20/CYLD double-deficient B cells and studied the development of several B cell subsets in CD19Cre/A20$^{F/F}$CYLD$^{-/-}$ mice, their response to B cell mitogens, and the impact of the combined loss of both DUBs on NF-κB activation.

In our studies, we did not uncover general functions for CYLD in B cell differentiation and activation. More importantly, compound loss of A20 and CYLD did not exacerbate the effects of A20 deficiency, with the possible exception of B cell activation in response to BCR cross-linking in vitro. Therefore, the discrepancy of the various reported effects of CYLD deficiency is not functional compensation by A20, and this issue awaits further experimental clarification.

Materials and Methods

Mice

All mouse strains employed in this study are published and were originally generated using C57BL/6 embryonic stem cells or backcrossed to C57BL/6 at least six times (11, 32). Mice were housed in a specific pathogen-free environment in the animal facility of the Max Planck Institute of Biochemistry, Martinsried, Germany, and all animal procedures were approved by the Regierung of Oberbayern.

Flow cytometry

Single-cell suspensions were prepared and stained as published (35) with the following mAbs conjugated to FITC, PE, PerCP, allophycocyanin, or biotin: AA4.1 (AA4.1), B220 (RA3-6B2), CD1d (1B1), CD19 (eBio1D3), CD21 (2D6), CD23 (B3B4), CD25 (PC61.5), CD38 (90), CD5 (53-7.3), IgM (II/41), CD95 (15A7), CD86 (GL-1), CD80 (16-10A1), IL-6 (MP5-20F3) (all from eBioscience), and PNA (Vector Laboratories). Dead cells were excluded from analysis by 7-aminoactinomycin D or ethidium monoazide bromide staining. All samples were acquired on an FACSCalibur or FACSCanto II (BD Pharmingen), and results were analyzed with FlowJo software (Tree Star). For intracellular cytokine staining, cells were treated for 5 h at 37°C with 10 nM brefeldin A (Applichem), incubated with Fc-block (eBioscience), washed, and surface-stained prior to fixation with 2% paraformaldehyde and permeabilization with 0.5% saponin.

In vitro cultures

For in vitro culture, cells were purified by MACS depletion of CD43-expressing cells (>85–90% pure; Miltenyi Biotec). Final concentrations of the stimuli for cellular activation were (unless otherwise indicated): 2.5 μg/ml anti-CD40 (HM40-3; eBioscience), 10 μg/ml anti-IgM (Jackson ImmunoResearch Laboratories), 0.1 μM CpG (Alexis Biochemical), and 20 μg/ml LPS (Sigma-Aldrich). ELISAs were conducted using Ab pairs to IL-6 (BD Biosciences) according to the manufacturer's instructions. To monitor cellular division, B cells were labeled in 1 ml 2.5 μM CFSE (Molecular Probes) in PBS per 10^7 cells at 37°C for 10 min.

EMSAs

Purified B cells were stimulated and lysed in whole-cell lysis buffer (20 mM HEPES [pH 7.9], 350 mM NaCl, 20% glycerin, 1 mM $MgCl_2$, 0.5 mM EDTA, 0.1 EGTA, 1% Nonidet P-40, 0.5 M NaF, 1 M DTT, 1 M β-glycerophosphate, 200 mM Na vanadate, and 25× Protease Inhibitor Mixture [Roche]) according to standard protocols. EMSAs were performed by using a [^{32}P]-dATP–labeled, dsNF-κB oligonucleotide probe (5′-CAGGGCTGGG-GATTCCCCATCTCCACAGG-3′). The samples were separated on native polyacrylamide gels prior to autoradiography. For EMSA supershift assays, whole-cell lysates were preincubated for 30 min on ice with anti-p50, anti-p65, or anti–c-Rel Abs (all from Santa Cruz Biotechnology).

Statistics

For comparisons of three and more groups, one-way ANOVA was used. The *p* values are presented in figure legends when a statistically significant difference was found.

Results

Loss of CYLD does not exacerbate the defects in A20-deficient B cell homeostasis

To study the consequences of the loss of both A20 and CYLD function in B cells, constitutive CYLD$^{-/-}$ KO mice (32) were intercrossed with CD19Cre/A20$^{F/F}$ mice (11), allowing B lineage-specific ablation of A20. In the resulting CD19Cre/A20$^{F/F}$ CYLD$^{-/-}$ mice, the CYLD deficiency was not restricted to the B lineage. However, in CYLD-deficient mice, B cell development was indistinguishable from wild-type mice, showing that complete CYLD deficiency does not affect the generation of B cells (Fig. 1A) (30). CYLD-deficient mice were also intercrossed with CD19cre mice to control for the heterozygous ablation of CD19 and the expression of the Cre recombinase.

We first assessed the impact of the combined deletion of A20 and CYLD on B cell development. To our surprise, loss of both DUBs did not exacerbate the defects in B cell subset differentiation caused by absence of A20 alone (11). The following developmental effects caused by absence of A20 in B cells were unchanged by additional absence of CYLD: 1) reduced proportions of mature recirculating B cells in the bone marrow (Fig. 1A); 2) increased proportions of transitional and reduced proportion of splenic mature B cells (Fig. 1B, *first panel*); 3) the expansion of CD23$^+$ marginal zone precursor (MZP) B cells (Fig. 1B, *third panel*); and 4) reduced percentages of B1, in particular B1a cells, in the peritoneal cavity (Fig. 1C).

In contrast, we observed that constitutive absence of CYLD caused a slight reduction in splenocyte numbers, which was not affected by the additional absence of A20 in B cells (Supplemental Fig. 1). A20 deficiency in B cells induces the expansion of myeloid and T cells, resulting in splenomegaly and chronic inflammation (11). It seems possible that loss of CYLD function in myelomonocytic cells, which impairs their responses to inflammatory stimuli (36), counteracts the inflammation caused by A20-deficient B cells to some extent. This could explain the reduction of splenocyte numbers in CD19Cre/A20$^{F/F}$CYLD$^{-/-}$ mice compared with CD19Cre/A20$^{F/F}$ mice.

A20/CYLD deficiency does not enhance formation of spontaneous germinal centers compared with loss of A20 alone

In previous studies, we and others (10, 11, 16) reported that A20-deficient B cells are hyperresponsive to stimulation caused by

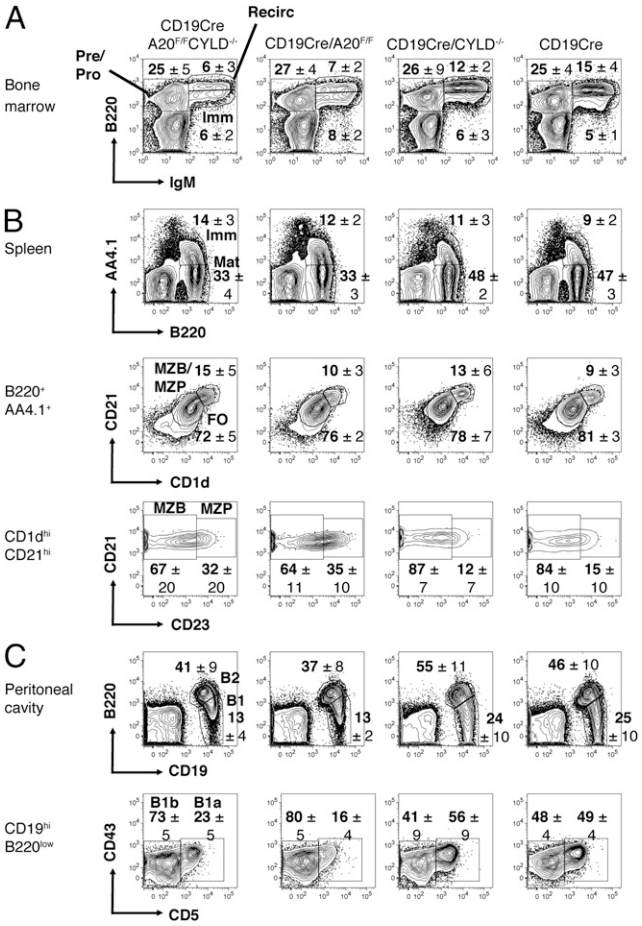

FIGURE 1. A20/CYLD-deficient B cells display similar developmental defects as A20-deficient B cells. (**A**) Proportions of pre/pro- ($B220^{+}IgM^{-}$), immature ($B220^{lo}IgM^{+}$), and mature/recirculating ($B220^{hi}IgM^{+}$) B cells of lymphocytes in the bone marrow. Numbers indicate mean and SD of five to six mice per genotype. (**B**) Proportions of transitional (Imm; $B220^{+}AA4.1^{+}$) and mature (Mat; $B220^{+}AA4.1^{-}$) B cells of total lymphocytes (*top panel*) and of follicular (FO: $CD1d^{int}CD21^{int}$) and marginal zone (MZ)/MZP ($CD1d^{high}CD21^{high}$) B cells of $B220^{+}$ B cells (*middle panel*) in the spleen. *Bottom panels*, Proportions of MZ ($CD1d^{hi}CD21^{hi}CD23^{lo}$) and MZP ($CD1d^{hi}CD21^{hi}CD23^{hi}$) B cells of $B220^{+}$ B cells. Numbers indicate mean and SD of nine mice per genotype. (**C**) Proportions of peritoneal B2 ($CD19^{+}B220^{+}$) and B1 ($CD19^{high}B220^{low}$) cells of total lymphocytes (*top panel*) and of B1a ($CD19^{high}B220^{low}CD5^{+}$) and B1b ($CD19^{high}B220^{low}CD5^{-}$) cells of total B1 cells (*bottom panel*). Numbers indicate mean and SD of nine mice per genotype.

enhanced NF-κB signaling due to lack of negative regulation. Given that CYLD has been suggested to also negatively regulate NF-κB in multiple cell types and was shown to restrict B cell activation (1), we asked whether combined loss of A20 and CYLD would cause additive effects during B cell activation.

To address this question in vivo, we studied spontaneous germinal center (GC) formation in the spleen and the GALT. Spontaneous GC formation was not enhanced in spleen and GALT of naive CYLD-deficient mice compared with control mice (Fig. 2). In contrast, naive CD19Cre/$A20^{F/F}CYLD^{-/-}$ and CD19Cre/$A20^{F/F}$ mice displayed the same slightly increased proportions of spontaneous splenic GC B cells compared with CYLD-deficient and control mice, although the differences did not reach statistical significance (Fig. 2). Similarly, the increased activation of A20-deficient B cells by bacterial Ags to form GCs in the mesenteric lymph nodes (mLN) and Peyer's patches was comparable in mice lacking both A20 and CYLD in B cells (Fig. 2).

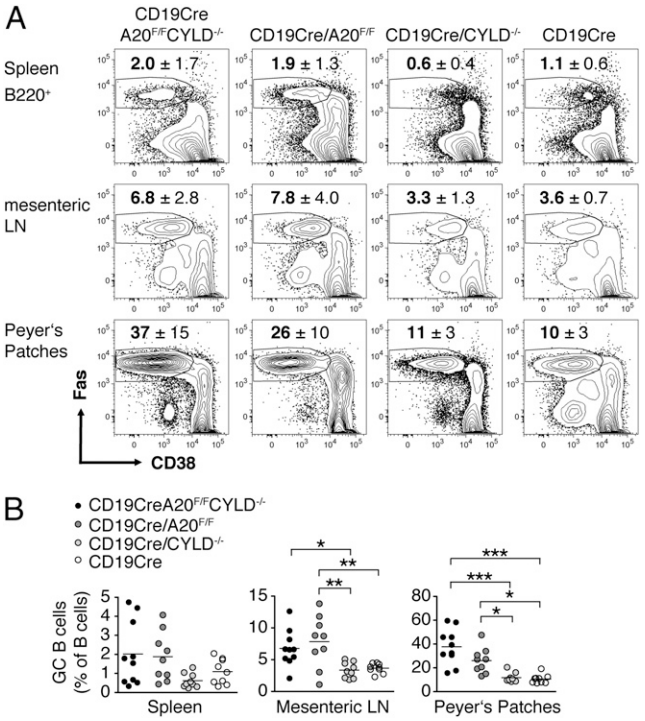

FIGURE 2. A20/CYLD deficiency in B cells enhances spontaneous GC formation to the same extent as A20 deficiency alone. (**A**) Proportions of GC B cells ($B220^{+}Fas^{hi}CD38^{lo}$) of total B cells in spleen (*top panel*), mLN (*middle panel*), and Peyer's patches (*bottom panel*); numbers indicate mean and SD of 9–10 mice per genotype. (**B**) Proportions of GC B cells in spleen, mLN, and Peyer's patches depicted as individual data points; bars indicate mean of 9–10 mice per group [same as in (A)]. $*p < 0.05$, $**p < 0.001$, $***p < 0.0001$, one-way ANOVA.

A20/CYLD deficiency does not enhance B cell activation and proliferation significantly more than absence of A20

We further compared B cell responses of A20/CYLD-deficient and A20-deficient B cells by measuring their activation, proliferation, and cytokine secretion in response to stimulation with B cell mitogens (anti-IgM, anti-CD40, LPS, and CpG) in vitro. Upon stimulation, B cells upregulate activation markers (CD25, CD80, CD86, MHC class II, and Fas) that were already slightly increased in resting A20/CYLD-deficient and A20-deficient B cells compared with CYLD-deficient and control B cells. Ex vivo-stimulated A20/CYLD-deficient and A20-deficient B cells expressed similar levels of activation markers, and these levels were considerably higher than in CYLD-deficient and control B cells (Fig. 3A, Table I). These data are consistent with the finding that the spontaneous GC formation rate in CD19Cre/$A20^{F/F}CYLD^{-/-}$ and CD19Cre/$A20^{F/F}$ mice was comparable with each other but significantly higher than in CD19Cre/$CYLD^{-/-}$ and control mice. A20/CYLD-deficient B cells proliferated in vitro to a similar extent as A20-deficient B cells in response to CD40 and CpG, judged by the calculation of different parameters of cellular division using CFSE dilution assays. In contrast, BCR cross-linking and LPS stimulation slightly enhanced the proliferation of A20/CYLD-deficient B cells compared with A20-deficient B cells. These observations support our previous finding that CYLD does not majorly contribute to the negative regulation of B cell response in the presence or absence of A20.

A20/CYLD-deficient B cells produce more IL-6 in response to BCR cross-linking, but not in response to the engagement of CD40 and TLRs

We recently demonstrated that A20 negatively controls canonical NF-κB activation in response to BCR cross-linking and CD40 and

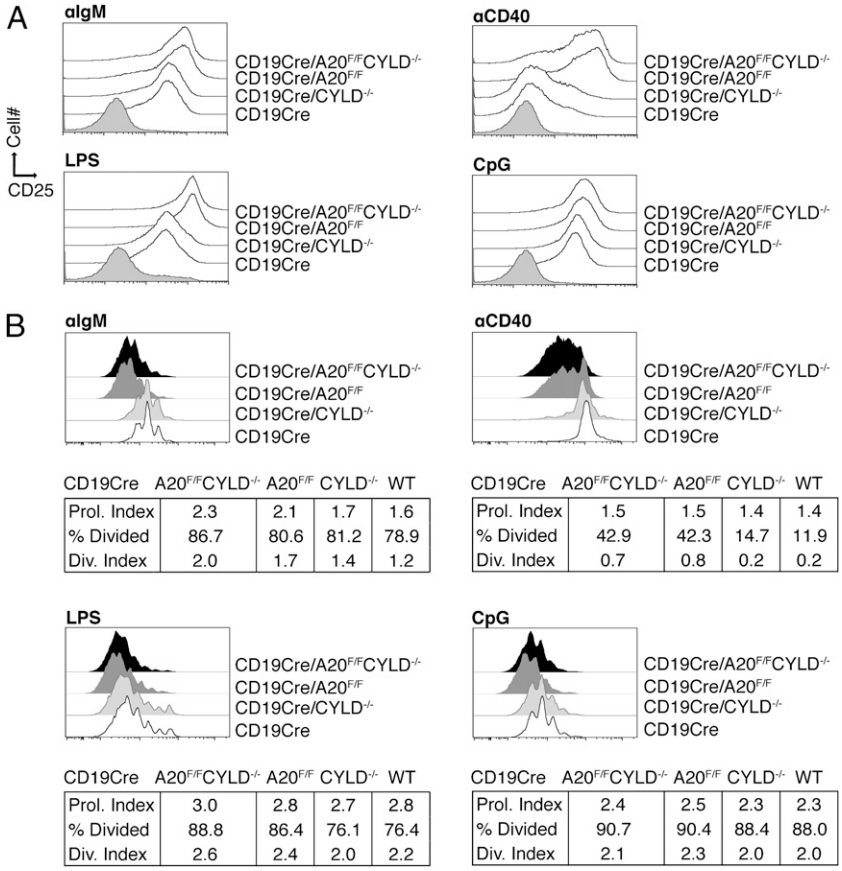

FIGURE 3. A20/CYLD-deficient B cells display similar pattern of hyperresponsiveness as A20-deficient B cells. (**A**) Expression level of the B cell activation marker CD25 after overnight stimulation with anti-IgM, anti-CD40, LPS, or CpG compared with the resting condition of control B cells (gray-filled histogram). The histograms are representative of two to three independent experiments. (**B**) CFSE proliferation assay: histograms show CFSE intensities 3 d after stimulation. The tables under each histogram depict the proliferation index (Prol. Index, average number of divisions of the proliferating cells), the percentage of dividing cells (% Divided, the proportion of cells that initially started to divide), and the division index (Div. Index, average number of divisions of all cells); values were calculated with the FlowJo software (Tree Star). Values represent means of four independent experiments.

TLR stimulation. In addition, we showed that the expression of IL-6, which is a direct target of NF-κB, correlates with the strength of NF-κB signaling in B cells (11).

Therefore, we evaluated the expression of IL-6 by ELISA (Fig. 4A) and intracellular FACS (Fig. 4B) of stimulated A20/CYLD-deficient and A20-deficient B cells compared with CYLD-deficient and control B cells. Both A20/CYLD and A20 deficiency alone led to an equivalent increase in the production of IL-6 after stimulation with anti-CD40, LPS, or CpG in B cells (Fig. 4A).

In contrast, BCR cross-linking caused elevated amounts of IL-6 (Fig. 4A) in A20/CYLD-deficient B cells compared with A20-deficient B cells. These results were in agreement with the observation that A20/CYLD deficiency enhanced the proliferation of B cells after BCR stimulation. Taking the median fluorescence

Table I. A20/CYLD-deficient and A20-deficient B cells express similar levels of activation markers

Stimuli	Genotype	CD25	CD80	CD86	MHC Class II	Fas
Resting	CD19Cre/A20$^{F/F}$CYLD$^{-/-}$	25	36	14	1241	51
	CD19Cre/A20$^{F/F}$	25	38	17	965	57
	CD19Cre/CYLD$^{-/-}$	18	27	11	547	36
	CD19Cre	18	28	9	573	33
Anti-IgM	CD19Cre/A20$^{F/F}$CYLD$^{-/-}$	621	63	519	3051	111
	CD19Cre/A20$^{F/F}$	552	63	704	3051	127
	CD19Cre/CYLD$^{-/-}$	340	45	737	2436	72
	CD19Cre	292	47	538	2890	63
Anti-CD40	CD19Cre/A20$^{F/F}$CYLD$^{-/-}$	396	91	355	3220	396
	CD19Cre/A20$^{F/F}$	487	102	519	2813	403
	CD19Cre/CYLD$^{-/-}$	39	42	130	1999	59
	CD19Cre	32	42	60	2227	45
LPS	CD19Cre/A20$^{F/F}$CYLD$^{-/-}$	1104	165	777	2763	205
	CD19Cre/A20$^{F/F}$	1165	179	791	2525	217
	CD19Cre/CYLD$^{-/-}$	319	56	704	2288	129
	CD19Cre	267	56	514	2738	95
CpG	CD19Cre/A20$^{F/F}$CYLD$^{-/-}$	414	98	328	2571	106
	CD19Cre/A20$^{F/F}$	441	91	368	2414	103
	CD19Cre/CYLD$^{-/-}$	346	57	382	1894	82
	CD19Cre	281	55	259	2267	68

Median fluorescence intensities of the B cell activation markers CD25, CD80, CD86, MHC class II, and Fas after overnight stimulation with anti-IgM, anti-CD40, LPS, or CpG compared with the resting condition of control B cells. Values represent the means of two to three independent experiments.

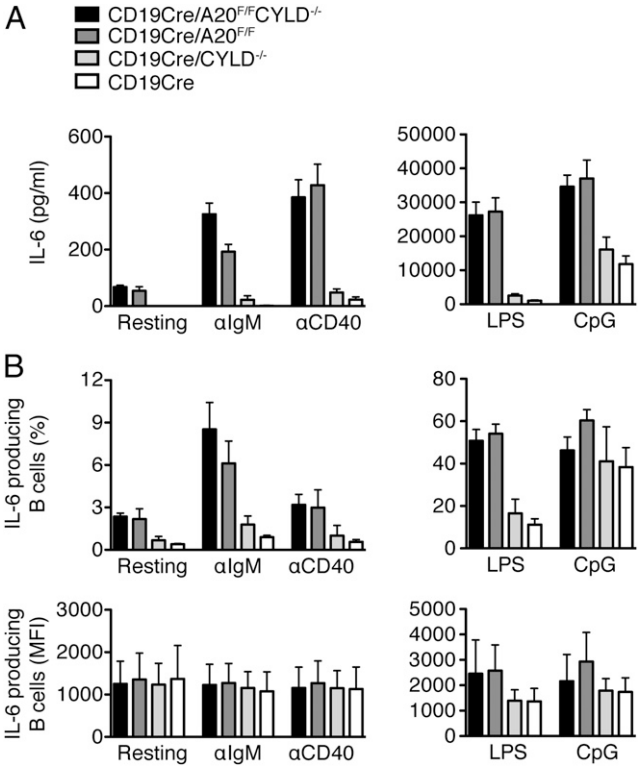

FIGURE 4. Proinflammatory IL-6 production is comparable between A20/CYLD-deficient and A20-deficient B cells. (**A**) Measurement of IL-6 production in overnight-stimulated B cells by ELISA. Bars represent means and SD of four independent experiments. (**B**) IL-6 production in overnight stimulated and brefeldin A-treated B cells assessed by intracellular FACS. *Top panel*, Percentage of IL-6–producing B cells. *Bottom panel*, Mean fluorescence intensity (MFI) of IL-6–producing B cells represents IL-6 amount per IL-6–producing cell. Bars depict means and SD of three independent experiments.

intensity as an estimate for the amount of IL-6 made per IL-6–producing cell suggests that B cells of all genotypes produce similar amounts of IL-6 in response to anti-IgM and anti-CD40 (Fig. 4B, *bottom panel*). Therefore, the differences between the genotypes most likely relate to the proportion of activated cells, rather than an increase in IL-6 secretion per cell. In contrast, stimulation with CpG and more so with LPS increased the IL-6 production per cell and the proportion of IL-6–producing cells (Fig. 4B) in both A20/CYLD-deficient and A20-deficient compared with CYLD-deficient and control B cells. However, the differences were entirely due to the lack of A20, whereas the loss of CYLD had essentially no effect.

Enhanced proliferation and IL-6 production in A20/CYLD-deficient compared with A20-deficient B cells in response to BCR cross-linking correlates with enhanced NF-κB activation

With two stimuli, we observed slightly enhanced in vitro responses in A20/CYLD-deficient compared with A20-deficient B cells: anti-IgM (proliferation and IL-6 production) and LPS (proliferation). To determine whether these enhanced responses correspond to increased NF-κB activation, we performed EMSAs from B cells stimulated with anti-IgM (Fig. 5A) and LPS (Fig. 5B). NF-κB DNA-binding complexes were verified by EMSA supershift assays using anti-p50, anti-p65, or anti–c-Rel Abs. The supershift assays reveal increased DNA-binding of mostly of p50/c-Rel and to a lesser extent of p50/p65 subunits following stimulation with anti-IgM or LPS (Supplemental Fig. 2).

We observed enhanced BCR cross-linking–induced NF-κB DNA binding in A20/CYLD-deficient and A20-deficient B cells at all investigated time points (10, 30, and 90 min) (Fig. 5A). In addition, A20/CYLD-deficient B cells displayed more robust NF-κB activation compared with A20-deficient B cells, with the strongest difference noted 10 min following stimulation (Fig. 5A). These data demonstrate that anti-IgM–induced NF-κB activity is slightly enhanced in A20/CYLD-deficient B cells compared with A20-deficient B cells. Possible explanations for this finding could be increased signal strength in individual B cells, the activation of a larger proportion of cells, or a combination of both.

In contrast, TLR4-mediated NF-κB signaling (Fig. 5B) yielded no consistent difference between A20/CYLD-deficient and A20-deficient B cells. These findings are in line with the comparable LPS-induced IL-6 production in A20/CYLD and A20-deficient B cells.

Discussion

In this study, we addressed potential overlapping physiological functions of the ubiquitin-editing enzyme A20 and the DUB CYLD in B cells. By ablating A20 and CYLD in B cells, we demonstrate that loss of both proteins does not exacerbate the impaired B cell homeostasis and in vivo B cell hyperresponsiveness that we previously reported for mice lacking A20 specifically in B cells. Mice with A20/CYLD deficiency or A20 deficiency in B cells display equally severe B cell developmental defects. Similarly, A20/CYLD-deficient and A20-deficient B cells exhibit comparable degrees of in vitro responses to B cell mitogens and NF-κB activation.

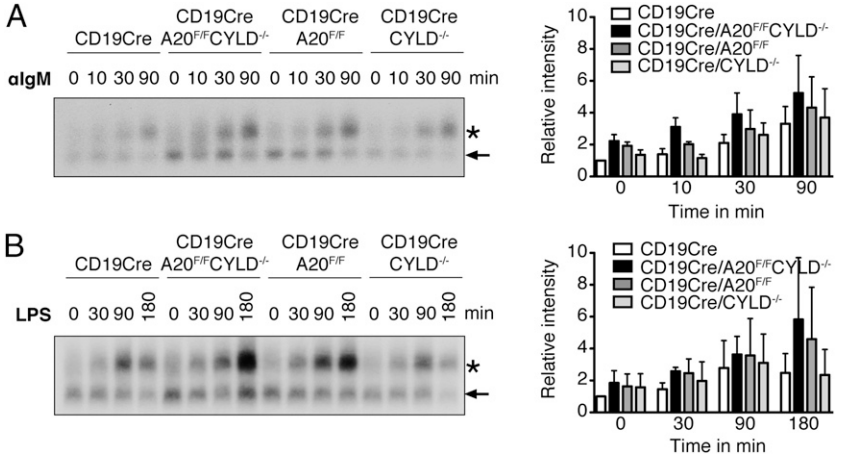

FIGURE 5. NF-κB activation in A20/CYLD-deficient compared with A20-deficient, CYLD-deficient, and control B cells in response to BCR cross-linking and LPS treatment. EMSA of anti-IgM–induced (**A**) and LPS-induced (**B**) NF-κB activation. The specific bands (asterisk) indicating NF-κB p50/c-Rel and p50/p65 heterodimer DNA-binding (*left panels*) were quantified and normalized to controls at time point 0. The lower bands (arrow) represent p50 homodimers. Bars depict means and SD of the relative band intensities, derived from four (A) or three (B) independent experiments (*right panels*).

Thus, our work indicates that A20 and CYLD do not functionally overlap in any significant fashion during B cell development and activation. The possible exception might be B cell responses and NF-κB activation after BCR cross-linking. However, we did not observe any significant consequences of the additive effects of A20 and CYLD deficiency on signaling downstream of the BCR in vivo. Because it is unclear to what extent BCR cross-linking accurately reflects recognition of Ag by the BCR in vivo, we did not pursue this observation in more detail.

Given that A20 and CYLD both contain DUB functions of K63-linked polyubiquitin chains and target similar molecular substrates including TRAF2, TRAF6, NF-κB essential modulator, and RIP1, it is surprising that both proteins do not functionally overlap. Key differences that could account for this lack of functional overlap are their molecular mode of action and CYLD's specificity to hydrolyze K63-linked (37) and linear polyubiquitin chains (38). In contrast, A20 does not act as a processive DUB for K63-linked polyubiquitin chains but (39) effectively cleaves entire K63-linked polyubiquitin chains from substrates such as TRAF6, thereby demonstrating specificity for particular polyubiquitinated substrates (40). In addition, A20 can limit NF-κB activation through noncatalytic mechanisms including lysosomal targeting of TRAF2 (41) and direct IκB kinase inhibition (42). In vivo, A20 is involved both in the addition of K48-linked polyubiquitin chains to induce the proteasomal degradation of various target proteins (43, 44) and the removal of K63-linked ubiquitin chains to terminate signaling (8, 43, 45, 46).

Another difference between A20 and CYLD include their distinct temporal expression and regulation. A20 depends functionally on its inducible expression upon signal-induced NF-κB activation (47), whereas CYLD is constitutively expressed. However, in response to mitogens and TNF-α, CYLD's DUB function is transiently inactivated by IκB kinase-mediated phosphorylation (48). Thus, it has been proposed that A20 and CYLD may regulate NF-κB activation at different phases (23). A20 function is crucial to terminate signal-induced NF-κB activation (7, 49). In contrast, CYLD acts constitutively to prevent spontaneous NF-κB activation (48).

In addition, different cell type-specific cofactor requirement and/or substrate-specific molecular mode of action could also explain the missing functional overlap between A20 and CYLD during the signal transduction pathways initiated upon B cell activation.

In contrast to another KO model (29) and the expression of a truncated CYLD protein (30), we did not observe major effects in our CYLD-deficient B cells with respect to cell numbers in mice, differentiation, and activation. Our findings are in agreement with the analysis of a third independently generated CYLD-KO mouse strain (31). It is also worth mentioning that our study is the only one that uses mice exclusively on the C57BL/6 genetic background. It cannot be excluded that some of the observed differences to the other studies are in part due to effects of the C57BL/6-129 mixed genetic background employed there (50).

In this study, we clearly demonstrate that the phenotypic differences between the mouse models are not due to a compensation for some of CYLD's functions by A20 in mice. Collectively, we conclude that A20 and CYLD do not significantly cooperate in the regulation of B cell development and activation.

Acknowledgments

We thank Reinhard Fässler for support, Julia Knogler and Barbara Habermehl for excellent technical assistance, and Christoph Vahl, Sarah Schmalbrock, Basma Abdel Motaal, and Klaus Heger for help with experiments and input.

Disclosures

The authors have no financial conflicts of interest.

References

1. Malynn, B. A., and A. Ma. 2010. Ubiquitin makes its mark on immune regulation. *Immunity* 33: 843–852.
2. Bhoj, V. G., and Z. J. Chen. 2009. Ubiquitylation in innate and adaptive immunity. *Nature* 458: 430–437.
3. Enesa, K., M. Zakkar, H. Chaudhury, A. Luong, L. Rawlinson, J. C. Mason, D. O. Haskard, J. L. E. Dean, and P. C. Evans. 2008. NF-kappaB suppression by the deubiquitinating enzyme Cezanne: a novel negative feedback loop in pro-inflammatory signaling. *J. Biol. Chem.* 283: 7036–7045.
4. Hymowitz, S. G., and I. E. Wertz. 2010. A20: from ubiquitin editing to tumour suppression. *Nat. Rev. Cancer* 10: 332–341.
5. Massoumi, R. 2010. Ubiquitin chain cleavage: CYLD at work. *Trends Biochem. Sci.* 35: 392–399.
6. Xu, G., X. Tan, H. Wang, W. Sun, Y. Shi, S. Burlingame, X. Gu, G. Cao, T. Zhang, J. Qin, and J. Yang. 2010. Ubiquitin-specific peptidase 21 inhibits tumor necrosis factor alpha-induced nuclear factor kappaB activation via binding to and deubiquitinating receptor-interacting protein 1. *J. Biol. Chem.* 285: 969–978.
7. Lee, E. G., D. L. Boone, S. Chai, S. L. Libby, M. Chien, J. P. Lodolce, and A. Ma. 2000. Failure to regulate TNF-induced NF-kappaB and cell death responses in A20-deficient mice. *Science* 289: 2350–2354.
8. Turer, E. E., R. M. Tavares, E. Mortier, O. Hitotsumatsu, R. Advincula, B. Lee, N. Shifrin, B. A. Malynn, and A. Ma. 2008. Homeostatic MyD88-dependent signals cause lethal inflamMation in the absence of A20. *J. Exp. Med.* 205: 451–464.
9. Vereecke, L., M. Sze, C. Mc Guire, B. Rogiers, Y. Chu, M. Schmidt-Supprian, M. Pasparakis, R. Beyaert, and G. van Loo. 2010. Enterocyte-specific A20 deficiency sensitizes to tumor necrosis factor-induced toxicity and experimental colitis. *J. Exp. Med.* 207: 1513–1523.
10. Tavares, R. M., E. E. Turer, C. L. Liu, R. Advincula, P. Scapini, L. Rhee, J. Barrera, C. A. Lowell, P. J. Utz, B. A. Malynn, and A. Ma. 2010. The ubiquitin modifying enzyme A20 restricts B cell survival and prevents autoimmunity. *Immunity* 33: 181–191.
11. Chu, Y., J. C. Vahl, D. Kumar, K. Heger, A. Bertossi, E. Wójtowicz, V. Soberon, D. Schenten, B. Mack, M. Reutelshöfer, et al. 2011. B cells lacking the tumor suppressor TNFAIP3/A20 display impaired differentiation and hyperactivation and cause inflammation and autoimmunity in aged mice. *Blood* 117: 2227–2236.
12. Lippens, S., S. Lefebvre, B. Gilbert, M. Sze, M. Devos, K. Verhelst, L. Vereecke, C. Mc Guire, C. Guérin, P. Vandenabeele, et al. 2011. Keratinocyte-specific ablation of the NF-κB regulatory protein A20 (TNFAIP3) reveals a role in the control of epidermal homeostasis. *Cell Death Differ.* 18: 1845–1853.
13. Matmati, M., P. Jacques, J. Maelfait, E. Verheugen, M. Kool, M. Sze, L. Geboes, E. Louagie, C. Mc Guire, L. Vereecke, et al. 2011. A20 (TNFAIP3) deficiency in myeloid cells triggers erosive polyarthritis resembling rheumatoid arthritis. *Nat. Genet.* 43: 908—912.
14. Kool, M., G. van Loo, W. Waelput, S. De Prijck, F. Muskens, M. Sze, J. van Praet, F. Branco-Madeira, S. Janssens, B. Reizis, et al. 2011. The ubiquitin-editing protein A20 prevents dendritic cell activation, recognition of apoptotic cells, and systemic autoimmunity. *Immunity* 35: 82–96.
15. Hammer, G. E., E. E. Turer, K. E. Taylor, C. J. Fang, R. Advincula, S. Oshima, J. Barrera, E. J. Huang, B. Hou, B. A. Malynn, et al. 2011. Expression of A20 by dendritic cells preserves immune homeostasis and prevents colitis and spondyloarthritis. *Nat. Immunol.* 12: 1184–1193.
16. Hövelmeyer, N., S. Reissig, N. T. Xuan, P. Adams-Quack, D. Lukas, A. Nikolaev, D. Schlüter, and A. Waisman. 2011. A20 deficiency in B cells enhances B-cell proliferation and results in the development of autoantibodies. *Eur. J. Immunol.* 41: 595–601.
17. Plenge, R. M., C. Cotsapas, L. Davies, A. L. Price, P. I. W. de Bakker, J. Maller, I. Pe'er, N. P. Burtt, B. Blumenstiel, M. DeFelice, et al. 2007. Two independent alleles at 6q23 associated with risk of rheumatoid arthritis. *Nat. Genet.* 39: 1477–1482.
18. Thomson, W., A. Barton, X. Ke, S. Eyre, A. Hinks, J. Bowes, R. Donn, D. Symmons, S. Hider, I. N. Bruce, et al; Wellcome Trust Case Control Consortium; YEAR Consortium. 2007. Rheumatoid arthritis association at 6q23. *Nat. Genet.* 39: 1431–1433.
19. Graham, R. R., C. Cotsapas, L. Davies, R. Hackett, C. J. Lessard, J. M. Leon, N. P. Burtt, C. Guiducci, M. Parkin, C. Gates, et al. 2008. Genetic variants near TNFAIP3 on 6q23 are associated with systemic lupus erythematosus. *Nat. Genet.* 40: 1059–1061.
20. Musone, S. L., K. E. Taylor, T. T. Lu, J. Nititham, R. C. Ferreira, W. Ortmann, N. Shifrin, M. A. Petri, M. I. Kamboh, S. Manzi, et al. 2008. Multiple polymorphisms in the TNFAIP3 region are independently associated with systemic lupus erythematosus. *Nat. Genet.* 40: 1062–1064.
21. Trynka, G., A. Zhernakova, J. Romanos, L. Franke, K. A. Hunt, G. Turner, M. Bruinenberg, G. A. Heap, M. Platteel, A. W. Ryan, et al. 2009. Coeliac disease-associated risk variants in TNFAIP3 and REL implicate altered NF-kappaB signalling. *Gut* 58: 1078–1083.
22. Bignell, G. R., W. Warren, S. Seal, M. Takahashi, E. Rapley, R. Barfoot, H. Green, C. Brown, P. J. Biggs, S. R. Lakhani, et al. 2000. Identification of the familial cylindromatosis tumour-suppressor gene. *Nat. Genet.* 25: 160–165.
23. Sun, S.-C. 2010. CYLD: a tumor suppressor deubiquitinase regulating NF-kappaB activation and diverse biological processes. *Cell Death Differ.* 17: 25–34.

24. Brummelkamp, T. R., S. M. B. Nijman, A. M. G. Dirac, and R. Bernards. 2003. Loss of the cylindromatosis tumour suppressor inhibits apoptosis by activating NF-kappaB. *Nature* 424: 797–801.
25. Kovalenko, A., C. Chable-Bessia, G. Cantarella, A. Israël, D. Wallach, and G. Courtois. 2003. The tumour suppressor CYLD negatively regulates NF-kappaB signalling by deubiquitination. *Nature* 424: 801–805.
26. Trompouki, E., E. Hatzivassiliou, T. Tsichritzis, H. Farmer, A. Ashworth, and G. Mosialos. 2003. CYLD is a deubiquitinating enzyme that negatively regulates NF-kappaB activation by TNFR family members. *Nature* 424: 793–796.
27. Lim, J. H., B. Stirling, J. Derry, T. Koga, H. Jono, C.-H. Woo, H. Xu, P. Bourne, U.-H. Ha, H. Ishinaga, et al. 2007. Tumor suppressor CYLD regulates acute lung injury in lethal *Streptococcus pneumoniae* infections. *Immunity* 27: 349–360.
28. Tauriello, D. V. F., A. Haegebarth, I. Kuper, M. J. Edelmann, M. Henraat, M. R. Canninga-van Dijk, B. M. Kessler, H. Clevers, and M. M. Maurice. 2010. Loss of the tumor suppressor CYLD enhances Wnt/beta-catenin signaling through K63-linked ubiquitination of Dvl. *Mol. Cell* 37: 607–619.
29. Jin, W., W. R. Reiley, A. J. Lee, A. Wright, X. Wu, M. Zhang, and S.-C. Sun. 2007. Deubiquitinating enzyme CYLD regulates the peripheral development and naive phenotype maintenance of B cells. *J. Biol. Chem.* 282: 15884–15893.
30. Hövelmeyer, N., F. T. Wunderlich, R. Massoumi, C. G. Jakobsen, J. Song, M. A. Wörns, C. Merkwirth, A. Kovalenko, M. Aumailley, D. Strand, et al. 2007. Regulation of B cell homeostasis and activation by the tumor suppressor gene CYLD. *J. Exp. Med.* 204: 2615–2627.
31. Zhang, J., B. Stirling, S. T. Temmerman, C. A. Ma, I. J. Fuss, J. M. J. Derry, and A. Jain. 2006. Impaired regulation of NF-kappaB and increased susceptibility to colitis-associated tumorigenesis in CYLD-deficient mice. *J. Clin. Invest.* 116: 3042–3049.
32. Massoumi, R., K. Chmielarska, K. Hennecke, A. Pfeifer, and R. Fässler. 2006. Cyld inhibits tumor cell proliferation by blocking Bcl-3-dependent NF-kappaB signaling. *Cell* 125: 665–677.
33. Shembade, N., and E. W. Harhaj. 2012. Regulation of NF-κB signaling by the A20 deubiquitinase. *Cell. Mol. Immunol.* 9: 123–130.
34. Schmidt, A., R. Schmitz, M. Giefing, J. I. Martin-Subero, S. Gesk, I. Vater, A. Massow, E. Maggio, M. Schneider, M.-L. Hansmann, et al. 2010. Rare occurrence of biallelic CYLD gene mutations in classical Hodgkin lymphoma. *Genes Chromosomes Cancer* 49: 803–809.
35. Sasaki, Y., E. Derudder, E. Hobeika, R. Pelanda, M. Reth, K. Rajewsky, and M. Schmidt-Supprian. 2006. Canonical NF-kappaB activity, dispensable for B cell development, replaces BAFF-receptor signals and promotes B cell proliferation upon activation. *Immunity* 24: 729–739.
36. Tsagaratou, A., D. L. Kontoyiannis, and G. Mosialos. 2011. Truncation of the deubiquitinating domain of CYLD in myelomonocytic cells attenuates inflammatory responses. *PLoS ONE* 6: e16397.
37. Komander, D., C. J. Lord, H. Scheel, S. Swift, K. Hofmann, A. Ashworth, and D. Barford. 2008. The structure of the CYLD USP domain explains its specificity for Lys63-linked polyubiquitin and reveals a B box module. *Mol. Cell* 29: 451–464.
38. Komander, D., F. Reyes-Turcu, J. D. F. Licchesi, P. Odenwaelder, K. D. Wilkinson, and D. Barford. 2009. Molecular discrimination of structurally equivalent Lys 63-linked and linear polyubiquitin chains. *EMBO Rep.* 10: 466–473.
39. Komander, D., and D. Barford. 2008. Structure of the A20 OTU domain and mechanistic insights into deubiquitination. *Biochem. J.* 409: 77–85.
40. Lin, S.-C., J. Y. Chung, B. Lamothe, K. Rajashankar, M. Lu, Y.-C. Lo, A. Y. Lam, B. G. Darnay, and H. Wu. 2008. Molecular basis for the unique deubiquitinating activity of the NF-kappaB inhibitor A20. *J. Mol. Biol.* 376: 526–540.
41. Li, L., D. W. Hailey, N. Soetandyo, W. Li, J. Lippincott-Schwartz, H.-B. Shu, and Y. Ye. 2008. Localization of A20 to a lysosome-associated compartment and its role in NFkappaB signaling. *Biochim. Biophys. Acta* 1783: 1140–1149.
42. Skaug, B., J. Chen, F. Du, J. He, A. Ma, and Z. J. Chen. 2011. Direct, noncatalytic mechanism of IKK inhibition by A20. *Mol. Cell* 44: 559–571.
43. Shembade, N., N. S. Harhaj, K. Parvatiyar, N. G. Copeland, N. A. Jenkins, L. E. Matesic, and E. W. Harhaj. 2008. The E3 ligase Itch negatively regulates inflammatory signaling pathways by controlling the function of the ubiquitin-editing enzyme A20. *Nat. Immunol.* 9: 254–262.
44. Shembade, N., A. Ma, and E. W. Harhaj. 2010. Inhibition of NF-kappaB signaling by A20 through disruption of ubiquitin enzyme complexes. *Science* 327: 1135–1139.
45. Hitotsumatsu, O., R.-C. Ahmad, R. Tavares, M. Wang, D. Philpott, E. E. Turer, B. L. Lee, N. Shiffin, R. Advincula, B. A. Malynn, et al. 2008. The ubiquitin-editing enzyme A20 restricts nucleotide-binding oligomerization domain containing 2-triggered signals. *Immunity* 28: 381–390.
46. Düwel, M., V. Welteke, A. Oeckinghaus, M. Baens, B. Kloo, U. Ferch, B. G. Darnay, J. Ruland, P. Marynen, and D. Krappmann. 2009. A20 negatively regulates T cell receptor signaling to NF-kappaB by cleaving Malt1 ubiquitin chains. *J. Immunol.* 182: 7718–7728.
47. Opipari, A. W., Jr., M. S. Boguski, and V. M. Dixit. 1990. The A20 cDNA induced by tumor necrosis factor alpha encodes a novel type of zinc finger protein. *J. Biol. Chem.* 265: 14705–14708.
48. Reiley, W., M. Zhang, X. Wu, E. Granger, and S.-C. Sun. 2005. Regulation of the deubiquitinating enzyme CYLD by IkappaB kinase gamma-dependent phosphorylation. *Mol. Cell. Biol.* 25: 3886–3895.
49. Boone, D. L., E. E. Turer, E. G. Lee, R.-C. Ahmad, M. T. Wheeler, C. Tsui, P. Hurley, M. Chien, S. Chai, O. Hitotsumatsu, et al. 2004. The ubiquitin-modifying enzyme A20 is required for termination of Toll-like receptor responses. *Nat. Immunol.* 5: 1052–1060.
50. Bygrave, A. E., K. L. Rose, J. Cortes-Hernandez, J. Warren, R. J. Rigby, H. T. Cook, M. J. Walport, T. J. Vyse, and M. Botto. 2004. Spontaneous autoimmunity in 129 and C57BL/6 mice-implications for autoimmunity described in gene-targeted mice. *PLoS Biol.* 2: E243.

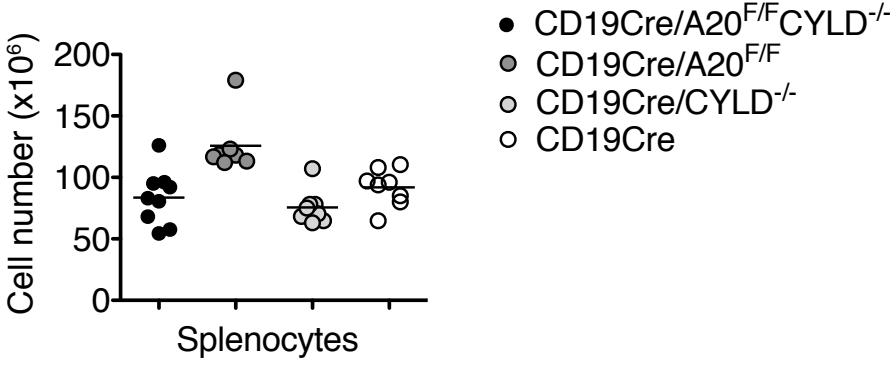

Supplemental figure 1. Combined loss of A20 and CYLD in B cells does not affect splenic cell numbers. Absolute cell numbers of splenocytes; n = 9 mice per genotype.

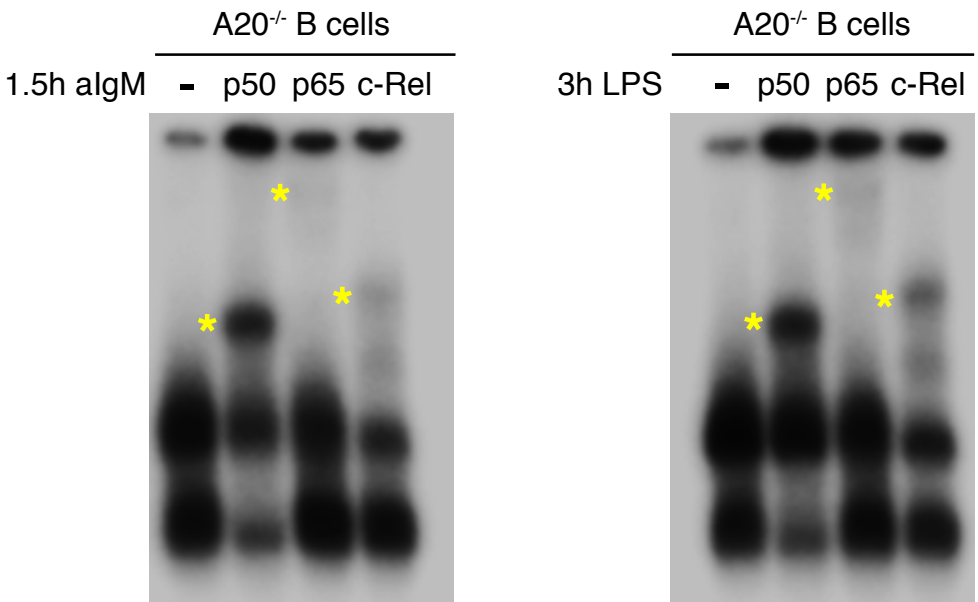

Supplemental figure 2. Canonical NF-κB activation in A20-deficient B cells. DNA-binding analysis of NF-κB subunits by EMSA supershift. The asterisks highlight the NF-κB subunits supershifted with the respective antibodies.